© PHYSBENCH: BENCHMARKING AND ENHANCING VISION-LANGUAGE MODELS FOR PHYSICAL WORLD UNDERSTANDING

Wei Chow^{*1}, Jiageng Mao^{*1}, Boyi Li², Daniel Seita¹, Vitor Guizilini³, Yue Wang¹ ¹University of Southern California, ²UC Berkeley, ³Toyota Research Institute

ABSTRACT

Understanding the physical world is a fundamental challenge in embodied AI, critical for enabling agents to perform complex tasks and operate safely in real-world environments. While Vision-Language Models (VLMs) have shown great promise in reasoning and task planning for embodied agents, their ability to comprehend physical phenomena remains extremely limited. To close this gap, we introduce PhysBench, a comprehensive benchmark designed to evaluate VLMs' physical world understanding capability across a diverse set of tasks. PhysBench contains 10,002 entries of interleaved video-image-text data, categorized into four major domains: physical object properties, physical object relationships, physical scene understanding, and physics-based dynamics, further divided into 19 subclasses and 8 distinct capability dimensions. Our extensive experiments, conducted on 75 representative VLMs, reveal that while these models excel in common-sense reasoning, they struggle with understanding the physical world-likely due to the absence of physical knowledge in their training data and the lack of embedded physical priors. To tackle the shortfall, we introduce PhysAgent, a novel framework that combines the generalization strengths of VLMs with the specialized expertise of vision models, significantly enhancing VLMs' physical understanding across a variety of tasks, including an 18.4% improvement on GPT-40. Furthermore, our results demonstrate that enhancing VLMs' physical world understanding capabilities can help embodied agents such as MOKA. We believe that PhysBench and PhysAgent offer valuable insights and contribute to bridging the gap between VLMs and physical world understanding. Project Page is here

1 INTRODUCTION

Understanding the physical world is a fundamental challenge in embodied AI (Gupta et al., 2021; Srivastava et al., 2021). Embodied agents are required to understand the physical properties of objects (e.g., mass, stiffness) to accurately interact with these objects. They also need to understand the relationships of physical objects to operate efficiently in cluttered environments, understand the structure of physical scenes for safe navigation and manipulation, and anticipate the outcomes of interactions and physics-based dynamics for better planning and preventing accidents. These capabilities of intuitive physics (McCloskey et al., 1983; Carey, 2000) are innate to humans and can also greatly benefit embodied agents, allowing them to perform complex tasks and operate safely in real-world scenarios (Kill & Kim, 2020).

Vision-language models (VLMs) (Liu et al., 2024c; Achiam et al., 2023; Team et al., 2023) have emerged as promising solutions for building embodied agents (Liu et al., 2024a; Nasiriany et al., 2024; Huang et al., 2023a). Trained on large amounts of human knowledge, these models have developed strong capabilities in reasoning and task planning (Yue et al., 2024; Lu et al., 2024b; Kim et al., 2024; Niu et al., 2024; Zhen et al., 2024). However, relying solely on these capabilities is insufficient for developing generalist embodied agents. A series of studies have highlighted a gap in understanding the physical world, leading to operational errors (Liu et al., 2024a), such as mishandling fragile objects (Wang et al., 2023c) or failing to recognize appropriate grasping affordances (Guo et al., 2024). Since these agents operate in and interact with the real world, VLMs must possess a comprehensive understanding of the physical world—a critical yet underexplored domain. This deficiency in physical world understanding limits the effective deployment of VLMs in embodied applications (Liu et al., 2024a; Guo et al., 2024; Gao et al., 2024a).

^{*}Equal contribution.

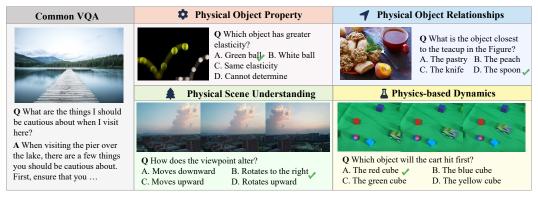


Figure 1: **Common VQA** tasks typically involve questions about visual content and general knowledge. **PhysBench** emphasizes understanding the physical world, encompassing 4 dimensions.

To further investigate this issue, we pose **two fundamental questions**: (1) Do VLMs possess an understanding of the physical world, and if not, what factors contribute to this limitation? (2) How can we enhance VLMs' physical world understanding capabilities and facilitate the effective deployment of embodied agents like MOKA?

To answer the above questions and comprehensively assess the extent of the gap between VLMs and physical world understanding, we introduce PhysBench, a dataset comprising 10,002 interleaved video-image-text entries. Given the difficulty of acquiring such data, where expressing specific properties often requires multiple images, we undertook a five-step process, spending a total of 4,000 hours on annotation. We systematically evaluate 75 representative VLM across four domains—physical object properties, physical object relationships, physical scene understanding, and physics-based dynamics—encompassing 19 sub-tasks, as shown in Figure 1. Our extensive experiments reveal that (1) most current VLMs exhibit poor understanding of the physical world, particularly in physical scene understanding and physics-based dynamics, with closed-source models significantly outperforming open-source ones; and (2) the training data for VLMs is likely a major factor contributing to their subpar performance, as it often lacks the necessary physical knowledge. Notably, when VLMs were fine-tuned on our physically grounded data, their performance improved.

To further improve VLM's physical world understanding capabilities, we propose PhysAgent, a unified framework that incorporates vision foundation models and a physics knowledge memory. By analyzing the sources of errors for VLMs on PhysBench, we identified perceptual inaccuracies and insufficient knowledge as the primary causes of mistakes. To address these issues, we incorporated vision foundation models to enhance perceptual capabilities and assist VLMs in handling tasks they typically struggle with, such as depth estimation and numerical distance calculation. Additionally, we integrated a knowledge memory module to embed essential knowledge about the physical world, which can be selectively invoked by PhysAgent. Unlike previous methods designed for physical reasoning (Zheng et al., 2024b; Tung et al., 2023), PhysAgent retains the strong generalization abilities of VLMs and their capacity to solve open-ended problems, without relying on manually predefined processing logic or being limited to specific tasks. Experimental results demonstrate that PhysAgent improves GPT-4o's zero-shot performance on PhysBench by 18.4%. Furthermore, we investigate how physical world understanding helps the deployment of embodied agents through extensive robotic manipulation experiments on MOKA (Liu et al., 2024a). Specifically, we employ two approaches: fine-tuning the VLM with PhysBench and utilizing PhysAgent for zero-shot inference across five representative manipulation tasks. The improvement in those tasks further validates that PhysBench and PhysAgent can facilitate the deployment of embodied agents like MOKA.

We hope this work offers valuable insights and contributes to bridging the gap between VLMs and physical world understanding, ultimately advancing embodied AI toward human-level capabilities. In summary, this paper has two technical contributions: (1) We present PhysBench, a large-scale benchmark for evaluating the performances of vision-language models in physical world understanding. We identify the key challenges through extensive studies and provide insights into why the existing VLMs have insufficient physical world understanding capabilities. (2) We propose PhysAgent, a unified approach that improves VLMs' physical world understanding abilities. Through extensive experiments, we demonstrate that enhancing VLMs' comprehension of physical environments can significantly facilitate the deployment of embodied agents.

2 RELATED WORK

Physical Comprehension Datasets. Early benchmarks (Riochet et al., 2018; Rajani et al., 2020) were developed primarily for vision-only models, while more recent efforts (Yi et al., 2019; Chen et al., 2022; Wang et al., 2024g) have predominantly focused on simple visual primitives, such as spheres, cubes, and rigid object collision events, often restricted to a limited set of simulated scenarios (Zheng et al., 2024b; Tung et al., 2023). We summarize the key features of these various benchmarks and compare them against our benchmark in Table 1. However, existing VQA datasets assessing physical knowledge (Lu et al., 2022; He et al., 2024) mainly focus on commonsense reasoning rather than physical world perception. Spatial VQA benchmarks (Chen et al., 2024a; Lyu et al., 2024; Bonnen et al., 2024; Wang et al., 2024d) emphasize geometric relationships in 3D sence, which represent only a part of the physical. In contrast, PhysBench is the first comprehensive dataset designed to evaluate models' understanding of the physical world, encompassing a wide variety of scenarios and tasks not covered by previous benchmarks.

Physical Reasoning Models. Models for understanding the physical world generally fall into two categories. The first comprises physics-specialized models (Guen & Thome, 2020; Duan et al., 2022), which are typically limited to predicting the next state and are not applicable to other tasks. The second includes physical oracle models (Zheng et al., 2024b; Tung et al., 2023), which are suitable for only a narrow range of tasks due to their reliance on predefined rules. These models often require training additional modules like R-CNN, and their probabilistic outputs restrict them to classification tasks, limiting their ability to handle open-ended questions. In contrast, PhysAgent offers greater flexibility and adaptability across a broader spectrum of problems without these limitations.

Vision-Language Models. Vision-Language Models (VLMs) are large-scale models that integrate visual modalities with language understanding (Wu et al., 2023b; Zhan et al., 2024; Dai et al., 2024). In recent years, there has been a surge of work leveraging VLMs as agents for embodied AI (Liu et al., 2024a; Nasiriany et al., 2024). Although these approaches are generalizable, they face challenges due to weak physical world understanding capabilities (Liu et al., 2024a; Guo et al., 2024). By employing PhysBench and PhysAgent, these shortcomings can be mitigated, enhancing the physical world understanding capabilities of VLMs and enabling more reliable robotic control. Additionally, spatial VLMs (Bonnen et al., 2024) have identified that most VLMs lack 3D spatial reasoning capabilities due to insufficient data. However, since spatial reasoning represents only a subset of physical world understanding, our work aims to provide a more comprehensive evaluation and improvement of VLMs' physical world understanding abilities. For additional related work, see Appendix G.

Table 1: A comparison between PhysBench and other physical understanding question-answering benchmarks. PhysBench is a comprehensive dataset, covering a wide range of tasks related to physical world understanding.

	Property	Attribute	Location	Motion	Temperature	Viewpoint	Light	Collision	Manipulation	Fluid	Interleaved	Size	More than cube
CLEVRER (Yi et al., 2019)	1	×	×	×	×	×	×	1	×	×	×	300,000	×
Cater (Girdhar & Ramanan, 2019)	1	×	×	X	×	×	×	1	×	×	×	5,500	×
CRIPP-VQA (Patel et al., 2022)	1	×	×	X	×	×	×	1	×	×	×	5,000	×
ComPhy (Chen et al., 2022)	1	×	×	X	×	×	×	1	×	×	×	99,844	×
EmbSpatial (Du et al., 2024)	×	×	1	X	×	×	×	×	×	×	×	3,600	1
Physion (Bear et al., 2021)	1	×	×	X	×	×	×	1	1	×	×	17,200	1
Physion++ (Tung et al., 2023)	1	1	×	X	×	×	×	1	×	×	×	2,000	1
ContPhy (Zheng et al., 2024b)	1	×	×	X	×	×	×	1	×	1	×	6,500	1
SuperCLEVR (Wang et al., 2024g)	1	×	×	1	×	×	×	1	×	×	×	1,200	×
PhysBench	1	1	1	1	1	1	1	1	1	~	1	10,002	1

3 PHYSBENCH

To assess VLMs' physical world understanding ability, we first define the concept of physical world understanding and introduce PhysBench in Section 3.1. Next, we provide a detailed description of the data collection process in Section 3.2. Utilizing PhysBench, we conduct experiments to determine whether VLMs can effectively comprehend the physical world in Section 3.3. Finally, in Section 3.4, we discuss the potential reasons for poor performance.

3.1 OVERVIEW OF PHYSBENCH

Understanding the physical world is essential yet fundamentally challenging for embodied AI, as systems must perceive, interpret, and predict the properties and dynamics of objects and environments. This involves comprehending object properties and relationships, interpreting environmental scenes, and anticipating interaction outcomes based on visual cues and core physical principles to ensure safe and effective operation.



Figure 2: Sampled PhysBench examples from four major dimensions mentioned in Section 3.1. Due to space constraints, we present only the correct answers (as each question in our dataset is a fouroption multiple-choice with one correct answer) and defer additional examples to Appendix C.

However, existing datasets often focus solely on image content and commonsense reasoning, neglecting the four fundamental aspects of the physical world mentioned above. To address this gap, we propose PhysBench, which comprehensively evaluates VLMs' perception of the physical world across four major task categories of the physical world: (1) Physical Object Property: Assessment of physical attributes of objects such as mass, size, density, tension, friction, bending stiffness, elasticity, and plasticity. (2) Physical Object Relationships: Evaluation of spatial relationships involving objects' relative or absolute positions and motions. (3) Physical Scene Understanding: Interpretation of environmental factors, including light sources, viewpoints, temperature, etc. (4) Physics-based Dynamics: Understanding of physical events like collisions, throwing, fluid dynamics, explosions, and other phenomena. Each category corresponds to specific sub-task types and ability types, whose distributions are shown in Figures 3. Detailed examples of specific tasks are illustrated in Figure 2, with additional examples provided in Appendix H. A comprehensive description of sub-task types and ability types is available in Appendix C.

PhysBench is structured as a multiple-choice questionnaire, presenting four options for each question, with only one correct answer. The primary statistics of PhysBench are presented in Table 2 and detailed in Appendix D. Recognizing that different types of tasks possess unique characteristics, we utilize videos and multiple images to effectively convey features that are difficult to capture in a single image—such as elasticity, mass, density, and environmental factors like temperature, humidity, light source, and viewpoint. The dataset also includes objects with similar initial states but differing properties, leading to different future outcomes. This enriches the dataset and allows for a wider range of observable physical behaviors. Consequently, PhysBench draws its data from the internet, real-world captures, and simulations, making it a mixed-format benchmark that integrates text, images, and videos. For convenience, PhysBench-test consists of 10,002 entries, organized into 19 subclasses, as the test set, and 200 entries as the validation set for parameter choosing. We also present 89,998 entries for further research. **The experimental results presented in this paper, unless otherwise specified, are based on the test set**. The performance of VLMs on PhysBench-val can be found in Appendix F.4. Benchmark release details can be found in Appendix B.8.



Table 2: Key statistics.

Figure 3: Subtype distribution and ability distribution

3.2 DATASET COLLECTION PROCESS

To ensure data quality, all questions were manually annotated by graduate students in STEM fields and further refined through a rigorous review process after collecting and clipping the raw images or videos. To maintain consistency in annotations, we implemented multiple rounds of cleaning and validation throughout the following steps. We have preserved intermediate outputs from the annotation process, such as depth and reflectance maps for simulator-generated data and human-annotated physical principles for many web-sourced videos. The process involves the following sequential steps: (a) Video Collection. Videos and images are gathered from web searches, simulations, and real-world captures. The collection process uses predefined simulation rules, LLM-guided queries, and other strategies to find related images or videos (see Appendix A). Human annotators further refine the data by clipping and annotating physical principles in the images or videos. (b) Video *Captioning.* Human-annotated raw videos are processed through automatic filtering, followed by GPT-40 annotations that generate captions with human check. (c) Questions Design. For videos annotated with physical principles, we generate physics-related questions using both manual design and GPT-40, following predefined rules. An automated filter and manual review processes eliminate irrelevant questions. (d) File Organization. The remaining valid questions are categorized by task, sub-task, and ability type by human experts. (e) Quality Check. The organized dataset undergoes a human review to ensure that the questions are physical world relevant, rely on all input information, are not grounded in common sense, and are accurately categorized with clear questions and corresponding answers. Due to space limitations, the collection guidelines are provided in Appendix B.

3.3 CAN VLMs UNDERSTAND THE PHYSICAL WORLD

To assess whether VLMs can understand the physical world, we evaluated 75 representative VLMs on PhysBench and found that a significant performance gap remains between VLMs and human-level understanding. The primary results are presented in Table 3, while detailed analyses of sub-task performance and ability types across the four task categories are provided in Appendix F.3.

Setup. Our evaluation was conducted under three configurations: (a) *Image VLMs*, which support only single-image input (e.g., LLaVA-1.5 and BLIP-2); (b) *Video VLMs*, designed for video comprehension (e.g., Chat-UniVi and PLLaVA); and (c) *General VLMs*, which support multiple images and interleaved inputs (e.g., VILA-1.5 and GPT-40). It is important to note that the data used for evaluating setups (a) and (b) is a subset of PhysBench test subset with interleaved QA pairs removed, whereas setup (c) was evaluated on the full dataset. For most models, we followed the standard protocol outlined in VLMEvalKit Contributors (2023), setting the temperature to 0. For models that do not support multiple images as input, we employed two methods: the *merge* method, where video frames are concatenated into a single image (Fu et al., 2024; Zhang et al., 2024a; Jiang et al., 2024), and the *seq* method, where video frames are input sequentially as individual images. Notably, only models using the *seq* setup can handle interleaved text-image sequences. For details on VLM prompts and hyperparameters, see Appendix E.

VLMs exhibit a limited understanding of the physical world. Our evaluation indicates that most models achieve an average accuracy of approximately 40%, which is significantly below human-level performance. Even the best-performing model, GPT-40, attains only 49.49% accuracy, underscoring the substantial gap between current VLMs and true comprehension of the physical world.

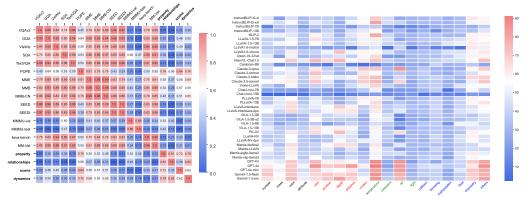


Figure 4: (a) Correlation map between 4 tasks in PhysBench and 15 other vision-language benchmarks. (b) The visualization of model performance across 19 sub-tasks is presented, where different colors represent the respective categories. The four colors, from left to right, represent physical object property, physical object relationships, physical scene, and physical-based dynamics.

	Size	Format	Property	✓Relationships	♣ Scene		Avg
Random Choice	-	-	25.00	25.00	25.00	25.00	25.00
Human	-	-	97.10	95.67	94.91	95.68	95.87
		Image V	/LM				
InstructBLIP-t5-xl (Dai et al., 2024)	4B	merge	35.35	36.67	37.45	35.95	36.24
InstructBLIP-t5-xxl (Dai et al., 2024)	12B	merge	41.11	38.47	37.89	36.42	38.51
InstructBLIP-7B (Dai et al., 2024)	7B	merge	21.94	29.00	19.53	27.45	23.82
InstructBLIP-13B (Dai et al., 2024)	13B	merge	31.69	33.19	23.13	30.64	29.94
BLIP-2 (Li et al., 2023c)	12B	merge	41.70	40.83	36.25	36.93	38.61
LLaVA-1.5-7B (Liu et al., 2023a)	7B	merge	38.44	41.53	38.60	42.69	40.09
LLaVA-1.5-13B (Liu et al., 2023a)	13B	merge	41.31	42.50	34.40	44.38	40.45
LLaVA1.6-mistral (Liu et al., 2024b)	7B	merge	29.77	22.22	8.54	20.58	20.30
LLaVA1.6-vicuna (Liu et al., 2024b)	7B	merge	40.26	59.72	38.60	42.65	42.28
Qwen-VL-Chat (Bai et al., 2023b)	9B	merge	35.97	43.33	26.47	41.27	35.63
InternVL-Chat1.5 (Chen et al., 2024c)	26B	merge	53.08	70.14	37.01	44.78	47.51 😈
Cambrian-8B (Tong et al., 2024)	8B	merge	23.27	17.92	23.02	29.29	24.61
Claude-3-opus (Anthropic, 2024)		merge	41.97	40.97	- 30.63 -	36.50	37.00
Claude-3-sonnet (Anthropic, 2024)	-	merge	37.86	40.00	32.23	36.89	36.18
Claude-3-haiku (Anthropic, 2024)	-	merge	43.28	53.33	30.06	39.93	39.44
Claude-3.5-sonnet (Anthropic, 2024)	-	merge	46.46	41.11	27.89	37.60	38.05
		Video V	/LM				
Video-LLaVA (Lin et al., 2023a)	7B	seq	36.82	36.11	33.69	40.52	37.04
Chat-Univi-7B (Jin et al., 2023)	7B	seq	19.28	20.97	18.86	28.46	22.19
Chat-Univi-13B (Jin et al., 2023)	13B	seq	4.30	11.53	15.67	11.47	10.36
PLLaVA-7B (Xu et al., 2024)	7B	seq	38.02	35.83	36.34	39.89	37.94😈
PLLaVA-13B (Xu et al., 2024)	13B	seq	39.91	38.33	31.52	40.76	37.70
			nterleaved d				
LLaVA-interleave (Li et al., 2024d)	7B	seq	47.23	44.62	35.64	37.21	41.00
LLaVA-interleave-dpo (Li et al., 2024d)	7B	seq	47.97	42.67	33.73	38.78	40.83
VILA-1.5-3B (Lin et al., 2023b)	3B	seq	32.40	33.02	34.84	35.78	34.11
VILA-1.5-3B-s2 (Lin et al., 2023b)	3B	seq	33.14	30.26	35.72	33.00	33.07
VILA-1.5-8B (Lin et al., 2023b)	8B	seq	33.41	29.88	30.85	35.91	32.85
VILA-1.5-13B (Lin et al., 2023b)	13B	seq	40.53	40.15	31.96	36.07	37.15
Phi-3V (Abdin et al., 2024)	4B	seq	43.67	37.92	34.93	36.92	38.42
LLaVA-NV (Zhang et al., 2024b)	7B	seq	38.33	30.83	34.00	37.17	35.42
LLaVA-NV-dpo (Zhang et al., 2024b)	7B	seq	38.83	44.31	33.86	37.21	37.43
Mantis-Idefics2 (Jiang et al., 2024)	8B	seq	41.97	41.44	29.53	36.56	37.39
Mantis-LLaVA (Jiang et al., 2024)	7B	seq	44.48	30.45	36.25	34.73	36.69
Mantis-siglip-llama3 (Jiang et al., 2024)		seq	42.47	32.78	36.83	37.51	37.64
Mantis-clip-llama3 (Jiang et al., 2024)	8B	seq	40.61	35.11	32.45	38.36	36.92
$\overline{\text{GPT-4V}}$ (Achiam et al., 2023)		seq	- 49.59	45.77	- 26.34 -	- 42.15	41.26
GPT-40 (Achiam et al., 2023)	-	seq	56.91	64.80	30.15	46.99	49.49🖲
GPT-4o-mini (Achiam et al., 2023)	-	seq	53.54	44.24	30.59	42.90	43.15
Gemini-1.5-flash (Team et al., 2023)	-	seq	57.41	52.24	34.32	40.93	46.07
Gemini-1.5-pro (Team et al., 2023)	-	seq	57.26	63.61	36.52	41.56	49.11

Table 3: Evaluation results for 39 VLMs. The evaluation of General VLMs is based on the data from Video and Image VLM evaluations, with the addition of interleaved data. "Seq" refers to sequential input of frames of videos, while "merge" refers to merging video frames into a single image. Bold indicates the best result, and <u>underline</u> indicates the second best in each group.

As shown in Figure 4(b), considerable room for improvement remains, particularly in tasks related to physical scene understanding and physics-based dynamics.

Closed-source models generally perform better. As shown in Figure 5(b), the GPT series and Gemini-1.5 models significantly outperform open-source models. Notably, GPT-4 surpasses the best open-source model, LLaVA-interleave, by 20.7%, indicating a substantial gap between open-source and closed-source models. However, we did not observe a clear advantage with Claude, a finding that aligns with results from other benchmarks (Cao et al., 2024; Wu et al., 2024c).

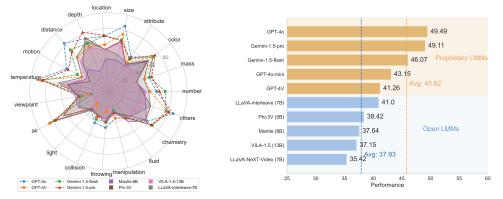


Figure 5: (a) The performance of 8 representative open-source General VLMs across 19 sub-tasks in PhysBench, which support interleaved inputs. The closer it is to the circular boundary, the better. (b) The overall performance of those 8 VLMs. Closed-source models generally perform better.

3.4 WHY DO VLMs STRUGGLE WITH PHYSICAL WORLD UNDERSTANDING

To further investigate why VLMs struggle with physical world understanding, we analyzed Phys-Bench and discovered that it differs significantly from common VQA tasks. Additionally, we found that the performance of larger model size or more training data does not result in clear improvements on PhysBench, which may be *due to a lack of physical world knowledge in the training data*. Furthermore, we found that many errors stem from this deficiency; when we augmented the models with physical world knowledge, their performance improved. This further suggests that the gap between VLMs and physical world understanding may be attributed to limitations in the training data.

Physical world understanding differs significantly from common VQA tasks. To assess the relationships between our tasks and other VLM benchmarks, we adopted the methodology proposed by (Tong et al., 2024; Fang et al., 2024) to construct a correlation map, as shown in Figure 4(a). Details on the construction of the correlation map are provided in Appendix F.6. Our analysis reveals that PhysBench differs significantly from traditional VLM benchmarks, exhibiting closer alignment with POPE (Li et al., 2023h) in tasks such as hallucination detection, while also showing that performance does not consistently improve with increased data or model scale.

VLMs's physical world understanding ability does not scale with model size, data, or frames. (1) Model Size Scalability. Figure 6(a) shows that increasing model size using the same dataset significantly enhances performance on common QA tasks. However, this improvement does not extend to PhysBench, where gains are limited or even negative. For instance, while VILA-1.5's performance improves by 7.1% on common QA tasks when scaling from 3B to 7B parameters, it

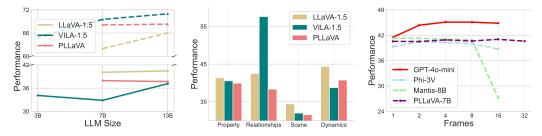


Figure 6: (a) Model size scalability. The solid line shows the average performance across 14 common QA tasks (Table 23), while the dashed line represents PhysBench results. (b) Data scalability. VILA and PLLaVA expand upon LLaVA's architecture by utilizing more data. (c) Frame scalability.

decreases by 3.8% on PhysBench. (2) Data Scalability. As shown in Figure 6(b), scaling up the dataset offers limited benefits for physical comprehension. PLLaVA and VILA-1.5, larger-data variants of LLaVA-1.5, exhibit minimal improvement or even a decline in performance on PhysBench compared to LLaVA-1.5. Analysis of the additional data (Appendix D.2) reveals it is predominantly descriptive, focusing on content description rather than enhancing physical understanding. Nevertheless, VILA-1.5's spatial reasoning abilities have significantly improved, aligning with trends observed in other benchmarks (Yu et al., 2023b; Li et al., 2023a). (3) Frame Scalability. Figure 6(c) indicates that the three open-source models are insensitive to the number of frames, performing similarly to single-frame inputs, with performance sometimes decreasing as frames increase. This suggests that current models cannot effectively utilize multi-frame information. Notably, increasing the number of frames led Mantis to frequently fail to follow instructions or refuse to answer, and expanding beyond eight frames did not yield further improvements.

Perceptual and knowledge gaps constitute the majority of errors. To investigate the poor performance of VLMs on PhysBench, we randomly selected 500 questions and obtained explanations from three models—GPT-40, Phi-3V, and Gemini-1.5-flash. Expert annotators classified the root causes of the mispredictions into six categories: perception errors, reasoning errors, lack of knowledge, refusal to answer, failure to follow instructions, and annotation errors in the dataset. The distribution of these error types is shown in Figure 7, with selected cases and detailed analyses provided in Appendix I. The error distribution reveals that perceptual errors account for 37%, 40%, and 45% of the mistakes made by GPT-40, Gemini-1.5-flash, and Phi-3V, respectively, while lack of knowledge constitutes 34%, 35%, and 23% of errors for these models. This analysis suggests that perceptual errors and knowledge gaps are the primary sources of mispredictions, indicating that while the models are adept at extracting information from text and visual inputs, their physical world understanding and complex reasoning abilities remain limited.

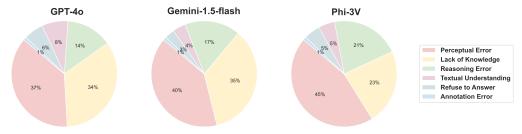


Figure 7: Distribution of error types for GPT-4V, Gemini-1.5-flash, Phi-3V.

Can VLMs transfer physical world knowledge? Our error analysis revealed that inadequate physical world knowledge and reasoning capabilities were key contributors to the models' poor performance. To investigate whether introducing additional examples could enhance performance, we conducted tests on 200 entries of PhysBench, pairing each with a similar example. These additional examples were incorporated through fine-tuning or in-context learning. As shown in Figure 9(b), the performance improvements after adding physical world knowledge examples indicate that VLMs can transfer physical knowledge to some extent. This suggests that the original data's lack of physical world knowledge was a significant factor in the models' suboptimal performance.

4 PHYSAGENT

Recognizing perceptual inaccuracies and knowledge gaps as key sources of error shown in Section 3.4, we introduce PhysAgent in Section 4.1 to improve VLMs' understanding of the physical world by integrating vision foundation models for enhanced perception and incorporating physical knowledge memory. To verify whether enhancing VLMs' physical understanding facilitates the deployment of embodied agents, we conducted five embodied agent tasks as detailed in Section 4.2.

4.1 HOW TO ENHANCE VLMs FOR PHYSICAL WORLD UNDERSTANDING

We propose PhysAgent, a novel framework that integrates knowledge memory and vision foundation models to enhance physical world understanding in VLMs. This framework is inspired by our findings in Section 3.4, where we identified perceptual errors and insufficient knowledge as the primary causes of mistakes in VLMs. To address these shortcomings, we establish a *knowledge memory* that provides prior physical world knowledge and rules. Additionally, we utilize vision *foundational models* namely Depth Anything (Yang et al., 2024b), SAM (Kirillov et al., 2023), and GroundingDINO (Liu et al., 2023b) to achieve enhanced visual perception. These models enable us to identify object types and spatial locations, and further acquire information about objects' dynamics through VLM reasoning or retrieval from memory. They also help solve problems that VLMs cannot address, such as estimating depth and numerical distances. Unlike prior physical reasoning models that are confined to specific tasks and struggle to adapt to natural language queries, our method aims to fully leverage the reasoning and generalization capabilities of VLMs. Experiments on PhyBench show that PhysAgent improves performance by 18.4% on GPT-40.

As illustrated in Figure 8, given a question, PhysAgent follows three key steps: (1) *Task-specific Prompt Activation*: PhysAgent first classifies the question (manually or automatically) and activates task-specific prompts, incorporating relevant physical knowledge for different tasks. For instance, for a question about light, it retrieves knowledge on the relationship between light source movement and shadow direction to assist the VLMs. (2) *Foundation Models Integration*: PhysAgent processes the foundation model's outputs, leveraging VLM reasoning capabilities. For example, it identifies objects in the scene using GroundingDINO and retrieves relevant attributes from the knowledge memory. (3) *Chain-of-Thoughts Reasoning*: PhysAgent then engages in chain-of-thought reasoning, conducting a self-verification step to ensure logical consistency before providing the final answer.

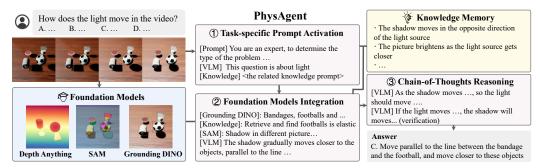


Figure 8: Architecture of PhysAgent. PhysAgent employs a three-step reasoning process to address the problem: activating task-specific prompts, integrating foundation models, and reasoning.

Baselines. We utilized three prompt methods: Chain of Thought (CoT) (Kojima et al., 2023), Desp-CoT (Wu et al., 2023d), and Pure Language Reasoning (PLR), in addition to an oracle method, ContPhy (Zheng et al., 2024b), which served as our baseline. Detailed descriptions of the prompt strategies and the implementation of ContPhy are provided in Appendix E.6 and Appendix E.7.

Results. The results in Figure 9(a), lead to the following conclusions: (1) Prompting methods are unstable, and using pure language yields catastrophic results. As observed, the CoT strategy has minimal impact, while both Desp-CoT and PLR show a decline in performance. This suggests that descriptive prompts are not particularly effective for addressing the questions, implying that our dataset requires a deeper understanding of the videos or images to answer accurately. (2) ContPhy even worsens performance. In three out of four tasks, ContPhy underperforms compared to its base model, GPT-40, due to suboptimal module invocation and limited flexibility in its logical templates, which struggle to adapt to diverse scenarios. Additionally, ContPhy relies on models like RCNN to process visual information instead of directly leveraging GPT-40, leading to potential information loss and subsequent performance degradation. (3) PhysAgent consistently improves zero-shot performance, notably achieving a 49.5% improvement for GPT-40 in Scene. Compared to the CoT, Desp-CoT, and PLR prompting strategies, our method demonstrates consistent improvements.

4.2 CAN PHYSICAL WORLD UNDERSTANDING HELP IN EMBODIED APPLICATIONS

Despite gaining significant attention in recent years for their strong generalization capabilities, VLMs as embodied agents (Liu et al., 2024a) still exhibit fundamental operational errors during physical world interactions. In this section, we investigate whether enhancing the physical world perception abilities of VLMs can improve their performance in downstream embodied agent tasks.

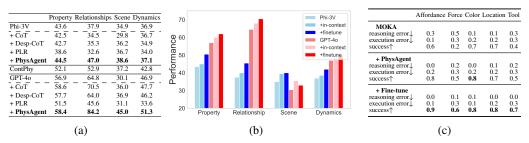


Figure 9: (a) Performance comparison of various methods. (b) Analysis of physical world knowledge transfer. (c) Performance evaluation across five embodied tasks as described in Figure 10.

To evaluate embodied agents, we designed five fundamental manipulation tasks as shown in Figure 10(a). The specifics of these tasks, along with the corresponding testing methods and language instructions, can be found in Appendix F.5. These tasks require the agents to possess a basic understanding of spatial relations and the physical properties of objects. Specifically, we utilized MuJoCo (Todorov et al., 2012) and the 7-DoF Franka Emika robotic arm from Menagerie (Zakka et al., 2022), building our simulation platform based on MOKA (Liu et al., 2024a) as the embodied agent approach to test these embodied tasks. The VLM we used in these tasks is GPT-40.

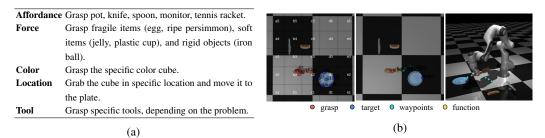


Figure 10: (a) Description of each of the testing tasks. (b) Marked observation, predicted affordances, and motion in MOKA. MOKA leverages a VLM to generate key points and waypoints, and then converts these affordance representations into executable motions for the robotic arm.

As illustrated in Figure 10(b), MOKA prompts the VLM to generate key points and additional attributes for affordance representation based on free-form language instructions and visual observations of the environment. Since the five tasks we tested were relatively basic and did not require decomposition into subtasks, we could directly invoke the VLM in a question-answering format to address the operational challenges. This approach ensures seamless compatibility between the pipelines of PhysAgent and MOKA. Once the key points and waypoints were obtained from the VLM, MOKA converted these affordance representations into executable motions for the robotic arm. To evaluate the impact of enhanced physical-world understanding on embodied tasks, we applied two methods to MOKA's VLM: (1) fine-tuning it with PhysBench, and (2) employing PhysAgent to zero-shot assist in reasoning about affordance representations.

As shown in Figure 9(c), we observe consistent improvements after fine-tuning with a subset of PhysBench, indicating that the benchmark's data is of high quality and suitable for use as demonstration data in open-world robotics tasks. Additionally, PhysAgent consistently yields stable zero-shot gains across all five tasks, with significant progress observed in the force task in Figure 10(a).

5 CONCLUSION

In conclusion, we introduce PhysBench, a benchmark designed to assess Vision-Language Models' understanding of the physical world. Through experiments on 75 models, we identified significant gaps in physical world understanding, particularly in open-source models, due to inadequate training data. To address this, we developed PhysAgent, a novel framework that improves physical reasoning by 18.4% on GPT-40. Additionally, we demonstrated the utility of our dataset and approach in robotic tasks, helping to advance the understanding of the physical world in machine intelligence.

Statement. We provide a detailed discussion of limitations, broader impacts, ethical considerations, and reproducibility in Appendix J.

ACKNOWLEDGMENTS

Jiageng Mao and Yue Wang acknowledge funding supports from Toyota Research Institute, Dolby, and Google DeepMind. Yue Wang is also supported by a Powell Faculty Research Award.

REFERENCES

- Marah Abdin, Sam Ade Jacobs, Ammar Ahmad Awan, Jyoti Aneja, Ahmed Awadallah, Hany Awadalla, Nguyen Bach, Amit Bahree, Arash Bakhtiari, Harkirat Behl, et al. Phi-3 technical report: A highly capable language model locally on your phone. *arXiv*, 2024.
- Josh Achiam, Steven Adler, Sandhini Agarwal, Lama Ahmad, Ilge Akkaya, Florencia Leoni Aleman, Diogo Almeida, Janko Altenschmidt, Sam Altman, Shyamal Anadkat, et al. Gpt-4 technical report. arXiv, 2023.
- 01. AI, :, Alex Young, Bei Chen, Chao Li, Chengen Huang, Ge Zhang, Guanwei Zhang, Heng Li, Jiangcheng Zhu, Jianqun Chen, Jing Chang, Kaidong Yu, Peng Liu, Qiang Liu, Shawn Yue, Senbin Yang, Shiming Yang, Tao Yu, Wen Xie, Wenhao Huang, Xiaohui Hu, Xiaoyi Ren, Xinyao Niu, Pengcheng Nie, Yuchi Xu, Yudong Liu, Yue Wang, Yuxuan Cai, Zhenyu Gu, Zhiyuan Liu, and Zonghong Dai. Yi: Open foundation models by 01.ai, 2024.
- Jean-Baptiste Alayrac, Jeff Donahue, Pauline Luc, Antoine Miech, Iain Barr, Yana Hasson, Karel Lenc, Arthur Mensch, Katherine Millican, Malcolm Reynolds, et al. Flamingo: a visual language model for few-shot learning. Advances in neural information processing systems, 35:23716– 23736, 2022.
- Zahid Ali, Chesser Luke, and Carbone Timothy. Unsplash, 2023.
- Anthropic. About claude models. https://docs.anthropic.com/en/docs/ about-claude/models, 2024. Accessed: 2024-09-03.
- Daman Arora, Himanshu Gaurav Singh, and Mausam. Have llms advanced enough? a challenging problem solving benchmark for large language models, 2023.
- Tayfun Ates, M Samil Atesoglu, Cagatay Yigit, Ilker Kesen, Mert Kobas, Erkut Erdem, Aykut Erdem, Tilbe Goksun, and Deniz Yuret. Craft: A benchmark for causal reasoning about forces and interactions. *arXiv*, 2020.
- AzureML. Phi-3.5-vision instruct (128k). https://github.com/marketplace/models/ azureml/Phi-3-5-vision-instruct, 2024. Architecture: Phi-3.5-vision has 4.2B parameters with image encoder, connector, projector, and Phi-3 Mini language model. Inputs: Text and Image (best suited for chat format). Context length: 128K tokens. GPUs: 256 A100-80G. Training time: 6 days. Training data: 500B tokens (vision + text tokens). Outputs: Generated text. Trained between July and August 2024. License: MIT. Release date: August 20, 2024. Status: Static model with offline text dataset cutoff on March 15, 2024.
- Jinbin Bai, Chunhui Liu, Feiyue Ni, Haofan Wang, Mengying Hu, Xiaofeng Guo, and Lele Cheng. Lat: latent translation with cycle-consistency for video-text retrieval. *arXiv*, 2022.
- Jinbin Bai, Wei Chow, Ling Yang, Xiangtai Li, Juncheng Li, Hanwang Zhang, and Shuicheng Yan. Humanedit: A high-quality human-rewarded dataset for instruction-based image editing. *arXiv*, 2024a.
- Jinbin Bai, Tian Ye, Wei Chow, Enxin Song, Qing-Guo Chen, Xiangtai Li, Zhen Dong, Lei Zhu, and Shuicheng Yan. Meissonic: Revitalizing masked generative transformers for efficient high-resolution text-to-image synthesis. *arXiv*, 2024b.
- Jinze Bai, Shuai Bai, Yunfei Chu, Zeyu Cui, Kai Dang, Xiaodong Deng, Yang Fan, Wenbin Ge, Yu Han, Fei Huang, Binyuan Hui, Luo Ji, Mei Li, Junyang Lin, Runji Lin, Dayiheng Liu, Gao Liu, Chengqiang Lu, Keming Lu, Jianxin Ma, Rui Men, Xingzhang Ren, Xuancheng Ren, Chuanqi Tan, Sinan Tan, Jianhong Tu, Peng Wang, Shijie Wang, Wei Wang, Shengguang Wu, Benfeng Xu, Jin Xu, An Yang, Hao Yang, Jian Yang, Shusheng Yang, Yang Yao, Bowen Yu, Hongyi Yuan,

Zheng Yuan, Jianwei Zhang, Xingxuan Zhang, Yichang Zhang, Zhenru Zhang, Chang Zhou, Jingren Zhou, Xiaohuan Zhou, and Tianhang Zhu. Qwen technical report. *arXiv*, 2023a.

- Jinze Bai, Shuai Bai, Shusheng Yang, Shijie Wang, Sinan Tan, Peng Wang, Junyang Lin, Chang Zhou, and Jingren Zhou. Qwen-vl: A frontier large vision-language model with versatile abilities. *arXiv*, 2023b.
- Max Bain, Arsha Nagrani, Gül Varol, and Andrew Zisserman. Frozen in time: A joint video and image encoder for end-to-end retrieval. In *Proceedings of the IEEE/CVF International Conference on Computer Vision*, pp. 1728–1738, 2021.
- Hritik Bansal, Zongyu Lin, Tianyi Xie, Zeshun Zong, Michal Yarom, Yonatan Bitton, Chenfanfu Jiang, Yizhou Sun, Kai-Wei Chang, and Aditya Grover. Videophy: Evaluating physical commonsense for video generation. arXiv, 2024.
- Fabien Baradel, Natalia Neverova, Julien Mille, Greg Mori, and Christian Wolf. Cophy: Counterfactual learning of physical dynamics. *arXiv*, 2019.
- Daniel M Bear, Elias Wang, Damian Mrowca, Felix J Binder, Hsiao-Yu Fish Tung, RT Pramod, Cameron Holdaway, Sirui Tao, Kevin Smith, Fan-Yun Sun, et al. Physion: Evaluating physical prediction from vision in humans and machines. *arXiv*, 2021.
- Ali Furkan Biten, Ruben Tito, Andres Mafla, Lluis Gomez, Marçal Rusinol, Ernest Valveny, CV Jawahar, and Dimosthenis Karatzas. Scene text visual question answering. In *Proceedings of* the IEEE/CVF international conference on computer vision, pp. 4291–4301, 2019.
- OC Blender. Blender—a 3d modelling and rendering package. *Retrieved. represents the sequence of Constructs1 to*, 4, 2018.
- Tyler Bonnen, Stephanie Fu, Yutong Bai, Thomas O'Connell, Yoni Friedman, Nancy Kanwisher, Joshua B Tenenbaum, and Alexei A Efros. Evaluating multiview object consistency in humans and image models. *arXiv*, 2024.
- Minwoo Byeon, Beomhee Park, Haecheon Kim, Sungjun Lee, Woonhyuk Baek, and Saehoon Kim. Coyo-700m: Image-text pair dataset, 2022.
- Holger Caesar, Varun Bankiti, Alex H. Lang, Sourabh Vora, Venice Erin Liong, Qiang Xu, Anush Krishnan, Yu Pan, Giancarlo Baldan, and Oscar Beijbom. nuscenes: A multimodal dataset for autonomous driving. *arXiv*, 2019.
- Xu Cao, Bolin Lai, Wenqian Ye, Yunsheng Ma, Joerg Heintz, Jintai Chen, Jianguo Cao, and James M Rehg. What is the visual cognition gap between humans and multimodal llms? *arXiv*, 2024.
- Susan Carey. The origin of concepts. Journal of Cognition and Development, 1(1):37-41, 2000.
- Keshigeyan Chandrasegaran, Agrim Gupta, Lea M. Hadzic, Taran Kota, Jimming He, Cristobal Eyzaguirre, Zane Durante, Manling Li, Jiajun Wu, and Fei-Fei Li. Hourvideo: 1-hour videolanguage understanding. In *Advances in Neural Information Processing Systems*, volume 37, 2024.
- Angel Chang, Angela Dai, Thomas Funkhouser, Maciej Halber, Matthias Niessner, Manolis Savva, Shuran Song, Andy Zeng, and Yinda Zhang. Matterport3d: Learning from rgb-d data in indoor environments. arXiv, 2017.
- Boyuan Chen, Zhuo Xu, Sean Kirmani, Brain Ichter, Dorsa Sadigh, Leonidas Guibas, and Fei Xia. Spatialvlm: Endowing vision-language models with spatial reasoning capabilities. In *Proceedings* of the IEEE/CVF Conference on Computer Vision and Pattern Recognition, pp. 14455–14465, June 2024a.
- Lin Chen, Jisong Li, Xiaoyi Dong, Pan Zhang, Conghui He, Jiaqi Wang, Feng Zhao, and Dahua Lin. Sharegpt4v: Improving large multi-modal models with better captions. *arXiv*, 2023a.
- Qiguang Chen, Libo Qin, Jin Zhang, Zhi Chen, Xiao Xu, and Wanxiang Che. M³cot: A novel benchmark for multi-domain multi-step multi-modal chain-of-thought, 2024b. URL https://arxiv.org/abs/2405.16473.

- Xi Chen, Xiao Wang, Lucas Beyer, Alexander Kolesnikov, Jialin Wu, Paul Voigtlaender, Basil Mustafa, Sebastian Goodman, Ibrahim Alabdulmohsin, Piotr Padlewski, Daniel Salz, Xi Xiong, Daniel Vlasic, Filip Pavetic, Keran Rong, Tianli Yu, Daniel Keysers, Xiaohua Zhai, and Radu Soricut. Pali-3 vision language models: Smaller, faster, stronger, 2023b. URL https: //arxiv.org/abs/2310.09199.
- Zhe Chen, Jiannan Wu, Wenhai Wang, Weijie Su, Guo Chen, Sen Xing, Muyan Zhong, Qinglong Zhang, Xizhou Zhu, Lewei Lu, Bin Li, Ping Luo, Tong Lu, Yu Qiao, and Jifeng Dai. Internvl: Scaling up vision foundation models and aligning for generic visual-linguistic tasks. *arXiv*, 2023c.
- Zhe Chen, Weiyun Wang, Hao Tian, Shenglong Ye, Zhangwei Gao, Erfei Cui, Wenwen Tong, Kongzhi Hu, Jiapeng Luo, Zheng Ma, et al. How far are we to gpt-4v? closing the gap to commercial multimodal models with open-source suites. *arXiv*, 2024c.
- Zhenfang Chen, Kexin Yi, Yunzhu Li, Mingyu Ding, Antonio Torralba, Joshua B Tenenbaum, and Chuang Gan. Comphy: Compositional physical reasoning of objects and events from videos. *arXiv*, 2022.
- An-Chieh Cheng, Hongxu Yin, Yang Fu, Qiushan Guo, Ruihan Yang, Jan Kautz, Xiaolong Wang, and Sifei Liu. Spatialrgpt: Grounded spatial reasoning in vision-language models. In *NeurIPS*, 2024.
- Wei-Lin Chiang, Zhuohan Li, Zi Lin, Ying Sheng, Zhanghao Wu, Hao Zhang, Lianmin Zheng, Siyuan Zhuang, Yonghao Zhuang, Joseph E. Gonzalez, Ion Stoica, and Eric P. Xing. Vicuna: An open-source chatbot impressing gpt-4 with 90%* chatgpt quality, March 2023. URL https: //lmsys.org/blog/2023-03-30-vicuna/.
- Wei Chow, Juncheng Li, Qifan Yu, Kaihang Pan, Hao Fei, Zhiqi Ge, Shuai Yang, Siliang Tang, Hanwang Zhang, and Qianru Sun. Unified generative and discriminative training for multi-modal large language models. *arXiv*, 2024.
- Hyung Won Chung, Le Hou, Shayne Longpre, Barret Zoph, Yi Tay, William Fedus, Yunxuan Li, Xuezhi Wang, Mostafa Dehghani, Siddhartha Brahma, et al. Scaling instruction-finetuned language models. *Journal of Machine Learning Research*, 25(70):1–53, 2024.
- OpenCompass Contributors. Opencompass: A universal evaluation platform for foundation models. *GitHub repository*, 2023.
- Chenhang Cui, Yiyang Zhou, Xinyu Yang, Shirley Wu, Linjun Zhang, James Zou, and Huaxiu Yao. Holistic analysis of hallucination in gpt-4v(ision): Bias and interference challenges, 2023. URL https://arxiv.org/abs/2311.03287.
- Angela Dai, Angel X Chang, Manolis Savva, Maciej Halber, Thomas Funkhouser, and Matthias Nießner. Scannet: Richly-annotated 3d reconstructions of indoor scenes. In *Proceedings of the IEEE conference on computer vision and pattern recognition*, pp. 5828–5839, 2017.
- Wenliang Dai, Junnan Li, Dongxu Li, Anthony Meng Huat Tiong, Junqi Zhao, Weisheng Wang, Boyang Li, Pascale N Fung, and Steven Hoi. Instructblip: Towards general-purpose visionlanguage models with instruction tuning. Advances in Neural Information Processing Systems, 36, 2024.
- Abhishek Das, Satwik Kottur, Khushi Gupta, Avi Singh, Deshraj Yadav, José MF Moura, Devi Parikh, and Dhruv Batra. Visual dialog. In *Proceedings of the IEEE conference on computer vision and pattern recognition*, pp. 326–335, 2017.
- Matt Deitke, Christopher Clark, Sangho Lee, Rohun Tripathi, Yue Yang, Jae Sung Park, Mohammadreza Salehi, Niklas Muennighoff, Kyle Lo, Luca Soldaini, et al. Molmo and pixmo: Open weights and open data for state-of-the-art multimodal models. *arXiv*, 2024.
- Mengfei Du, Binhao Wu, Zejun Li, Xuanjing Huang, and Zhongyu Wei. Embspatial-bench: Benchmarking spatial understanding for embodied tasks with large vision-language models. *arXiv*, 2024.

- Jiafei Duan, Samson Yu, Soujanya Poria, Bihan Wen, and Cheston Tan. Pip: Physical interaction prediction via mental simulation with span selection. In *European Conference on Computer Vision*, pp. 405–421. Springer, 2022.
- Desmond Elliott, Stella Frank, Khalil Sima'an, and Lucia Specia. Multi30k: Multilingual englishgerman image descriptions. *arXiv*, 2016.
- Taoran Fang, Wei Zhou, Yifei Sun, Kaiqiao Han, Lvbin Ma, and Yang Yang. Exploring correlations of self-supervised tasks for graphs. *arXiv*, 2024.
- Taoran Fang, Tianhong Gao, Chunping Wang, Yihao Shang, Wei Chow, Lei Chen, and Yang Yang. Kaa: Kolmogorov-arnold attention for enhancing attentive graph neural networks. *arXiv*, 2025.
- Yuxin Fang, Wen Wang, Binhui Xie, Quan Sun, Ledell Wu, Xinggang Wang, Tiejun Huang, Xinlong Wang, and Yue Cao. Eva: Exploring the limits of masked visual representation learning at scale. In *Proceedings of the IEEE/CVF Conference on Computer Vision and Pattern Recognition*, pp. 19358–19369, 2023.
- Xingyu Fu, Yushi Hu, Bangzheng Li, Yu Feng, Haoyu Wang, Xudong Lin, Dan Roth, Noah A Smith, Wei-Chiu Ma, and Ranjay Krishna. Blink: Multimodal large language models can see but not perceive. *arXiv*, 2024.
- Chuang Gan, Jeremy Schwartz, Seth Alter, Damian Mrowca, Martin Schrimpf, James Traer, Julian De Freitas, Jonas Kubilius, Abhishek Bhandwaldar, Nick Haber, et al. Threedworld: A platform for interactive multi-modal physical simulation. *arXiv*, 2020.
- Jensen Gao, Bidipta Sarkar, Fei Xia, Ted Xiao, Jiajun Wu, Brian Ichter, Anirudha Majumdar, and Dorsa Sadigh. Physically grounded vision-language models for robotic manipulation. In *International Conference on Robotics and Automation*. IEEE, 2024a.
- Zhangwei Gao, Zhe Chen, Erfei Cui, Yiming Ren, Weiyun Wang, Jinguo Zhu, Hao Tian, Shenglong Ye, Junjun He, Xizhou Zhu, et al. Mini-internvl: A flexible-transfer pocket multimodal model with 5% parameters and 90% performance. *arXiv*, 2024b.
- Zhiqi Ge, Juncheng Li, Qifan Yu, Wei Zhou, Siliang Tang, and Yueting Zhuang. Demon24: Acm mm24 demonstrative instruction following challenge. In *Proceedings of the 32nd ACM International Conference on Multimedia*, pp. 11426–11428, 2024.
- James J Gibson. *The ecological approach to visual perception: classic edition*. Psychology press, 2014.
- Rohit Girdhar and Deva Ramanan. Cater: A diagnostic dataset for compositional actions and temporal reasoning. *arXiv*, 2019.
- Raghav Goyal, Samira Ebrahimi Kahou, Vincent Michalski, Joanna Materzynska, Susanne Westphal, Heuna Kim, Valentin Haenel, Ingo Fruend, Peter Yianilos, Moritz Mueller-Freitag, et al. The" something something" video database for learning and evaluating visual common sense. In *Proceedings of the IEEE international conference on computer vision*, pp. 5842–5850, 2017a.
- Yash Goyal, Tejas Khot, Douglas Summers-Stay, Dhruv Batra, and Devi Parikh. Making the v in vqa matter: Elevating the role of image understanding in visual question answering. In *Proceedings of the IEEE conference on computer vision and pattern recognition*, pp. 6904–6913, 2017b.
- Kristen Grauman, Andrew Westbury, Eugene Byrne, Zachary Chavis, Antonino Furnari, Rohit Girdhar, Jackson Hamburger, Hao Jiang, Miao Liu, Xingyu Liu, et al. Ego4d: Around the world in 3,000 hours of egocentric video. In *Proceedings of the IEEE/CVF Conference on Computer Vision and Pattern Recognition*, pp. 18995–19012, 2022.
- Cylingo Group. Xinyuan-vl-2b: A high-performance multimodal large model. https:// huggingface.co/Cylingo/Xinyuan-VL-2B, 2024. Accessed: 2024-12-02.

- Shuhao Gu, Jialing Zhang, Siyuan Zhou, Kevin Yu, Zhaohu Xing, Liangdong Wang, Zhou Cao, Jintao Jia, Zhuoyi Zhang, Yixuan Wang, Zhenchong Hu, Bo-Wen Zhang, Jijie Li, Dong Liang, Yingli Zhao, Yulong Ao, Yaoqi Liu, Fangxiang Feng, and Guang Liu. Infinity-mm: Scaling multimodal performance with large-scale and high-quality instruction data, 2024. URL https: //arxiv.org/abs/2410.18558.
- Vincent Le Guen and Nicolas Thome. Disentangling physical dynamics from unknown factors for unsupervised video prediction. In *Proceedings of the IEEE/CVF conference on computer vision and pattern recognition*, pp. 11474–11484, 2020.
- Dingkun Guo, Yuqi Xiang, Shuqi Zhao, Xinghao Zhu, Masayoshi Tomizuka, Mingyu Ding, and Wei Zhan. Phygrasp: Generalizing robotic grasping with physics-informed large multimodal models, 2024. URL https://arxiv.org/abs/2402.16836.
- Agrim Gupta, Silvio Savarese, Surya Ganguli, and Li Fei-Fei. Embodied intelligence via learning and evolution. *Nature communications*, 12(1):5721, 2021.
- Danna Gurari, Qing Li, Abigale J Stangl, Anhong Guo, Chi Lin, Kristen Grauman, Jiebo Luo, and Jeffrey P Bigham. Vizwiz grand challenge: Answering visual questions from blind people. In Proceedings of the IEEE conference on computer vision and pattern recognition, pp. 3608–3617, 2018.
- John K Haas. A history of the unity game engine. Diss. Worcester Polytechnic Institute, 2014.
- Chaoqun He, Renjie Luo, Yuzhuo Bai, Shengding Hu, Zhen Leng Thai, Junhao Shen, Jinyi Hu, Xu Han, Yujie Huang, Yuxiang Zhang, et al. Olympiadbench: A challenging benchmark for promoting agi with olympiad-level bilingual multimodal scientific problems. *arXiv*, 2024.
- Kaiming He, Xiangyu Zhang, Shaoqing Ren, and Jian Sun. Deep residual learning for image recognition. In *Proceedings of the IEEE conference on computer vision and pattern recognition*, pp. 770–778, 2016.
- Kaiming He, Georgia Gkioxari, Piotr Dollár, and Ross Girshick. Mask r-cnn. In *Proceedings of the IEEE international conference on computer vision*, pp. 2961–2969, 2017.
- Dan Hendrycks, Collin Burns, Steven Basart, Andy Zou, Mantas Mazeika, Dawn Song, and Jacob Steinhardt. Measuring massive multitask language understanding. *arXiv*, 2020.
- Jinchang Hou, Chang Ao, Haihong Wu, Xiangtao Kong, Zhigang Zheng, Daijia Tang, Chengming Li, Xiping Hu, Ruifeng Xu, Shiwen Ni, and Min Yang. E-eval: A comprehensive chinese k-12 education evaluation benchmark for large language models, 2024.
- Shengding Hu, Yuge Tu, Xu Han, Chaoqun He, Ganqu Cui, Xiang Long, Zhi Zheng, Yewei Fang, Yuxiang Huang, Weilin Zhao, et al. Minicpm: Unveiling the potential of small language models with scalable training strategies. *arXiv*, 2024.
- Wenlong Huang, Chen Wang, Ruohan Zhang, Yunzhu Li, Jiajun Wu, and Li Fei-Fei. Voxposer: Composable 3d value maps for robotic manipulation with language models. *arXiv*, 2023a.
- Xuanwen Huang, Wei Chow, Yang Wang, Ziwei Chai, Chunping Wang, Lei Chen, and Yang Yang. One graph model for cross-domain dynamic link prediction. *arXiv*, 2024.
- Yuzhen Huang, Yuzhuo Bai, Zhihao Zhu, Junlei Zhang, Jinghan Zhang, Tangjun Su, Junteng Liu, Chuancheng Lv, Yikai Zhang, Jiayi Lei, Yao Fu, Maosong Sun, and Junxian He. C-eval: A multi-level multi-discipline chinese evaluation suite for foundation models, 2023b.
- Drew A Hudson and Christopher D Manning. Gqa: A new dataset for real-world visual reasoning and compositional question answering. In *Proceedings of the IEEE/CVF conference on computer* vision and pattern recognition, pp. 6700–6709, 2019.
- Aaron Jaech, Adam Kalai, Adam Lerer, Adam Richardson, Ahmed El-Kishky, Aiden Low, Alec Helyar, Aleksander Madry, Alex Beutel, Alex Carney, et al. Openai o1 system card. *arXiv*, 2024.

- Baoxiong Jia, Yixin Chen, Huangyue Yu, Yan Wang, Xuesong Niu, Tengyu Liu, Qing Li, and Siyuan Huang. Sceneverse: Scaling 3d vision-language learning for grounded scene understanding. In European Conference on Computer Vision, pp. 289–310. Springer, 2025.
- Albert Q Jiang, Alexandre Sablayrolles, Arthur Mensch, Chris Bamford, Devendra Singh Chaplot, Diego de las Casas, Florian Bressand, Gianna Lengyel, Guillaume Lample, Lucile Saulnier, et al. Mistral 7b. arXiv, 2023.
- Dongfu Jiang, Xuan He, Huaye Zeng, Cong Wei, Max W.F. Ku, Qian Liu, and Wenhu Chen. Mantis: Interleaved multi-image instruction tuning. arXiv, 2024.
- Peng Jin, Ryuichi Takanobu, Caiwan Zhang, Xiaochun Cao, and Li Yuan. Chat-univi: Unified visual representation empowers large language models with image and video understanding. *arXiv*, 2023.
- Justin Johnson, Bharath Hariharan, Laurens Van Der Maaten, Li Fei-Fei, C Lawrence Zitnick, and Ross Girshick. Clevr: A diagnostic dataset for compositional language and elementary visual reasoning. In *Proceedings of the IEEE conference on computer vision and pattern recognition*, pp. 2901–2910, 2017.
- Kushal Kafle and Christopher Kanan. An analysis of visual question answering algorithms. In *Proceedings of the IEEE international conference on computer vision*, pp. 1965–1973, 2017.
- Andrej Karpathy and Li Fei-Fei. Deep visual-semantic alignments for generating image descriptions. In *Proceedings of the IEEE conference on computer vision and pattern recognition*, pp. 3128–3137, 2015.
- Will Kay, Joao Carreira, Karen Simonyan, Brian Zhang, Chloe Hillier, Sudheendra Vijayanarasimhan, Fabio Viola, Tim Green, Trevor Back, Paul Natsev, et al. The kinetics human action video dataset. *arXiv*, 2017.
- Alexander Khazatsky, Karl Pertsch, Suraj Nair, Ashwin Balakrishna, Sudeep Dasari, Siddharth Karamcheti, Soroush Nasiriany, Mohan Kumar Srirama, Lawrence Yunliang Chen, Kirsty Ellis, Peter David Fagan, Joey Hejna, Masha Itkina, Marion Lepert, Yecheng Jason Ma, Patrick Tree Miller, Jimmy Wu, Suneel Belkhale, Shivin Dass, Huy Ha, Arhan Jain, Abraham Lee, Youngwoon Lee, Marius Memmel, Sungjae Park, Ilija Radosavovic, Kaiyuan Wang, Albert Zhan, Kevin Black, Cheng Chi, Kyle Beltran Hatch, Shan Lin, Jingpei Lu, Jean Mercat, Abdul Rehman, Pannag R Sanketi, Archit Sharma, Cody Simpson, Quan Vuong, Homer Rich Walke, Blake Wulfe, Ted Xiao, Jonathan Heewon Yang, Arefeh Yavary, Tony Z. Zhao, Christopher Agia, Rohan Baijal, Mateo Guaman Castro, Daphne Chen, Qiuyu Chen, Trinity Chung, Jaimyn Drake, Ethan Paul Foster, Jensen Gao, David Antonio Herrera, Minho Heo, Kyle Hsu, Jiaheng Hu, Donovon Jackson, Charlotte Le, Yunshuang Li, Kevin Lin, Roy Lin, Zehan Ma, Abhiram Maddukuri, Suvir Mirchandani, Daniel Morton, Tony Nguyen, Abigail O'Neill, Rosario Scalise, Derick Seale, Victor Son, Stephen Tian, Emi Tran, Andrew E. Wang, Yilin Wu, Annie Xie, Jingyun Yang, Patrick Yin, Yunchu Zhang, Osbert Bastani, Glen Berseth, Jeannette Bohg, Ken Goldberg, Abhinav Gupta, Abhishek Gupta, Dinesh Jayaraman, Joseph J Lim, Jitendra Malik, Roberto Martín-Martín, Subramanian Ramamoorthy, Dorsa Sadigh, Shuran Song, Jiajun Wu, Michael C. Yip, Yuke Zhu, Thomas Kollar, Sergey Levine, and Chelsea Finn. Droid: A large-scale in-the-wild robot manipulation dataset. 2024.
- Jihyung Kil, Zheda Mai, Justin Lee, Zihe Wang, Kerrie Cheng, Lemeng Wang, Ye Liu, Arpita Chowdhury, and Wei-Lun Chao. Compbench: A comparative reasoning benchmark for multimodal llms. arXiv, 2024.
- Carina Kill and Ohnshim Kim. Mental mechanics: How humans reason through a physical world. *Mental*, 2020.
- Moo Jin Kim, Karl Pertsch, Siddharth Karamcheti, Ted Xiao, Ashwin Balakrishna, Suraj Nair, Rafael Rafailov, Ethan Foster, Grace Lam, Pannag Sanketi, Quan Vuong, Thomas Kollar, Benjamin Burchfiel, Russ Tedrake, Dorsa Sadigh, Sergey Levine, Percy Liang, and Chelsea Finn. Openvla: An open-source vision-language-action model. *arXiv*, 2024.

- Alexander Kirillov, Eric Mintun, Nikhila Ravi, Hanzi Mao, Chloe Rolland, Laura Gustafson, Tete Xiao, Spencer Whitehead, Alexander C Berg, Wan-Yen Lo, et al. Segment anything. In Proceedings of the IEEE/CVF International Conference on Computer Vision, pp. 4015–4026, 2023.
- Takeshi Kojima, Shixiang Shane Gu, Machel Reid, Yutaka Matsuo, and Yusuke Iwasawa. Large language models are zero-shot reasoners. *Advances in neural information processing systems*, 35:22199–22213, 2022.
- Takeshi Kojima, Shixiang Shane Gu, Machel Reid, Yutaka Matsuo, and Yusuke Iwasawa. Large language models are zero-shot reasoners, 2023. URL https://arxiv.org/abs/2205. 11916.
- Eric Kolve, Roozbeh Mottaghi, Winson Han, Eli VanderBilt, Luca Weihs, Alvaro Herrasti, Matt Deitke, Kiana Ehsani, Daniel Gordon, Yuke Zhu, et al. Ai2-thor: An interactive 3d environment for visual ai. *arXiv*, 2017.
- Jonathan Krause, Justin Johnson, Ranjay Krishna, and Li Fei-Fei. A hierarchical approach for generating descriptive image paragraphs. In *Proceedings of the IEEE conference on computer vision and pattern recognition*, pp. 317–325, 2017.
- Zihang Lai, Senthil Purushwalkam, and Abhinav Gupta. The functional correspondence problem. In *Proceedings of the IEEE/CVF International Conference on Computer Vision*, pp. 15772–15781, 2021.
- Paul Lerner, Olivier Ferret, Camille Guinaudeau, Hervé Le Borgne, Romaric Besançon, José G Moreno, and Jesús Lovón Melgarejo. Viquae, a dataset for knowledge-based visual question answering about named entities. In Proceedings of the 45th International ACM SIGIR Conference on Research and Development in Information Retrieval, pp. 3108–3120, 2022.
- Aitor Lewkowycz, Anders Andreassen, David Dohan, Ethan Dyer, Henryk Michalewski, Vinay Ramasesh, Ambrose Slone, Cem Anil, Imanol Schlag, Theo Gutman-Solo, Yuhuai Wu, Behnam Neyshabur, Guy Gur-Ari, and Vedant Misra. Solving quantitative reasoning problems with language models, 2022.
- Bohao Li, Rui Wang, Guangzhi Wang, Yuying Ge, Yixiao Ge, and Ying Shan. Seed-bench: Benchmarking multimodal llms with generative comprehension. *arXiv*, 2023a.
- Bohao Li, Yuying Ge, Yixiao Ge, Guangzhi Wang, Rui Wang, Ruimao Zhang, and Ying Shan. Seed-bench: Benchmarking multimodal large language models. In *Proceedings of the IEEE/CVF Conference on Computer Vision and Pattern Recognition*, pp. 13299–13308, 2024a.
- Boyi Li, Yue Wang, Jiageng Mao, Boris Ivanovic, Sushant Veer, Karen Leung, and Marco Pavone. Driving everywhere with large language model policy adaptation. In *Proceedings of the IEEE/CVF Conference on Computer Vision and Pattern Recognition*, pp. 14948–14957, 2024b.
- Boyi Li, Ligeng Zhu, Ran Tian, Shuhan Tan, Yuxiao Chen, Yao Lu, Yin Cui, Sushant Veer, Max Ehrlich, Jonah Philion, et al. Wolf: Captioning everything with a world summarization framework. *arXiv*, 2024c.
- Feng Li, Renrui Zhang, Hao Zhang, Yuanhan Zhang, Bo Li, Wei Li, Zejun Ma, and Chunyuan Li. Llava-next-interleave: Tackling multi-image, video, and 3d in large multimodal models, 2024d. URL https://arxiv.org/abs/2407.07895.
- Juncheng Li, Kaihang Pan, Zhiqi Ge, Minghe Gao, Wei Ji, Wenqiao Zhang, Tat-Seng Chua, Siliang Tang, Hanwang Zhang, and Yueting Zhuang. Fine-tuning multimodal llms to follow zero-shot demonstrative instructions. In *The Twelfth International Conference on Learning Representations*, 2023b.
- Junnan Li, Dongxu Li, Silvio Savarese, and Steven Hoi. Blip-2: Bootstrapping language-image pre-training with frozen image encoders and large language models. In *International conference* on machine learning, pp. 19730–19742. PMLR, 2023c.
- KunChang Li, Yinan He, Yi Wang, Yizhuo Li, Wenhai Wang, Ping Luo, Yali Wang, Limin Wang, and Yu Qiao. Videochat: Chat-centric video understanding. *arXiv*, 2023d.

- Kunchang Li, Yali Wang, Yinan He, Yizhuo Li, Yi Wang, Yi Liu, Zun Wang, Jilan Xu, Guo Chen, Ping Luo, Limin Wang, and Yu Qiao. Mvbench: A comprehensive multi-modal video understanding benchmark, 2023e.
- Kunchang Li, Yali Wang, Yinan He, Yizhuo Li, Yi Wang, Yi Liu, Zun Wang, Jilan Xu, Guo Chen, Ping Luo, et al. Mvbench: A comprehensive multi-modal video understanding benchmark. In Proceedings of the IEEE/CVF Conference on Computer Vision and Pattern Recognition, pp. 22195–22206, 2024e.
- Lei Li, Yuwei Yin, Shicheng Li, Liang Chen, Peiyi Wang, Shuhuai Ren, Mukai Li, Yazheng Yang, Jingjing Xu, Xu Sun, Lingpeng Kong, and Qi Liu. M³it: A large-scale dataset towards multimodal multilingual instruction tuning. arXiv, 2023f.
- Yanwei Li, Chengyao Wang, and Jiaya Jia. Llama-vid: An image is worth 2 tokens in large language models. arXiv, 2023g.
- Yifan Li, Yifan Du, Kun Zhou, Jinpeng Wang, Wayne Xin Zhao, and Ji-Rong Wen. Evaluating object hallucination in large vision-language models. *arXiv*, 2023h.
- Yuncheng Li, Yale Song, Liangliang Cao, Joel Tetreault, Larry Goldberg, Alejandro Jaimes, and Jiebo Luo. Tgif: A new dataset and benchmark on animated gif description. In *Proceedings of* the IEEE Conference on Computer Vision and Pattern Recognition, pp. 4641–4650, 2016.
- Yunzhu Li, Jiajun Wu, Russ Tedrake, Joshua B Tenenbaum, and Antonio Torralba. Learning particle dynamics for manipulating rigid bodies, deformable objects, and fluids. *arXiv*, 2018.
- Zekun Li, Xianjun Yang, Kyuri Choi, Wanrong Zhu, Ryan Hsieh, HyeonJung Kim, Jin Hyuk Lim, Sungyoung Ji, Byungju Lee, Xifeng Yan, et al. Mmsci: A multimodal multi-discipline dataset for phd-level scientific comprehension. arXiv, 2024f.
- Bin Lin, Bin Zhu, Yang Ye, Munan Ning, Peng Jin, and Li Yuan. Video-llava: Learning united visual representation by alignment before projection. *arXiv*, 2023a.
- Ji Lin, Hongxu Yin, Wei Ping, Yao Lu, Pavlo Molchanov, Andrew Tao, Huizi Mao, Jan Kautz, Mohammad Shoeybi, and Song Han. Vila: On pre-training for visual language models, 2023b.
- Xiongkun Linghu, Jiangyong Huang, Xuesong Niu, Xiaojian Ma, Baoxiong Jia, and Siyuan Huang. Multi-modal situated reasoning in 3d scenes. *arXiv*, 2024.
- Fangchen Liu, Kuan Fang, Pieter Abbeel, and Sergey Levine. Moka: Open-vocabulary robotic manipulation through mark-based visual prompting. *arXiv*, 2024a.
- Haotian Liu, Chunyuan Li, Yuheng Li, and Yong Jae Lee. Improved baselines with visual instruction tuning, 2023a.
- Haotian Liu, Chunyuan Li, Yuheng Li, Bo Li, Yuanhan Zhang, Sheng Shen, and Yong Jae Lee. Llava-next: Improved reasoning, ocr, and world knowledge, January 2024b. URL https:// llava-vl.github.io/blog/2024-01-30-llava-next/.
- Haotian Liu, Chunyuan Li, Qingyang Wu, and Yong Jae Lee. Visual instruction tuning. Advances in neural information processing systems, 36, 2024c.
- Junpeng Liu, Yifan Song, Bill Yuchen Lin, Wai Lam, Graham Neubig, Yuanzhi Li, and Xiang Yue. Visualwebbench: How far have multimodal llms evolved in web page understanding and grounding?, 2024d.
- Shilong Liu, Zhaoyang Zeng, Tianhe Ren, Feng Li, Hao Zhang, Jie Yang, Chunyuan Li, Jianwei Yang, Hang Su, Jun Zhu, et al. Grounding dino: Marrying dino with grounded pre-training for open-set object detection. arXiv, 2023b.
- Yuan Liu, Haodong Duan, Yuanhan Zhang, Bo Li, Songyang Zhang, Wangbo Zhao, Yike Yuan, Jiaqi Wang, Conghui He, Ziwei Liu, et al. Mmbench: Is your multi-modal model an all-around player? *arXiv*, 2023c.

- Yuanxin Liu, Shicheng Li, Yi Liu, Yuxiang Wang, Shuhuai Ren, Lei Li, Sishuo Chen, Xu Sun, and Lu Hou. Tempcompass: Do video llms really understand videos? *arXiv*, 2024e.
- Zhijian Liu, Ligeng Zhu, Baifeng Shi, Zhuoyang Zhang, Yuming Lou, Shang Yang, Haocheng Xi, Shiyi Cao, Yuxian Gu, Dacheng Li, Xiuyu Li, Yunhao Fang, Yukang Chen, Cheng-Yu Hsieh, De-An Huang, An-Chieh Cheng, Vishwesh Nath, Jinyi Hu, Sifei Liu, Ranjay Krishna, Daguang Xu, Xiaolong Wang, Pavlo Molchanov, Jan Kautz, Hongxu Yin, Song Han, and Yao Lu. Nvila: Efficient frontier visual language models, 2024f. URL https://arxiv.org/abs/2412. 04468.
- Haoyu Lu, Wen Liu, Bo Zhang, Bingxuan Wang, Kai Dong, Bo Liu, Jingxiang Sun, Tongzheng Ren, Zhuoshu Li, Yaofeng Sun, Chengqi Deng, Hanwei Xu, Zhenda Xie, and Chong Ruan. Deepseek-vl: Towards real-world vision-language understanding, 2024a.
- Pan Lu, Swaroop Mishra, Tanglin Xia, Liang Qiu, Kai-Wei Chang, Song-Chun Zhu, Oyvind Tafjord, Peter Clark, and Ashwin Kalyan. Learn to explain: Multimodal reasoning via thought chains for science question answering. *Advances in Neural Information Processing Systems*, 35:2507–2521, 2022.
- Pan Lu, Hritik Bansal, Tony Xia, Jiacheng Liu, Chunyuan Li, Hannaneh Hajishirzi, Hao Cheng, Kai-Wei Chang, Michel Galley, and Jianfeng Gao. Mathvista: Evaluating mathematical reasoning of foundation models in visual contexts. In *International Conference on Learning Representations*, 2024b.
- Ruiyuan Lyu, Tai Wang, Jingli Lin, Shuai Yang, Xiaohan Mao, Yilun Chen, Runsen Xu, Haifeng Huang, Chenming Zhu, Dahua Lin, et al. Mmscan: A multi-modal 3d scene dataset with hierarchical grounded language annotations. arXiv, 2024.
- Xiaojian Ma, Silong Yong, Zilong Zheng, Qing Li, Yitao Liang, Song-Chun Zhu, and Siyuan Huang. Sqa3d: Situated question answering in 3d scenes. In *International Conference on Learning Representations*, 2023. URL https://openreview.net/forum?id=IDJx97BC38.
- Muhammad Maaz, Hanoona Rasheed, Salman Khan, and Fahad Shahbaz Khan. Video-chatgpt: Towards detailed video understanding via large vision and language models. *arXiv*, 2023a.
- Muhammad Maaz, Hanoona Rasheed, Salman Khan, and Fahad Shahbaz Khan. Video-chatgpt: Towards detailed video understanding via large vision and language models. *arXiv:2306.05424*, 2023b.
- Arjun Majumdar, Anurag Ajay, Xiaohan Zhang, Pranav Putta, Sriram Yenamandra, Mikael Henaff, Sneha Silwal, Paul Mcvay, Oleksandr Maksymets, Sergio Arnaud, Karmesh Yadav, Qiyang Li, Ben Newman, Mohit Sharma, Vincent Berges, Shiqi Zhang, Pulkit Agrawal, Yonatan Bisk, Dhruv Batra, Mrinal Kalakrishnan, Franziska Meier, Chris Paxton, Sasha Sax, and Aravind Rajeswaran. Openeqa: Embodied question answering in the era of foundation models. In *Conference on Computer Vision and Pattern Recognition*, 2024.
- Karttikeya Mangalam, Raiymbek Akshulakov, and Jitendra Malik. Egoschema: A diagnostic benchmark for very long-form video language understanding. Advances in Neural Information Processing Systems, 36, 2024.
- Jiageng Mao, Yuxi Qian, Junjie Ye, Hang Zhao, and Yue Wang. Gpt-driver: Learning to drive with gpt. *arXiv*, 2023a.
- Jiageng Mao, Junjie Ye, Yuxi Qian, Marco Pavone, and Yue Wang. A language agent for autonomous driving. *arXiv*, 2023b.
- Jiageng Mao, Siheng Zhao, Siqi Song, Tianheng Shi, Junjie Ye, Mingtong Zhang, Haoran Geng, Jitendra Malik, Vitor Guizilini, and Yue Wang. Learning from massive human videos for universal humanoid pose control. *arXiv*, 2024.
- Kenneth Marino, Mohammad Rastegari, Ali Farhadi, and Roozbeh Mottaghi. Ok-vqa: A visual question answering benchmark requiring external knowledge. In *Conference on Computer Vision and Pattern Recognition*, 2019.

- Minesh Mathew, Dimosthenis Karatzas, and CV Jawahar. Docvqa: A dataset for vqa on document images. In Proceedings of the IEEE/CVF winter conference on applications of computer vision, pp. 2200–2209, 2021.
- Michael McCloskey, Allyson Washburn, and Linda Felch. Intuitive physics: the straight-down belief and its origin. *Journal of Experimental Psychology: Learning, Memory, and Cognition*, 9(4):636, 1983.
- Fanqing Meng, Jin Wang, Chuanhao Li, Quanfeng Lu, Hao Tian, Jiaqi Liao, Xizhou Zhu, Jifeng Dai, Yu Qiao, Ping Luo, Kaipeng Zhang, and Wenqi Shao. Mmiu: Multimodal multi-image understanding for evaluating large vision-language models, 2024. URL https://arxiv.org/abs/2408.02718.
- Antoine Miech, Dimitri Zhukov, Jean-Baptiste Alayrac, Makarand Tapaswi, Ivan Laptev, and Josef Sivic. Howto100m: Learning a text-video embedding by watching hundred million narrated video clips. In *Proceedings of the IEEE/CVF international conference on computer vision*, pp. 2630–2640, 2019.
- Anand Mishra, Shashank Shekhar, Ajeet Kumar Singh, and Anirban Chakraborty. Ocr-vqa: Visual question answering by reading text in images. In *International Conference on Document Analysis* and Recognition, pp. 947–952. IEEE, 2019.
- Niklas Muennighoff, Luca Soldaini, Dirk Groeneveld, Kyle Lo, Jacob Morrison, Sewon Min, Weijia Shi, Pete Walsh, Oyvind Tafjord, Nathan Lambert, Yuling Gu, Shane Arora, Akshita Bhagia, Dustin Schwenk, David Wadden, Alexander Wettig, Binyuan Hui, Tim Dettmers, Douwe Kiela, Ali Farhadi, Noah A. Smith, Pang Wei Koh, Amanpreet Singh, and Hannaneh Hajishirzi. Olmoe: Open mixture-of-experts language models, 2024. URL https://arxiv.org/abs/2409. 02060.
- Soroush Nasiriany, Fei Xia, Wenhao Yu, Ted Xiao, Jacky Liang, Ishita Dasgupta, Annie Xie, Danny Driess, Ayzaan Wahid, Zhuo Xu, Quan Vuong, Tingnan Zhang, Tsang-Wei Edward Lee, Kuang-Huei Lee, Peng Xu, Sean Kirmani, Yuke Zhu, Andy Zeng, Karol Hausman, Nicolas Heess, Chelsea Finn, Sergey Levine, and Brian Ichter. Pivot: Iterative visual prompting elicits actionable knowledge for vlms. *arXiv*, 2024.
- Dantong Niu, Yuvan Sharma, Giscard Biamby, Jerome Quenum, Yutong Bai, Baifeng Shi, Trevor Darrell, and Roei Herzig. Llarva: Vision-action instruction tuning enhances robot learning. *arXiv*, 2024.
- Octo Model Team, Dibya Ghosh, Homer Walke, Karl Pertsch, Kevin Black, Oier Mees, Sudeep Dasari, Joey Hejna, Charles Xu, Jianlan Luo, Tobias Kreiman, You Liang Tan, Lawrence Yunliang Chen, Pannag Sanketi, Quan Vuong, Ted Xiao, Dorsa Sadigh, Chelsea Finn, and Sergey Levine. Octo: An open-source generalist robot policy. In *Proceedings of Robotics: Science and Systems*, Delft, Netherlands, 2024.
- Kaihang Pan, Siliang Tang, Juncheng Li, Zhaoyu Fan, Wei Chow, Shuicheng Yan, Tat-Seng Chua, Yueting Zhuang, and Hanwang Zhang. Auto-encoding morph-tokens for multimodal llm. *arXiv*, 2024.
- Maitreya Patel, Tejas Gokhale, Chitta Baral, and Yezhou Yang. Cripp-vqa: Counterfactual reasoning about implicit physical properties via video question answering. *arXiv*, 2022.
- Zhiliang Peng, Wenhui Wang, Li Dong, Yaru Hao, Shaohan Huang, Shuming Ma, and Furu Wei. Kosmos-2: Grounding multimodal large language models to the world. ArXiv, abs/2306.14824, 2023. URL https://api.semanticscholar.org/CorpusID:259262263.
- Charles R Qi, Hao Su, Kaichun Mo, and Leonidas J Guibas. Pointnet: Deep learning on point sets for 3d classification and segmentation. In *Proceedings of the IEEE conference on computer vision and pattern recognition*, pp. 652–660, 2017.
- Alec Radford, Jong Wook Kim, Chris Hallacy, Aditya Ramesh, Gabriel Goh, Sandhini Agarwal, Girish Sastry, Amanda Askell, Pamela Mishkin, Jack Clark, et al. Learning transferable visual models from natural language supervision. In *International conference on machine learning*, pp. 8748–8763. PMLR, 2021.

- Nazneen Fatema Rajani, Rui Zhang, Yi Chern Tan, Stephan Zheng, Jeremy Weiss, Aadit Vyas, Abhijit Gupta, Caiming Xiong, Richard Socher, and Dragomir Radev. Esprit: Explaining solutions to physical reasoning tasks. *arXiv*, 2020.
- Tianhe Ren, Shilong Liu, Ailing Zeng, Jing Lin, Kunchang Li, He Cao, Jiayu Chen, Xinyu Huang, Yukang Chen, Feng Yan, et al. Grounded sam: Assembling open-world models for diverse visual tasks. *arXiv*, 2024.
- Ronan Riochet, Mario Ynocente Castro, Mathieu Bernard, Adam Lerer, Rob Fergus, Véronique Izard, and Emmanuel Dupoux. Intphys: A framework and benchmark for visual intuitive physics reasoning. *arXiv*, 2018.
- Paul-Edouard Sarlin, Daniel DeTone, Tomasz Malisiewicz, and Andrew Rabinovich. Superglue: Learning feature matching with graph neural networks. In *Proceedings of the IEEE/CVF confer*ence on computer vision and pattern recognition, pp. 4938–4947, 2020.
- Piyush Sharma, Nan Ding, Sebastian Goodman, and Radu Soricut. Conceptual captions: A cleaned, hypernymed, image alt-text dataset for automatic image captioning. In *Proceedings of ACL*, 2018.
- Oleksii Sidorov, Ronghang Hu, Marcus Rohrbach, and Amanpreet Singh. Textcaps: a dataset for image captioning with reading comprehension. In *Computer Vision–ECCV 2020: 16th European Conference, Glasgow, UK, August 23–28, 2020, Proceedings, Part II 16*, pp. 742–758. Springer, 2020.
- Karen Simonyan and Andrew Zisserman. Very deep convolutional networks for large-scale image recognition. *arXiv*, 2014.
- Amanpreet Singh, Vivek Natarajan, Meet Shah, Yu Jiang, Xinlei Chen, Dhruv Batra, Devi Parikh, and Marcus Rohrbach. Towards vqa models that can read. In *Proceedings of the IEEE/CVF conference on computer vision and pattern recognition*, pp. 8317–8326, 2019.
- Noah Snavely, Steven M. Seitz, and Richard Szeliski. Photo tourism: Exploring photo collections in 3d. In SIGGRAPH Conference Proceedings, pp. 835–846, New York, NY, USA, 2006. ACM Press. ISBN 1-59593-364-6.
- Sanjana Srivastava, Chengshu Li, Michael Lingelbach, Roberto Mart, Fei Xia, Kent Vainio, Zheng Lian, Cem Gokmen, Shyamal Buch, Karen Liu, Silvio Savarese, Hyowon Gweon, Jiajun Wu, and Li Fei-Fei. Behavior: Benchmark for everyday household activities in virtual, interactive, and ecological environments. In *Conference in Robot Learning*, pp. accepted, 2021.
- Andreas Steiner, André Susano Pinto, Michael Tschannen, Daniel Keysers, Xiao Wang, Yonatan Bitton, Alexey Gritsenko, Matthias Minderer, Anthony Sherbondy, Shangbang Long, Siyang Qin, Reeve Ingle, Emanuele Bugliarello, Sahar Kazemzadeh, Thomas Mesnard, Ibrahim Alabdulmohsin, Lucas Beyer, and Xiaohua Zhai. Paligemma 2: A family of versatile vlms for transfer. *arXiv*, 2024.
- Alane Suhr, Mike Lewis, James Yeh, and Yoav Artzi. A corpus of natural language for visual reasoning. In *Proceedings of the 55th Annual Meeting of the Association for Computational Linguistics*, pp. 217–223, 2017.
- Alane Suhr, Stephanie Zhou, Ally Zhang, Iris Zhang, Huajun Bai, and Yoav Artzi. A corpus for reasoning about natural language grounded in photographs. *arXiv*, 2018.
- Deborah Sulsky, Shi-Jian Zhou, and Howard L Schreyer. Application of a particle-in-cell method to solid mechanics. *Computer physics communications*, 87(1-2):236–252, 1995.
- Ddac Surs, Sachit Menon, and Carl Vondrick. Vipergpt: Visual inference via python execution for reasoning. In *Proceedings of the IEEE/CVF International Conference on Computer Vision*, pp. 11888–11898, 2023.
- Ryota Tanaka, Kyosuke Nishida, and Sen Yoshida. Visualmrc: Machine reading comprehension on document images. In *Proceedings of the AAAI Conference on Artificial Intelligence*, volume 35, pp. 13878–13888, 2021.

- Gemini Team, Rohan Anil, Sebastian Borgeaud, Yonghui Wu, Jean-Baptiste Alayrac, Jiahui Yu, Radu Soricut, Johan Schalkwyk, Andrew M Dai, Anja Hauth, et al. Gemini: a family of highly capable multimodal models. *arXiv*, 2023.
- Gemma Team, Morgane Riviere, Shreya Pathak, Pier Giuseppe Sessa, Cassidy Hardin, Surya Bhupatiraju, Léonard Hussenot, Thomas Mesnard, Bobak Shahriari, Alexandre Ramé, et al. Gemma 2: Improving open language models at a practical size. *arXiv*, 2024.
- Emanuel Todorov, Tom Erez, and Yuval Tassa. Mujoco: A physics engine for model-based control. In 2012 IEEE/RSJ international conference on intelligent robots and systems, pp. 5026–5033. IEEE, 2012.
- Shengbang Tong, Ellis Brown, Penghao Wu, Sanghyun Woo, Manoj Middepogu, Sai Charitha Akula, Jihan Yang, Shusheng Yang, Adithya Iyer, Xichen Pan, Austin Wang, Rob Fergus, Yann LeCun, and Saining Xie. Cambrian-1: A fully open, vision-centric exploration of multimodal llms. arXiv, 2024.
- Hugo Touvron, Thibaut Lavril, Gautier Izacard, Xavier Martinet, Marie-Anne Lachaux, Timothée Lacroix, Baptiste Rozière, Naman Goyal, Eric Hambro, Faisal Azhar, et al. Llama: Open and efficient foundation language models. *arXiv*, 2023.
- Fish Tung, Mingyu Ding, Zhenfang Chen, Daniel M. Bear, Chuang Gan, Joshua B. Tenenbaum, Daniel L. K. Yamins, Judith Fan, and Kevin A. Smith. Physion++: Evaluating physical scene understanding that requires online inference of different physical properties. *arXiv*, 2023.
- Andong Wang, Bo Wu, Sunli Chen, Zhenfang Chen, Haotian Guan, Wei-Ning Lee, Li Erran Li, and Chuang Gan. Sok-bench: A situated video reasoning benchmark with aligned open-world knowledge. In *Proceedings of the IEEE/CVF Conference on Computer Vision and Pattern Recognition*, pp. 13384–13394, 2024a.
- Chen Wang, Linxi Fan, Jiankai Sun, Ruohan Zhang, Li Fei-Fei, Danfei Xu, Yuke Zhu, and Anima Anandkumar. Mimicplay: Long-horizon imitation learning by watching human play. *arXiv*, 2023a.
- Fei Wang, Xingyu Fu, James Y Huang, Zekun Li, Qin Liu, Xiaogeng Liu, Mingyu Derek Ma, Nan Xu, Wenxuan Zhou, Kai Zhang, et al. Muirbench: A comprehensive benchmark for robust multi-image understanding. *arXiv*, 2024b.
- Peng Wang, Shuai Bai, Sinan Tan, Shijie Wang, Zhihao Fan, Jinze Bai, Keqin Chen, Xuejing Liu, Jialin Wang, Wenbin Ge, Yang Fan, Kai Dang, Mengfei Du, Xuancheng Ren, Rui Men, Dayiheng Liu, Chang Zhou, Jingren Zhou, and Junyang Lin. Qwen2-vl: Enhancing vision-language model's perception of the world at any resolution. arXiv, 2024c.
- Tai Wang, Xiaohan Mao, Chenming Zhu, Runsen Xu, Ruiyuan Lyu, Peisen Li, Xiao Chen, Wenwei Zhang, Kai Chen, Tianfan Xue, Xihui Liu, Cewu Lu, Dahua Lin, and Jiangmiao Pang. Embodiedscan: A holistic multi-modal 3d perception suite towards embodied ai. In *Conference on Computer Vision and Pattern Recognition*, 2024d.
- Weihan Wang, Qingsong Lv, Wenmeng Yu, Wenyi Hong, Ji Qi, Yan Wang, Junhui Ji, Zhuoyi Yang, Lei Zhao, Xixuan Song, et al. Cogvlm: Visual expert for pretrained language models. arXiv, 2023b.
- Weiyun Wang, Zhe Chen, Wenhai Wang, Yue Cao, Yangzhou Liu, Zhangwei Gao, Jinguo Zhu, Xizhou Zhu, Lewei Lu, Yu Qiao, and Jifeng Dai. Enhancing the reasoning ability of multimodal large language models via mixed preference optimization. *arXiv*, 2024e.
- Xiaoxuan Wang, Ziniu Hu, Pan Lu, Yanqiao Zhu, Jieyu Zhang, Satyen Subramaniam, Arjun R. Loomba, Shichang Zhang, Yizhou Sun, and Wei Wang. Scibench: Evaluating college-level scientific problem-solving abilities of large language models, 2024f.
- Xingrui Wang, Wufei Ma, Angtian Wang, Shuo Chen, Adam Kortylewski, and Alan Yuille. Compositional 4d dynamic scenes understanding with physics priors for video question answering. *arXiv*, 2024g.

- Yi Ru Wang, Jiafei Duan, Dieter Fox, and Siddhartha Srinivasa. Newton: Are large language models capable of physical reasoning? *arXiv*, 2023c.
- Jason Wei, Maarten Bosma, Vincent Y Zhao, Kelvin Guu, Adams Wei Yu, Brian Lester, Nan Du, Andrew M Dai, and Quoc V Le. Finetuned language models are zero-shot learners. *arXiv*, 2021.
- Johannes Welbl, Nelson F. Liu, and Matt Gardner. Crowdsourcing multiple choice science questions. In Leon Derczynski, Wei Xu, Alan Ritter, and Tim Baldwin (eds.), *Proceedings of the 3rd Workshop on Noisy User-generated Text*, pp. 94–106, Copenhagen, Denmark, September 2017. Association for Computational Linguistics. doi: 10.18653/v1/W17-4413. URL https://aclanthology.org/W17-4413.
- Bo Wu, Shoubin Yu, Zhenfang Chen, Joshua B Tenenbaum, and Chuang Gan. Star: A benchmark for situated reasoning in real-world videos. *arXiv*, 2024a.
- Haoning Wu, Zicheng Zhang, Erli Zhang, Chaofeng Chen, Liang Liao, Annan Wang, Chunyi Li, Wenxiu Sun, Qiong Yan, Guangtao Zhai, et al. Q-bench: A benchmark for general-purpose foundation models on low-level vision. arXiv, 2023a.
- Haoning Wu, Dongxu Li, Bei Chen, and Junnan Li. Longvideobench: A benchmark for long-context interleaved video-language understanding. *arXiv*, 2024b.
- Jiajun Wu, Joseph J Lim, Hongyi Zhang, Joshua B Tenenbaum, and William T Freeman. Physics 101: Learning physical object properties from unlabeled videos. In *BMVC*, volume 2, pp. 7, 2016.
- Qiucheng Wu, Handong Zhao, Michael Saxon, Trung Bui, William Yang Wang, Yang Zhang, and Shiyu Chang. Vsp: Assessing the dual challenges of perception and reasoning in spatial planning tasks for vlms. *arXiv*, 2024c.
- Shengqiong Wu, Hao Fei, Leigang Qu, Wei Ji, and Tat-Seng Chua. Next-gpt: Any-to-any multimodal llm. ArXiv, abs/2309.05519, 2023b. URL https://api.semanticscholar.org/ CorpusID:261696650.
- Weijia Wu, Yuzhong Zhao, Zhuang Li, Jiahong Li, Hong Zhou, Mike Zheng Shou, and Xiang Bai. A large cross-modal video retrieval dataset with reading comprehension. *arXiv*, 2023c.
- Yifan Wu, Pengchuan Zhang, Wenhan Xiong, Barlas Oguz, James C. Gee, and Yixin Nie. The role of chain-of-thought in complex vision-language reasoning task, 2023d. URL https:// arxiv.org/abs/2311.09193.
- Yuxin Wu, Alexander Kirillov, Francisco Massa, Wan-Yen Lo, and Ross Girshick. Detectron2. https://github.com/facebookresearch/detectron2, 2019.
- Junbin Xiao, Xindi Shang, Angela Yao, and Tat-Seng Chua. Next-qa: Next phase of questionanswering to explaining temporal actions. In Proceedings of the IEEE/CVF conference on computer vision and pattern recognition, pp. 9777–9786, 2021a.
- Junbin Xiao, Xindi Shang, Angela Yao, and Tat-Seng Chua. Next-qa: Next phase of questionanswering to explaining temporal actions. In *Proceedings of the IEEE/CVF conference on computer vision and pattern recognition*, pp. 9777–9786, 2021b.
- Binzhu Xie, Sicheng Zhang, Zitang Zhou, Bo Li, Yuanhan Zhang, Jack Hessel, Jingkang Yang, and Ziwei Liu. Funqa: Towards surprising video comprehension. *arXiv*, 2023.
- Dejing Xu, Zhou Zhao, Jun Xiao, Fei Wu, Hanwang Zhang, Xiangnan He, and Yueting Zhuang. Video question answering via gradually refined attention over appearance and motion. In *Proceedings of the 25th ACM international conference on Multimedia*, pp. 1645–1653, 2017.
- Jun Xu, Tao Mei, Ting Yao, and Yong Rui. Msr-vtt: A large video description dataset for bridging video and language. In *Proceedings of the IEEE conference on computer vision and pattern* recognition, pp. 5288–5296, 2016.

- Lin Xu, Yilin Zhao, Daquan Zhou, Zhijie Lin, See Kiong Ng, and Jiashi Feng. Pllava : Parameterfree llava extension from images to videos for video dense captioning, 2024.
- Antoine Yang, Antoine Miech, Josef Sivic, Ivan Laptev, and Cordelia Schmid. Just ask: Learning to answer questions from millions of narrated videos. In *Proceedings of the IEEE/CVF international* conference on computer vision, pp. 1686–1697, 2021.
- Jihan Yang, Shusheng Yang, Anjali W Gupta, Rilyn Han, Li Fei-Fei, and Saining Xie. Thinking in space: How multimodal large language models see, remember, and recall spaces. *arXiv*, 2024a.
- Lihe Yang, Bingyi Kang, Zilong Huang, Zhen Zhao, Xiaogang Xu, Jiashi Feng, and Hengshuang Zhao. Depth anything v2. *arXiv:2406.09414*, 2024b.
- Yuan Yao, Tianyu Yu, Ao Zhang, Chongyi Wang, Junbo Cui, Hongji Zhu, Tianchi Cai, Haoyu Li, Weilin Zhao, Zhihui He, Qianyu Chen, Huarong Zhou, Zhensheng Zou, Haoye Zhang, Shengding Hu, Zhi Zheng, Jie Zhou, Jie Cai, Xu Han, Guoyang Zeng, Dahai Li, Zhiyuan Liu, and Maosong Sun. Minicpm-v: A gpt-4v level mllm on your phone. *arXiv*, 2024. URL https://arxiv.org/abs/2408.01800.
- Jiabo Ye, Haiyang Xu, Haowei Liu, Anwen Hu, Ming Yan, Qi Qian, Ji Zhang, Fei Huang, and Jingren Zhou. mplug-owl3: Towards long image-sequence understanding in multi-modal large language models, 2024. URL https://arxiv.org/abs/2408.04840.
- Kexin Yi, Chuang Gan, Yunzhu Li, Pushmeet Kohli, Jiajun Wu, Antonio Torralba, and Joshua B Tenenbaum. Clevrer: Collision events for video representation and reasoning. *arXiv*, 2019.
- Shukang Yin, Chaoyou Fu, Sirui Zhao, Ke Li, Xing Sun, Tong Xu, and Enhong Chen. A survey on multimodal large language models. *arXiv*, 2023.
- Kaining Ying, Fanqing Meng, Jin Wang, Zhiqian Li, Han Lin, Yue Yang, Hao Zhang, Wenbo Zhang, Yuqi Lin, Shuo Liu, Jiayi Lei, Quanfeng Lu, Runjian Chen, Peng Xu, Renrui Zhang, Haozhe Zhang, Peng Gao, Yali Wang, Yu Qiao, Ping Luo, Kaipeng Zhang, and Wenqi Shao. Mmt-bench: A comprehensive multimodal benchmark for evaluating large vision-language models towards multitask agi, 2024.
- Qifan Yu, Juncheng Li, Yu Wu, Siliang Tang, Wei Ji, and Yueting Zhuang. Visually-prompted language model for fine-grained scene graph generation in an open world. In *Proceedings of the IEEE/CVF International Conference on Computer Vision*, pp. 21560–21571, 2023a.
- Qifan Yu, Wei Chow, Zhongqi Yue, Kaihang Pan, Yang Wu, Xiaoyang Wan, Juncheng Li, Siliang Tang, Hanwang Zhang, and Yueting Zhuang. Anyedit: Mastering unified high-quality image editing for any idea. *arXiv*, 2024a.
- Qifan Yu, Juncheng Li, Longhui Wei, Liang Pang, Wentao Ye, Bosheng Qin, Siliang Tang, Qi Tian, and Yueting Zhuang. Hallucidoctor: Mitigating hallucinatory toxicity in visual instruction data. In Proceedings of the IEEE/CVF Conference on Computer Vision and Pattern Recognition, 2024b.
- Weihao Yu, Zhengyuan Yang, Linjie Li, Jianfeng Wang, Kevin Lin, Zicheng Liu, Xinchao Wang, and Lijuan Wang. Mm-vet: Evaluating large multimodal models for integrated capabilities. arXiv, 2023b.
- Zhou Yu, Dejing Xu, Jun Yu, Ting Yu, Zhou Zhao, Yueting Zhuang, and Dacheng Tao. Activitynetqa: A dataset for understanding complex web videos via question answering. In *Proceedings of the AAAI Conference on Artificial Intelligence*, volume 33, pp. 9127–9134, 2019.
- Shenghai Yuan, Jinfa Huang, Yongqi Xu, Yaoyang Liu, Shaofeng Zhang, Yujun Shi, Ruijie Zhu, Xinhua Cheng, Jiebo Luo, and Li Yuan. Chronomagic-bench: A benchmark for metamorphic evaluation of text-to-time-lapse video generation. *arXiv*, 2024.
- Xiang Yue, Yuansheng Ni, Kai Zhang, Tianyu Zheng, Ruoqi Liu, Ge Zhang, Samuel Stevens, Dongfu Jiang, Weiming Ren, Yuxuan Sun, Cong Wei, Botao Yu, Ruibin Yuan, Renliang Sun, Ming Yin, Boyuan Zheng, Zhenzhu Yang, Yibo Liu, Wenhao Huang, Huan Sun, Yu Su, and Wenhu Chen. Mmmu: A massive multi-discipline multimodal understanding and reasoning benchmark for expert agi. In *Proceedings of the IEEE/CVF Conference on Computer Vision and Pattern Recognition*, 2024.

- Kevin Zakka, Yuval Tassa, and MuJoCo Menagerie Contributors. MuJoCo Menagerie: A collection of high-quality simulation models for MuJoCo, 2022. URL http://github.com/ google-deepmind/mujoco_menagerie.
- Michał Zawalski, William Chen, Karl Pertsch, Oier Mees, Chelsea Finn, and Sergey Levine. Robotic control via embodied chain-of-thought reasoning. *arXiv*, 2024a.
- Michał Zawalski, William Chen, Karl Pertsch, Oier Mees, Chelsea Finn, and Sergey Levine. Robotic control via embodied chain-of-thought reasoning. *arXiv*, 2024b.
- Xiaohua Zhai, Basil Mustafa, Alexander Kolesnikov, and Lucas Beyer. Sigmoid loss for language image pre-training, 2023.
- Jun Zhan, Junqi Dai, Jiasheng Ye, Yunhua Zhou, Dong Zhang, Zhigeng Liu, Xin Zhang, Ruibin Yuan, Ge Zhang, Linyang Li, Hang Yan, Jie Fu, Tao Gui, Tianxiang Sun, Yugang Jiang, and Xipeng Qiu. Anygpt: Unified multimodal llm with discrete sequence modeling. ArXiv, abs/2402.12226, 2024. URL https://api.semanticscholar.org/ CorpusID:267750101.
- Hang Zhang, Xin Li, and Lidong Bing. Video-Ilama: An instruction-tuned audio-visual language model for video understanding. arXiv, 2023. URL https://arxiv.org/abs/2306. 02858.
- Jieyu Zhang, Weikai Huang, Zixian Ma, Oscar Michel, Dong He, Tanmay Gupta, Wei-Chiu Ma, Ali Farhadi, Aniruddha Kembhavi, and Ranjay Krishna. Task me anything. *arXiv*, 2024a.
- Yuanhan Zhang, Bo Li, haotian Liu, Yong jae Lee, Liangke Gui, Di Fu, Jiashi Feng, Ziwei Liu, and Chunyuan Li. Llava-next: A strong zero-shot video understanding model, April 2024b. URL https://llava-vl.github.io/blog/2024-04-30-llava-next-video/.
- Haoyu Zhen, Xiaowen Qiu, Peihao Chen, Jincheng Yang, Xin Yan, Yilun Du, Yining Hong, and Chuang Gan. 3d-vla: 3d vision-language-action generative world model. *arXiv*, 2024.
- Chujie Zheng, Zhenru Zhang, Beichen Zhang, Runji Lin, Keming Lu, Bowen Yu, Dayiheng Liu, Jingren Zhou, and Junyang Lin. Processbench: Identifying process errors in mathematical reasoning, 2024a. URL https://arxiv.org/abs/2412.06559.
- Zhicheng Zheng, Xin Yan, Zhenfang Chen, Jingzhou Wang, Qin Zhi Eddie Lim, Joshua B Tenenbaum, and Chuang Gan. Contphy: Continuum physical concept learning and reasoning from videos. In *International Conference on Machine Learning*. PMLR, 2024b.
- Junjie Zhou, Yan Shu, Bo Zhao, Boya Wu, Shitao Xiao, Xi Yang, Yongping Xiong, Bo Zhang, Tiejun Huang, and Zheng Liu. Mlvu: A comprehensive benchmark for multi-task long video understanding. *arXiv*, 2024.
- Luowei Zhou, Chenliang Xu, and Jason Corso. Towards automatic learning of procedures from web instructional videos. In *Proceedings of the AAAI Conference on Artificial Intelligence*, 2018.
- Shuyan Zhou, Frank F Xu, Hao Zhu, Xuhui Zhou, Robert Lo, Abishek Sridhar, Xianyi Cheng, Yonatan Bisk, Daniel Fried, Uri Alon, et al. Webarena: A realistic web environment for building autonomous agents. *arXiv*, 2023.
- Wanrong Zhu, Jack Hessel, Anas Awadalla, Samir Yitzhak Gadre, Jesse Dodge, Alex Fang, Youngjae Yu, Ludwig Schmidt, William Yang Wang, and Yejin Choi. Multimodal c4: An open, billionscale corpus of images interleaved with text. Advances in Neural Information Processing Systems, 36, 2024.

CONTENTS

A	Deta	iled Dataset Collection Process	28
	A.1	Simulation	28
	A.2	Web	28
	A.3	Real-world	29
B	Data	Annotation Protocol	29
	B .1	General Guidelines	29
	B.2	Data Format and Structure	30
	B.3	Quality Control and Validation	30
	B.4	Handling Ambiguities	31
	B.5	Ethical Considerations	31
	B.6	Data Contamination Considerations	31
	B.7	Annotation Platform	31
	B.8	Benchmark Preparation and Release	31
	B.9	More Details of the Annotation Pipeline	32
С	Deta	iled Task Description	33
	C.1	Ability Description	33
	C.2	Physical Object Property Sub-task	33
	C.3	Physical Object Relationships Sub-task	33
	C.4	Physical Scene Understanding Sub-task	35
	C.5	Physics-based Dynamics Sub-task	35
D	Mor	e Dataset Analysis	36
	D.1	Global Statics	36
	D.2	Word Statics and Word Cloud	37
Е	Mor	e Details on the Setup	39
	E.1	Prompt for LLMs	39
	E.2	3D Assets	41
	E.3	Model Hyperparameters	41
		E.3.1 Image VLM	41
		E.3.2 Video VLM	44
		E.3.3 General VLM	44
	E.4	Prompt for VLM test	47
	E.5	Reference Datasets Summary	48
	E.6	Prompt Strategies	48
	E.7	ViperGPT Implementation	49
	E.8	Human Performance	50
F	Mor	e Experiments Results	50

	F.1	GroundingDINO Configuration	50
	F.2	Effect of Visual Prompting	50
	F.3	More PhysBench Results	51
	F.4	PhysBench-val Results	59
	F.5	Embodied Tasks Detailed Description	60
	F.6	Correlation Map	61
	F.7	Performance on Related Benchmarks	62
G	Mor	e Related Works	63
Н	Mor	e Examples	65
	H.1	Physical Object Property Sub-task	65
	H.2	Physical Object Relationships Sub-task	65
	H.3	Physical Scene Understanding Sub-task	65
	H.4	Physics-based Dynamics Sub-task	65
I	Erro	or Study	79
	I.1	Detailed Statics	79
	I.2	Main Reason Analysis	79
	I.3	Case Study	79
J	Disc	ussion and Statement	141
	J.1	Limitation	141
	J.2	Boarder Impact	141
	J.3	Ethics Statement	142
	J.4	Reproducibility Statement	142
K	Late	est Results	142

A DETAILED DATASET COLLECTION PROCESS

A.1 SIMULATION

We use (Blender, 2018) as our simulation platform. We utilized 679 objects and 470 HDR images to generate simulated videos and images. During each simulation, we concurrently save images or videos of depth, normal, and albedo, as well as the corresponding configuration files, which include the position, angle, movement ,and other properties of the object light source.

Image generation. In addition to ambient lighting, we employed two point lights and one sunlight. To ensure data diversity, the positions of the camera and the arrangement of objects (ensuring no overlap and that all objects are captured by the camera) were randomized to some extent. Drawing from the object attribute annotation methods described in Newton (Wang et al., 2023c), we cleaned and re-annotated our data to develop a comprehensive table of objects and their attributes. Utilizing this table, we delineate the relational semantics between different objects and the corresponding queries. Following the approach in BLINK (Fu et al., 2024), each object in the simulated images is demarcated with a bounding box rather than being explicitly mentioned in the text, thereby enhancing the evaluation of the model's image comprehension capabilities.

Despite imposing considerable constraints on our code and meticulously annotating the 3D assets, there remains the possibility of minor object overlaps or incomplete captures of objects by the camera. To ensure that objects in the data are clearly identifiable, we employed GroundingDINO (Liu et al., 2023b) for detection. We only accept images where the labels detected by GroundingDINO match exactly in content and quantity with the generated labels. This process also provides us with the bounding boxes of objects for subsequent annotation. During the later stages of annotation, manual inspection of the images is conducted to ensure accuracy. To improve the detection success rate of GroundingDINO and reduce the probability of false detections, we set the box_threshold to 0.2 and the text_threshold to 0.2. Specifically, these parameter settings were obtained through a grid search, with detailed results presented in Table 14.

Videos with varying lighting conditions. We used only one point light source and arranged objects on a plane to render shadows. The variations in lighting include three aspects: the color of the light, the position of the light source, and the intensity of the light. In terms of the light source position, the movement involves translations along the x, y, and z axes. To avoid ambiguity in lateral directions (Du et al., 2024), during the dataset generation, the movement questions are typically framed in terms of moving along the line connecting two objects rather than simply asking for the direction of movement.

Videos with varying camera conditions. We used the same lighting and other configurations as in the image generation process. During video recording, we randomly altered the camera's position or shooting angle to capture the videos.

Fulid. We used assets from ContPhy (Zheng et al., 2024b) and Unity (Haas, 2014) to generate videos across four types: fluid, rope, cloth, and ball, with 350, 250, 200, and 200 videos respectively. The videos were then manually annotated.

A.2 Web

For web data collection, we primarily use predefined topics (e.g., gases) to retrieve relevant videos or images from the internet (such as middle school physics experiments). After filtering and cleaning the data, we proceed with annotation. Additionally, we leverage large language models (LLMs) to generate suitable descriptions of physics-related concepts, which we then use to search for corresponding videos, followed by further cleaning and annotation.

In addition to the network data collection process described in Section 3.2, we employ the following methods to gather data.

Unsplash. We use high-quality and high-resolution images from Unsplash Ali et al. (2023). 57,859 images are downloaded, and finally we use only about 6,000 images.

Manipulation. We sampled approximately 500 videos from DROID (Khazatsky et al., 2024), Ego4D (Grauman et al., 2022), and MimicPlay (Wang et al., 2023a), providing detailed annotations to generate QA pairs categorized under object-manipulation tasks. The primary focus of these questions is to determine the appropriate sequence of actions based on given instructions, which are derived from the original datasets' descriptions of actions. Figure 42's both first and second examples provide an example of this task. First, we filtered the videos to select those with a strong alignment between the instructions and the visuals, ensuring that the videos were clear, unambiguous, and matched the instructions well. Next, we identified 3-4 keyframes from these videos. The task involved sorting these key frames in the correct order to execute the instructions properly. Additionally, we used FunKPoint (Lai et al., 2021) to annotate the affordance (Gibson, 2014) points in individual images from the original dataset. Specific examples of these annotations can be found in Figure 42's third and fourth examples.

nuScenes. We cropped and annotated videos from the nuScenes (Caesar et al., 2019) mini and test datasets, ultimately obtaining 1,356 QA pairs for spatial movement tasks. We categorized the questions into types such as left turn, straight, and right turn, and included arrows on the images to indicate the direction. The questions asked participants to identify which image they might see based on the indicated direction, as illustrated in Figure 28.

Visual Prompt. In certain tasks, we utilized Visual Prompts (Fu et al., 2024), and through experimentation, we identified an alternative annotation method, detailed in Appendix F.2. For tasks using Visual Prompts, we set the image size to 1024×1024 pixels. In this scale, we standardized the Visual Prompt to a red circle with a 30-pixel radius and white text options with a font size of 65 pixels. The positions of the options' centers in the dataset are recorded in the following format:

"A": [734, 922], "B": [202, 898], "C": [343, 115], "D": [410, 559]

Visual Correspondences. Drawing inspiration from Fu et al. (2024); Sarlin et al. (2020), we also annotated a portion of the corresponding point data using visual prompts. Specific examples can be found in Figure 24.

A.3 REAL-WORLD

We also collected some real-world videos and images, primarily covering sub-tasks related to light, camera, and physical dynamics such as collisions. An iPhone 13 Pro Max was used as the recording device, and all images are in RGBD format.

B DATA ANNOTATION PROTOCOL

B.1 GENERAL GUIDELINES

As previously discussed, there is a significant gap in existing benchmarks, which primarily assess vision-language models (VLMs) based on descriptive tasks without adequately addressing their physical perception and reasoning abilities. To bridge this gap, our benchmark, PhysBench, is designed to provide a comprehensive evaluation framework for physical perception, integrating visual understanding with the assessment of physical properties, spatial relationships, and dynamic phenomena. This approach aims to advance AI systems toward more general-purpose capabilities in real-world physical environments. Our benchmark follows the guidelines outlined below for data collection:

• General Principles:

- Annotations must be accurate, consistent, and adhere to a high standard of academic rigor.
- It covers multiple tasks and topics to mirror real-world applications.
- It incorporates diverse visual contexts and physics knowledge to foster a well-rounded evaluation.
- It offers varying levels of challenge to effectively probe and uncover the potential limitations of current models.

- It provides robust evaluation settings for deterministic assessments.

• Specific Instructions:

- All questions must contain one or more images.
- All questions should be written in English.
- All questions should meet the college-level difficulty.
- Questions should not be ambiguous and must be answerable with one of the given options.
- Clearly categorize each question.
- Annotate all fields, including the question, answer options and other things that follow the format requirement.
- **Review Process:** Ensure that every annotation undergoes a peer review to maintain high standards and minimize errors.

Annotations such as physical properties, spatial relationships, dynamic interactions, and environmental factors are also collected, providing detailed examples that demonstrate the physical perception and reasoning capabilities of the models for further analysis and usage.

B.2 DATA FORMAT AND STRUCTURE

Detailed examples of annotated question examples as shown in Figure 11 are provided in the guidance to serve as a reference for the annotators.

- **JSON File Format:** The structured JSON format will include fields for number, question type, question text, answer options (for multiple-choice), correct answer, question difficulty, and explanation (if there exists).
- Naming Conventions:
 - Each collected sample will be stored in a separate JSON file following a standard naming rule: **subject_{Number}**.json
 - Image Files: **image**_{QuesNum}_{ImageNum}.png

	<pre>{ "scene": "black background", "object": ["glass", "rubber bullet"</pre>
Following the content of the video, which option's corresponding picture will happen first?], "source": "web",
○ A	"file_name": ["iNINchj5IAqn.mp4", "iNINchj5IAqj.png", "iNINchj5IAqk.png",
• B.	<pre>"iNINChj51Aql.png", "iNINChj51Aqm.png"], "question": "Following the content of the <video>, which option's</video></pre>
• C.	<pre>corresponding picture will happen first?\nA. <image/>\nB. <image/>\nC. <image/>\nD. <image/>", "answer": "A", "task type": "dynamics", "task type": "dynamics",</pre>
O D.	<pre>"sub_type": "collision", "ability_type": "prediction", "description": null, "mode": "general" },</pre>

Figure 11: A question-answer pair case in PhysBench and its JSON representation.

B.3 QUALITY CONTROL AND VALIDATION

- A secondary review team will rigorously vet annotations for quality and adherence to guidelines.
- Regular audits of random samples from the dataset will be conducted to ensure sustained quality and consistency.
- Periodic training sessions will be held to update annotators on best practices and any changes in annotation guidelines.
- Feedback mechanisms will be established to promptly address and rectify any identified errors or inconsistencies in the annotations.

B.4 HANDLING AMBIGUITIES

Instances of ambiguity or unclear data should be flagged for detailed review. These instances will be collaboratively examined during team meetings to establish a standardized approach for annotation.

- **B.5** ETHICAL CONSIDERATIONS
 - **Copyright and Licensing:** Adherence to copyright and licensing regulations is strictly enforced. Data from sources that prohibit copying or redistribution will be explicitly avoided.
 - **Data Privacy:** Compliance with privacy laws and ethical standards in data handling is paramount. Annotators must avoid collecting questions that contain any private information.
 - Ethical Data Usage: All data collection and usage must respect ethical guidelines. This includes avoiding biased or harmful content and ensuring that the datasets promote fairness and inclusivity.

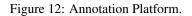
B.6 DATA CONTAMINATION CONSIDERATIONS

The risk of data contamination can be mitigated by assigning annotators to carefully select questions that extend beyond straightforward queries with easily accessible answers. It is essential that tasks rely on provided videos or images for answers rather than the common knowledge of large language models. This approach is beneficial for creating benchmarks that genuinely test the model's ability to comprehend and synthesize information from diverse and challenging sources.

B.7 ANNOTATION PLATFORM

We developed a GUI-based annotation platform, as shown in Figure 12, designed to assist human experts in the data annotation process. Through this program, experts can easily view various media content, such as videos and images, and perform annotations and edits directly within an intuitive interface. The streamlined layout enhances the user experience, ensuring that experts can complete annotation tasks efficiently and accurately, thereby improving the quality and efficiency of the annotations. The purpose of this tool is to simplify the complex annotation workflow, reduce manual effort, and make the annotation process more efficient.

Video and Images Data Overview	Cr Vdro k			S ingr	G tage
Scene		Task Type		Description	
black background		phenomena	11	No description provided	1.
Objects		Sub Type		Mode	
glass, rubber bullet		collision	1	general	1.
Source		Ability Type		Answer	
web		prediction		A	1
Question					
	NChj5IAqn.mp4, which option's corresponding	picture will happen first?			



B.8 BENCHMARK PREPARATION AND RELEASE

For convenience, PhysBench-test consists of 10,002 entries, organized into 19 subclasses, as the test set, and 200 entries as the validation set for parameter choosing (PhysBench-val) since the answers

for the PhysBench will not be publicly available and are hosted similarly to Yue et al. (2024). We also present 89,998 entries for further research. The experimental results presented in this paper, unless otherwise specified, are based on the test set. Importantly, the answer labels for the remaining set will not be publicly released to prevent data leakage, and we will maintain an online evaluation platform. It should be noted that the scores we refer to for PhysBench are based on the entire test dataset, including the validation split.

To ensure that each source dataset is well represented in the validation split and that the distribution of sub-task types and ability types in the validation set is similar to that of the entire dataset, we adopted the following sampling strategy: 1. Randomly sample questions to ensure that the distribution of sub-task and ability types in the validation set matches the full dataset. 2. Randomly sample the remaining questions from each source dataset based on its proportion in the entire dataset.

Additionally, we conducted several quality checks to address any potential errors.

B.9 More Details of the Annotation Pipeline

As described in Section 3.2, all questions were manually annotated by graduate students in STEM fields and subsequently refined through a rigorous review process. The detailed workflow is depicted in Figure 13, where the icon 4 denotes stages involving human participation. The annotators were divided into three groups, each comprising six individuals. During the annotation process, either a GUI interface similar to Figure 12 or direct editing of JSON files was employed. The first group was responsible for video collection, the final group handled quality checks, and the intermediate group completed the remaining steps. A comprehensive explanation of this process is provided below.

Video Collection. Videos and images were sourced through web searches, simulations, and realworld recordings. The collection process utilized predefined simulation rules, LLM-guided queries, and other strategies to identify relevant content. Specifically, for data that could be simulated, we generated it using pre-written simulation scripts, as described in Section A. Additionally, we conducted YouTube searches for videos, leveraging captions generated by GPT to guide annotators in collecting videos. We also sought compilations on topics like "interesting physical phenomena." For real-world recordings, we pre-designed scenarios and objects to capture. Given the complexity of collecting such data, we employed GPT as heuristic tools to expand the search scope and enrich the dataset's diversity. Finally, annotators curated the videos by trimming them to retain only relevant segments and provided detailed physical descriptions, such as the direction of shadow movement or the causes of observed events.

Question Design. In the previous step, we utilized GPT to generate annotations for videos. This approach was adopted after observing that directly inputting a video and prompting GPT to generate question-answer pairs in an in-context learning format often led to suboptimal adherence to instructions. Instead of focusing on generating questions, GPT tended to explain the video content. Additionally, inputting videos directly consumed more tokens, increasing computational costs. Furthermore, annotating videos with captions was considered beneficial for subsequent research leveraging our dataset. Given the complexity of collecting such data, we employed GPT as a heuristic strategy to broaden the scope of search and enhance the diversity of our dataset. GPT generated questions using an in-context learning approach, with the templates provided in Appendix E.1. Notably, all final questions were curated and verified by human annotators, with GPT serving only as a reference.

File Organization. We presented annotators with examples and detailed classification criteria, as outlined in Appendix C and Appendix H. Annotators were then instructed to categorize tasks accordingly and structure each task in the JSON format shown in Figure 11.

Quality Check. After organizing the dataset, we conduct a two-stage review process to ensure its quality. The dataset undergoes human verification to confirm that the questions are relevant to the physical world, rely on all provided input information, are not solely based on common sense, and are accurately categorized with clear questions and corresponding answers. The first stage involves filtering and refining the questions, while the second stage focuses on thorough validation to ensure data accuracy and consistency.

Given the difficulty of acquiring such data, where expressing spe- cific properties often requires multiple images, we undertook a five-step process, spending a total of **4,000 hours** on annotation.



Figure 13: Annotation Pipeline. Icon 🗳 indicate stages involving human participation.

C DETAILED TASK DESCRIPTION

This section primarily introduces the definitions of the various capabilities and sub-tasks. Specific examples can be found in Appendix H. As illustrated in Figure 1, humans not only accurately comprehend visual content but also draw upon knowledge to explain and reason about the scenes they observe. This is the primary goal of most VQA datasets. Building on this foundation, several studies have focused on the commonsense understanding of the geometric relationships and properties within the 3D world. However, the real physical world encompasses not only 3D geometric relationships (e.g., velocity, acceleration, depth), physical scene and environmental factors understanding (e.g., temperature, camera parameters, lighting conditions), and the principles and mechanisms of physical dynamics (e.g., the sequence of collisions, energy transfer, fluid flow, simple physical and chemical reactions, optical and electromagnetic dynamics). To address this gap, we propose PhysBench, which aims to bring Vision-Language Models closer to achieving spatial intelligence (Gupta et al., 2021; Srivastava et al., 2021).

C.1 ABILITY DESCRIPTION

Table 4 presents the description of capability types for PhysBench. The tasks are categorized into four types: physical properties, physical object relationships, physical scene, and physics-based dynamics. Each task type corresponds to different capability types such as recognition, comparison, prediction, judgment, reasoning, and perception, with detailed descriptions provided for each. Specifically, the physical properties task type includes the recognition of object properties and comparisons between the physical properties of different objects. The physical object relationships task type distinguishes between static and dynamic relationships of objects. The physical scene understanding task type involves the prediction, judgment, reasoning, and perception of changes in environmental conditions. The physics-based dynamics task type evaluates the ability to predict, judge, reason, and perceive various physics-based dynamics or phenomena.

C.2 PHYSICAL OBJECT PROPERTY SUB-TASK

Table 5 describes the sub-tasks for object types in PhysBench. The object types are divided into four subcategories: number, mass, color, and attributes. Specifically, the "number" subcategory involves the count of certain objects or changes in their quantity; the "mass" subcategory focuses on approximate changes in object mass, mass estimation, or mass comparison; the "color" subcategory describes the color of objects or color changes; and the "attributes" subcategory covers object characteristics such as rigidity, fluidity, gas, hardness, malleability, elasticity, smoothness, and sharpness.

Notably, our dataset imposes more rigorous evaluations on conventional attributes like mass and color. For instance, in the case of counting tasks, previous works (Kafle & Kanan, 2017; Yi et al., 2019; Chen et al., 2022) typically only require identifying the number of objects in an image. In contrast, our dataset often ties quantities to specific object attributes (e.g., "How many objects of a certain color are outside the plate?" or "How many objects are not blurred by the camera?").

C.3 PHYSICAL OBJECT RELATIONSHIPS SUB-TASK

Table 6 presents the descriptions of physical object relationships sub-tasks in PhysBench. The relationships types are divided into five subcategories: size, location, depth, distance, and movement.

Task type	Ability type	Description
Physical Object Property	Identify	Identify a physical property of an object.
Thysical Object Hoperty	Comparison	Comparison of the same physical property between different
		objects, or changes in a specific property over time.
Physical Object Relationships	Static	The static spatial properties of an object.
r nysieur object iterationsinps	Dynamic	The dynamic spatial properties of an object, meaning the spatial
		properties are changing dynamically.
Physical	Prediction	Predict what might happen if a certain environmental condition
Scene		is changed, or what will happen next.
Understanding	Judgment	Judge what will be different if a certain environmental condition
Chaerstanding		is modified.
	Reasoning	Explain the occurrence reason or condition of the environment.
	Perception	Understand what environment condition change has occurred
		and what its definition is, or determine the environmental at-
		tributes that caused the phenomenon to occur.
Physics-	Prediction	Predict what might happen if a certain object or object attribute
based		in the video is changed, or what will happen next.
Dynamics	Judgment	Judge what will change if a certain attribute is modified, or, for
Dynamies		example, the sequence in which actions occur.
	Reasoning	Explaining the occurrence reason or condition of phenomena.
	Perception	Understand what phenomenon has occurred and what its def-
		inition is, or determine the physical attributes that caused the
		phenomenon to occur.

Table 4: Ability Type Description for PhysBench.

Table 5: Sub-task Description for Physical Object Property Type in PhysBench.

Sub type	Description
Number	The number of certain objects or changes in the number of objects.
Mass	Approximate changes in mass, mass estimation, or mass com- parisons.
Color	Color of an object or changes in color.
Attribute	The attributes or types of objects, such as rigid body, fluid, gas, stiffness, malleability, elasticity, smoothness, sharpness, <i>etc.</i>

Specifically, the "size" subcategory relates to the dimensions of an object; the "location" subcategory describes the absolute and relative positions of objects, including tasks related to object localization and spatial information processing; the "depth" subcategory focuses on an object's depth relative to the camera or depth comparisons between different objects; the "distance" subcategory involves the comparison or estimation of distances between objects as well as their absolute size; and the "move-ment" subcategory addresses the analysis of movement direction, changes in speed, and changes in acceleration.

Table 6: Sub-task Description for Physical Object Relationships Type in PhysBench.

Sub type	Description
Size	The size of the object.
Location	Positional relationships (absolute and relative), including di- rectly or indirectly locating objects and other tasks involving spatial information.
Depth	Depth of an object relative to the camera or depth comparisons between different objects.
Distance	Comparison or estimation of distances between objects or their absolute sizes.
Motion	Motion, velocity, acceleration and the direction of movement, changes in speed, or changes in acceleration.

C.4 PHYSICAL SCENE UNDERSTANDING SUB-TASK

Table 7 describes the sub-tasks for physical scene understanding types in PhysBench. The physical scene understanding types are divided into four subcategories: temperature, camera, gas, and light. Specifically, the "temperature" subcategory involves temperature and its fluctuations, as well as dynamics caused by these changes; the "camera" subcategory focuses on changes in camera position and the resulting effects; the "gas" subcategory covers conditions of the gas environment, such as high pressure, low pressure, or vacuum states; and the "light" subcategory describes the color tone of the light source (warm or cool), changes in the position of the light source, light intensity, and the nature of the light source (point or surface).

Table 7: Sub-task Descri	ption for Physical Scene	Understanding Type in PhysBench.
fuele /. Bue tubit Debell	iption for i hybroar beene	enderstanding Type in Thysbenen.

Sub type	Description
Temperature	The temperature and its changes, as well as phenomena caused by temperature fluctuations.
Viewpoint	The position of the camera and its changes, along with phenom- ena caused by shifts in camera position.
Air	The air environment encompasses conditions such as air pres- sure, humidity, airflow direction, and intensity.
Light	Includes the color tone of the light source (warm or cool), changes in the position of the light source, its intensity, and the nature of the light source (point or surface).

C.5 PHYSICS-BASED DYNAMICS SUB-TASK

Table 8 describes the sub-tasks for physics-based dynamics types in PhysBench. The physics-based dynamics types are divided into six subcategories: collision, throwing, manipulation, fluid, chemistry, and other physics-based dynamics. Specifically, the "collision" subcategory includes physics-based dynamics such as friction between objects, collisions, and explosions; the "throwing" subcategory involves physical world dynamics and phenomena such as throwing and falling; the "manipulation" subcategory focuses on the manipulation of deformable objects and affordance-based sequence arrangements; the "fluid" subcategory covers fluid motion, shapes, and other fluid-related dynamics; the "chemistry" subcategory involves basic chemical reactions or other dynamics or phenomena related to chemistry in the physical world; and the "other" subcategory includes various other dynamics related to the physical world.

Table 8: Sub-task Description for Physics-based Dynamics Type in PhysBench

Sub type	Description
Collision	Friction between objects, collisions, explosions, and similar dy- namics.
Throwing	Throwing, falling, and other physical world dynamics.
Manipulation	Manipulation of deformable objects and affordance-based se- quence arrangements.
Fluid	Fluid motion, shapes, and other fluid-related dynamics.
Chemistry	Basic chemical reactions or other dynamics involving chemical knowledge in the physical world.
Others	Other dynamics related to the physical world.

All of our questions are designed as multiple-choice, with only one correct answer among the four options. Referring to BLINK (Fu et al., 2024), the visual prompt is set as a red circle with a 10px size, which has been found to be the most suitable.

D MORE DATASET ANALYSIS

D.1 GLOBAL STATICS

Question Distribution. Figure 14 further elucidates the distribution of word counts, highlighting the diverse patterns of questions. The average word of the questions within PhysBench is 16.53, while the maximum number of words in a question reaches 48.

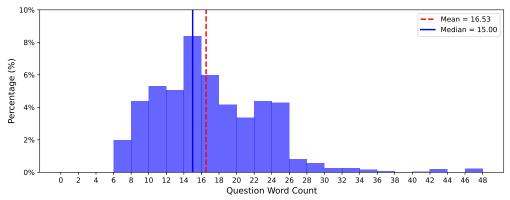


Figure 14: The distribution of the number of words per question in PhysBench. Questions with a length greater than 48 are categorized as 47 for visualization simplicity.

Option Distribution. Figure 15 further elucidates the distribution of word counts, highlighting the diverse patterns of options. The average number of words in the options within PhysBench is 4.36, while the maximum number of words in a question reaches 20. It is worth noting that an "option" here refers to the text following a choice, such as "A. Point A," where the character length is 2.

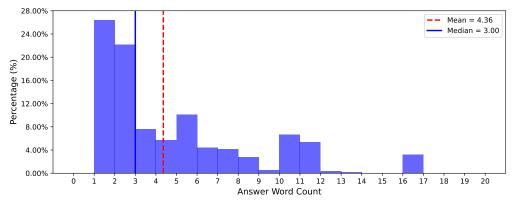


Figure 15: The distribution of the number of words per question in PhysBench. Options with a length greater than 20 are categorized as 20 for visualization simplicity.

Image Resolution. The resolution of most images falls within the 1024-2048 range, accounting for approximately 79.7% of the total images. Only four images in the dataset have a resolution below 256. The minimum resolution is 183, while the maximum is 7201.

Video Resolution. Similarly, the majority of videos have a resolution between 1024-2048, covering about 98.6% of the total videos. Only 1.3% of videos have a resolution below 1024. The highest video resolution is 1920, and the lowest is 370.

Video Frames. Considering that VLMs typically extract keyframes when processing videos—generally selecting 6-8 frames—the total number of frames in the videos doesn't need to be large. However, this doesn't imply that our videos are limited to 6–8 frames. The frame counts are primarily distributed in the ranges of 30–45 frames and 60+ frames, accounting for 59.4% and 35.9% of the total, respectively. The distribution charts for image and video resolution, as well as video frame counts, can be seen in Figure 16.

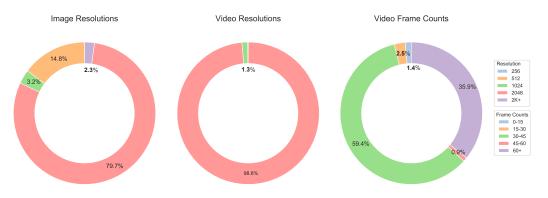


Figure 16: The distribution charts for image and video resolution, as well as video frame counts. From left to right: the distribution of image resolution, the distribution of video resolution, and the distribution of video frame counts.

D.2 WORD STATICS AND WORD CLOUD

We created a word cloud and word frequency chart for our dataset, as shown in Figure 17. It reveals a significant presence of terms related to physical world perception, such as "direction," "camera," "phenomenon," "effects," "relationship," and "light." Additionally, we generated a word cloud and word frequency chart for the **LLaVA-1.5-13B** training data, which includes 595K pretraining samples and 665K instruction-tuning samples, as illustrated in Figure 18.

VILA-1.5-13B. In the pretraining data, CC3M (Sharma et al., 2018) and COYO (Byeon et al., 2022) 25M primarily consist of image captions, while MMC4 (Zhu et al., 2024) 25M includes webpage descriptions, none of which significantly contribute to the model's understanding of the physical world. Therefore, we mainly focus on the instruction-tuning data. The LLaVA-1.5-SFT-665K instruction-tuning data has already been used in LLaVA-1.5-13B, so it is not considered further. Additionally, FLAN (Wei et al., 2021) consists purely of text data and is thus also excluded from consideration.

The data used for VILA-1.5-13B includes the following:

- Captioning: Image Paragraph Captioning (Krause et al., 2017), MSR-VTT (Xu et al., 2016), TextCaps (Sidorov et al., 2020)
- Reasoning: CLEVR (Johnson et al., 2017), NLVR (Suhr et al., 2017), VisualMRC (Tanaka et al., 2021)
- Translation: Multi30k (Elliott et al., 2016)
- VQA: ActivityNet-QA (Yu et al., 2019), DocVQA (Mathew et al., 2021), GQA (Hudson & Manning, 2019), iVQA (Yang et al., 2021), MSRVTT-QA (Xu et al., 2017), MSVD-QA (Xu et al., 2017), OCR-VQA (Mishra et al., 2019), ST-VQA (Biten et al., 2019), Vi-QuAE (Lerner et al., 2022), VQAv2 (Goyal et al., 2017b), Visual Dialog (Das et al., 2017)

According to the guidelines from the VILA repository, the aforementioned instruction-tuning data is all included in M³IT (Li et al., 2023f). Therefore, we use M³IT to analyze the training data for VILA-1.5. The final word frequency statistics and word cloud for the VILA-1.5-13B training data are shown in Figure 19.

PLLaVA-13B. PLLaVA-13B is based on LLaVA-Next (Liu et al., 2024b), with LLaVA-Next incorporating additional data from ShareGPT-4V (Chen et al., 2023a) compared to LLaVA-1.5-13B. The main enhancement from LLaVA-Next to PLLaVA-13B is the addition of 783k instructional video-to-text tuning data, enabling LLaVA-Next to handle video input. Specifically, the training data are sourced from the dataset used in VideoChat2 (Li et al., 2023e), which includes data for various video understanding tasks, such as 27k conversation videos from VideoChat (Li et al., 2023d) and Video-ChatGPT (Maaz et al., 2023b), 80k classification task data from Kinetics (Kay et al., 2017) and SthSthV2 (Goyal et al., 2017a), 450k captioned data from Webvid (Bain et al., 2021), YouCook2 (Zhou et al., 2018), TextVR (Wu et al., 2023c), and VideoChat, 117 reasoning data points from NextQA (Xiao et al., 2021b) and CLEVRER (Yi et al., 2019), and 109k annotated questionanswering samples from Webvid, TGIF (Li et al., 2016), and Ego4D (Grauman et al., 2022). We used ShareGPT-4V and downloaded all the training data from the PLLaVA repository, creating a word cloud and word frequency chart of the training data, as shown in Figure 20.

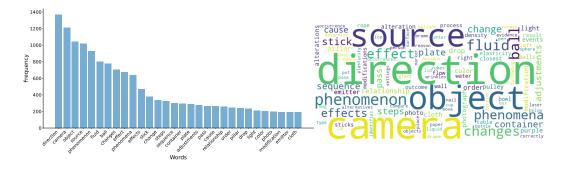


Figure 17: Word Statics and Word Cloud for PhysBench.

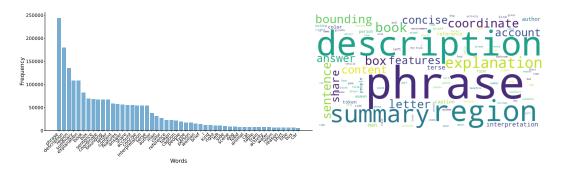


Figure 18: Word Statics and Word Cloud for LLaVA-1.5-13B Training Data.

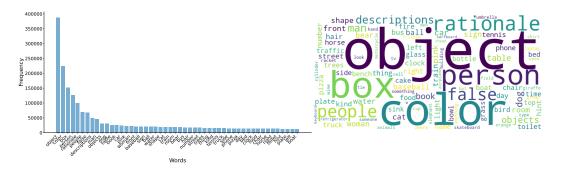


Figure 19: Word Statics and Word Cloud for VILA-1.5-13B Training Data.

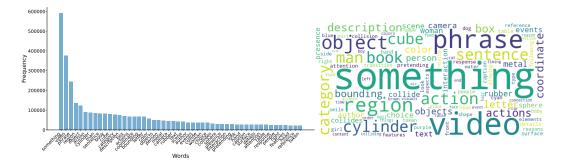


Figure 20: Word Statics and Word Cloud for PLLaVA-13B Training Data.

Observing Figure 18 19 20, we can see that the most frequent words in the training data of LLaVA-1.5-13B, VILA-1.5-13B, and PLLaVA-13B are terms like 'description', 'phrase', 'summary', 'region', and similar words. Keywords such as 'direction' appear much less frequently. We have listed the frequency of several key terms from our dataset in the training data of LLaVA-1.5-13B, VILA-1.5-13B, and PLLaVA-13B, as shown in Figure 21. Although PLLaVA-13B includes words like 'collides' and 'camera', they are primarily used to describe phenomena without addressing the underlying physical mechanisms, which may explain why PLLaVA-13B shows no substantial improvement.

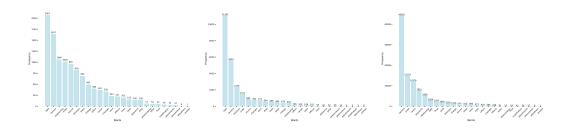


Figure 21: The frequency of common terms in PhysBench within the training data of the LLaVA-1.5-13B, VILA-1.5-13B, and PLLaVA-13B models.

E MORE DETAILS ON THE SETUP

E.1 PROMPT FOR LLMS

Video Cases Prompt. The general system prompt for LLMs to generate video or image cases is as follows:

You are an assistant that communicates only in JSON and is an expert in physics. Do not write normal text.

Your response should be in JSON format with the following string fields:

1. 'video description': A description of the video.

2. 'question': A multiple-choice question based on the video's content.

3. 'answer': A response to the question, with one of the values being 'A', 'B', 'C', or 'D'.

For the same 'video description', you may provide multiple question-answer pairs, which should be presented in a list format.

Important notes: 1. The 'question' should not contain details from the 'video description'. 2. The relationship between each question-answer pair is one of juxtaposition, not progression.

The following is a conversation between the user and the assistant. Ensure that the assistant's answers are as rich and informative as possible.

Then we will the below sentence as the first turn chat and let the LLMs give the more cases in the latter turns. We replace the examples provided in the first turn to enable GPT to generate more diverse responses. Notably, some of the examples generated by GPT do not fully align with the data standards defined in Appendix B. We use these examples solely as references to collect more diverse data. However, as described in Section 3.2, the subsequent data annotation undergoes a rigorous five-step manual process to ensure high data quality.

The process of generating VQA templates is similar: questions are generated based on the captions of the input video or image. However, QA templates are more focused, targeting specific types of relationships, such as those related to spatial positioning.

{"role": "system", "content": (Contents of the color block above)}
{"role": "user", "content": "give me some cases"}
{"role": "assistant", "content":

• Video Description: A ball thrown horizontally from a cliff

– Questions:

- 1. What causes the ball to fall downward?
 - A. Air resistance
 - B. Gravitational force
 - C. Magnetism
 - D. Elastic collision
- 2. Which of the following affects how far the ball travels horizontally?
 - A. Mass of the ball
 - B. Initial velocity of the ball
 - C. Color of the ball
 - D. Shape of the ball
- 3. What happens if the ball is thrown with a higher initial velocity?
 - A. It travels farther horizontally
 - B. It travels shorter horizontally
 - C. It stops mid-air
 - D. It moves vertically upward
- Answers: [B, B, A]
- Video Description: A feather falling in a vacuum chamber
 - Questions:
 - 1. What happens if the vacuum chamber is filled with air?
 - A. The feather falls faster
 - B. The feather falls at the same speed
 - C. The feather floats
 - D. The feather rises upward
 - 2. What would happen to the action if it happened in a strong magnetic field?
 - A. It would fall faster
 - B. It would float
 - C. It would fall slower
 - D. It would remain unaffected
 - Answers: [A, D]

},

{"role": "user", "content": "give me some cases"}

Caption. video or image caption system prompt is as follows:

You are an outstanding video annotator and physicist.

Your task is to provide a detailed description of a given video based on the user's input video and a brief description of the video.

The description should include, but is not limited to, the following aspects:

- 1. The content of the video.
- 2. The principles behind the phenomena observed in the video.
- The properties of certain objects within the video, such as estimated size, mass, color, and type.
 Various spatial information, including relative and absolute positions, sizes, distances, and movements.

Ensure that the descriptions are thorough, precise, and reflect your expertise in physics.

Answer Extraction. The prompt used to instruct GPT-40 is illustrated as follows:

The following sentences contain answers (one of A, B, C, D) and corresponding analysis. Your role is to find the answer.

Please return only one of the four letters: A, B, C, or D.

The sentences are:

E.2 3D ASSETS

The overview of the 3D assets is shown in Figure 22. After defining the object attribute table, we selected 678 objects and annotated their attributes accordingly. For each object, we then adjusted its size and position to ensure that multiple objects (typically 4-5 in our dataset) do not overlap and remain clearly visible. These objects were subsequently used for simulations.



Figure 22: **3D** Assets Sample. We have 678 objects and 470 HDR environment in total for simulation.

E.3 MODEL HYPERPARAMETERS

In our experiments, we conducted comparisons with some of the most recent and representative MLLMs in the following. In our experiments, we conducted comparisons with some of the most recent and representative MLLMs in the following. We divided the models into three categories: **Image VLM**, **Video VLM**, and **General VLM**, according to whether they support only one image input, support a video input (also supports image), or support interlaced video and multiple images.

Following Zhang et al. (2024a), for Image VLMs, we concatenate multiple frames from a video (defaulting to 8 frames) into a single image, arranged from left to right and bottom to top, before inputting it into the model. Thus, both Image VLMs and Video VLMs were tested on question-answer pairs involving only a single image or video, which represent a subset of PhysBench. In contrast, General VLMs, which support interleaved image-text sequences, were tested on the full PhysBench test split.

For most open-source models, we used the hyperparameter torch_dtype = torch.float16. However, for some models that only support torch_dtype = torch.bfloat16, we used torch_dtype = torch.bfloat16 for those cases. Additionally, for other parameter settings, we generally followed the configurations provided in the original papers, their code repositories, or the examples from Hugging Face.

E.3.1 IMAGE VLM

The following is a description of the specific models reviewed, as well as the specific parameter configurations, can be found in Table 9.

- **BLIP-2** (Li et al., 2023c) employs a dual-stage strategy to bridge the modality gap effectively, utilizing a lightweight Q-Former pre-trained on 129 million image-text pairs. In the first stage, the model initiates the learning of vision-language representations by leveraging a frozen image encoder, ViT-g/14 from EVA-CLIP (Fang et al., 2023). In the subsequent stage, a frozen LLM, FlanT5 (Chung et al., 2024), is employed to facilitate vision-to-language generative learning. This innovative approach enables effective zero-shot instructed image-to-text generation. The tested version is BLIP2-t5-xxl (we call it as BLIP-2 in this paper).
- **InstructBLIP** (Dai et al., 2024) is derived from the pre-trained BLIP-2 model (Li et al., 2023c), which integrates a ViT-g/14 image encoder, a Vicuna (Chiang et al., 2023), and a Q-Former that bridges these two components. During the vision-language instruction tuning process, only the Q-Former is fine-tuned, utilizing data from 13 distinct visual question-answering datasets. The tested version is InstructBLIP-t5-xl (we call it as InstructBLIP-

t5-xl in this paper), InstructBLIP-t5-xxl (we call it as InstructBLIP-t5-xxl in this paper), InstructBLIP-vicuna-7b (we call it as InstructBLIP-7B in this paper) and InstructBLIP-vicuna-13b (we call it as InstructBLIP-13B in this paper). It is worth noting that both InstructBLIP-vicuna-7b and InstructBLIP-vicuna-13b provided no responses to a small part of questions. For these instances, we disregarded these questions and did not assign any scores.

- LLaVA-1.5 Liu et al. (2023a). LLaVA (Liu et al., 2024c) establishes a connection between the visual encoder ViT-L/14 from CLIP (Radford et al., 2021) and the language decoder LLaMA (Touvron et al., 2023) using a lightweight, fully connected (FC) layer. Initially, the system trains this FC layer with 595K image-text pairs, while keeping both the visual encoder and LLM static. Subsequently, LLaVA fine-tunes both the FC layer and the LLM using a dataset of 158K instructional vision-language pairs. LLaVa-1.5 (Liu et al., 2023a) is an enhanced version of LLaVA, trained on additional datasets. The tested version is LLaVa-1.5-7b and LLaVa-1.5-13b (we call it as LLaVA-1.5-7B and LLaVA-1.5-13B in this paper).
- Qwen-VL-Chat (Bai et al., 2023b) introduces a series of large-scale vision-language models (LVLMs) designed to perceive and understand both text and images. The Qwen-VL series is built upon the Qwen-LM (Bai et al., 2023a) foundation, augmented with visual capabilities through a meticulously designed visual receptor, input-output interface, and a three-stage training pipeline using a multilingual multimodal cleaned corpus. These models excel in image description, question-answering, grounding, and text-reading by aligning image-caption-box tuples. The series includes Qwen-VL and Qwen-VL-Chat, both of which achieve state-of-the-art performance on a broad range of visual-centric benchmarks and real-world dialog benchmarks, demonstrating their superiority over existing vision-language chatbots. The tested version is Qwen-VL-Chat, as Qwen-VL-Chat have stronger instruction fellow ability than Qwen-VL.
- LLaVA-NeXT (Liu et al., 2024b) is the latest iteration in the LLaVA series (Liu et al., 2024c), building upon the foundation of LLaVA-1.5 (Liu et al., 2023a). This new model enhances visual reasoning, OCR, and world knowledge capabilities. It increases input image resolution to four times more pixels, supporting resolutions up to 672x672, 336x1344, and 1344x336. LLaVA-NeXT features an improved visual instruction tuning data mixture, further enhancing its visual reasoning and OCR capabilities. Additionally, it supports better visual conversations across various scenarios and applications, demonstrating improved world knowledge and logical reasoning. Despite these enhancements, LLaVA-NeXT maintains the minimalist design and data efficiency of its predecessor, utilizing less than 1M visual instruction tuning samples. The tested versions are LLaVA-NeXT-mistral-7b (LLaVA1.6-mistral) and LLaVA-NeXT-vicuna-7b (LLaVA1.6-vicuna), with the base models being Mistral-7b (Jiang et al., 2023) and Vicuna-7b (Chiang et al., 2023), respectively (we call it as LLaVA1.6-mistral and LLaVA1.6-vicuna in this paper).
- InternVL-Chat-V1-5 (Chen et al., 2024c) is an open-source multimodal large language model with enhanced visual understanding through a continuous learning vision encoder, dynamic high-resolution image processing, and a high-quality bilingual dataset. The tested version is InternVL-Chat-V1-5-quantable (we call it as InternVL-Chat1.5), as the GPU memory size restriction of 40G A6000.
- **Cambrian-1** (Tong et al., 2024) is a family of multimodal large language models (MLLMs) designed with a vision-centric approach. This model series addresses the gap between language models and visual representation learning by thoroughly evaluating various visual representations. Cambrian-1 introduces the Spatial Vision Aggregator (SVA), a dynamic and spatially-aware connector that integrates high-resolution vision features with large language models (LLMs) via cross-attention layers (Dai et al., 2024) while reducing the number of tokens. The tested version is Cambrian-1-8b (we call it as Cambrian-8B in this paper).
- MiniCPM-V (Yao et al., 2024). MiniCPM-V2 is a robust multimodal large language model designed for efficient end-side deployment. The model is constructed by integrating SigLip-400M (Zhai et al., 2023) and MiniCPM-2.4B (Hu et al., 2024), connected through a perceiver resampler. The latest iteration, MiniCPM-V2.5, further improves upon

its predecessors. Built on SigLip-400M and Llama3-8B-Instruct with a total of 8B parameters, MiniCPM-V2.5 demonstrates significant performance enhancements over MiniCPM-V2. The most recent and advanced model in the MiniCPM-V series, MiniCPM-V2.6, is built on SigLip-400M and Qwen2-7B (Bai et al., 2023a), also with a total of 8B parameters. MiniCPM-V2.6 shows substantial performance improvements over MiniCPM-Llama3-V2.5 and introduces new capabilities for multi-image and video understanding.

- MolmoE (Deitke et al., 2024). MolmoE is a family of open vision-language models developed by the Allen Institute for AI. The Molmo models are trained on PixMo, a dataset of 1 million highly curated image-text pairs, and exhibit state-of-the-art performance among multimodal models of similar size, while remaining fully open-source. MolmoE-1B is a multimodal Mixture-of-Experts large language model (LLM) with 1.5B active and 7.2B total parameters, based on OLMoE-1B-7B-0924 (Muennighoff et al., 2024). It closely matches the performance of GPT-4V on both academic benchmarks and human evaluations, achieving state-of-the-art performance among similarly-sized open multimodal models. Molmo 7B-O, based on OLMo-7B-1024 (a preview of the next generation of OLMo models), utilizes OpenAI CLIP as its vision backbone, performing between GPT-4V and GPT-40 on both academic benchmarks and human evaluations. Molmo 7B-D, based on Qwen2-7B and also using OpenAI CLIP as its vision backbone, performs similarly, sitting between GPT-4V and GPT-4o in both academic benchmarks and human evaluations. It powers the Molmo demo available at molmo.allenai.org. Finally, Molmo 72B, based on Qwen2-72B with OpenAI CLIP as the vision backbone, achieves the highest academic benchmark score and ranks second in human evaluations, trailing GPT-40 by only a small margin.
- Xinyuan-VL (Group, 2024). Xinyuan-VL-2B is a high-performance multimodal large model developed by the Cylingo Group for end-user applications. It is fine-tuned based on Qwen2-VL-2B (Wang et al., 2024c) and trained on over 5 million multimodal data samples, with additional training on a small amount of plain text data.
- Aquila-VL (Gu et al., 2024). The Aquila-VL-2B model is a VLM trained using the LLava framework. The Qwen2.5-1.5B (Wang et al., 2024c) model serves as the LLM, while siglip-so400m-patch14-384 is employed as the vision tower. The model was trained on our custom-built Infinity-MM dataset, which consists of approximately 40 million image-text pairs. This dataset combines open-source data collected from the internet with synthetic instruction data generated using open-source VLM models.
- **DeepSeek-VL** (Lu et al., 2024a). DeepSeek-VL is an open-source Vision-Language (VL) model designed for real-world applications involving vision and language understanding. It demonstrates broad multimodal capabilities, enabling the processing of logical diagrams, web pages, formula recognition, scientific literature, natural images, and embodied intelligence in complex scenarios. The models we tested, with sizes of 1B and 7B parameters, are respectively sourced from deepseek-ai/deepseek-vl-1.3b-chat and deepseek-ai/deepseek-vl-7b-chat.

PaliGemma 2 (Steiner et al., 2024) represents a significant advancement in visionlanguage modeling, building upon its predecessor by incorporating the sophisticated Gemma 2 architecture. Following the approach of PaLI-3 (Chen et al., 2023b), the PaliGemma model family utilizes open-source components, specifically combining the SigLIP vision model with Gemma 2 language models (Team et al., 2024). This multimodal system effectively processes both visual and textual inputs to generate multilingual outputs. The architecture has been optimized to achieve superior fine-tuning performance across a comprehensive range of vision-language tasks, including image and short video captioning, visual question answering, optical character recognition, object detection, and instance segmentation. The model variants include paligemma2-10b-ft-docci-448, paligemma2-3bft-docci-448.

• Claude (Anthropic, 2024) is a large language model developed by Anthropic with a strong focus on safety, interpretability, and alignment. It has been designed to align with human intent and values, using various methodologies like reinforcement learning from human feedback (RLHF) to ensure that the model behaves as intended. Claude integrates mechanisms to reduce harmful or biased outputs and is optimized for interactive dialogue across a range of domains. In this paper, the tested version is Claude-3-opus, Claude-3-sonnet,

Claude-3-haiku, Claude-3.5-sonnet. Except for Claude-3-haiku, where images were used in their original size, the images for the other three models were resized to 128×128 due to cost considerations. Notably, both Claude-3-sonnet and Claude-3.5-sonnet demonstrated poor adherence to instructions, often failing to provide direct answers as requested in the prompt, instead offering explanations alongside the options. Therefore, we used GPT-40 to extract the answers for scoring, with the prompt provided in Appendix E.1.

E.3.2 VIDEO VLM

The following is a description of the specific models reviewed, as well as the specific parameter configurations, can be found in Table 10.

- **Chat-Univi** (Jin et al., 2023) is a unified vision-language model capable of comprehending and engaging in conversations involving both images and videos through a unified visual representation. Chat-Univi employs a set of dynamic visual tokens to uniformly represent images and videos, enabling it to efficiently utilize a limited number of visual tokens to capture the spatial details necessary for images and the comprehensive temporal relationships required for videos. This approach is supported by a multiscale representation that allows the model to perceive both high-level semantic concepts and low-level visual details. The tested version is Chat-Univi-7B and Chat-Univi-13B.
- Video-LLaVA (Lin et al., 2023a)is a sophisticated multi-modal framework designed to empower large language models (LLMs) with the ability to understand both visual and auditory content in videos. Unlike previous models that handle either visual or audio signals independently, Video-LLaVA integrates both to achieve comprehensive video comprehension. The tested version is Video-LLaVA-7b (we call it as Video-LLaVA in this paper).
- **PLLaVA** (Xu et al., 2024)(Pooling LLaVA) is an advanced video understanding model designed to extend image-based models to video, enabling dense video caption generation. The model employs a simple yet powerful pooling module to bridge image-finetuned Vision-Language Models (Vision-LLM) into the video domain, achieving significant performance improvements in video captioning tasks. The tested versions are PLLaVA-7B and PLLaVA-13B. Notably, since the model uses num_frame as a parameter during loading, our approach for processing images involved duplicating the image for the num_frames input.

We also evaluated VideoChatGPT (Maaz et al., 2023a), Video-LLaMA (Zhang et al., 2023), and VideoChat2 (Li et al., 2024e), and observed that these models exhibit poor instruction-following capabilities. Despite repeatedly prompting them to provide options, the models consistently responded with descriptions of the video or image content rather than addressing the questions posed. As a result, we did not include specific evaluation metrics for these models in our study.

E.3.3 GENERAL VLM

The following is a description of the specific models reviewed, as well as the specific parameter configurations, can be found in Table 11, 12.

- LLaVA-NeXT-Interleave (Li et al., 2024d) is a multimodal large language model that extends LLaVA's capabilities to handle multi-image, video, and 3D data. By using an interleaved data format, it unifies single-image and multi-modal tasks, enabling it to transfer knowledge across different scenarios. The model is trained on the M4-Instruct dataset, which includes over a million samples spanning multi-image, video, and 3D tasks. The tested versions are llava-interleave-qwen-7b-hf (we call it as LLaVA-interleave) and llava-interleave-qwen-7b-dpo-hf (we call it as LLaVA-interleave-dpo in this paper).
- VILA-1.5 (Lin et al., 2023b) is a multimodal visual language model (VLM) designed to handle both multi-image and video understanding tasks. It is pretrained on large-scale interleaved image-text data, which enhances its ability to perform tasks such as video reasoning and in-context learning. The tested versions are VILA-1.5-3B, VILA-1.5-3B-s2, VILA-1.5-8B and VILA-1.5-13B.
- **NVILA** (Liu et al., 2024f) is a family of open Vision-Language Models (VLMs) optimized for efficient video and multi-image understanding. We enhance VILA's architecture

Model	Generation Setup
BLIP-2	torch_dtype = torch.float16, max_new_tokens = 200
InstructBLIP-t5-xl	torch_dtype = torch.float16, max_new_tokens = 200
InstructBLIP-t5-xxl	torch_dtype = torch.float16, max_new_tokens = 200
InstructBLIP-7B	torch_dtype = torch.float16, max_new_tokens = 200
InstructBLIP-13B	torch_dtype = torch.float16, max_new_tokens = 200
LLaVA-1.5-7B	torch_dtype = torch.float16, max_new_tokens = 200, do_sample = False
LLaVA-1.5-13B	torch_dtype = torch.float16, max_new_tokens = 200, do_sample = False
Qwen-VL-Chat	torch_dtype = torch.bfloat16
LLaVA1.6-mistral	torch_dtype = torch.float16, max_new_tokens = 200, do_sample = False
LLaVA1.6-vicuna	torch_dtype = torch.float16, max_new_tokens = 200, do_sample = False
InternVL-Chat1.5	torch_dtype = torch.bfloat16, max_new_tokens = 512, num_beams = 1, do_sample = False
Cambrian-8B	torch_dtype = torch.float16, max_new_tokens = 512, temperature = 0, num_beams = 1, use_cache = True
MiniCPM-V2	dtype = torch.float32, context = None, sampling = False, temperature = 0.1, max_new_token = 10
MiniCPM-V2.5	dtype = torch.float32, context = None, sampling = False, temperature = 0.1, max_new_token = 10
MiniCPM-V2.6	dtype = torch.float32, context = None, sampling = False, temperature = 0.1, max_new_token = 10
MolmoE-1B	<pre>dtype = torch.float32, stop_strings = stop_strings="< endoftext >", dtype = 'auto', max_new_tokens = 200</pre>
MolmoE-7B-O	<pre>dtype = torch.float32, stop_strings = stop_strings="< endoftext >", dtype = 'auto', max_new_tokens = 200</pre>
MolmoE-7B-D	<pre>dtype = torch.float32, stop_strings = stop_strings="< endoftext >", dtype = 'auto', max_new_tokens = 200</pre>
MolmoE-72B	<pre>dtype = torch.float32, stop_strings = stop_strings="< endoftext >", dtype = 'auto', max_new_tokens = 200</pre>
Xinyuan-VL	max_new_tokens = 128, resize = (1024, 1024)
Aquila-VL	do_sample = False, temperature = 0, max_new_tokens = 4096
DeepSeek-VL-1B dtype = torch.bfloat16, max_new_tokens = 10, do_sample=False, use_cache=True	
DeepSeek-VL-7B dtype = torch.bfloat16, max_new_tokens = 10, do_sample=False, use_cache=True	
Claude-3-opus	max_new_tokens = 1000, temperature = 0
Claude-3-sonnet	max_new_tokens = 1000, temperature = 0
Claude-3-haiku	max_new_tokens = 1000, temperature = 0
Claude-3.5-sonnet	max_new_tokens = 1000, temperature = 0

Table 9: Generating parameters for Image VLM. Parameters not explicitly stated indicate the use of the model's default system settings.

Model	Generation Setup
Video-LLaVA	torch_dtype = torch.float16, max_new_tokens = 1024, temperature = 0.1, use_cache = True, do_sample = True
Chat-Univi-7B	torch_dtype = torch.float16, max_new_tokens = 10, temperature = 0, num_beams = 1, use_cache = True, do_sample = False, top_p = None, out- put_scores = True, return_dict_in_generate = True, length_penalty = 1
Chat-Univi-13B	torch_dtype = torch.float16, max_new_tokens = 10, temperature = 0, num_beams = 1, use_cache = True, do_sample = False, top_p = None, out- put_scores = True, return_dict_in_generate = True, length_penalty = 1
PLLaVA-7B	conv_mode = conv_eval_videoqabench, max_new_tokens = 256, do_sample = False
PLLaVA-13B	conv_mode = conv_eval_videoqabench, max_new_tokens = 256, do_sample = False

Table 10: Generating parameters for Video VLM. Parameters not explicitly stated indicate the use of the model's default system settings.

through a 'scale-then-compress' approach, increasing spatial and temporal resolutions before compressing visual tokens, enabling efficient processing of high-resolution images and long videos. Through systematic optimization across training, fine-tuning, and deployment phases, NVILA achieves comparable or superior performance to leading VLMs while reducing training costs by 4.5×, fine-tuning memory by 3.4×, and latency by up to 2.8×. The code and models are publicly available for reproducibility.

- **Phi-3V** (Abdin et al., 2024). Phi-3 is a family of open AI models developed by Microsoft, designed to be the most capable and cost-effective small language models (SLMs) available. Phi-3 models outperform other models of the same size and even those in the next size up across various language, reasoning, coding, and math benchmarks. Phi-3V is the VLM based on Phi-3. The tested version is Phi-3V-128k (we call it as Phi-3V in this paper).
- Phi-3.5V (AzureML, 2024). Phi-3.5V, released on November 15, 2024, is an advanced version of Phi-3V. This state-of-the-art, lightweight multimodal model is built on datasets comprising synthetic data and curated, publicly available web content, with a focus on high-quality, reasoning-rich data in both text and vision. As part of the Phi-3 model family, the multimodal version supports a context length of 128K tokens. The model has undergone a comprehensive enhancement process, including supervised fine-tuning and direct preference optimization, to ensure accurate adherence to instructions and robust safety measures.
- mPLUG-Owl3 (Ye et al., 2024). Here's a refined version of your sentence: mPLUG-Owl3 is a state-of-the-art multimodal large language model designed to address the challenges of understanding long image sequences. mPLUG-Owl3 introduces *Hyper Attention*, a method that enhances the speed of visual sequence processing in multimodal large language models by sixfold, enabling the handling of sequences up to eight times longer. Simultaneously, mPLUG-Owl3 maintains exceptional performance across single-image, multi-image, and video tasks. The tested versions are mPLUG-Owl3-1B (mPLUG-Owl3-1B-241014), mPLUG-Owl3-2B (mPLUG-Owl3-2B-241014) and mPLUG-Owl3-7B (mPLUG-Owl3-7B-241101).
- InternVL2 (Wang et al., 2024e). InternVL 2.0 is the latest iteration in the InternVL series of multimodal large language models. It includes a range of instruction-tuned models, with parameter sizes ranging from 1 billion to 108 billion. In comparison to state-of-theart open-source multimodal large language models, InternVL 2.0 outperforms most opensource alternatives and demonstrates competitive performance that rivals proprietary commercial models. Its capabilities include document and chart comprehension, infographics question answering, scene text understanding and OCR tasks, scientific and mathematical problem-solving, as well as cultural understanding and integrated multimodal processing. InternVL 2.0 is trained with an 8K context window and incorporates training data consisting of long texts, multiple images, and videos. This training significantly enhances its ability to process and understand these types of inputs, surpassing the capabilities of InternVL

1.5 (Chen et al., 2023c). For larger model variants, we implement a merge-based approach rather than sequential processing for video data to optimize GPU memory consumption, as demonstrated in Table 28.

- InternVL 2.5 (Gao et al., 2024b) was released on December 9, 2024, representing an advanced iteration in the multimodal large language model (MLLM) series. While maintaining the core architecture of InternVL 2.0, it introduces significant enhancements in training strategies, testing methodologies, and data quality. The model preserves the "ViT-MLP-LLM" paradigm established by its predecessors, InternVL 1.5 and 2.0. This new version integrates a newly incrementally pre-trained InternViT with various pre-trained LLMs, including InternLM 2.5 and Qwen 2.5, utilizing a randomly initialized MLP projector. Consistent with previous implementations, InternVL 2.5 employs a pixel unshuffle operation, reducing visual tokens to one-quarter of their original count, and adopts a dynamic resolution strategy similar to InternVL 1.5, processing images in 448×448 pixel tiles. A significant advancement since InternVL 2.0 is the expansion of capabilities to include multi-image and video data processing. For larger model variants, we implement a merge-based approach rather than sequential processing for video data to optimize GPU memory consumption, as demonstrated in Table 28.
- LLaVA-NeXT-Video (Zhang et al., 2024b) is a multimodal large language model designed to excel in video understanding tasks through zero-shot modality transfer. Trained primarily on image data, it demonstrates impressive performance on video tasks by leveraging deep learning models with DPO training and AI feedback. The model supports various deployment scenarios, from cloud environments to edge devices, making it highly versatile. It is part of the broader LLaVA-NeXT suite, focused on advancing visual-language integration. The tested version are LLaVA-NeXT-Video-7B-Qwen and LLaVA-NeXT-Video-7B-Qwen-dpo, we call them as LLaVA-NV and LLaVA-NV-dpo respectively in this paper.
- Mantis (Jiang et al., 2024) is a multimodal large language model designed for interleaved multi-image tasks. Built on the LLaMA-3 architecture, it excels in co-reference, reasoning, comparison, and temporal understanding. Mantis uses the Mantis-Instruct dataset, containing 721K examples, to train on various multi-image skills. It achieves state-of-theart performance on some interleaved benchmarks, while maintaining strong single-image performance on par with CogVLM (Wang et al., 2023b). The tested version are Mantis-Idefics2, Mantis-LLaVA, Mantis-siglip-llama3 and Mantis-clip-llama3.
- **GPT** (Achiam et al., 2023). GPT-4V is an advanced multimodal model that extends GPT-4's capabilities with integrated vision processing, allowing it to understand and generate text based on visual inputs. GPT-4o is an optimized variant designed for better performance in language tasks while maintaining lower computational requirements. GPT-4o-mini is a more lightweight version of GPT-4o, designed for deployment in resource-constrained environments while still providing strong performance in language understanding and generation tasks. The version of GPT-4V used is GPT-4-turbo. Notably, due to token length limitations, all images were resized to 512×512 before being input into GPT. Our testing was conducted around mid-August 2024, using the most advanced model available at that time. The remaining models were also tested during this period.
- **Gemini-1.5** (Team et al., 2023). Gemini-1.5-Flash and Gemini-1.5-Pro are advanced multimodal large language models, each designed with distinct capabilities for different performance needs. Gemini-1.5-Flash emphasizes fast processing and efficient memory usage, making it ideal for tasks requiring speed on devices with limited resources. Our testing of Gemini-1.5-Flash and Gemini-1.5-Pro was conducted around mid-August 2024.

E.4 PROMPT FOR VLM TEST

Referring to Liu et al. (2024c), during testing, we appended an end prompt to each question-answer pair (i.e., the value corresponding to the "question" key in the Figure 11). The end prompt is as follows:

Answer with the option's letter from the given choices directly. You can only answer one letter from A, B, C, or D.

Consistent with Zhang et al. (2024a), when asking video-related questions to Image VLMs, we prepend the prompt with the following statement:

This is a series of images sampled at equal intervals from the beginning to the end of a video. Based on the series of images, output the best option for the question.

For Video VLMs, due to their weaker instruction-following capabilities, we provided additional prompts during testing to guide the models in selecting the correct answer rather than simply describing the video content. (Despite this, many models still responded with video descriptions rather than answering the questions, as noted in Appendix E.3.2.) For Video LLMs, if the question involves only a single image input, we prepend the following statement:

Based on the image, output the best option for the question. You must only output the option.

Add the last line in the prompt:

The best choice option is:

If the input involves only a single video, we prepend the following statement:

This is a series of images sampled at equal intervals from the beginning to the end of a video. Based on the series of images, answer the question. Based on the video, output the best option for the question. You must only output the option.

E.5 REFERENCE DATASETS SUMMARY

Our dataset was entirely annotated by humans and underwent two rounds of rigorous filtering and screening. The data sources we utilized, along with their respective uses, are detailed in Table 13.

E.6 **PROMPT STRATEGIES**

In Section 4.1, we explore several prompting strategies:Chain of Thought (CoT) (Kojima et al., 2023) with the prompt "Let's think step-by-step!"; Desp-CoT (Wu et al., 2023d), which begins with an image description prompt; and Pure Language Reasoning (PLR), similar to Mathvista (Lu et al., 2024b). The specific prompt content can be found in Appendix E.6. Following the settings of Kojima et al. (2022); Chen et al. (2024b), we extract the final generated answer through GPT-4o-mini. In this section, we provide the prompts used to implement these three strategies. Note that for Phi-3V:

(1.1) The prompt for CoT (Kojima et al., 2023) is:

Let's think step by step! Start by selecting the correct option's letter from the given choices, then provide a detailed explanation of your thought process.

(1.2) The prompt for Desp-CoT (Wu et al., 2023d) is:

Each image or video is followed by a description, which you can refer to. Answer with the option's letter from the given choices directly.

(1.3) The prompt for PLR is:

Each image or video is replaced by description. Answer with the option's letter from the given choices directly.

For GPT-40:

(2.1) The prompt for CoT (Kojima et al., 2023) is:

Let's think step by step! Start by selecting the correct option's letter from the given choices, then provide a detailed explanation of your thought process.

(2.2) The prompt for Desp-CoT (Wu et al., 2023d) is:

Each image or video is followed by a description, which you can refer to. Answer with the option's letter from the given choices directly.

(2.3) The prompt for PLR is:

Each image or video is replaced by description. Answer with the option's letter from the given choices directly.

We used the following prompts to generate the corresponding descriptions for each model (for image descriptions, "video" is replaced with "image" where applicable):

Give me the description of this video.

E.7 VIPERGPT IMPLEMENTATION

Following the methodology described in ContPhy (Zheng et al., 2024b), since the code for its model, ContPro, has not been released, we implemented an oracle neural-symbolic model using ViperGPT (Surs et al., 2023), which we refer to as ContPhy, and evaluated it on the PhysBench. Similar to ContPhy (Zheng et al., 2024b), we decomposed the question-answering task into four main modules: video perception, physical simulation, program parser, and symbolic execution.

Given a raw video, the video perception module detects objects and their associated static attributes using the MASK-RCNN detector (He et al., 2017). The physical simulator takes point clouds as input and predicts object dynamics across various scenarios using dynamic prediction models (Li et al., 2018; Sulsky et al., 1995). The program parser, powered by a large language model (we use GPT-4o), translates the question query into executable Python programs. Based on the detected object attributes and predicted dynamics, the symbolic executor runs the programs to derive the answer to the question.

Since neuro-symbolic approaches rely on pre-trained domain-specific modules to extract objects' static attributes, physical properties, and dynamic trajectories, this method is not suitable for the complex and diverse tasks in PhysBench. For instance, in ContPhy, simulating four types of tasks—rope, cloth, ball, and fluid—requires pre-training three models: MASK R-CNN (He et al., 2017) based on Detectron2 (Wu et al., 2019), DPI-Net (Li et al., 2018), and Material Point Method (MPM) (Sulsky et al., 1995). Given the variety of tasks in PhysBench, where even individual tasks within certain subcategories can differ significantly, it is impractical to design and call a specific module for every task. Therefore, we designed an Oracle model for the QA pairs generated through specific simulations to ensure that the tasks are similar enough to allow the use of consistent logical processing templates following Zheng et al. (2024b), while GPT-4o directly provided answers for the remaining questions without invoking additional modules or running Python code.

Following the approach in ContPhy, we use ResNet-50 (He et al., 2016) as the backbone for MASK R-CNN to densely detect object locations in each frame and associate static attributes such as color and material. We use the default config from Detectron2, while the number of classes is different across scenarios. Specifically, the batch size is 16 for 8 GPUs thus each mini-batch has 2 images per GPU. We train the model for about 10k iterations, with a learning rate of 0.01. For image size, we keep the original resolution.

We fine-tune the network using the training set data from all simulations. For scenes involving fluid and soft-body dynamics, we adopt MPM, while DPI-Net is used for other tasks. The training data for these two modules is similar to that of MASK R-CNN, and the overall training procedure is comparable to ContPhy. After extracting objects' static attributes, physical properties, and dynamic trajectories, and parsing the natural language query into an executable program, we run the program using the object states as input and produce the predicted answer. Due to the rich diversity and versatile resources of our dataset, it is challenging to ensure that templates perfectly fit all predefined modules. For example, some videos become significantly distorted when rescaled into a square format, and in certain videos, fluids are difficult to extract as points due to their similar color to the environment. For the specific training parameters of MPM and DPI-Net, we have kept them consistent with ContPhy.

E.8 HUMAN PERFORMANCE

To evaluate human performance on PhysBench, we recruited 12 graduate students in STEM fields and provided monetary compensation for their participation. Each question was assigned to all annotators. To ensure the quality of the results, we followed the methodology of MathVista (Lu et al., 2024b) by implementing qualification questions during participant recruitment. These questions tested basic knowledge of physical world concepts, and only those who answered the qualification questions correctly were deemed eligible for the study. Given the large number of questions in PhysBench, the testing was divided into 10 sessions, delivered as online questionnaires with no time constraints for completion. The average score across all participants was used as the final measure of human performance.

F MORE EXPERIMENTS RESULTS

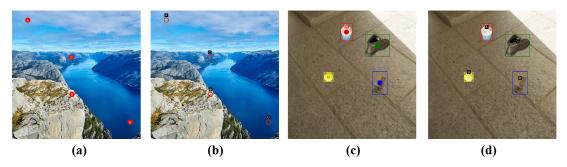
F.1 GROUNDINGDINO CONFIGURATION

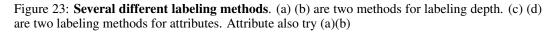
GroundingDINO has two key parameters: box_threshold and text_threshold. The box_threshold parameter is used to filter predictions based on the confidence level of the detected bounding boxes, ensuring that only boxes with confidence scores above this threshold are retained. On the other hand, the text_threshold parameter filters predictions based on their relevance to the input text prompt, retaining only those that meet or exceed this threshold.

It is important to note that the filtered phrases may contain a significant number of duplicates. To address this, we consider a prediction successful only if the set of output phrases matches exactly with the set of input phrases, ensuring both completeness and accuracy. The detailed experimental results are presented in Table 14.

F.2 EFFECT OF VISUAL PROMPTING

To enhance the VLM's responsiveness to visual prompts, we assessed its sensitivity to these prompts. The images used in our tests were all 1024×1024 pixels. We employed two different annotation methods for depth and attribute sub-tasks, as illustrated in Figure 23, drawing on BLINK (Fu et al., 2024) for reference. For depth, the default color for circles is red. Method (a) follows the approach introduced in the BLINK paper, while the second method aligns exactly with the instances in BLINK-eval. Additionally, the prompts for both methods are largely similar to those in the BLINK-eval examples. Similarly, for attributes, we experimented with two annotation methods, denoted as (c) and (d) in Figure 23. However, since the white text doesn't look very clear in the yellow checkbox in the first method, the yellow color was selected.





The test images comprise 1000 samples, with a uniform circle radius of 20 pixels and a font size of 25 pixels. The detailed experimental results are presented in Table 15. For samples (a) and (b), the text prompts require selecting the location or object indicated by the prompt, while samples (c) and

(d) involve identifying a bounding box or point. For instance, answers for (c) and (d) might be "A. The object enclosed in the red box at point A" using both color and letter identifiers.

Based on the experimental results, we find that the outcomes for (a) and (b) are similar in terms of depth and attribute, though (a) performs slightly better. For attributes, (c) and (d) yield results close to random, likely because the tested models cannot perceive color differences in the bounding boxes, thus failing to answer effectively. However, (a) and (b) significantly improve accuracy. Therefore, we ultimately decided to use the annotation method in (a).

Building on the findings of the previous experiment, we further tested the impact of varying circle sizes using the annotation method, which showed the best model performance. The corresponding results are detailed in Table 16. Additionally, the text size was consistently 5 pixels larger than the center of the circle. Based on the previous experiment, we adopted the annotation method (a) for all subsequent annotations. Therefore, we used method (a) to test depth, with a sample size of 1000 images.

We have tested 6 scales as shown in Figure 24 and the results indicate that for LLaVA-1.5, larger sizes generally yield better results. For Phi-3V and VILA-1.5, the optimal radius is 30 pixels, although performance does not show a significant relationship on either side of 30 pixels. Most models show low sensitivity to size variations, except for LLaVA-1.5-7b. To balance performance and aesthetics, we ultimately selected a radius size of 30 pixels.



Figure 24: Visual Prompt with Different Size.

F.3 MORE PHYSBENCH RESULTS

The performance of 39 models across 8 ability categories in PhysBench is presented in Table 17. Note that the ability classifications for the physical scene understanding and physics-based dynamics categories are identical, though their content differs slightly; these are combined here for clarity. Detailed descriptions of the ability classifications can be found in Appendix C.1, while the remaining 36 newly tested models are listed in Appendix K.

The details for Ability Type, Physical Object Property, Physical Object Relationships, Physical Scene Understanding, and Physics-based Dynamics can be found in Table 17, Table 18, Table 19, Table 20, Table 21, respectively.

Model	Generation Setup
LLaVA-interleave	torch_dtype = torch.float16, max_new_tokens = 10, do_sample = False
LLaVA-interleave-dpo	torch_dtype = torch.float16, max_new_tokens = 10, do_sample = False
VILA-1.5-3B	torch_dtype = torch.float16, max_new_tokens = 4000, temperature = 0.1, num_beams = 1, use_cache = False, do_sample = False, top_p = None
VILA-1.5-3B-s2	torch_dtype = torch.float16, max_new_tokens = 4000, temperature = 0.1, num_beams = 1, use_cache = False, do_sample = False, top_p = None
VILA-1.5-8B	torch_dtype = torch.float16, max_new_tokens = 4000, temperature = 0.1, num_beams = 1, use_cache = False, do_sample = False, top_p = None
VILA-1.5-13B	torch_dtype = torch.float16, max_new_tokens = 4000, temperature = 0.1, num_beams = 1, use_cache = False, do_sample = False, top_p = None
Phi-3V	torch_dtype = torch.float16, max_new_tokens = 500, temperature = 0, do_sample = False, length_penalty = 1, repetition_penalty = 1 (When in error analysis the max_new_tokens is set to 5000)
Phi-3.5V	torch_dtype = torch.float16, max_new_tokens = 500, temperature = 0, do_sample = False, length_penalty = 1, repetition_penalty = 1 (When in error analysis the max_new_tokens is set to 5000)
LLaVA-NV	torch_dtype = torch.float16, max_new_tokens = 10
LLaVA-NV-dpo	torch_dtype = torch.bfloat16, max_new_tokens = 10
Mantis-Idefics2	torch_dtype = torch.bfloat16, max_new_tokens = 10, do_sample = False
Mantis-LLaVA	torch_dtype = torch.bfloat16, max_new_tokens = 1, num_beams = 1, do_sample = False, length_penalty = 1, repetition_penalty = 1
Mantis-siglip-llama3	torch_dtype = torch.bfloat16, max_new_tokens = 1, num_beams = 1, do_sample = False
Mantis-clip-llama3	torch_dtype = torch.bfloat16, max_new_tokens = 1, num_beams = 1, do_sample = False
mPLUG-Owl3-1B	max_new_tokens = 100, decode_text = True
mPLUG-Owl3-2B	max_new_tokens = 100, decode_text = True
mPLUG-Owl3-7B	max_new_tokens = 100, decode_text = True
InternVL2-1B	dtype = torch.bfloat16, max_new_tokens = 10, do_sample = False, max_num = 12
InternVL2-2B	dtype = torch.bfloat16, max_new_tokens = 10, do_sample = False, max_num = 12
InternVL2-4B	dtype = torch.bfloat16, max_new_tokens = 10, do_sample = False, max_num = 12
InternVL2-8B	dtype = torch.bfloat16, max_new_tokens = 10, do_sample = False, max_num = 12
InternVL2-26B	dtype = torch.bfloat16, max_new_tokens = 10, do_sample = False, max_num = 1
InternVL2-40B	dtype = torch.bfloat16, max_new_tokens = 10, do_sample = False, max_num = 1
InternVL2-76B	dtype = torch.bfloat16, max_new_tokens = 10, do_sample = False, max_num = 1
GPT-40	max_new_tokens = 300, temperature = 0, seed = 42 (When in error analysis the max_new_tokens is set to 2000)
GPT-4o-mini	$max_new_tokens = 300$, temperature = 0, seed = 42
GPT-4V	max_new_tokens = 300, temperature = 0, seed = 42
Gemini-1.5-flash	stream = True
Gemini-1.5-pro	stream = True

Table 11: Generating parameters for General VLM. Parameters not explicitly stated indicate the use of the model's default system settings.

Model	Generation Setup
InternVL2.5-1B	dtype = torch.bfloat16, max_new_tokens = 10, do_sample = False, max_num = 12
InternVL2.5-2B	dtype = torch.bfloat16, max_new_tokens = 10, do_sample = False, max_num = 12
InternVL2.5-4B	dtype = torch.bfloat16, max_new_tokens = 10, do_sample = False, max_num = 12
InternVL2.5-8B	dtype = torch.bfloat16, max_new_tokens = 10, do_sample = False, max_num = 12
InternVL2.5-26B	dtype = torch.bfloat16, max_new_tokens = 10, do_sample = False, max_num = 1
InternVL2.5-38B	dtype = torch.bfloat16, max_new_tokens = 10, do_sample = False, max_num = 1
InternVL2.5-78B	dtype = torch.bfloat16, max_new_tokens = 10, do_sample = False, max_num = 1
NVILA-8B	default
NVILA-15B	default
NVILA-Lite-8B	default
NVILA-Lite-15B	default

Table 12: Generation parameters for more models (continued from Table 11). All other parameters not specified here use the default model configurations.

Table 13: Datasets Reference for our PhysBench.	'None' indicates that the dataset does not explic-
itly state which license is being used.	

Dataset	License	Description of usage
Unsplash Ali et al. (2023)	https://unsplash.com/license	We crawled some images for annotation and labeling.
ContPhy Zheng et al. (2024b)	CC-BY 4.0	We used his code to generate some of the simulation data.
ChronoMagic-Bench Yuan et al. (2024)	Apache 2.0	As source data, we annotated some QA.
DROID Khazatsky et al. (2024)	CC-BY 4.0	As source data, we annotated some QA data belonging to physics-based dynamics-manuplation type.
Ego4D Grauman et al. (2022)	CC-BY 4.0	As source data, we annotated some QA data belonging to physics-based dynamics-manuplation type.
MimicPlay Wang et al. (2023a)	CC-BY 4.0	As source data, we annotated some QA data belonging to physics-based dynamics-manuplation type.
nuScenes Caesar et al. (2019)	CC BY-NC-SA 4.0	As source data, we annotated some QA data belonging to spatial movement type.
Netwon Wang et al. (2023c)	CC-BY 4.0	As reference data for us to create the attribute table for objects.
FunKPoint Lai et al. (2021)	None	As source data, we annotated some QA data belonging to physics-based dynamics-manuplation type.
PhotoTourism Snavely et al. (2006)	None	As source data, we annotated some QA data belonging to physical scene understanding-camera type.

Table 14: GroundingDINO Acc	uracy with differe	nt box threshold	and text threshold.	The
number of samples tested is 1000.				

text threshold	0.1	0.2	0.3	0.4	0.5	0.6	0.7
0.1	0.015	0	0	0	0	0	0
0.2	0.015	0.075	0.005	0.005	0	0	0
0.3	0.01	0.03	0.06	0.01	0.005	0	0
0.4	0.005	0.015	4	4	0	0	0
0.5	0.005	0.005	0	0	0	0	0
0.6	0.005	0	0	0	0	0	0
0.7	0.005	0	0	0	0	0	0

 Table 15: Comparison of Visual Prompts for Depth and Attribute Annotation.

	De	pth		Attribute				
	Prompt (a)	Prompt (b)	Prompt (a)	Prompt (b)	Prompt (c)	Prompt(d)		
LLaVA-1.5-7b	27.3	27.2	31.5	29.9	25.3	25.2		
LLaVA-1.5-13b	21.2	20.2	41.1	38.5	26.0	25.6		
Phi-3V-128k	78.2	75.8	41.2	40.1	24.8	25.1		
VILA-1.5-8b	19.9	20.3	27.9	26.1	25.9	24.7		

	10	20	30	40	50	60
LLaVA-1.5-7b	19.2	27.3	27.3	28.4	30.9	31.2
LLaVA-1.5-13b	19.9	21.2	24.9	25.2	25.8	27.9
Phi-3V-128k	74.7	78.2	78.8	76.8	73.1	73.0
VILA-1.5-8b	20.3	19.9	26.9	25.3	26.7	22.2

Table 16: Effects of different visual prompt circle radius on Depth task performance.

48.30 57.63		e VLM		-								
	25.20	Image VLM										
57 62	25.39	36.38	35.76	40.06	34.07	42.74	35.83					
57.05	28.40	33.21	53.64	41.90	32.62	47.58	36.28					
25.02	19.31	30.98	24.50	32.21	23.74	29.91	18.28					
39.49	25.70	32.46	35.33	35.88	27.12	33.62	20.18					
55.97	30.78	36.01	53.64	42.51	33.24	48.15	34.29					
47.78	31.26	40.30	45.70	47.40	39.90	45.01	37.38					
52.48	32.70	42.16	42.38	51.17	40.87	43.02	32.65					
36.79	23.82	23.13	21.19	29.15	15.93	28.21	4.97					
52.48	30.78	65.49	42.38	49.75	39.08	43.30	37.13					
51.44	23.75	44.96	39.74	45.16	37.09	50.14	24.25					
64.78	43.96	74.81	56.29	53.62	41.35	44.16	34.39					
28.60	18.57	20.52	13.25	22.02	33.65	11.68	25.65					
53.71	32.70	35.82	58.28	43.93	32.90	43.30	27.83					
47.78	29.97	36.75	52.32	38.43	36.47	43.02	30.22					
53.71	34.95	52.05	60.93	47.20	35.71	43.87	27.73					
61.46	34.33	36.19	58.94	43.32	34.00	47.01	25.15					
	Vide	o VLM										
47.08	29.15	35.45	35.10	42.71	40.59	43.59	31.16					
25.46	14.54	18.10	31.79	24.16	29.74	31.05	18.29					
6.10	3.07	12.50	7.95	13.86	9.00	9.69	17.10					
47.95	30.31	31.72	49.67	42.71	39.42	40.46	34.74					
50.39	31.60	36.94	43.71	44.44	39.77	41.60	29.17					
59.37	37.68	44.21	49.02	47.40	39.07	28.52	32.74					
61.73	37.41	42.90	36.60	47.81	40.84	28.77	31.40					
38.01	28.46	32.15	40.52	39.65	36.15	32.99	33.65					
38.71	29.22	29.12	39.87	39.04	30.97	31.71	34.99					
39.06	29.15	28.97	39.87	37.41	42.48	21.23	30.54					
50.74	32.90	39.25	47.71	44.24	35.94	31.97	29.44					
55.01	34.68	36.64	52.94	47.81	35.06	32.35	32.74					
47.78	31.26	29.85	38.56	42.41	38.76	31.63	32.22					
47.52	32.22	45.28	40.52	43.53	38.35	32.01	31.74					
55.36	31.88	41.18	41.83	42.92	36.76	33.25	27.00					
59.81	32.76	29.28	41.18	41.18	36.28	30.43	33.75					
55.01	32.63	32.72	30.72	42.41	40.84	31.46	34.47					
52.40	31.60	34.71	36.60	40.16	42.75	31.33	30.68					
65.13	37.41	44.05	64.71	55.15	34.99	41.43	24.41					
71.23	45.73	64.20	71.90	56.37	42.75	43.99	28.63					
74.46	36.86	42.90	60.13	55.45	41.25	35.04	27.96					
74.89	43.55	51.51	60.78	54.23	39.05	33.76	31.69					
72.28	45.46	63.57	65.36	53.41	37.92	37.08	34.85					
	55.97 47.78 52.48 52.48 51.44 54.78 28.60 53.71 53.71 51.46 47.78 53.71 61.46 47.78 53.71 61.46 47.95 50.39 (55.37 51.73 38.01 38.71 39.06 59.37 51.73 38.01 38.71 39.07 55.36 55.01 47.78 55.36 55.01 55.40 55.13 71.23 74.46 74.89	$\begin{array}{cccccccccccccccccccccccccccccccccccc$	$\begin{array}{cccccccccccccccccccccccccccccccccccc$	$\begin{array}{cccccccccccccccccccccccccccccccccccc$	$\begin{array}{cccccccccccccccccccccccccccccccccccc$	$\begin{array}{cccccccccccccccccccccccccccccccccccc$	$\begin{array}{cccccccccccccccccccccccccccccccccccc$					

Table 17: **Evaluation Results for 39 VLMs Categorized by Ability Dimensions**. PhysBench includes two evaluation dimensions: ability and task. Table 3 presents results categorized by the task-type dimension.

$\begin{tabular}{ c c c c c c c c c c c c c c c c c c c$	Model		Mass	Color	Attribute					
$\begin{tabular}{ c c c c c c c c c c c c c c c c c c c$										
$\begin{tabular}{ c c c c c c c c c c c c c c c c c c c$		47.14	22.18	44.33	31.37					
$ InstructBLIP-13B Dai et al. (2024) 29.12 28.67 43.33 30.77 \\ BLIP-2 Li et al. (2023c) 51.30 50.85 47.33 34.63 \\ LLaVA-1.5-7B Liu et al. (2023a) 38.99 36.86 52.67 35.63 \\ LLaVA-1.5-13B Liu et al. (2023b) 41.59 52.22 56.67 35.63 \\ LLaVA-1.6-mistral Liu et al. (2024b) 41.07 35.15 61.33 36.41 \\ Qwen-VL-Chat Bai et al. (2024b) 41.07 35.15 61.33 30.45 \\ InternVL-Chat J.5 Chen et al. (2024c) 53.73 57.68 71.00 48.12 \\ Cambrian-8B Tong et al. (2024) 38.13 14.68 25.67 18.52 \\ Claude-3-opus Anthropic (2024) 45.75 54.95 50.33 35.77 \\ Claude-3-opus Anthropic (2024) 40.73 53.24 62.00 38.18 \\ Claude-3-apus Anthropic (2024) 40.73 53.24 62.00 38.18 \\ Claude-3-haiku Anthropic (2024) 40.73 53.24 62.00 38.18 \\ Claude-3-sonnet Anthropic (2024) 56.67 58.02 60.33 36.69 \\ \hline Video-LLaVA Lin et al. (2023) 22.70 22.87 23.00 16.32 \\ Chat-Univi-7B Jin et al. (2023) 24.3 3.07 4.00 5.32 \\ PLaVA-13B Xu et al. (2024) 35.36 48.46 56.33 33.07 \\ PLaVA-13B Xu et al. (2024) 35.36 48.46 56.33 33.07 \\ PLaVA-13B Xu et al. (2024) 55.29 41.30 67.33 42.23 \\ VILA-1.5-3B Lin et al. (2023b) 39.17 29.01 27.00 31.37 \\ VILA-1.5-3B Lin et al. (2023b) 39.86 24.23 33.33 32.72 \\ VILA-1.5-3B Lin et al. (2023b) 39.86 24.23 33.33 32.72 \\ VILA-1.5-3B Lin et al. (2024b) 35.70 38.57 55.67 35.70 \\ LLaVA-NV Zhang et al. (2024b) 35.70 38.57 55.67 35.70 \\ LLaVA-NV Zhang et al. (2024b) 35.70 38.57 55.67 35.70 \\ LLaVA-NV Zhang et al. (2024b) 35.70 38.57 55.67 35.70 \\ LLaVA-NV Zhang et al. (2024b) 35.70 38.57 55.67 35.70 \\ LLaVA-NV Zhang et al. (2024b) 35.70 38.57 55.67 35.70 \\ LLaVA-NV Zhang et al. (2024b) 35.70 38.57 55.67 35.70 \\ LLaVA-NV Zhang et al. (2024b) 35.70 38.57 55.67 35.70 \\ LLaVA-NV Zhang et al. (2024b) 35.70 38.57 55.67 35.70 \\ LLaVA-NV Zhang et al. (2024b) 35.70 38.57 55.67 35.70 \\ LAVA-NV Zhang et al. (2024b) 35.70 38.57 55.67 35.70 \\ LAVA-NV Zhang et al. (2024b) 35.70 38.57 55.67 35.70 \\ L$	InstructBLIP-t5-xxl Dai et al. (2024)	52.86	43.00	54.00	33.22					
$\begin{array}{c c c c c c c c c c c c c c c c c c c $	InstructBLIP-7B Dai et al. (2024)	11.23	34.93	35.57						
$ \begin{array}{c} LLaVA-1.5-7B\ Liu et al. (2023a) \\ 38.99 \\ 36.86 \\ 52.67 \\ 35.63 \\ LLaVA.1.5-ni3tral\ Liu et al. (2024b) \\ 34.49 \\ 32.42 \\ 32.43 \\ 30.74 \\ 40.0 \\ 5.32 \\ PLLaVA-1B\ Lin et al. (2024) \\ 34.84 \\ 47.44 \\ 65.00 \\ 35.06 \\ \hline \\ $	InstructBLIP-13B Dai et al. (2024)	29.12	28.67	43.33	30.77					
$ \begin{array}{c} \text{LLaVA-1.5-13B Liu et al. (2023a)} & 41.59 & 52.22 & 56.67 & 35.63 \\ \text{LLaVA1.6-mistral Liu et al. (2024b)} & 34.49 & 32.42 & 32.67 & 26.76 \\ \text{LLaVA1.6-vicuna Liu et al. (2024b)} & 41.07 & 35.15 & 61.33 & 36.41 \\ \text{Qwen-VL-Chat Bai et al. (2023b)} & 48.35 & 21.50 & 51.33 & 30.45 \\ \text{InternVL-Chat I.5 Chen et al. (2024c)} & 53.73 & 57.68 & 71.00 & 48.12 \\ \text{Cambrian-8B Tong et al. (2024)} & 48.13 & 14.68 & 25.67 & 18.52 \\ \text{Claude-3-opus Anthropic (2024)} & 45.75 & 54.95 & 50.33 & 35.77 \\ \text{Claude-3-sonnet Anthropic (2024)} & 45.75 & 54.95 & 50.33 & 35.77 \\ \text{Claude-3-sonnet Anthropic (2024)} & 40.73 & 53.24 & 62.00 & 38.18 \\ \text{Claude-3-sonnet Anthropic (2024)} & 40.73 & 53.24 & 62.00 & 38.18 \\ \text{Claude-3-sonnet Anthropic (2024)} & 56.67 & 58.02 & 60.33 & 36.69 \\ \hline & Video-LLaVA Lin et al. (2023) & 22.70 & 22.87 & 23.00 & 16.32 \\ \text{Chat-Univi-TB Jin et al. (2023)} & 2.70 & 22.87 & 23.00 & 16.32 \\ \text{Chat-Univi-13B Jin et al. (2024)} & 35.36 & 48.46 & 56.33 & 33.07 \\ PLLaVA-7B Xu et al. (2024) & 35.36 & 48.46 & 56.33 & 33.07 \\ PLLaVA-1B Xu et al. (2024) & 51.30 & 47.44 & 65.00 & 35.06 \\\hline & \hline & General VLM + Interleaved Data \\\hline & LaVA-interleave Li et al. (2024b) & 39.17 & 29.01 & 27.00 & 31.37 \\ VILA-1.5-3B Lin et al. (2023b) & 39.17 & 29.01 & 27.00 & 31.37 \\ VILA-1.5-3B Lin et al. (2023b) & 39.86 & 24.23 & 33.33 & 32.72 \\ VILA-1.5-3B Lin et al. (2023b) & 39.86 & 24.23 & 33.33 & 32.72 \\ VILA-1.5-3B Lin et al. (2024b) & 35.70 & 38.57 & 55.67 & 35.70 \\ LaVA-NV Zhang et al. (2024b) & 36.40 & 39.59 & 54.67 & 36.34 \\ Mantis-Idefics2 Jiang et al. (2024) & 52.51 & 48.81 & 71.00 & 33.598 \\ Mantis-LaVA Jiang et al. (2024) & 45.41 & 37.88 & 61.00 & 38.11 \\ Mantis-Clip-Ilama3 Jiang et al. (2024) & 45.41 & 37.88 & 61.00 & 38.11 \\ Mantis-clip-Ilama3 Jiang et al. (2024) & 45.41 & 37.88 & 61.00 & 38.11 \\ Mantis-clip-Ilama3 Jiang et al. (2024) & 45.41 & 37.88 & 61.00 & 38.11 \\ Mantis-clip-Ilama3 Jiang et al. (2024) & 45.41 & 37.88 & 61.00 & 38.11 \\ Mantis-clip-Ilama3 Jiang et al. (2024) & 45.41 & 37.88 & 61.00 & 38.11 \\$	BLIP-2 Li et al. (2023c)	51.30	50.85	47.33	34.63					
$ \begin{array}{c} \text{LLaVA1.6-mistral Liu et al. (2024b)} & 34.49 & 32.42 & 32.67 & 26.76 \\ \text{LLaVA1.6-vicuna Liu et al. (2024b)} & 41.07 & 35.15 & 61.33 & 36.41 \\ \text{Qwen-VL-Chat Bai et al. (2023b)} & 48.35 & 21.50 & 51.33 & 30.45 \\ \text{InternVL-Chat I.5 Chen et al. (2024c)} & 53.73 & 57.68 & 71.00 & 48.12 \\ \text{Cambrian-8B Tong et al. (2024)} & 38.13 & 14.68 & 25.67 & 18.52 \\ \text{Claude-3-opus Anthropic (2024)} & 45.75 & 54.95 & 50.33 & 35.77 \\ \text{Claude-3-sonnet Anthropic (2024)} & 45.75 & 54.95 & 50.33 & 35.77 \\ \text{Claude-3-sonnet Anthropic (2024)} & 40.73 & 53.24 & 62.00 & 38.18 \\ \text{Claude-3-sonnet Anthropic (2024)} & 40.73 & 53.24 & 62.00 & 38.18 \\ \text{Claude-3-sonnet Anthropic (2024)} & 56.67 & 58.02 & 60.33 & 36.69 \\ \hline & Video VLM \\ \hline & Video-LLaVA Lin et al. (2023) & 22.70 & 22.87 & 23.00 & 16.32 \\ \text{Chat-Univi-7B Jin et al. (2023)} & 2.70 & 22.87 & 23.00 & 16.32 \\ \text{Chat-Univi-13B Jin et al. (2023)} & 2.43 & 3.07 & 4.00 & 5.32 \\ \hline & \text{PLLaVA-7B Xu et al. (2024)} & 35.36 & 48.46 & 56.33 & 33.07 \\ \hline & \text{PLLaVA-13B Xu et al. (2024)} & 51.30 & 47.44 & 65.00 & 35.06 \\ \hline & \hline & \text{General VLM + Interleaved Data} \\ \hline & \text{LLaVA-interleave Dp Li et al. (2024d)} & 55.29 & 41.30 & 67.33 & 42.23 \\ \hline & \text{VILA-1.5-3B Lin et al. (2023b)} & 39.17 & 29.01 & 27.00 & 31.37 \\ \hline & \text{VILA-1.5-3B Lin et al. (2023b)} & 39.86 & 24.23 & 33.33 & 32.72 \\ \hline & \text{VILA-1.5-3B Lin et al. (2024b)} & 35.70 & 38.57 & 55.67 & 35.70 \\ \hline & \text{LaVA-NV Zhang et al. (2024b)} & 36.40 & 39.59 & 54.67 & 36.34 \\ \hline & \text{Mantis-Idefics2 Jiang et al. (2024)} & 45.41 & 37.88 & 61.00 & 38.11 \\ \hline & \text{Mantis-clip-Ilama3 Jiang et al. (2024)} & 45.21 & 47.49 & 32.76 & 65.33 & 35.98 \\ \hline & \text{Mantis-LLaVA Jiang et al. (2024)} & 45.41 & 37.88 & 61.00 & 38.11 \\ \hline & \text{Mantis-clip-Ilama3 Jiang et al. (2024)} & 45.41 & 37.88 & 61.00 & 38.11 \\ \hline & \text{Mantis-clip-Ilama3 Jiang et al. (2024)} & 45.41 & 37.88 & 61.00 & 38.11 \\ \hline & \text{Mantis-clip-Ilama3 Jiang et al. (2024)} & 45.41 & 37.88 & 61.00 & 38.11 \\ \hline & \text{Mantis-clip-Ilama3 Jiang et al. (2023)} & 61.18 & 54.27 & 71.00 & 52.52 \\ \hline & GPT-$	LLaVA-1.5-7B Liu et al. (2023a)	38.99	36.86	52.67	35.42					
$ \begin{array}{c} LLaVA1.6-vicuna Liu et al. (2024b) & 41.07 & 35.15 & 61.33 & 36.41 \\ Qwen-VL-Chat Bai et al. (2023b) & 48.35 & 21.50 & 51.33 & 30.45 \\ InternVL-Chat1.5 Chen et al. (2024c) & 53.73 & 57.68 & 71.00 & 48.12 \\ Cambrian-8B Tong et al. (2024) & 38.13 & 14.68 & 25.67 & 18.52 \\ Claude-3-opus Anthropic (2024) & 45.75 & 54.95 & 50.33 & 35.77 \\ Claude-3-sonnet Anthropic (2024) & 40.73 & 53.24 & 62.00 & 38.18 \\ Claude-3-haiku Anthropic (2024) & 40.73 & 53.24 & 62.00 & 38.18 \\ Claude-3.5-sonnet Anthropic (2024) & 56.67 & 58.02 & 60.33 & 36.69 \\ \hline \\ $	LLaVA-1.5-13B Liu et al. (2023a)	41.59	52.22	56.67	35.63					
Qwen-VL-Chat Bai et al. (2023b) 48.35 21.50 51.33 30.45 InternVL-Chat 1.5 Chen et al. (2024c) 53.73 57.68 71.00 48.12 Cambrian-8B Tong et al. (2024) 38.13 14.68 25.67 18.52 Claude-3-opus Anthropic (2024) 45.75 54.95 50.33 35.77 Claude-3-sonnet Anthropic (2024) 40.73 53.24 62.00 38.18 Claude-3-sonnet Anthropic (2024) 40.73 53.24 62.00 38.18 Claude-3.5-sonnet Anthropic (2024) 56.67 58.02 60.33 36.69 Video VLMVideo VLMVideo VLMVideo VLMGeneral VLM + Interleaved DataLavA-7B Xu et al. (2023) 2.43 3.07 4.00 5.32 PLaVA-13B Xu et al. (2024) 51.30 47.44 65.33 41.66 LaVA-interleave Li et al. (2024d) 51.30 47.44 65.33 41.66 LaVA-interleave-dpo Li et al. (2024d) 55.29 41.30 67.33 42.23 VILA-1.5-3B Lin et al. (2023b) 39.86 24.23 33.33 32.72 VILA-1.5-3B Lin et al. (2023b) 39.86 24.23 33.33 32.72 VILA-1.5-3B Lin et al. (2024b) 35.70 38.57 55.67 35.70 LaVA-NV Apo Zhang et al. (2024b) 36.40 39.59 54.67 36.34 Mathreat al	LLaVA1.6-mistral Liu et al. (2024b)	34.49	32.42	32.67	26.76					
InternVL-Chat1.5 Chen et al. (2024c) 53.73 57.68 71.00 48.12 Cambrian-8B Tong et al. (2024) 38.13 14.68 25.67 18.52 Claude-3-opus Anthropic (2024) 45.75 54.95 50.33 35.77 Claude-3-sonnet Anthropic (2024) 46.73 53.24 62.00 38.18 Claude-3-baiku Anthropic (2024) 56.67 58.02 60.33 36.69 Video VLMVideo-LLaVA Lin et al. (2023a) 22.70 22.87 23.00 16.32 Chat-Univi-7B Jin et al. (2023) 2.43 3.07 4.00 5.32 PLLaVA-7B Xu et al. (2024) 35.36 48.46 56.33 33.07 PLLaVA-13B Xu et al. (2024) 34.84 47.44 65.00 35.06 General VLM + Interleaved DataLLaVA-interleave Li et al. (2024d) 51.30 47.44 65.33 41.66 LLaVA-interleave-dpo Li et al. (2023b) 39.17 29.01 27.00 32.29 VILA-1.5-3B Lin et al. (2023b) 39.17 29.01 27.00 31.37 VILA-1.5-3B Lin et al. (2023b) 39.86 24.23 33.33 32.72 VILA-1.5-3B Lin et al. (2023b) 39.86 24.23 33.33 32.72 VILA-1.5-3B Lin et al. (2024b) 35.70 38.57 55.67 35.70 LaVA-NV Zhang et al. (2024) 47.49 32.76 65.33 36.69 Mantis-Idefics2 Jiang et al. (2024b) 36.40 39.59 54.67 36.34	LLaVA1.6-vicuna Liu et al. (2024b)	41.07	35.15	61.33	36.41					
$\begin{array}{c} \mbox{Cambrian-8B Tong et al. (2024)} & 38.13 & 14.68 & 25.67 & 18.52 \\ \mbox{Claude-3-opus Anthropic (2024)} & 45.75 & 54.95 & 50.33 & 35.77 \\ \mbox{Claude-3-sonnet Anthropic (2024)} & 38.30 & 44.71 & 50.00 & 33.64 \\ \mbox{Claude-3-haiku Anthropic (2024)} & 40.73 & 53.24 & 62.00 & 38.18 \\ \mbox{Claude-3.5-sonnet Anthropic (2024)} & 56.67 & 58.02 & 60.33 & 36.69 \\ \hline & Video VLM \\ \hline & Video-LLaVA Lin et al. (2023a) & 28.13 & 28.33 & 53.00 & 34.49 \\ \mbox{Chat-Univi-7B Jin et al. (2023)} & 22.70 & 22.87 & 23.00 & 16.32 \\ \mbox{Chat-Univi-7B Jin et al. (2023)} & 2.43 & 3.07 & 4.00 & 5.32 \\ \mbox{PLaVA-7B Xu et al. (2024)} & 35.36 & 48.46 & 56.33 & 33.07 \\ \mbox{PLaVA-7B Xu et al. (2024)} & 34.84 & 47.44 & 65.00 & 35.06 \\ \hline & \hline$	Qwen-VL-Chat Bai et al. (2023b)	48.35	21.50	51.33	30.45					
$\begin{array}{c} \mbox{Cambrian-8B Tong et al. (2024)} & 38.13 & 14.68 & 25.67 & 18.52 \\ \mbox{Claude-3-opus Anthropic (2024)} & 45.75 & 54.95 & 50.33 & 35.77 \\ \mbox{Claude-3-sonnet Anthropic (2024)} & 38.30 & 44.71 & 50.00 & 33.64 \\ \mbox{Claude-3-haiku Anthropic (2024)} & 40.73 & 53.24 & 62.00 & 38.18 \\ \mbox{Claude-3.5-sonnet Anthropic (2024)} & 56.67 & 58.02 & 60.33 & 36.69 \\ \hline & Video VLM \\ \hline & Video-LLaVA Lin et al. (2023a) & 28.13 & 28.33 & 53.00 & 34.49 \\ \mbox{Chat-Univi-7B Jin et al. (2023)} & 22.70 & 22.87 & 23.00 & 16.32 \\ \mbox{Chat-Univi-7B Jin et al. (2023)} & 2.43 & 3.07 & 4.00 & 5.32 \\ \mbox{PLaVA-7B Xu et al. (2024)} & 35.36 & 48.46 & 56.33 & 33.07 \\ \mbox{PLaVA-7B Xu et al. (2024)} & 34.84 & 47.44 & 65.00 & 35.06 \\ \hline & \hline$	InternVL-Chat1.5 Chen et al. (2024c)	53.73	57.68	71.00	48.12					
$\begin{array}{c} \mbox{Claude-3-opus Anthropic (2024)} & 45.75 & 54.95 & 50.33 & 35.77 \\ \mbox{Claude-3-sonnet Anthropic (2024)} & 38.30 & 44.71 & 50.00 & 33.64 \\ \mbox{Claude-3-baiku Anthropic (2024)} & 40.73 & 53.24 & 62.00 & 38.18 \\ \mbox{Claude-3.5-sonnet Anthropic (2024)} & 56.67 & 58.02 & 60.33 & 36.69 \\ \hline & Video VLM \\ \hline & Video-LLaVA Lin et al. (2023a) & 22.70 & 22.87 & 23.00 & 16.32 \\ \mbox{Chat-Univi-7B Jin et al. (2023)} & 2.43 & 3.07 & 4.00 & 5.32 \\ \mbox{PLLaVA-7B Xu et al. (2024)} & 35.36 & 48.46 & 56.33 & 33.07 \\ \mbox{PLAVA-7B Xu et al. (2024)} & 34.84 & 47.44 & 65.00 & 35.06 \\ \hline & \hline$		38.13	14.68	25.67	18.52					
$\begin{array}{c} \mbox{Claude-3-sonnet Anthropic (2024)} & 38.30 & 44.71 & 50.00 & 33.64 \\ \mbox{Claude-3-haiku Anthropic (2024)} & 40.73 & 53.24 & 62.00 & 38.18 \\ \mbox{Claude-3.5-sonnet Anthropic (2024)} & 56.67 & 58.02 & 60.33 & 36.69 \\ \hline & Video VLM \\ \hline & Video-LLaVA Lin et al. (2023a) & 38.13 & 28.33 & 53.00 & 34.49 \\ \mbox{Chat-Univi-7B Jin et al. (2023)} & 22.70 & 22.87 & 23.00 & 16.32 \\ \mbox{Chat-Univi-13B Jin et al. (2023)} & 2.43 & 3.07 & 4.00 & 5.32 \\ \mbox{PLLaVA-7B Xu et al. (2024)} & 35.36 & 48.46 & 56.33 & 33.07 \\ \mbox{PLLaVA-13B Xu et al. (2024)} & 34.84 & 47.44 & 65.00 & 35.06 \\ \hline & & & & & & & & & & & & & & & & & &$		45.75	54.95	50.33	35.77					
$\begin{array}{c} \mbox{Claude-3-haiku Anthropic (2024)} & 40.73 & 53.24 & 62.00 & 38.18 \\ \mbox{Claude-3.5-sonnet Anthropic (2024)} & 56.67 & 58.02 & 60.33 & 36.69 \\ \hline & Video VLM \\ \hline \\ \hline Video-LLaVA Lin et al. (2023a) & 38.13 & 28.33 & 53.00 & 34.49 \\ \mbox{Chat-Univi-7B Jin et al. (2023)} & 22.70 & 22.87 & 23.00 & 16.32 \\ \mbox{Chat-Univi-13B Jin et al. (2023)} & 2.43 & 3.07 & 4.00 & 5.32 \\ \mbox{PLLaVA-7B Xu et al. (2024)} & 35.36 & 48.46 & 56.33 & 33.07 \\ \mbox{PLLaVA-13B Xu et al. (2024)} & 34.84 & 47.44 & 65.00 & 35.06 \\ \hline \\ $		38.30	44.71	50.00	33.64					
$\begin{tabular}{ c c c c c c c c c c c c c c c c c c c$		40.73	53.24		38.18					
Video VLM Video-LLaVA Lin et al. (2023a) 38.13 28.33 53.00 34.49 Chat-Univi-7B Jin et al. (2023) 22.70 22.87 23.00 16.32 Chat-Univi-13B Jin et al. (2023) 2.43 3.07 4.00 5.32 PLLaVA-7B Xu et al. (2024) 35.36 48.46 56.33 33.07 PLLaVA-13B Xu et al. (2024) 34.84 47.44 65.00 35.06 General VLM + Interleaved Data LLaVA-interleave Li et al. (2024d) 51.30 47.44 65.33 42.23 VILA-1.5-3B Lin et al. (2023b) 39.17 29.01 27.00 31.37 VILA-1.5-3B-s2 Lin et al. (2023b) 38.82 30.72 28.00 32.29 VILA-1.5-3B Lin et al. (2023b) 39.86 24.23 33.33 32.72 VILA-1.5-13B Lin et al. (2023b) 48.01 36.52 40.00 38.47 Phi-3V Abdin et al. (2024) 43.15 37.88 63.00 40.81 LLaVA-NV Zhang et al. (2024b) 36.70 38.57 55.67 35.70		56.67	58.02	60.33	36.69					
$\begin{array}{c ccccccccccccccccccccccccccccccccccc$		/LM								
$\begin{array}{c ccccccccccccccccccccccccccccccccccc$	Video-LLaVA Lin et al. (2023a)	38.13	28.33	53.00	34.49					
$\begin{array}{c ccccccccccccccccccccccccccccccccccc$										
PLLaVA-7B Xu et al. (2024) 35.36 48.46 56.33 33.07 PLLaVA-13B Xu et al. (2024) 34.84 47.44 65.00 35.06 General VLM + Interleaved DataLLaVA-interleave Li et al. (2024d) 51.30 47.44 65.33 41.66 LLaVA-interleave Li et al. (2024d) 55.29 41.30 67.33 42.23 VILA-1.5-3B Lin et al. (2023b) 39.17 29.01 27.00 31.37 VILA-1.5-3B-s2 Lin et al. (2023b) 38.82 30.72 28.00 32.29 VILA-1.5-8B Lin et al. (2023b) 39.86 24.23 33.33 32.72 VILA-1.5-13B Lin et al. (2023b) 48.01 36.52 40.00 38.47 Phi-3V Abdin et al. (2024) 43.15 37.88 63.00 40.81 LLaVA-NV Zhang et al. (2024b) 36.40 39.59 54.67 36.34 Mantis-Idefics2 Jiang et al. (2024) 47.49 32.76 65.33 36.69 Mantis-LaVA Jiang et al. (2024) 58.41 40.27 61.33 35.98 Mantis-clip-Ilama3 Jiang et al. (2024) 52.51 48.81 71.00 43.79 GPT-40 Achiam et al. (2023) 61.18 54.27 71.00 52.52 GPT-40-mini Achiam et al. (2023) 69.67 50.85 72.33 43.29 Gemini-1.5-flash Team et al. (2023) 72.10 54.95 72.33 48.65 <td></td> <td>2.43</td> <td>3.07</td> <td>4.00</td> <td>5.32</td>		2.43	3.07	4.00	5.32					
$\begin{array}{c c c c c c c c c c c c c c c c c c c $										
LLaVA-interleave Li et al. (2024d)51.3047.4465.3341.66LLaVA-interleave-dpo Li et al. (2024d)55.2941.3067.3342.23VILA-1.5-3B Lin et al. (2023b)39.1729.0127.0031.37VILA-1.5-3B-s2 Lin et al. (2023b)38.8230.7228.0032.29VILA-1.5-8B Lin et al. (2023b)39.8624.2333.3332.72VILA-1.5-13B Lin et al. (2023b)48.0136.5240.0038.47Phi-3V Abdin et al. (2024)43.1537.8863.0040.81LLaVA-NV Zhang et al. (2024b)35.7038.5755.6735.70LLaVA-NV-dpo Zhang et al. (2024b)36.4039.5954.6736.34Mantis-Idefics2 Jiang et al. (2024)47.4932.7665.3336.69Mantis-LaVA Jiang et al. (2024)58.4140.2761.3335.98Mantis-siglip-llama3 Jiang et al. (2024)42.2940.9657.6736.05GPT-4v Achiam et al. (2023)52.5148.8171.0043.79GPT-4o-mini Achiam et al. (2023)69.6750.8572.3343.29Gemini-1.5-flash Team et al. (2023)72.1054.9572.3348.65		34.84	47.44	65.00	35.06					
LLaVA-interleave-dpo Li et al. (2024d)55.2941.3067.3342.23VILA-1.5-3B Lin et al. (2023b)39.1729.0127.0031.37VILA-1.5-3B-s2 Lin et al. (2023b)38.8230.7228.0032.29VILA-1.5-8B Lin et al. (2023b)39.8624.2333.3332.72VILA-1.5-13B Lin et al. (2023b)48.0136.5240.0038.47Phi-3V Abdin et al. (2024)43.1537.8863.0040.81LLaVA-NV Zhang et al. (2024b)35.7038.5755.6735.70LLaVA-NV-dpo Zhang et al. (2024b)36.4039.5954.6736.34Mantis-Idefics2 Jiang et al. (2024)47.4932.7665.3336.69Mantis-LLaVA Jiang et al. (2024)58.4140.2761.3335.98Mantis-clip-llama3 Jiang et al. (2024)42.2940.9657.6736.05GPT-4v Achiam et al. (2023)52.5148.8171.0043.79GPT-4o-mini Achiam et al. (2023)69.6750.8572.3343.29Gemini-1.5-flash Team et al. (2023)72.1054.9572.3348.65	General VLM + In	nterleaved I	Data							
VILA-1.5-3B Lin et al. (2023b)39.1729.0127.0031.37VILA-1.5-3B-s2 Lin et al. (2023b)38.8230.7228.0032.29VILA-1.5-8B Lin et al. (2023b)39.8624.2333.3332.72VILA-1.5-13B Lin et al. (2023b)48.0136.5240.0038.47Phi-3V Abdin et al. (2024)43.1537.8863.0040.81LLaVA-NV Zhang et al. (2024b)35.7038.5755.6735.70LLaVA-NV-dpo Zhang et al. (2024b)36.4039.5954.6736.34Mantis-Idefics2 Jiang et al. (2024)47.4932.7665.3336.69Mantis-LLaVA Jiang et al. (2024)58.4140.2761.3335.98Mantis-clip-llama3 Jiang et al. (2024)42.2940.9657.6736.05GPT-4v Achiam et al. (2023)52.5148.8171.0043.79GPT-4o-mini Achiam et al. (2023)69.6750.8572.3343.29Gemini-1.5-flash Team et al. (2023)72.1054.9572.3348.65	LLaVA-interleave Li et al. (2024d)	51.30	47.44	65.33	41.66					
VILA-1.5-3B Lin et al. (2023b)39.1729.0127.0031.37VILA-1.5-3B-s2 Lin et al. (2023b)38.8230.7228.0032.29VILA-1.5-8B Lin et al. (2023b)39.8624.2333.3332.72VILA-1.5-13B Lin et al. (2023b)48.0136.5240.0038.47Phi-3V Abdin et al. (2024)43.1537.8863.0040.81LLaVA-NV Zhang et al. (2024b)35.7038.5755.6735.70LLaVA-NV-dpo Zhang et al. (2024b)36.4039.5954.6736.34Mantis-Idefics2 Jiang et al. (2024)47.4932.7665.3336.69Mantis-LLaVA Jiang et al. (2024)58.4140.2761.3335.98Mantis-clip-llama3 Jiang et al. (2024)42.2940.9657.6736.05GPT-4v Achiam et al. (2023)52.5148.8171.0043.79GPT-4o-mini Achiam et al. (2023)69.6750.8572.3343.29Gemini-1.5-flash Team et al. (2023)72.1054.9572.3348.65	LLaVA-interleave-dpo Li et al. (2024d)	55.29	41.30	67.33	42.23					
VILA-1.5-8B Lin et al. (2023b)39.8624.2333.3332.72VILA-1.5-13B Lin et al. (2023b)48.0136.5240.0038.47Phi-3V Abdin et al. (2024)43.1537.8863.0040.81LLaVA-NV Zhang et al. (2024b)35.7038.5755.6735.70LLaVA-NV-dpo Zhang et al. (2024b)36.4039.5954.6736.34Mantis-Idefics2 Jiang et al. (2024)47.4932.7665.3336.69Mantis-LLaVA Jiang et al. (2024)58.4140.2761.3335.98Mantis-clip-llama3 Jiang et al. (2024)42.2940.9657.6736.05GPT-4V Achiam et al. (2023)52.5148.8171.0043.79GPT-4o Achiam et al. (2023)69.6750.8572.3343.29Gemini-1.5-flash Team et al. (2023)72.1054.9572.3348.65	VILA-1.5-3B Lin et al. (2023b)	39.17	29.01	27.00	31.37					
VILA-1.5-13B Lin et al. (2023b)48.0136.5240.0038.47Phi-3V Abdin et al. (2024)43.1537.8863.0040.81LLaVA-NV Zhang et al. (2024b)35.7038.5755.6735.70LLaVA-NV-dpo Zhang et al. (2024b)36.4039.5954.6736.34Mantis-Idefics2 Jiang et al. (2024)47.4932.7665.3336.69Mantis-LLaVA Jiang et al. (2024)58.4140.2761.3335.98Mantis-clip-llama3 Jiang et al. (2024)45.4137.8861.0038.11Mantis-clip-llama3 Jiang et al. (2024)42.2940.9657.6736.05GPT-4v Achiam et al. (2023)52.5148.8171.0043.79GPT-4o-mini Achiam et al. (2023)69.6750.8572.3343.29Gemini-1.5-flash Team et al. (2023)72.1054.9572.3348.65	VILA-1.5-3B-s2 Lin et al. (2023b)	38.82	30.72	28.00	32.29					
Phi-3V Abdin et al. (2024)43.1537.8863.0040.81LLaVA-NV Zhang et al. (2024b)35.7038.5755.6735.70LLaVA-NV-dpo Zhang et al. (2024b)36.4039.5954.6736.34Mantis-Idefics2 Jiang et al. (2024)47.4932.7665.3336.69Mantis-LLaVA Jiang et al. (2024)58.4140.2761.3335.98Mantis-clip-llama3 Jiang et al. (2024)45.4137.8861.0038.11Mantis-clip-llama3 Jiang et al. (2024)52.5148.8171.0043.79GPT-4v Achiam et al. (2023)61.1854.2771.0052.52GPT-4o-mini Achiam et al. (2023)69.6750.8572.3343.29Gemini-1.5-flash Team et al. (2023)72.1054.9572.3348.65	VILA-1.5-8B Lin et al. (2023b)	39.86	24.23	33.33	32.72					
Phi-3V Abdin et al. (2024)43.1537.8863.0040.81LLaVA-NV Zhang et al. (2024b)35.7038.5755.6735.70LLaVA-NV-dpo Zhang et al. (2024b)36.4039.5954.6736.34Mantis-Idefics2 Jiang et al. (2024)47.4932.7665.3336.69Mantis-LLaVA Jiang et al. (2024)58.4140.2761.3335.98Mantis-clip-llama3 Jiang et al. (2024)45.4137.8861.0038.11Mantis-clip-llama3 Jiang et al. (2024)52.5148.8171.0043.79GPT-4v Achiam et al. (2023)61.1854.2771.0052.52GPT-4o-mini Achiam et al. (2023)69.6750.8572.3343.29Gemini-1.5-flash Team et al. (2023)72.1054.9572.3348.65	VILA-1.5-13B Lin et al. (2023b)	48.01	36.52	40.00	38.47					
LLaVA-NV-dpo Zhang et al. (2024b)36.4039.5954.6736.34Mantis-Idefics2 Jiang et al. (2024)47.4932.7665.3336.69Mantis-LLaVA Jiang et al. (2024)58.4140.2761.3335.98Mantis-clip-llama3 Jiang et al. (2024)45.4137.8861.0038.11Mantis-clip-llama3 Jiang et al. (2024)42.2940.9657.6736.05GPT-4V Achiam et al. (2023)52.5148.8171.0043.79GPT-4o Achiam et al. (2023)61.1854.2771.0052.52GPT-4o-mini Achiam et al. (2023)69.6750.8572.3343.29Gemini-1.5-flash Team et al. (2023)72.1054.9572.3348.65		43.15	37.88	63.00	40.81					
LLaVA-NV-dpo Zhang et al. (2024b)36.4039.5954.6736.34Mantis-Idefics2 Jiang et al. (2024)47.4932.7665.3336.69Mantis-LLaVA Jiang et al. (2024)58.4140.2761.3335.98Mantis-clip-llama3 Jiang et al. (2024)45.4137.8861.0038.11Mantis-clip-llama3 Jiang et al. (2024)42.2940.9657.6736.05GPT-4V Achiam et al. (2023)52.5148.8171.0043.79GPT-4o Achiam et al. (2023)61.1854.2771.0052.52GPT-4o-mini Achiam et al. (2023)69.6750.8572.3343.29Gemini-1.5-flash Team et al. (2023)72.1054.9572.3348.65	LLaVA-NV Zhang et al. (2024b)	35.70	38.57	55.67	35.70					
Mantis-Idefics2 Jiang et al. (2024)47.4932.7665.3336.69Mantis-LLaVA Jiang et al. (2024)58.4140.2761.3335.98Mantis-siglip-llama3 Jiang et al. (2024)45.4137.8861.0038.11Mantis-clip-llama3 Jiang et al. (2024)42.2940.9657.6736.05GPT-4V Achiam et al. (2023)52.5148.8171.0043.79GPT-4o Achiam et al. (2023)61.1854.2771.0052.52GPT-4o-mini Achiam et al. (2023)69.6750.8572.3343.29Gemini-1.5-flash Team et al. (2023)72.1054.9572.3348.65		36.40	39.59	54.67	36.34					
Mantis-LLaVA Jiang et al. (2024)58.4140.2761.3335.98Mantis-siglip-llama3 Jiang et al. (2024)45.4137.8861.0038.11Mantis-clip-llama3 Jiang et al. (2024)42.2940.9657.6736.05GPT-4V Achiam et al. (2023)52.5148.8171.0043.79GPT-4o Achiam et al. (2023)61.1854.2771.0052.52GPT-4o-mini Achiam et al. (2023)69.6750.8572.3343.29Gemini-1.5-flash Team et al. (2023)72.1054.9572.3348.65		47.49	32.76	65.33	36.69					
Mantis-siglip-llama3 Jiang et al. (2024)45.4137.8861.0038.11Mantis-clip-llama3 Jiang et al. (2024)42.2940.9657.6736.05GPT-4V Achiam et al. (2023)52.5148.8171.0043.79GPT-4o Achiam et al. (2023)61.1854.2771.0052.52GPT-4o-mini Achiam et al. (2023)69.6750.8572.3343.29Gemini-1.5-flash Team et al. (2023)72.1054.9572.3348.65		58.41	40.27	61.33	35.98					
Mantis-clip-llama3 Jiang et al. (2024)42.2940.9657.6736.05GPT-4V Achiam et al. (2023)52.5148.8171.0043.79GPT-4o Achiam et al. (2023)61.1854.2771.0052.52GPT-4o-mini Achiam et al. (2023)69.6750.8572.3343.29Gemini-1.5-flash Team et al. (2023)72.1054.9572.3348.65				61.00						
GPT-4V Achiam et al. (2023)52.5148.8171.0043.79GPT-4o Achiam et al. (2023)61.1854.2771.0052.52GPT-4o-mini Achiam et al. (2023)69.6750.8572.3343.29Gemini-1.5-flash Team et al. (2023)72.1054.9572.3348.65			40.96	57.67	36.05					
GPT-4o Achiam et al. (2023)61.1854.2771.0052.52GPT-4o-mini Achiam et al. (2023)69.6750.8572.3343.29Gemini-1.5-flash Team et al. (2023)72.1054.9572.3348.65										
GPT-4o-mini Achiam et al. (2023)69.6750.8572.3343.29Gemini-1.5-flash Team et al. (2023)72.1054.9572.3348.65										
Gemini-1.5-flash Team et al. (2023) 72.10 54.95 72.33 48.65										
			54.95	72.33	48.65					
	Gemini-1.5-pro Team et al. (2023)									

Table 18: Evaluation Results for 39 VLMs in PhysBench Physical Object Property Sub-task (the fifth last column of Table 3).

LM 0 38.72 1 41.35	30.53		
1 41.35	30.53		
		41.67	53.93
	27.72	51.67	57.30
3 30.92	26.35	20.00	37.08
9 39.10	25.26	43.33	48.31
3 44.74	29.47	46.67	59.55
	35.09	41.67	51.69
4 46.24	32.63	45.00	60.67
9 19.55	24.56	10.00	37.08
9 51.88	72.98	51.67	59.55
3 42.11	45.96	38.33	52.81
0 66.17	76.14	58.33	61.80
9 7.89	31.93	11.67	5.62
0 38.72	31.23	46.67	71.91
1 42.11	28.77	31.67	62.92
9 54.14	47.37	51.67	68.54
3 46.24	25.96	36.67	69.66
LM			
9 40.60	27.72	43.33	50.56
7 19.55	17.89	25.00	35.96
6 16.17	6.32	11.67	15.73
1 34.59	28.42	41.67	60.67
0 42.86	28.42	38.33	57.30
	ıta		
1 53.95	69.47	60.00	37.48
7 53.26	62.46	63.33	36.17
0 40.89	45.61	46.67	28.42
4 37.80	37.19	36.67	26.76
0 22.34	29.47	40.00	31.47
9 52.92	60.35	53.33	32.57
7 53.61	74.39	48.33	26.69
4 35.40	49.47	45.00	26.00
4 35.74	53.68	45.00	50.55
9 58.42	65.61	65.00	32.50
0 47.08	31.93	46.67	26.56
7 41.58	27.72	38.33	32.23
6 39.86	33.68	43.33	33.89
0 59.45	61.40	58.33	38.87
1 70.45	73.33	83.33	60.58
4 51.55	57.19	63.33	39.21
6 70.79	66.32	71.67	44.81
7 71.48	82.11	68.33	58.30
7921729025224725320420015201125030753	79 39.10 39 44.74 29 43.23 14 46.24 79 19.55 29 51.88 33 42.11 20 66.17 29 7.89 50 38.72 21 42.11 29 54.14 43 46.24 LM 29 40.60 57 19.55 36 16.17 21 34.59 20 42.86 terleaved Da 21 53.95 37 53.26 30 40.89 14 35.40 14 35.74 29 52.92 37 53.61 14 35.74 29 58.42 50 47.08 37 41.58 36 39.86 30 59.45 71 70.45 54 51.55 36 70.79	79 39.10 25.26 33 44.74 29.47 29 43.23 35.09 14 46.24 32.63 79 19.55 24.56 29 51.88 72.98 33 42.11 45.96 00 66.17 76.14 29 7.89 31.93 50 38.72 31.23 21 42.11 28.77 29 54.14 47.37 43 46.24 25.96 \overline{LM} $\overline{29}$ 40.60 27.72 719.55 17.89 36 16.17 6.32 21 34.59 28.42 20 42.86 28.42 21 53.95 69.47 77 53.26 62.46 20 42.86 28.42 21 53.95 69.47 77 53.26 62.46 20 42.86 28.42 21 53.95 69.47 77 53.26 62.46 20 42.86 28.42 21 53.95 69.47 77 53.61 74.39 14 35.40 49.47 14 35.40 49.47 14 35.40 49.47 14 35.40 49.47 14 35.40 49.47 23 58.42 65.61 50 59.45 61.40 71 70.45 73.33 54 51.55 <	79 39.10 25.26 43.33 93 44.74 29.47 46.67 29 43.23 35.09 41.67 14 46.24 32.63 45.00 79 19.55 24.56 10.00 29 51.88 72.98 51.67 93 42.11 45.96 38.33 90 66.17 76.14 58.33 29 7.89 31.93 11.67 50 38.72 31.23 46.67 21 42.11 28.77 31.67 29 54.14 47.37 51.67 43 46.24 25.96 36.67 LM 29 40.60 27.72 43.33 57 19.55 17.89 25.00 36 16.17 6.32 11.67 21 53.95 69.47 60.00 07 53.26 62.46 63.33 00 42.86 28.42 38.33

Table 19: Evaluation Results for 39 VLMs in PhysBench Object **A**Relationships Sub-task (the forth last column of Table 3).

Model	Temperature	Viewpoint	Air	Light
	e VLM			
InstructBLIP-t5-xl Dai et al. (2024)	70.59	43.26	26.00	30.03
InstructBLIP-t5-xxl Dai et al. (2024)	80.88	43.36	40.00	30.30
InstructBLIP-7B Dai et al. (2024)	36.76	22.94	12.00	14.74
InstructBLIP-13B Dai et al. (2024)	57.35	21.61	30.61	19.86
BLIP-2 Li et al. (2023c)	79.41	40.90	30.00	29.48
LLaVA-1.5-7B Liu et al. (2023a)	61.76	44.58	24.00	31.76
LLaVA-1.5-13B Liu et al. (2023a)	50.00	40.06	38.00	28.03
LLaVA1.6-mistral Liu et al. (2024b)	45.59	5.66	40.00	8.01
LLaVA1.6-vicuna Liu et al. (2024b)	57.35	44.67	32.00	31.76
Qwen-VL-Chat Bai et al. (2023b)	66.18	20.55	20.00	29.66
InternVL-Chat1.5 Chen et al. (2024c)	72.06	40.43	34.00	31.48
Cambrian-8B Tong et al. (2024)	11.76	22.05	20.00	24.66
Claude-3-opus Anthropic (2024)	72.06	29.59	86.00	27.93
Claude-3-sonnet Anthropic (2024)	54.41	31.39	36.00	31.30
Claude-3-haiku Anthropic (2024)	73.53	26.86	42.00	29.94
Claude-3.5-sonnet Anthropic (2024)	75.00	27.80	68.00	24.48
Video	o VLM			
Video-LLaVA Lin et al. (2023a)	67.65	39.40	30.00	26.02
Chat-Univi-7B Jin et al. (2023)	50.00	14.80	20.00	20.75
Chat-Univi-13B Jin et al. (2023)	20.59	13.29	16.00	17.93
PLLaVA-7B Xu et al. (2024)	60.29	40.81	22.00	31.12
PLLaVA-13B Xu et al. (2024)	66.18	30.63	36.00	30.39
General VLM +	- Interleaved Da	ta		
LLaVA-interleave Li et al. (2024d)	64.71	36.48	41.82	32.85
LLaVA-interleave-dpo Li et al. (2024d)	61.76	35.34	47.27	30.21
VILA-1.5-3B Lin et al. (2023b)	54.41	43.26	14.55	26.11
VILA-1.5-3B-s2 Lin et al. (2023b)	51.47	46.18	10.91	25.48
VILA-1.5-8B Lin et al. (2023b)	44.12	36.29	23.64	25.02
VILA-1.5-13B Lin et al. (2023b)	60.29	32.52	14.55	30.21
Phi-3V Abdin et al. (2024)	52.94	38.93	65.45	29.48
LLaVA-NV Zhang et al. (2024b)	52.94	36.29	18.18	31.12
LLaVA-NV-dpo Zhang et al. (2024b)	51.47	35.25	20.00	31.94
Mantis-Idefics2 Jiang et al. (2024)	63.24	27.43	47.27	29.39
Mantis-LLaVA Jiang et al. (2024)	58.82	41.28	23.64	30.57
Mantis-siglip-llama3 Jiang et al. (2024)	51.47	42.41	43.64	30.57
Mantis-clip-llama3 Jiang et al. (2024)	52.94	33.93	27.27	30.21
GPT-4V Achiam et al. (2023)	88.24	25.07	85.45	22.02
GPT-40 Achiam et al. (2023)	91.18	22.05	83.64	32.67
GPT-40-mini Achiam et al. (2023)	82.35	28.56	83.64	27.75
Gemini-1.5-flash Team et al. (2023)	85.29	33.74	78.18	30.48
Gemini-1.5-pro Team et al. (2023)	85.29	37.32	76.36	31.85

Table 20: Evaluation Results for 39 VLMs in PhysBench Physical **\$**Scene Understanding Sub-task (the third last column of Table 3).

Model			Manipulation	Fluid	Chemistry	Others
		ge VLM				
InstructBLIP-t5-xl Dai et al. (2024)	31.49	34.68	27.89	32.41	62.16	58.16
InstructBLIP-t5-xxl Dai et al. (2024)	32.72	31.35	29.90	33.33	52.70	58.84
InstructBLIP-7B Dai et al. (2024)	19.97	26.60	27.96	29.94	27.03	38.10
InstructBLIP-13B Dai et al. (2024)	28.26	15.44	27.89	35.65	33.78	46.60
BLIP-2 Li et al. (2023c)	33.64	35.39	30.40	31.17	59.46	58.84
LLaVA-1.5-7B Liu et al. (2023a)	36.25	37.77	41.21	45.37	59.46	55.10
LLaVA-1.5-13B Liu et al. (2023a)	33.18	34.92	46.73	50.15	60.81	60.20
LLaVA1.6-mistral Liu et al. (2024b)	24.12	11.64	12.81	7.56	62.16	50.34
LLaVA1.6-vicuna Liu et al. (2024b)	33.03	35.39	44.97	45.22	52.70	61.90
Qwen-VL-Chat Bai et al. (2023b)	32.57	33.25	37.19	47.84	59.46	59.86
InternVL-Chat1.5 Chen et al. (2024c)	35.94	39.90	42.71	43.67	55.41	73.47
Cambrian-8B Tong et al. (2024)	24.88	39.43	28.89	30.56	36.49	23.47
Claude-3-opus Anthropic (2024)	35.79	28.98	25.63	27.78	58.11	69.73
Claude-3-sonnet Anthropic (2024)	38.25	30.64	26.13	35.19	44.59	57.48
Claude-3-haiku Anthropic (2024)	35.94	39.90	34.42	30.40	67.57	68.37
Claude-3.5-sonnet Anthropic (2024)	34.25	37.05	27.64	28.09	50.00	71.09
	Vid	eo VLM				
Video-LLaVA Lin et al. (2023a)	35.48	38.48	29.15	46.30	54.05	53.74
Chat-Univi-7B Jin et al. (2023)	29.80	37.77	5.78	26.39	52.70	40.48
Chat-Univi-13B Jin et al. (2023)	5.38	12.59	12.81	11.27	20.27	17.01
PLLaVA-7B Xu et al. (2024)	33.79	40.86	28.89	41.20	59.46	57.14
PLLaVA-13B Xu et al. (2024)	36.25	39.43	29.90	39.20	58.11	63.61
Ge		+ Interleave	ed Data			
LLaVA-interleave Li et al. (2024d)	31.98	41.57	26.30	40.43	45.95	56.40
LLaVA-interleave-dpo Li et al. (2024d)	33.63	40.38	28.59	44.60	50.00	54.22
VILA-1.5-3B Lin et al. (2023b)	31.07	38.00	30.88	39.35	35.14	45.78
VILA-1.5-3B-s2 Lin et al. (2023b)	25.64	35.63	30.76	33.02	40.54	45.78
VILA-1.5-8B Lin et al. (2023b)	35.29	37.05	18.58	52.16	51.35	41.42
VILA-1.5-13B Lin et al. (2023b)	32.43	35.87	30.88	38.73	45.95	46.87
Phi-3V Abdin et al. (2024)	33.18	35.39	28.95	35.34	59.46	56.68
LLaVA-NV Zhang et al. (2024b)	29.71	41.57	29.35	44.44	59.46	45.90
LLaVA-NV-dpo Zhang et al. (2024b)	29.41	39.43	30.92	44.44	54.05	46.45
Mantis-Idefics2 Jiang et al. (2024)	32.88	33.25	28.59	38.43	41.89	57.49
Mantis-LLaVA Jiang et al. (2024)	27.75	40.14	28.11	40.74	43.24	41.96
Mantis-siglip-llama3 Jiang et al. (2024)	34.09	35.87	25.33	46.14	60.81	50.14
Mantis-clip-llama3 Jiang et al. (2024)	36.95	41.33	22.92	45.06	52.70	56.13
GPT-4V Achiam et al. (2023)	35.29	- 25.18 -	35.22	41.20	70.27	81.20
GPT-40 Achiam et al. (2023)	43.74	46.32	35.22	39.20	62.16	86.92
GPT-4o-mini Achiam et al. (2023)	37.41	39.90	25.33	46.76	71.62	78.75
Gemini-1.5-flash Team et al. (2023)	38.86	38.95	24.61	38.43	70.27	77.38
Gemini-1.5-pro Team et al. (2023)	34.24	39.43	27.62	39.81	68.92	80.93

Table 21: Evaluation Results for 39 VLMs in PhysBench Physics-based Δ Dynamics Sub-task (the second last column of Table 3).

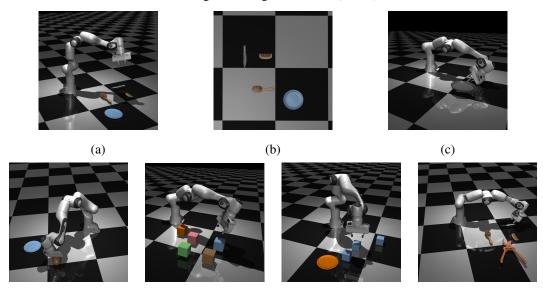
F.4 PHYSBENCH-VAL RESULTS

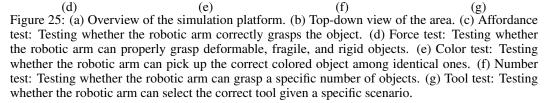
		Format		√ Relationships			Avg
Random Choice	-	-	25.00	25.00	25.00	25.00	25.00
		Image					
InstructBLIP-t5-xl Dai et al. (2024)	4B	merge	40.54	47.62	45.95	44.44	44.69
InstructBLIP-t5-xxl Dai et al. (2024)	12B	merge	48.65	52.38	43.24	49.21	48.60
InstructBLIP-7B Dai et al. (2024)	7B	merge	28.57	30.95	36.36	35.48	33.14
InstructBLIP-13B Dai et al. (2024)	13B	merge	30.56	32.50	60.00	36.51	37.80
BLIP-2 Li et al. (2023c)	12B	merge	51.35	52.38	37.84	46.03	46.93
LLaVA-1.5-7B Liu et al. (2023a)	7B	merge	37.84	54.76	43.24	52.38	48.04
LLaVA-1.5-13B Liu et al. (2023a)	13B	merge	56.76	52.38	29.73	42.86	45.25
LLaVA1.6-mistral Liu et al. (2024b)	7B	merge	43.24	30.95	35.14	39.68	37.43
LLaVA1.6-vicuna Liu et al. (2024b)	7B	merge	59.46	42.86	37.84	49.21	47.49
Qwen-VL-Chat Bai et al. (2023b)	9B	merge	40.54	45.24	40.54	44.44	43.02
InternVL-Chat1.5 Chen et al. (2024c)	26B	merge	62.16	61.90	54.05	57.14	58.66😈
Cambrian-8B Tong et al. (2024)	8B	merge	8.11	21.43	21.62	28.57	21.23
Claude-3-opus Anthropic (2024)		merge	45.95	61.90	45.95	57.14	53.63
Claude-3-sonnet Anthropic (2024)	-	merge	40.54	66.67	43.24	38.10	46.37
Claude-3-haiku Anthropic (2024)	-	merge	56.76	59.52	35.14	49.21	50.28
Claude-3.5-sonnet Anthropic (2024)	-	merge	54.05	69.05	40.54	50.79	53.63 🗑
· · · · · · · · · · · · · · · · · · ·		Video '	VLM				
Video-LLaVA Lin et al. (2023a)	7B	seq	43.24	33.33	48.65	52.38	45.25
Chat-Univi-7B Jin et al. (2023)	7B	seq	24.32	28.57	29.73	33.33	29.61
Chat-Univi-13B Jin et al. (2023)	13B	seq	8.11	21.43	18.92	17.46	16.76
PLLaVA-7B Xu et al. (2024)	7B	seq	48.65	47.62	32.43	53.97	46.93
PLLaVA-13B Xu et al. (2024)	13B	seq	51.35	50.00	40.54	58.73	51.40
· · · · · ·		1	interleaved d				
LLaVA-interleave Li et al. (2024d)	7B	seq	48.65	59.57	43.24	51.90	51.50
LLaVA-interleave-dpo Li et al. (2024d)	7B	seq	40.54	48.94	48.65	50.63	48.00
VILA-1.5-3B Lin et al. (2023b)	3B	seq	37.84	51.06	43.24	36.71	41.50
VILA-1.5-3B-s2 Lin et al. (2023b)	3B	seq	35.14	51.06	43.24	36.71	41.00
VILA-1.5-8B Lin et al. (2023b)	8B	seq	24.32	29.79	43.24	36.71	34.00
VILA-1.5-13B Lin et al. (2023b)	13B	seq	32.43	51.06	37.84	45.57	43.00
Phi-3V Abdin et al. (2024)	4B	seq	54.05	61.70	51.35	49.37	53.50
LLaVA-NV Zhang et al. (2024b)	7B	seq	45.95	40.43	32.43	46.15	42.21
LLaVA-NV-dpo Zhang et al. (2024b)	7B	seq	48.65	41.86	29.73	46.15	42.56
Mantis-Idefics2 Jiang et al. (2024)	8B	seq	40.54	46.81	43.24	45.57	44.50
Mantis-LLaVA Jiang et al. (2024)	7B	seq	43.24	29.79	45.95	35.44	37.50
Mantis-siglip-llama3 Jiang et al. (2024)	8B	seq	67.57	34.04	40.54	40.51	44.00
Mantis-clip-llama3 Jiang et al. (2024)	8B	seq	54.05	42.55	35.14	44.30	44.00
$\overline{\text{GPT-4V}}$ Achiam et al. (2023)		seq -	62.16	68.09	43.24	67.09	62.00
GPT-40 Achiam et al. (2023)	-	seq	72.97	74.47	54.05	62.03	65.50 °
GPT-40-mini Achiam et al. (2023)	_	seq	64.86	57.45	45.95	63.29	59.00
Gemini-1.5-flash Team et al. (2023)	-	seq	64.86	74.47	54.05	63.29	64.50
Gemini-1.5-pro Team et al. (2023)	_	seq	59.46	70.21	56.76	68.35	65.00
Gemmi-1.3-pro reall et al. (2023)	-	seq	57.40	/0.21	50.70	00.33	00.000

Table 22: **Evaluation results for 39 vision-language models in PhysBench-val.** Note that the evaluation of General VLMs is based on the data from Video and Image VLM evaluations, with the addition of interleaved data, meaning that the full test dataset of PhysBench is being assessed. In this context, "seq" refers to the sequential input of images after frame selection from videos, while "merge" refers to merging video frames into a single image.

F.5 EMBODIED TASKS DETAILED DESCRIPTION

To further validate the effectiveness of our data and method, we built a simulation platform using MuJoCo (Todorov et al., 2012) and the Franka Emika Panda from Menagerie (Zakka et al., 2022), and conducted tests on five embodied tasks. Using the proposed mark-based visual prompting technique with GroundedSAM (Ren et al., 2024) and farthest point sampling (Qi et al., 2017), MOKA (Liu et al., 2024a) converts affordance reasoning into a series of visual question-answering problems that pre-trained VLMs can solve. The setup matches MOKA, and the general visual setup can be seen in Figure 25(a)(b). Our tabletop environment only has one top-down camera, which is the primary camera used in MOKA to capture RGBD images. For each task, we report the number of successes out of 10 trials following the setting of Liu et al. (2024a).





We present the specific language instructions given to the VLM in Figure 26. It is important to note that, for each task, we only provide a single example. For instance, while we tested five objects in the Affordance task—pot, knife, spoon, monitor, and tennis racket—we only used the tennis racket as an example here. For each task, we report the success rate over 10 trials, following the MOKA protocol. "Specifically, the test content and evaluation methods for each task are as follows: (1) Affordance test: This test evaluates whether the robotic arm can correctly grasp various objects. Figure 25(c) illustrates the robotic arm successfully grasping a pot. In total, we tested the grasping ability on 10 items, including a pot, knife, spoon, spatula, monitor, tennis racket, phone, and others. Specifically, we tested 5 objects—pot, knife, spoon, monitor, and tennis racket—attempting to grasp each object twice. (2) Force Test: This test evaluates the robotic arm's capacity to properly grasp deformable, fragile, and rigid objects. Due to simulation constraints, the evaluation was based on the robotic arm's output metrics. We tested fragile items (e.g., egg, ripe persimmon), soft items (e.g., jelly, plastic cup), and rigid objects (e.g., iron ball), with two attempts per object. It should be noted that the simulation system models all objects as rigid bodies, meaning that breakage during grasping is not depicted. Furthermore, while using the MOKA system to control the Panda robotic arm, we were unable to directly manipulate the gripper's size. Instead, we provided the VLM with approximate object dimensions, allowing the VLM to determine the necessary gripping force to evaluate success or failure." (3) Color test: This test evaluates whether the robotic arm can accurately pick up the correctly colored object from a set of identical items. As shown in Figure 25(e), the blocks are identical except for their color, and the task requires selecting the object of the designated color. We tested five colors—blue, pink, brown, green, and orange—conducting two trials for each color.

(4) Location test: This test evaluates whether the robotic arm can correctly grasp objects at specific locations. The goal is to ensure that the robotic arm accurately grasps the required objects based on their positions. Specifically, we tested with three blocks, requiring the arm to grasp the middle block (4 attempts), the block farthest from the plate (3 attempts), and the block closest to the plate (3 attempts). (5) Tool test: This test assesses whether the robotic arm can select the appropriate tool for a given task. For instance, as shown in Figure 25(g), the task is: "If you need to cut a watermelon, which tool should you grasp?" In this scenario, the robotic arm is expected to grasp the fruit knife. In total, we posed 5 questions, with 2 attempts per question, requiring the robotic arm to select and grasp different target tools for each task.

On the other hand, these five tasks require minimal consideration of height (or depth) information, making the evaluation more fundamental. For MOKA's waypoints selected from free space, their height must be explicitly specified for accurate deprojection into 3D space, as they are not anchored to any objects. For this reason, in typical tabletop manipulation scenarios, MOKA primarily focuses on cases where the waypoints are at the same height as the target point.

Affordance	Grasp the tennis racket.
Force	Grasp the egg.
Color	Grasp the blue cube.
Location	Grab the block farthest from the plate and move it to the plate.
Tool	Grasp the tools for cutting a watermelon.

Figure 26: The language description of the testing tasks.

We present an overview of our implementation of MOKA in Algorithm 1. Our experiments aim to enhance the VLM's ability to understand the physical world and validate its impact on downstream embodied agent tasks. Specifically, we employ two methods to improve the VLM: first, fine-tuning the VLM using PhysBench, and second, incorporating the PhysAgent to assist during VLM inference. It is worth noting that the five tasks we address are relatively fundamental, unlike the complex multi-action tasks described in the MOKA paper, which require hierarchical decomposition from high- to low-level actions. In our case, the tasks can be executed directly without such decomposition."

Algorithm 1 MOKA Pipeline

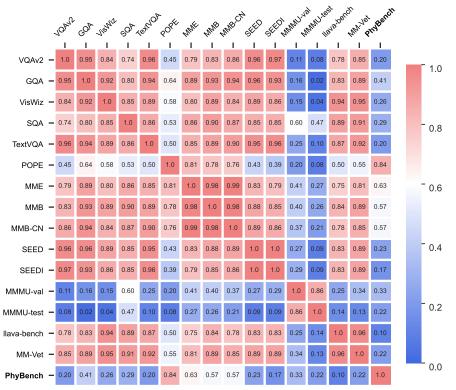
- 1: **Input:** Vision-language Model \mathcal{M} , Task instruction l, text prompt for low-level reasoning p_{low} and initial observation s
- 2: Get observation s from the top-down camera
- 3: Propose keypoint and waypoint candidates and get annotated image $f(s_k)$
- 4: Query \mathcal{M} for low-level motion reasoning, obtain $y_{low} = \mathcal{M}([p_{low}, l, f(s)])$
- 5: Execute y_{low} on the robot in simulation

F.6 CORRELATION MAP

Following the approach of Tong et al. (2024); Fang et al. (2024; 2025), we used the Pearson correlation coefficient to construct a relationship matrix. The data used to build this matrix can be found in Table 23.

	VQAv2	GQA	VisWiz	SQA	TextVQA	POPE	MME	MMB	MMBCN	SEED	SEEDI	MMMUval	MMMUtest	LLaVA-bench
LLaVA-1.5-7B	78.5	62.0	50.0	66.8	58.2	85.9	1510.7	64.3	58.3	61.5	67.0	33.2	31.1	63.4
LLaVA-1.5-13B	80.0	63.3	53.6	71.6	61.3	85.9	1531.3	67.7	63.6	62.4	68.2	36.4	33.6	70.7
InstructBLIP-7B	61.1	49.2	34.5	60.5	50.1	78.8	1210.1	36.0	23.7	53.4	58.8	32.9	30.6	60.9
InstructBLIP-13B	62.3	49.5	33.4	63.1	50.7	78.9	1212.8	42.0	25.0	55.2	61.7	35.7	33.8	58.2
Qwen-VL-Chat	78.2	57.5	38.9	68.2	61.5	85.6	1487.5	60.6	56.7	58.2	65.4	35.9	32.9	64.1
VILA-1.5-3B	80.4	61.5	53.5	69.0	60.4	85.9	1442.4	63.4	52.7	60.9	67.9	33.3	30.8	75.9
VILA-1.5-3B-s2	79.8	61.4	61.3	69.6	63.4	85.3	1431.7	62.8	52.2	60.0	66.4	32.8	31.3	76.7
VILA-1.5-8B	80.9	61.9	58.7	79.9	66.3	84.4	1577.0	72.3	66.2	64.2	71.4	36.9	36.0	80.0
VILA-1.5-13B	82.8	64.3	62.6	80.1	65.0	86.3	1569.6	74.9	66.3	65.1	72.6	37.9	33.6	80.8
BLIP-2	41.0	44.6	29.4	61.0	42.1	85.3	1293.8	44.0	27.0	46.4	49.7	35.4	34.0	56.2

Table 23: The performance of the 10 models used to construct the correlation map across 15 other VLM benchmarks.



The correlation presented in Figure 4(a) illustrates the relationships between the four major categories in PhysBench and other tasks. Additionally, we provide a detailed correlation map between PhysBench and 15 other vision-language benchmarks in Figure 27 below.

Figure 27: Correlation map between PhysBench and 15 other vision-language benchmarks.

F.7 PERFORMANCE ON RELATED BENCHMARKS

To further evaluate the contribution of our data and model to understanding the physical world, we conducted tests on three existing benchmarks related to physical-world perception. Notably, these benchmarks focus on specific aspects of physical-world perception, whereas our PhysBench provides a more comprehensive and holistic evaluation, as summarized in Table 1. Furthermore, since these datasets were not originally designed for VLMs, we applied necessary preprocessing to adapt them for our evaluations.

Setup. EmbSpatial (Du et al., 2024) is a benchmark designed to evaluate spatial understanding within embodied environments with source image come from MP3D (Chang et al., 2017), ScanNet (Dai et al., 2017) and AI2-THOR (Kolve et al., 2017). We utilized its benchmark dataset for testing purposes. ContPhy (Zheng et al., 2024b) is a benchmark aimed at assessing visual models' capabilities in perceiving continuous physical phenomena and properties. It comprises four simulation systems based on Unity3D: Fluid Hourglass, Rope-Pulley System, Cloth Magic Trick, and Ball Playground. Since ContPhy primarily targets visual and physical models, we selected 200 items for each of the four categories (split evenly between property-based and dynamics-based tasks) and translate them into multiple-choice format suitable for VLMs. The question prompts were modified to better align with the answering capabilities of VLMs. Physion++ (Tung et al., 2023) evaluates the impact of physical properties such as mass, friction, elasticity, and deformability on physical phenomena. It leverages the ThreeDWorld simulation platform (Gan et al., 2020) to generate a series of videos, each paired with a corresponding question. The videos consist of an inference phase, where artificial systems can identify objects' mechanical properties, followed by a prediction phase, where the model must predict whether two specified objects will collide after the video ends. Physion++ is primarily designed for vision models such as ResNet (He et al., 2016) and VGG (Simonyan & Zisserman, 2014), with answers in the form of binary classification (yes/no), derived by converting model outputs into probabilities. To adapt Physion++ for VLMs, we processed the videos and

reformulated the questions into natural language prompts, adding necessary contextual hints. For example, if a video includes a transition phase, we explicitly include a statement like, "The black screen in the video marks a transition in objects or scenes" in the prompt. Due to the small size of the test set, we combined the train and test sets, resulting in 250 VQA pairs for evaluation. During fine-tuning with PhysBench, we modified the options to an open-ended format. The results, presented in Table 24, are reported in terms of accuracy. All parameter settings and configurations are kept consistent with those outlined in the main text.

Table 24: Performance on Three Related Benchmarks.

	ContPhy-Property	ContPhy-Dynamics	Physion++	EmbSpatial
Phi-3V	49.25	43.25	68.80	55.91
Phi-3V + finetune	64.50	62.75	82.20	66.95
Phi-3V + PhysAgent	52.00	44.75	78.40	62.28

Results. As presented in Table 24, leveraging PhysBench data for fine-tuning or in a zero-shot setting with PhysAgent leads to performance improvements across the benchmarks, particularly in Physion++, where improvements of 19.50% and 9.6% are observed, with fine-tuning achieving the most significant gains. These results highlight the effectiveness of our data and methods in enhancing the capability of Vision-Language Models to comprehend the physical world.

G MORE RELATED WORKS

Vision-Language Models. Vision-Language Models (VLMs) are large language models that integrate visual modalities, such as images and videos, with language knowledge (Wu et al., 2023b; Huang et al., 2024; Bai et al., 2022; Zhan et al., 2024; Dai et al., 2024; Bai et al., 2024b). Notable models like BLIP-2 (Li et al., 2023c) and LLaVA (Liu et al., 2024c) have advanced image-captioning datasets and visual instruction tuning, with LLaVA-Next further improving single-image performance at higher computational costs (Liu et al., 2024b). Subsequent models, such as QwenVL (Bai et al., 2023b), CogVLM (Wang et al., 2023b), and Yi-VL (AI et al., 2024), have followed a similar architecture to LLaVA. As single-image and text interaction technologies continue to mature, many recent VLMs (Alayrac et al., 2022; Peng et al., 2023; Pan et al., 2024; Lin et al., 2023b) are now capable of handling complex visual tasks with interleaved images or videos, enabling VLMs to tackle more sophisticated tasks (Lu et al., 2024b; Yu et al., 2024b) and paving the way for interactions with the real physical world.

Vision-Language Benchmarks VLMs (Liu et al., 2024c; Achiam et al., 2023; Pan et al., 2024; Yu et al., 2023a; Chow et al., 2024; **?**; Li et al., 2024b; have inherited and advanced many intriguing features from text-only LMs. Benchmarks for VLMs have rapidly emerged to evaluate performance in areas such as image question answering (Ying et al., 2024), in-context response (Yu et al., 2023b), chart understanding (Li et al., 2024f), and web comprehension (Liu et al., 2024d; Zhou et al., 2023). Some benchmarks cover spatial relations understanding (Li et al., 2024a), but often overlook the ability to devise complex spatial action plans based on physical world comprehension. Recently, new benchmarks have also emerged that focus on the ability to understand multiple images in long contexts (Zhang et al., 2024a; Kil et al., 2024; Jiang et al., 2024; Wu et al., 2023a; Li et al., 2024e; Ge et al., 2024) and complex realistic environments (Fu et al., 2024; Bai et al., 2024a). However, these benchmarks—whether based on answering questions from images, videos, or tables, or using visual prompts (Fu et al., 2024; Yu et al., 2024a)—ultimately rely on responding to the content of the given images rather than the true perception of the physical world, thus falling short of achieving spatial intelligence (Gupta et al., 2021; Yang et al., 2024a).

Video Benchmarks. With the growing interest in video understanding, the development of benchmarks for VLMs has become increasingly emphasized. In video comprehension, the research community has made significant strides, particularly for short videos. There are specialized benchmarks for temporal perception (Yu et al., 2019; Wu et al., 2024a), action understanding (Liu et al., 2024e; Mangalam et al., 2024), video classification (Kay et al., 2017), video reasoning (Xiao et al., 2021a; Xie et al., 2023), video captioning (Miech et al., 2019; Xu et al., 2016), video question-answering (Zhou et al., 2024; Li et al., 2023g; 2024e), long video comprehension (Wu et al., 2024b; Chandrasegaran et al., 2024), video generation (Bansal et al., 2024), and interleaved video-text

Table 25: **Comparison between PhysBench and other vision-language benchmarks**. In the format, I, T, V present text, image, and video. Annotated means annotate the existing dataset, like MSCOCO Karpathy & Fei-Fei (2015). LLaVA^{Wd}: LLaVA-Bench(In-the-Wild)-Detail Liu et al. (2024c). Reasoning means that it requires the VLMs' reasoning ability to answer the question.

Dataset	Size (k)	Format	Interleaving	Source	Domain	Reasoning
VQA-v2 Goyal et al. (2017b)	1,105,904	I+T	×	Annotated	Image content	×
GQA Hudson & Manning (2019)	22,669,678	I+T	×	Annotated	Image content	×
VizWiz Gurari et al. (2018)	32,000	I+T	×	Annotated	Image content	×
TextVQA Singh et al. (2019)	45,000	I+T	×	Annotated	Image content	×
OKVQA Marino et al. (2019)	14,000	I+T	×	Annotated	Image content	×
SEED Li et al. (2023a)	19,000	V+I+T	×	Annotated	Image and video content	×
MMBench Liu et al. (2023c)	3,000	I+T	×	Annotated	Image content	×
MME Yin et al. (2023)	1,297	I+T	×	Annotated	Image content	×
POPE Li et al. (2023h)	18,000	I+T	×	Annotated	Image hallucination detection	×
MM-Vet Yu et al. (2023b)	200	I+T	×	Annotated	Image chat	×
LLaVAWd Liu et al. (2024c)	60	I+T	×	Annotated	Image chat	×
SQA ^I Lu et al. (2022)	6,000	I+T	×	Annotated	Image content	×
NLVR2 Suhr et al. (2018)	6,967	I+T	×	Annotated	Image content	×
MathVista Lu et al. (2024b)	6,141	I+T	×	Annotated	Math	1
BLINK Fu et al. (2024)	1,901	I+T	1	Annotated, Chart	Visual prompt	×
Mantis-eval Jiang et al. (2024)	217	I+T	1	Annotated	Image chat	×
Q-Bench Wu et al. (2023a)	2,990	I+T	1	Annotated	Image content	×
MMMU Yue et al. (2024)	11,500	I+T	1	Annotated, Web, Textbook	Image content	×
PhysBench	10,002	V+I+T	1	Annotated, Web, Simulation, Real-world	Physical property and dynamics	1

question-answering (Wang et al., 2024a). However, these works primarily focus on evaluating video content and do not explore the underlying mechanisms of video representation or address true physical world perception. Furthermore, during our experiments, we observed significant challenges with current video VLMs in following instructions and answering questions, as the models frequently output descriptions of the video rather than directly addressing the posed questions.

Interleaved Vision-Language Benchmarks. VLMs are increasingly processing longer and more complex inputs. Along with this development, several benchmarks with interleaved inputs have emerged (Li et al., 2023b; Wang et al., 2024b; Meng et al., 2024). For example, SEED-Bench (Li et al., 2023a; 2024a) focuses on video understanding, BLINK (Fu et al., 2024) introduces visual prompts, and NLVR2 (Suhr et al., 2018) differentiates between two images. However, all of these benchmarks still primarily assess content description based on images, without evaluating physical understanding or perception abilities. Furthermore, current interleaved benchmarks only involve images and text, while PhysBench is a dataset that interweaves video, image, and text inputs. A detailed comparison with the previously mentioned benchmarks and other vision-language benchmarks can be found in Table 25.

Science-related Benchmarks. In addition to the benchmarks related to physical world comprehension mentioned in Section 2, there are also benchmarks that assess models' understanding through middle or university-level physics exam questions. SciQ (Welbl et al., 2017), ScienceQA (Lu et al., 2022), E-EVAL (Hou et al., 2024), MMLU-STEM (Hendrycks et al., 2020), and C-Eval-STEM (Huang et al., 2023b) include some physics-related questions, but these datasets often allow questions to be answered simply by analyzing the provided images, lacking the complexity of reasoning and computational tasks. JEEBench (Arora et al., 2023) requires multistep reasoning with physics knowledge but is limited in scope and purely text-based. SciBench (Wang et al., 2024f), OlympiadBench (He et al., 2024), MathVista (Lu et al., 2024b), and OCWCourses (Lewkowycz et al., 2022) provide college-level physics questions. However, these benchmarks mainly consist of homework and exam-style questions, focusing more on mathematical reasoning (Zheng et al., 2024a) and general knowledge rather than true physical world comprehension. In contrast, our PhysBench is the first systematic and comprehensive question-answering benchmark specifically designed for understanding the real physical world.

Table 26: A comparison between PhysBench and other physical understanding benchmarks not in question-answering format.

	Property	Attribute	Location	Velocity	Temperature	Camera	Light	Collision	Manipulation	Fluid	Interleaved	Size
Physics 101 Wu et al. (2016)	×	X	X	×	×	×	×	1	×	×	×	17,408
IntPhys Riochet et al. (2018)	1	×	×	×	×	×	×	×	×	X	×	15,000
ESPRIT Rajani et al. (2020)	×	×	×	×	×	×	×	1	×	×	×	2,441
CRAFT Ates et al. (2020)	1	×	×	×	×	×	×	1	×	×	×	57,000
CoPhy Baradel et al. (2019)	1	×	1	×	×	×	×	1	×	×	×	216,000
PhysBench	1	1	1	1	1	1	1	1	1	~	1	10,002

3D Scence VQA. Recently, multi-modal 3D perception has garnered increasing attention due to its connection to the physical world, driving rapid advancements in the field. SQA3D (Ma et al., 2023) highlights the importance of "situations" within contextual understanding. EmbodiedScan (Wang et al., 2024d) and SceneVerse (Jia et al., 2025) expand the scope by collecting more scenes or annotating additional objects, scaling annotations to the millions. OpenEQA (Majumdar et al., 2024), SpatialRGPT-Bench (Cheng et al., 2024), MMScan (Lyu et al., 2024), and MSNN (Linghu et al., 2024) integrate comprehensive annotations, adapting the task into a VQA format. However, these studies primarily focus on geometric relationships, which represent only a subset of the broader understanding of the physical world, as discussed in Section 2. Our work prioritizes a more holistic evaluation of the physical world perception capabilities of VLMs across four major task categories: Physical Object Properties, Physical Object Relationships, Physical Scene Understanding, and Physics-based Dynamics. Additionally, the spatial components in our dataset differ significantly from those in existing Spatial VQA datasets. While such benchmarks typically rely on 3D point cloud scenes or interleaved 2D images from multiple viewpoints, our dataset uses interleaved images to capture physical world dynamics, such as viewpoint rotations and the progression of physical phenomena.

VLMs for Robotic Manipulation. Recently, two main approaches have been proposed for applying Vision-Language Models (VLMs) (Liu et al., 2024c; Achiam et al., 2023; Team et al., 2023; Mao et al., 2023a;b) to robotic manipulation: (*a*) directly generating actions (Kim et al., 2024; Octo Model Team et al., 2024; Zawalski et al., 2024a; Niu et al., 2024; Zawalski et al., 2024b) and (*b*) employing VLMs as agents (Liu et al., 2024a; Nasiriany et al., 2024; Huang et al., 2023a). Approach (a) involves directly outputting actions, which requires extensive training—for instance, OpenVLA was trained using $64 \times A100$ GPUs—and produces embodied-specific actions that necessitate targeted fine-tuning. In contrast, approach (b) generates affordance representations through VLMs, which are subsequently converted into actions. This method requires less training and exhibits stronger generalization capabilities. However, it suffers from weaker perception capabilities in the physical world, leading to performance limitations (Liu et al., 2024a; Mao et al., 2024).

H MORE EXAMPLES

We use red color as right answer. We use red to indicate the correct answer (correct answer). It is important to note that, to reduce difficulty and facilitate evaluation, we employed a multiple-choice format rather than open-ended responses. For space-saving purposes, the example figures in the main text do not display the available options.

H.1 PHYSICAL OBJECT PROPERTY SUB-TASK



The color of the original spots on the chameleon's body has not changed during the process of changing its color. What color are these spots?

Answer

A. Black B. Green C. White D. Blue

Figure 28: Example for property color. Ability Type is identify.

- H.2 PHYSICAL OBJECT RELATIONSHIPS SUB-TASK
- H.3 PHYSICAL SCENE UNDERSTANDING SUB-TASK
- H.4 PHYSICS-BASED DYNAMICS SUB-TASK



The weight of the object about the size of a ping-pong ball is closest to which of the options?

Answer

A. 5g B. 50g C. 500g D. 5kg

Question



Which fruit in the picture is most likely to be the heaviest individually?

Answer

A. Watermelon B. Pear C. Plum D. Peach

Question



What can be said about the mass of the brown cube compared to the white sphere?

Answer

```
A. The brown cube is less massive B. The white sphere is less massive C. They have the same mass D. Cannot answer
```

Figure 29: Three examples related to property mass, categorized by the following ability types: identification, comparison, and comparison.



How many blueberries are there outside the plate?

Answer

A. 1 B. 2 C. 3 D. 4

Question



How many of the books pictured have covers with titles beginning with P?

Answer

A. 1 B. 2 C. 3 D. 4

Question



Following the content of the ¡video¿, How many eggs were broken?

Answer

A. 1 B. 2 C. 3 D. 4

Question



How many balls are moving close together without separating?

Answer A. 2 B. 3 C. 4 D. 6

Figure 30: Four examples related to property number, ability types are all identification.



In the photo, which point with option signifies the object with the most sharp?

Answer

A. Point A B. Point B C. Point C D. Point D

Question



Can you tell me which point with option in the image points to the object that has the least

brittle? Answer

A. Point A B. Point B C. Point C D. Point D

Question



Which point with option in the photograph pinpoints the object with the most stiff?

Answer

A. Point A B. Point B C.	Point C D. Point D
--------------------------	--------------------

Question



Which point with option in the image marks the object that exhibits the most elastic?

Answer

A. Point A B. Point B C. Point C D. Point D

Question



Which point with option in the photograph captures the object that has the most malleable?

Answer

A. Point A B. Point B C. Point C D. Point D

Question



Which point with option in the image isolates the object with the most soft?

Answer A. Point A B. Point B C. Point C D. Point D

Figure 31: Six examples of property attributes include sharpness, brittleness, stiffness, elasticity, malleability, and softness.



Moving according to the arrow in the picture, which of the following options are you

most likely to encounter?

Answer

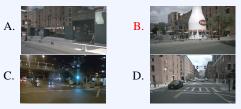


Question

Following the direction indicated by the arrow in the picture, which of the following

options are you most likely to encounter?

Answer



Question



What is the

relationship between the speeds of the two objects in the video after they begin to fall?

Answer

- A. Both objects have the same speed.
- B. The egg consistently falls faster than the feather.
- C. The feather consistently falls faster than the egg.
- D. Initially, the egg falls faster, but the feather eventually surpasses it.

Figure 32: Three examples for relationships motion, categorized by the following ability types: static, static and dynamic.

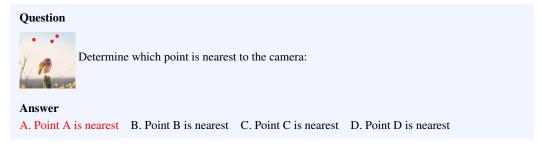


Figure 33: An example for relationships depth. Ability Type is static.



Find the point that is closest to the river:

Answer

A. Point A is the closest B. Point B is the closest C. Point C is the closest D. Point D is the closest

Question



What value is the distance between each of the three small bowls placed side by side

closest to?

Answer A.3mm B.3cm C.10cm D.20cm

Question



What is farthest from the key in the picture?

Answer

A. Pen B. Camera C. Watch D. Glasses

Figure 34: Three examples for relationships distance. Ability Type is static, static and dynamic.

Question What is happening to the size of the ice cube in the video? Answer A. Increasing B. Decreasing C. No change D. Increasing first and then decreasing Question Question Which object is the biggest in volume? Answer A. red cube B. purple cube C. green cube D. orange cube

Figure 35: Two examples for relationships size. Ability Type is dynamic and static.



Among these points, which one is not on the same sunflower as the other 3 points?

Answer

A. Point A B. Point B C. Point C D. Point D

Question



What is the object above the egg?

Answer

A. Milk B. Yogurt C. Banana D. Egg

Question

				L	L	L
How does the	e moon pass thr	ough the sun in	the video?			
Answer						
B. From the C. From the B	upper left corne lower right corr	er to the upper ri er to the lower ri her to the upper l her to the lower	ght corner of the left corner of	ne picture ne picture		
Question						
1	with the option		COT O	rresponds to the	e reference poir	nt P in the
How does the	e moon pass thr	ough the sun in	the video?			
Answer						
A. Point A	B. Point B	C. Point C	D. Point D			

Figure 36: Four examples for relationships location. Ability Type is static, static, dynamic and static.



Where is the light source in the picture?

Answer

- A. In the clouds on the upper right of the screen
- B. In the lower left corner of the screen
- C. A little above the center of the screen
- D. In the exact center of the screen

Question



Reflecting on the events in the video, which of the following alterations to the light source is most likely to result in the phenomenon observed?

Answer

- A. The color of the light changes from yellow to pink
- B. It's just that the light source is weaker and the light source position remains the same
- C. Move parallel to the line between the drumstick and the ballet skirt
- D. It's just that the light source is stronger and the light source position remains the same

Question



From the events in the video, which of the listed changes to the light source is most likely to have resulted in the observed phenomenon?

Answer

- A. Move parallel to the line between the postcard and the cake
- B. The color of the light changes from orange to blue
- C. The color of the light changes from lime yellow to green
- D. The light source moves downward

Question



Taking into account the phenomena observed in the video, which of the following changes to the light source is most likely to have led to this result?

Answer

- A. It's just that the light source is stronger and the light source position remains the same
- B. It's just that the light source is weaker and the light source position remains the same
- C. The color of the light changes from red to purple
- D. The color of the light changes from yellow to blue

Figure 37: Four examples illustrating scene environmental lighting conditions. The corresponding ability types are perception, reasoning, reasoning, and reasoning.

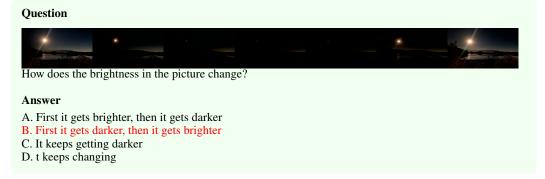


Figure 38: Examples for scene environmental lighting conditions (Continued). Ability Type is judgement.

Question			
What happens t	o the gas pressure	inside the bottle before	e open it?
Answer			
A. Increases	B. Decreases	C. Stays the same	D. Varies randomly

Figure 39: Example for scene environmental air conditions and the ability type of it is perception.

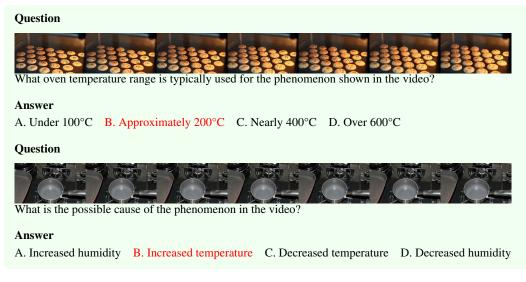


Figure 40: Two examples for scene temperature conditions and the ability types of them are all perception.

Question



Answer

- A. Focus length remains unchanged
- B. Focus length increases
- C. Focus length decreases
- D. Unknown

Question



Based on the phenomenon in the video, which of the following camera changes can produce the effect in the video?

Answer

- A. Move parallel to the line between the motor and the wash basin
- B. Move parallel to the line between the bunk bed and the wash basin
- C. The camera moves upward or downward
- D. The camera rotates along the horizontal axis (left or right)

Question



From the video, which of these camera changes could be responsible for the depicted phenomenon?

Answer

- A. The camera is farther away from the objects
- B. Move parallel to the line between the cupcake and the sponge
- C. The camera is closer to the objects
- D. Move parallel to the line between the cupcake and the blackboard

Question



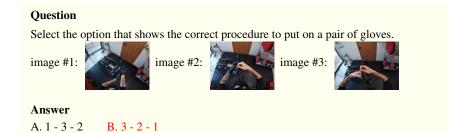
Based on the phenomenon in the video, which of the following camera changes can produce the effect in the video?

Answer

- A. The camera rotates along the vertical axis (upside or downside).
- B. The camera is closer to the objects
- C. The camera rotates along the horizontal axis (left or right).
- D. The camera moves upward or downward

Figure 41: Four examples illustrating scene viewpoint conditions. The corresponding ability types are perception, reasoning, reasoning and reasoning.

D. 1 - 2 - 3



C. 2 - 1 - 3 **Question**

Which of the following options lists the steps in the correct sequence to put the carrot in the microwave?



Answer

A. 2 - 1 - 4 - 3	B. 1 - 3 - 2 - 4
C. 2 - 3 - 1 - 4	D. 2 - 4 - 3 - 1

Question



To poke the watering can, which point is most suitable?

Answer

A. B. C.	D.
----------	----

Question



In order to pick up the cup, which of the following color points has reasonable affordance?

Answer

A. B. C. **D**.

Question

What operation is used to transform the object from Image





Answer

- A. Remove the small ball from the clay block.
- B. Add another ball to the clay block.
- C. Air-dry the clay block.
- D. Press the small ball into the clay block.

Figure 42: Five examples illustrating dynamics manipulation. The corresponding ability types are judgment, judgment, perception, perception and reasoning.

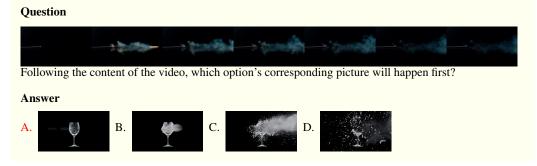
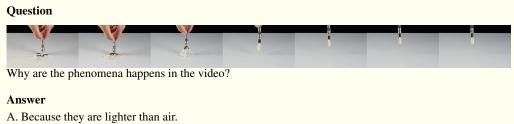
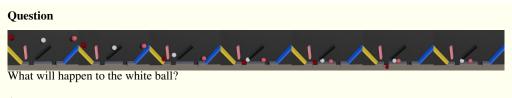


Figure 43: Example for dynamics collision and the ability type of it is prediction.



- B. Due to the presence of ferric oxide in the match heads.
- C. Because they are coated with a special glue.
- D. Due to static electricity on the magnet.

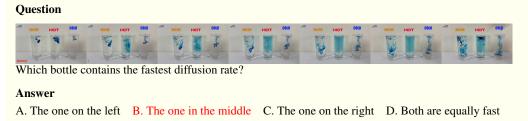
Figure 44: Example for dynamics chemistry and the ability type of it is perception.



Answer

A. It will drop into the right pit.B. It will not drop into the right pit.C. Its movement cannot be determined.D. It will drop into the left pit.

Figure 45: Example for dynamics throwing and the ability type of it is prediction.



Question

-			F
		E Star	

We already know that the liquid poured in is water, so what is the original yellow liquid?

Answer

A. Orange juice B. Oil C. Beer D. Urine

Question

	A AA	nnn	non	noa	nna
Which color object look					

Which color object looks the most viscous in the video?

Answer

A. Transparent liquid B. Light yellow color liquid C. Thick yellow liquid D. Dark blue liquid

Question



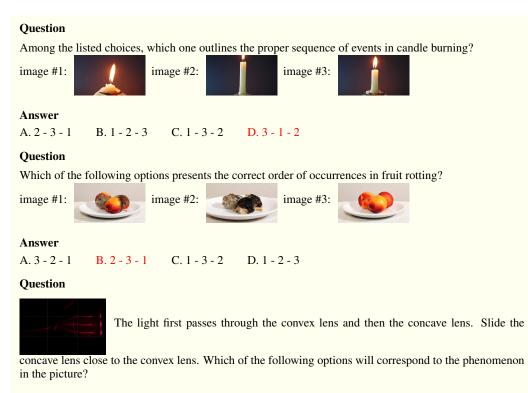
We already know that the red particles in the picture are liquid particles. In which

area of the picture does the liquid flow fastest?

Answer

- A. All parts of the image are at the same speed.
- B. the leftmost part of the picture
- C. the middle part of the picture
- D. the rightmost part of the picture

Figure 46: Four examples illustrating dynamics fluid. The corresponding ability types are perception, reasoning, perception and perception.





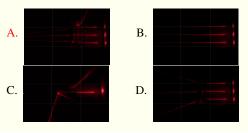


Figure 47: Three examples illustrating dynamics others. The corresponding ability types are reasoning, reasoning and prediction.

I ERROR STUDY

I.1 DETAILED STATICS

In this section, we present a case study analysis of the error types made by GPT-4V, Gemini-1.5flash, and Phi-3V across various tasks. The errors are classified into the following five categories. Other less frequent error types are not included in this analysis. For the analysis, as mentioned in Section 3.4, we selected 500 samples for each model, but due to space limitations, we present only 60 of them here, as shown in Table 27.

Perception Error : VLMs fail to recognize, classify, or detect the objects or content in images. VLMs are constrained by the representation power of visual encoders, and these errors account for the majority of them. See examples in Figure 48, Figure 50, *etc*.

Reasoning Error : VLMs can recognize the text and visual content exactly but make errors in reasoning, leading to incorrect results. See examples in Figure 65, Figure 81, *etc.*

Lack of Knowledge : VLMs do not have specific knowledge, so they finally get a wrong answer. See examples in Figure 57, Figure 71.

Refuse to Answer : VLMs refuse to answer questions and stop answering immediately. See examples in Figure 54.

Fail to Follow Instruction: VLMs fail to correctly understand instructions and provide erroneous answers. For example, VLMs may not understand the specified conditions in the instruction (see Figure 74).

I.2 MAIN REASON ANALYSIS

Perceptual Errors: Perceptual errors can be classified into two categories: basic perceptual errors and domain-specific perceptual errors. Basic perceptual errors occur when the model successfully understands the given information but fails to interpret fundamental visual objects correctly. In contrast, domain-specific perceptual errors arise when the model misinterprets visual inputs due to a lack of understanding of specialized conditions. Moreover, GPT-4V often exhibits a bias towards textual information, prioritizing text over visual inputs—a trend highlighted in recent studies Cui et al. (2023). A notable example is shown in Figure 68, where the model mistakenly identified the plate as part of the background, leading to incorrect depth estimation. This underscores the importance of seeking a balanced approach to enhance the model's interpretative capabilities.

Reasoning Errors: Sometimes, even when the model correctly interprets the text, images, and question, it fails to establish a rigorous logical chain, leading to incorrect conclusions. These types of mistakes, known as reasoning errors, are illustrated in Figures 65 and 78. In the first example, the model mistakenly assumes that friction can only exist if the machine rotates faster than the object, overlooking the presence of another object, which results in an incorrect answer. In the second example, while the model correctly identifies that the temperature of the wrapped paper is significantly lower than that of the other object, it incorrectly attributes this phenomenon to the flame's temperature, leading to an erroneous conclusion.

Lack of Knowledge: Another major cause of errors is the model's lack of relevant knowledge. A notable example is shown in Figure 71, where the model incorrectly assumes that light bending in water is due to refraction. The model clearly does not understand the concept of total internal reflection in water, leading to an incorrect conclusion.

Other Errors: The remaining errors, such as those related to textual understanding, refusal to answer, annotation mistakes, and answer extraction issues, account for only a small proportion. However, they remain significant and should not be overlooked.

I.3 CASE STUDY

Case Figure	Meta-task	Subtask	GPT-40	Gemini-1.5-flash	Phi-3V
Figure 48	Scene	Light	Perception Error	Perception Error	Perception Error
Figure 49	Dynamics	Collision	Reasoning Error	Perception Error	Reasoning Error
Figure 50	Dynamics	Throwing	Perception Error	Perception Error	Perception Error
Figure 51	Scene	Light	Perception Error	Perception Error	Perception Error
Figure 52	Scene	Viewpoint	Perception Error	Reasoning Error	Reasoning Error
Figure 53	Scene	Viewpoint	Perception Error	Reasoning Error	Success
Figure 54	Dynamics	Chemistry	Reasoning Error	Refuse to Answer	Success
Figure 55	Dynamics	Manipulation	Perception Error	Perception Error	Perception Error
Figure 56	Dynamics	Manipulation	Perception Error	Perception Error	Perception Error
Figure 57	Property	Attribute	Perception Error	Perception Error	Reasoning Error
Figure 58	Property	Color	Perception Error	Reasoning Error	Perception Error
Figure 59	Property	Mass	Reasoning Error	Success	Perception Error
Figure 60	Property	Mass	Success	Success	Success
Figure 61	Property	Number	Perception Error	Perception Error	Refuse to Answer
Figure 62	Property	Number	Perception Error	Perception Error	Success
Figure 63	Property	Attribute	Lack of Knowledge	Lack of Knowledge	Perception Error
Figure 64	Relationships	Motion	Perception Error	Perception Error	Reasoning Error
Figure 65	Relationships	Motion	Reasoning Error	Reasoning Error	Reasoning Error
Figure 66	Relationships	Depth	Reasoning Error	Reasoning Error	Success
Figure 67	Relationships	Depth	Success	Success	Success
Figure 68	Relationships	Distance	Perception Error	Reasoning Error	Success
Figure 69	Relationships	Distance	Reasoning Error	Reasoning Error	Lack of Knowledge
Figure 70	Relationships	Size	Perception Error	Reasoning Error	Reasoning Error
Figure 71	Dynamics	Others	Lack of Knowledge	Lack of Knowledge	Lack of Knowledge
Figure 72	Relationships	Size	Success	Success	Success
Figure 73	Scene	Viewpoint	Perception Error	Perception Error	Success
Figure 74	Relationships	Location	Perception Error	Perception Error	Fail to follow instruction
Figure 75	Relationships	Location	Perception Error	Perception Error	Reasoning Error
Figure 76	Scene	Viewpoint	Perception Error	Perception Error	Success
Figure 77	Scene	Temperature	Perception Error	Perception Error	Perception Error
Figure 78	Scene	Temperature	Reasoning Error	Reasoning Error	Reasoning Error
Figure 79	Dynamics	Air	Perception Error	Perception Error	Perception Error
Figure 80	Dynamics	Air	Reasoning Error	Reasoning Error	Reasoning Error
Figure 81	Dynamics	Manipulation	Reasoning Error	Reasoning Error	Reasoning Error
Figure 82	Relationships	Depth	Reasoning Error	Perception Error	Perception Error
Figure 83	Dynamics	Fluid	Perception Error	Perception Error	Perception Error
Figure 84	Dynamics	Others	Perception Error	Perception Error	Perception Error
Figure 85	Dynamics	Others	Perception Error	Perception Error	Perception Error
Figure 86	Dynamics	Collision	Perception Error	Perception Error	Perception Error
Figure 87	Scene	Light	Reasoning Error	Perception Error	Success
Figure 88	Scene	Viewpoint	Perception Error	Perception Error	Perception Error
Figure 89	Relationships	Location	Success	Perception Error	Perception Error
Figure 90	Property	Attribute	Perception Error	Reasoning Error	Perception Error
Figure 90	Dynamics	Manipulation	Perception Error	Success	Perception Error
Figure 91 Figure 92	Scene	Viewpoint	Perception Error	Perception Error	Perception Error
Figure 92 Figure 93	Scene	Light	Perception Error	Perception Error	Perception Error
Figure 95 Figure 94	Relationships	Location	Perception Error	Perception Error	Perception Error
Figure 94 Figure 95	Relationships	Location	Perception Error	Perception Error Perception Error	Perception Error
Figure 95 Figure 96	Dynamics	Others	Reasoning Error	Reasoning Error	Reasoning Error
Figure 96 Figure 97	Scene	Viewpoint	Perception Error	Reasoning Error	Success
-	Scene	-	-		
Figure 98		Light	Reasoning Error	Reasoning Error	Reasoning Error
Figure 99	Dynamics Dynamics	Manipulation Colligion	Perception Error	Success Beneantian Error	Reasoning Error
Figure 100	Dynamics Brownerty	Collision	Perception Error	Perception Error	Success Bassening Error
Figure 101	Property	Attribute	Perception Error	Perception Error	Reasoning Error
Figure 102	Scene	Light	Success	Reasoning Error	Success
Figure 103	Scene	Light	Perception Error	Perception Error	Perception Error
Figure 104	Scene	Light	Perception Error	Perception Error	Reasoning Error
Figure 105	Scene	Light	Success	Perception Error	Reasoning Error
Figure 106	Scene	Light	Reasoning Error	Perception Error	Reasoning Error
Figure 107	Scene	Light	Perception Error	Perception Error	Perception Error

Table 27: Table index of case study figures by meta-task with associated error categories.



Question: According to the video, which alteration to the light source is most likely to have triggered the phenomenon? <video 1>

Option:

- (A) The color of the light changes from yellow to cyan
- (B) The color of the light changes from green to red
- (C) It's just that the light source is weaker and the light source position remains the same (D) It's just that the light source is stronger and the light source position remains the same



<video 1>

The answer is C. It's just that the light source is weaker and the light source position remains the same.

Here's the reasoning

1. Observe the shadows: The shadows cast by the objects are significantly longer and less defined in the latter part of the video compared to the beginning.

- 2. Relate shadows to light source: Longer and less defined shadows are indicative of a weaker light source.
- 3. Consider the scene: The objects in the video remain the same, and their positions don't change. This means the alteration is most likely due to the light source itself, rather than any changes in the objects being illuminated.
- 4. Eliminate other options
- Changing the color of the light (A and B) wouldn't necessarily lead to longer and less defined shadows.
 A stronger light source (D) would result in shorter and sharper shadows.

Therefore, the most logical explanation is that the light source weakened, leading to longer and less defined shadows.

Choice: C. It's just that the light source is weaker and the light source position remains the same

- Reasoning Chain:
- Observation of Images:

 The series of images show a consistent scene with a ball, a backpack, and some other objects on a wooden surface.
 The shadows and lighting on the objects remain consistent in terms of direction and shape throughout the series of images.
- 2. Analysis of Light Intensity:
 The primary noticeable change in the images is the overall brightness.
 The images progressively become darker, indicating a reduction in the intensity of the light source.
- Elimination of Color Change Options:

 Option A (Yellow to Cyan): A change in light color from yellow to cyan would result in a noticeable shift in the color tones of the objects and shadows. This is not observed in the images.

 t observed in the images. - Option B (Green to Red): Similarly, a change from green to red would also alter the color tones significantly, which is not evident in the images.
- 4. Elimination of Light Source Strengthening - Option D (Stronger Light Source): If the light source were getting stronger, the images would progressively become brighter. This is contrary to what is
- observed.
- 5. Conclusion: The consistent direction and shape of the shadows indicate that the position of the light source has not changed.
 The progressive darkening of the images suggests that the light source is becoming weaker. Therefore, the most likely alteration to the light source that triggered the phenomenon is that the light source is weaker while its position remains the

The phenomenon in the image is the casting of shadows on the wooden floor, which suggests that there is a light source above the objects. The shadows are consistent in shape and size, indicating that the light source is not moving. The most likely alteration to the light source that would trigger this phenomenon is a change in the light source's intensity. Therefore, the correct answer is C. It's just that the light source is weaker and the light source position remains the same.

Figure 48: A sample case of physical scene understanding-light. Back to List of Figures.

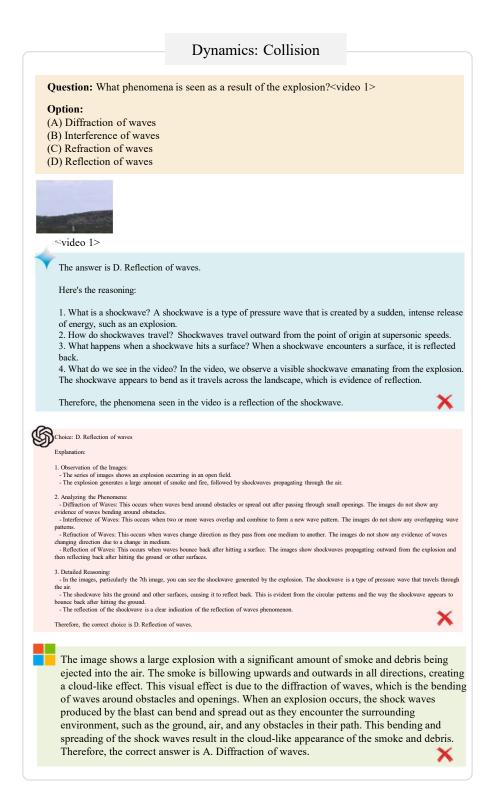


Figure 49: A sample case of physics-based dynamics-collision. Back to List of Figures.

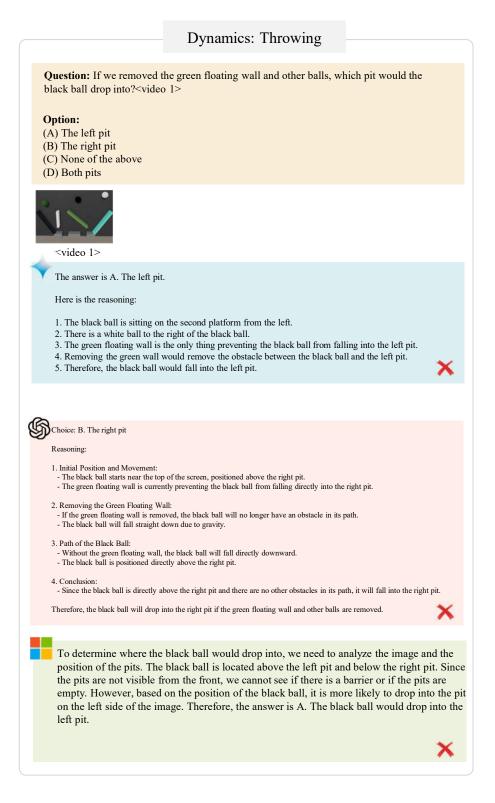


Figure 50: A sample case of physics-based dynamics-throwing. Back to List of Figures.

Scene: Light

Question: Observing the phenomena in the video, which of the following alterations to the light source is most likely to produce such an effect?<video 1>

Option:

(A) It's just that the light source is weaker and the light source position remains the same (B) It's just that the light source is stronger and the light source position remains the same

- (C) The color of the light changes from limeyellow to blue
- (D) The color of the light changes from red to pink



<video 1>

The answer is A. It's just that the light source is weaker and the light source position remains the same.

Here's the reasoning:

1. Observation: The objects in the video cast elongated shadows, indicating that the light source is positioned at a low angle. The shadows are also relatively faint and indistinct, suggesting the light source is not very strong

2. Elimination:

* B. Stronger light source: A stronger light source would produce sharper, more defined shadows. The shadows in the video are too blurry for a strong light source.

* C & D. Color changes: While color changes can affect the perceived appearance of objects, they wouldn't directly cause the elongated and faint shadows observed in the video.

3. Conclusion: The most likely explanation is that the light source is weaker. A weaker light source produces less intense light, resulting in softer, more blurred shadows. The low angle of the light source would still contribute to the elongated shadow shapes

Choice: B. It's just that the light source is stronger and the light source position remains the same

Detailed Explanation:

- 1. Observation of Shadows:
- In the series of images, the shadows of the objects on the ground are clearly visible and consistent in shape and position. - The shadows do not change in size, shape, or direction, indicating that the position of the light source remains constant.
- 2. Intensity of Shadows:
- The shadows appear to be well-defined and dark, suggesting that the light source is strong and casting distinct shadows. - If the light source were weaker, the shadows would be less defined and lighter in appearance.
- 3. Color of Light
- The images do not show any noticeable change in the color of the light. The ground and objects maintain a consistent color throughout the series of image
- If the color of the light had changed (options C or D), there would be a visible shift in the color tones of the objects and the ground. 4. Conclusion:

- Since the shadows are well-defined and there is no change in the color of the light, the most likely alteration is that the light source has become stronger while its position remains the same. - Therefore, the correct choice is B. It's just that the light source is stronger and the light source position remains the same

The most likely explanation for the observed effect is that the light source is weaker and the light source position remains the same. This is because a weaker light source would result in less intense shadows, making them appear more diffuse and less defined. Additionally, if the position of the light source remains the same, the shadows would still be cast in the same direction, but they would be less pronounced due to the reduced intensity of the light. This would result in the shadows appearing more blurred and less distinct, as seen in the video. Therefore, the correct answer is A. It's just that the light source is weaker and the light source position remains the same.

Figure 51: A sample case of physical scene understanding–light. Back to List of Figures.

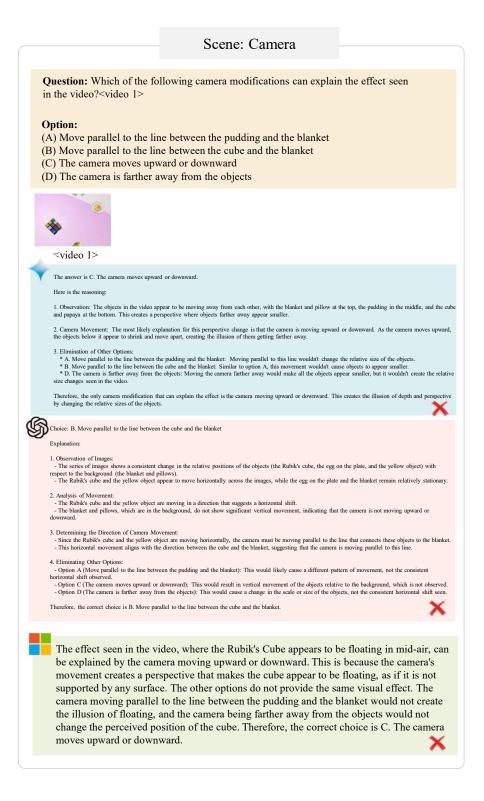


Figure 52: A sample case of physical scene understanding-viewpoint. Back to List of Figures.

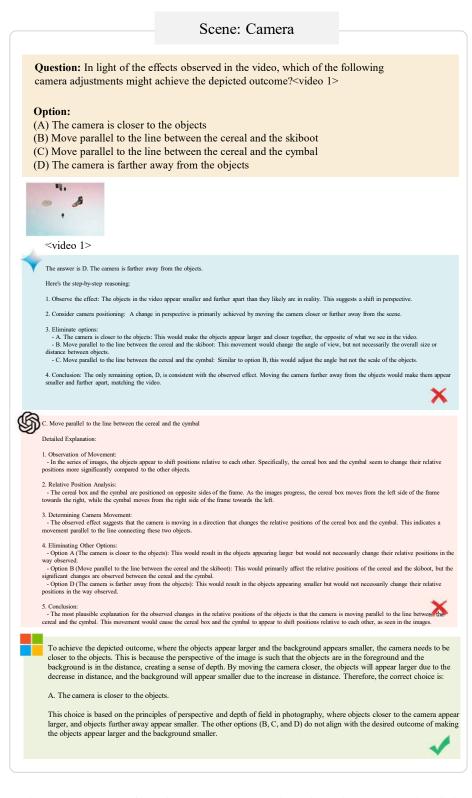


Figure 53: A sample case of physical scene understanding-viewpoint. Back to List of Figures.

Dy	namics: Chemistry	
Question: What action is displayed	in the video? <video 1=""></video>	
Option: (A) Candle being blown out delibera (B) Candle causing wax to overflow (C) Candle burning with a double w (D) Candle being used in a romantic	ick	
≤video 1>		
The answer is C. Candle burning	with a double wick.	
Here's the reasoning:		
1. Visual Cues: The video shows flame at the top suggests the cand	•	honeycomb pattern. The
2. Flame Observation: The flame than-normal amount of fuel being	11 2	l wide, indicating a larger-
3. Double Wick Inference: This s	uggests that the candle	×
B. Candle causing wax to overflow		
Detailed Explanation: 1. Observation of Candle Burning: The s consistent and does not show signs of be change in the flame's behavior).	-	-
2. Wax Overflow: In the last two images This indicates that the candle has been bu		
 No Double Wick: The images do not s centered, which is typical for a single-wi 		. The flame is singular and
4. No Romantic Setting: The background a romantic setting (such as dim lighting,		
Based on these observations, the correct	choice is B. Candle causing wax to o	verflow.
The image shows a single candle with a 'THE 100% NATURAL ROLLING C. The repeated logos suggest that the can indicates that the candle is currently bu based on the context of the image, it is intended purpose, which could be for li candle is being used in a romantic settin Therefore, the choice is:	ANDLES' and 'THE NATURAL CA dle is a product being advertised, and rning. The action displayed in the vid reasonable to infer that the candle is l ghting, ambiance, or decoration. The	NDLE FACTORY EST. 1969 I the presence of the flame leo is not explicitly shown, but being used, likely for its most likely action is that the
D. Candle being used in a romantic set	ing	1

Figure 54: A sample case of physics-based dynamics——chemistry. Back to List of Figures.

Dynamics: Manipulation
Question: Among the listed choices, which one outlines the proper sequence to close the open cabinet door? <image 1=""/> <image 2=""/> <image 3=""/>
Option: (A) 1 - 3 - 2 (B) 3 - 2 - 1 (C) 1 - 2 - 3 (D) 2 - 1 - 3
<image 1=""/> <image 2=""/> <image 3=""/>
The answer is C. 1 - 2 - 3.
Here's the reasoning:
 * Image 1: The robotic arm is fully extended and reaches the cabinet door. * Image 2: The arm starts to close the cabinet door. * Image 3: The cabinet door is fully closed and the robotic arm retracts back to its original position.
Choice: C. 1 - 2 - 3
Reasoning Chain:
 Image #1: The cabinet door is fully open. This is the starting point where the door is in its most open position.
 Image #2: The cabinet door is partially closed. This indicates that the door is in the process of being closed but has not yet reached the fully closed position.
3. Image #3:The cabinet door is fully closed. This is the final position where the door is completely shut.
Step-by-Step Explanation:
 Step 1: Start with the cabinet door fully open (Image #1). Step 2: Move to the partially closed position (Image #2). Step 3: Finally, close the door completely (Image #3).
Thus, the proper sequence to close the open cabinet door is 1 - 2 - 3.
To determine the proper sequence to close the open cabinet door, let's analyze the images:
image #1 shows the cabinet door open, image #2 shows the cabinet door closed, and image #3 shows the cabinet door open again.
Based on this information, the correct sequence to close the open cabinet door would be:
 Open the cabinet door (image #1) Close the cabinet door (image #2) Open the cabinet door (image #3)
So, the answer is A. 1 - 3 - 2.

Figure 55: A sample case of physics-based dynamics—manipulation. Back to List of Figures.

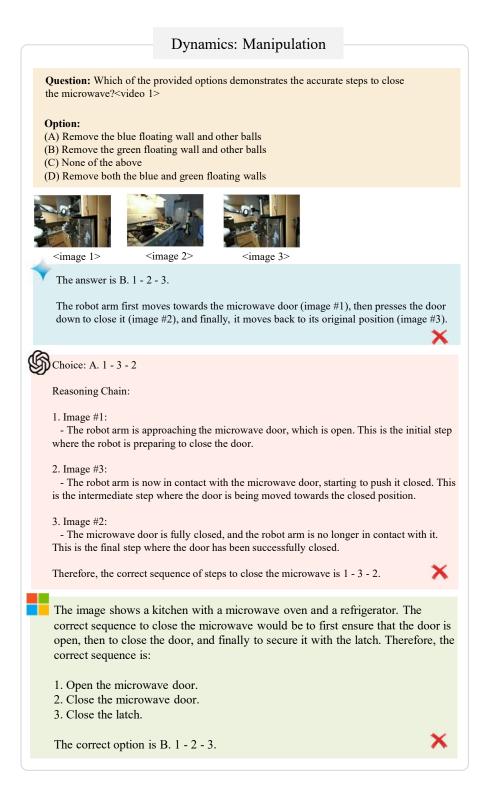


Figure 56: A sample case of physics-based dynamics----throwing. Back to List of Figures.

	Property: Attribute	
Question: How does the flexibic cloth? <video 1=""></video>	lity of the left cloth compare to the o	other
Option: (A) It is more flexible (B) It is equally flexible (C) It is harder to bend (D) It is softer		
<video 1=""></video>		
A. It is more flexible		
Here's the reasoning:		
	table, one brown and one plaid. ed over the objects on the table. The brown cloth dr	apes in a more fluid and uneven
of the objects more easily. This suggests	nd uneven drape of the brown cloth indicates that it t is more flexible. her hand, drapes in a more rigid and uniform manne	
Therefore, based on the way the cloths dr	ape, we can infer that the brown cloth is more flexit	ble than the plaid cloth.
		×
A. It is more flexible		
Step-by-step explanation:		
1. Initial Observation: In the first two imag cloth is orange, and the right cloth is check	es, we see two cloths placed on a table with some or ered.	objects underneath them. The left
Cloth Placement: In the third image, bot (checkered) are both pinned at the corners.	h cloths are being placed on the objects. The left clo	oth (orange) and the right cloth
- In the fourth image, the left cloth (orang to the right cloth (checkered).	l over the objects, we can observe their behavior: ge) starts to show more pronounced draping and ber) continues to show more flexibility, conforming m	
object underneath it. - In the sixth and seventh images, the left	cloth (orange) appears to be more fluid and flexibl hich maintains a more structured and less flexible a	e, showing more folds and curves
4. Final Observation: By the last image, th	e left cloth (orange) has clearly shown more flexibil ath it, while the right cloth (checkered) appears stif	lity in its ability to drape and
Based on these observations, the left cloth	(orange) is more flexible compared to the right clot	th (checkered).
the image and look for any d appear to move. The left clot cloth is on the right side. We other cloth, which is more ex	of the left cloth compared to the othe ifferences in the way the cloths are p h is positioned on the left side of the can observe that the left cloth is not tended towards the right side of the han the other cloth. Therefore, the cl	ositioned or how they table, while the other as stretched out as the table. This suggests that

Figure 57: A sample case of physical object property-attribute. Back to List of Figures.

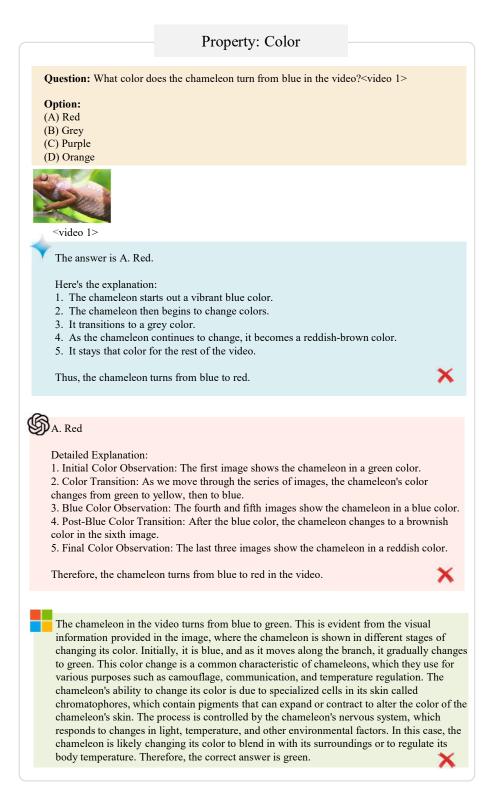


Figure 58: A sample case of physical object property-color. Back to List of Figures.

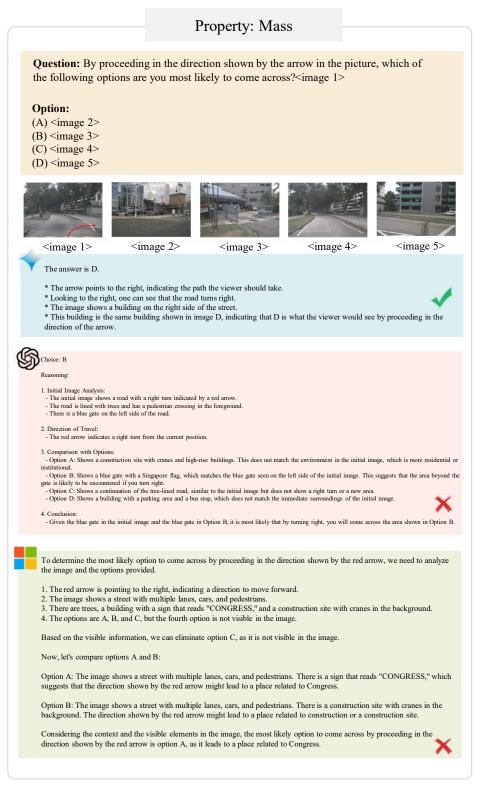


Figure 59: A sample case of physical object property-mass. Back to List of Figures.

_	Property: Mass
	Question: Which fruit in the picture is most likely to be the heaviest individually? <image 1=""/>
	Option: (A) Watermelon (B) Pear (C) Plum (D) Peach
	<pre><video 1=""></video></pre>
	A. Watermelon
	Here's the reasoning:1. Visual Size: The watermelon is noticeably larger than all the other fruits in the picture. This suggests it has a greater volume.2. Density: While we don't know the exact densities of the fruits, watermelons are known to be mostly water, making them relatively dense.3. Combined: A larger volume combined with higher density leads to a greater overall mass, which translates to a heavier weight.
	Therefore, it's safe to assume the watermelon is the heaviest fruit in the picture.
C	A. Watermelon
	 Reasoning: 1. Visual Inspection: By looking at the image, the watermelon appears significantly larger in size compared to the other fruits. 2. Typical Weight: Generally, watermelons are known to be much heavier than pears, plums, and peaches. Even a small watermelon can weigh several pounds, whereas the other fruits typically weigh much less. 3. Density and Volume: Watermelons have a high water content and a large volume, contributing to their weight. Pears, plums, and peaches, while also containing water, are much smaller in volume and thus weigh less individually.
	Therefore, based on size and typical weight characteristics, the watermelon is most likely to be the heaviest fruit individually in the picture.
	To determine which fruit is most likely to be the heaviest individually, we need to consider the average weight of each type of fruit.
	 A. Watermelon: A typical watermelon can weigh between 20 to 30 pounds. B. Pear: A pear can weigh between 0.25 to 0.5 pounds. C. Plum: A plum can weigh between 0.1 to 0.2 pounds. D. Peach: A peach can weigh between 0.1 to 0.2 pounds.
	Based on the average weights, the watermelon is most likely to be the heaviest fruit individually.
_	

Figure 60: A sample case of physical object property-mass. Back to List of Figures.



Figure 61: A sample case of physical object property-number. Back to List of Figures.

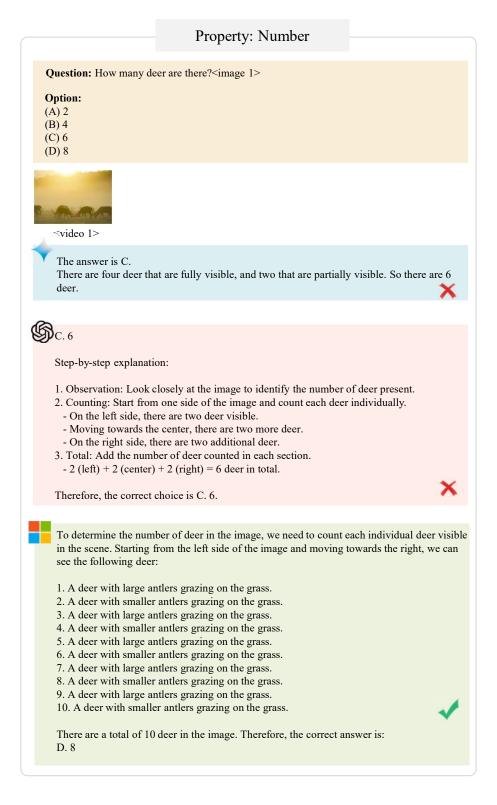


Figure 62: A sample case of physical object property-number. Back to List of Figures.

Property: Attribute	
Question: Can you tell me which point with option in the image points to the object that has the least brittle? <image 1=""/>	
Option: (A) Point A (B) Point B (C) Point C (D) Point D	
<video 1=""></video>	
The answer is B. Here's why:	
 Brittle means easily broken or shattered. A is a wooden clothespin, which can break with enough force. B is a camera lens, made of strong glass and metal, it's designed to withstand impacts and pressure. C is a ceramic plate, which is brittle and easily broken. D is a ceramic mug, also brittle and easily broken. 	
Therefore, the object pointed by B has the least brittle nature.	
×	
Choice: D. Point D	
Reasoning Chain: 1. Understanding Brittleness: Brittleness is a material property that describes the tendency of a material to fracture or break without significant deformation when subjected to stress.	
 Analyzing Objects: Point A (Clothespins): Clothespins are typically made of wood or plastic. Both materials can be somewhat brittle, especially if they are thin and subjected to bending forces. Point B (Camera Lens): Camera lenses are made of glass and metal. Glass is very brittle and can shatter easily upon impact. Point C (Plate): Plates are usually made of ceramic or glass, both of which are brittle materials that can break easily if dropped Point D (Mug): Mugs are often made of ceramic, which is brittle. However, if the mug is made of plastic, it would be much less brittle compared to the other materials listed. 	
 3. Determining the Least Brittle Object: Among the materials listed, plastic is generally the least brittle. Since the mug (Point D) could be made of plastic, it is likely to be the least brittle object in the image. 	
Therefore, the object at Point D (the mug) is the least brittle among the options provided.	
To determine which object is the least brittle, we need to consider the materials and typical usage of each object.	
A. A paperclip is made of metal and is designed to hold papers together. It is not typically brittle, but it can bend or break if subjected to excessive force.	
B. A camera lens is made of glass and is designed to focus light onto a sensor. Glass is a brittle material and can easily break if dropped or subjected to impact.	
C. A plate is made of ceramic or porcelain and is designed to hold food. Ceramic and porcelain are brittle materials and can brea if dropped or subjected to impact.	k
D. A mug is made of ceramic or porcelain and is designed to hold liquids. Ceramic and porcelain are brittle materials and can break if dropped or subjected to impact.	
Based on this analysis, the object with the least brittle material is the paperclip (Option A).	

Figure 63: A sample case of physical object property-attribute. Back to List of Figures.

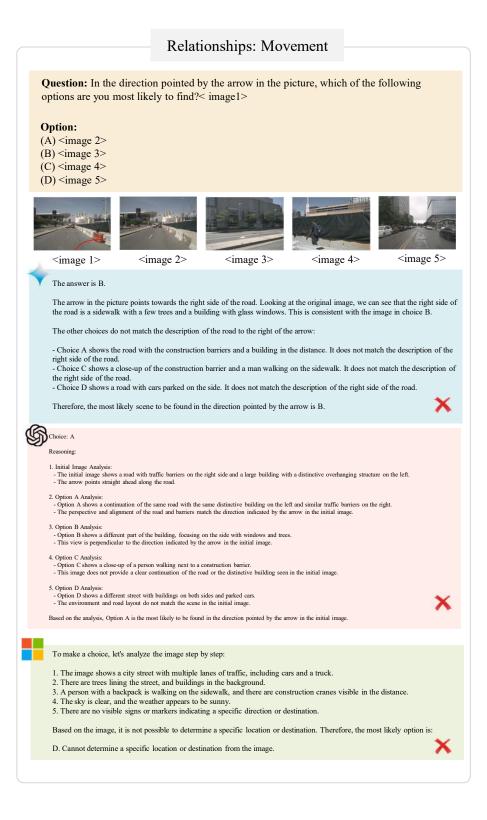


Figure 64: A sample case of physical object relationships-motion. Back to List of Figures.

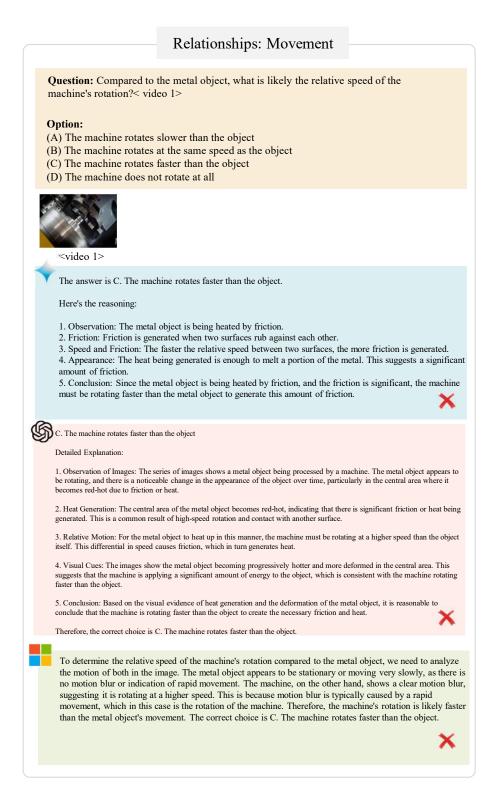


Figure 65: A sample case of physical object relationships-motion. Back to List of Figures.

Relationships: Depth
Question: In terms of depth relative to the camera, where is the bridge primarily located?< video 1>
Option: (A) Closer to the camera than the car (B) Equidistant from the car and the camera (C) Farther from the camera than the car (D) Cannot be determined
<video 1=""></video>
The answer is C. Farther from the camera than the car.
 Here's the reasoning: 1. Identify the key elements: We see a car on the bridge and the bridge itself, with the camera positioned on the bridge surface. 2. Focus on perspective: The car appears closer to the camera because it is in the foreground. The bridge structure extends beyond the car and towards the horizon. 3. Apply the concept of perspective: In perspective, objects farther away appear smaller and less detailed. The bridge appears much larger in scale than the car, suggesting it is farther away from the camera. 4. Conclude: Based on the visual cues of size and distance within the frame, we can conclude that the bridge is farther from the camera than the car.
SC. Farther from the camera than the car
Detailed Explanation: 1. Observation of Images: The series of images shows a bridge with a car on it. The car appears to be in the middle of the bridge, and the bridge structure extends both in front of and behind the car.
2. Relative Positioning: In the images, the car is positioned on the bridge, and the bridge extends further into the background beyond the car. This indicates that the bridge continues past the car, making the bridge structure farther from the camera than the car.
3. Depth Perception: The bridge's towers and cables are visible in the background, indicating that the bridge extends into the distance. The car is closer to the camera than these structures.
4. Conclusion: Since the bridge extends beyond the car and the car is positioned on the bridge, the bridge is primarily located farther from the camera than the car.
Therefore, the correct choice is C. Farther from the camera than the car.
To determine the depth of the bridge relative to the camera, we need to analyze the image and the perspective from which it is taken. The bridge appears to be in the foreground, as it is in sharp focus and there is a clear view of the cables and the road surface. The car, on the other hand, is in the background, as it is out of focus and appears smaller due to the perspective. The bridge is also closer to the camera because the cables and the road surface are in clear view, while the car is not. Therefore, the bridge is primarily located closer to the camera than the car.

Figure 66: A sample case of physical object relationships-depth. Back to List of Figures.

Relationships: Depth				
Question: Identify the closest point to the camera. < image 1> Option: (A) Point A is closest (B) Point B is closest (C) Point C is closest (D) Point D is closest				
<image 1=""/>				
 The answer is D. Here's why: 1. Perspective: We can use the concept of perspective to determine distance. Objects further away appear smaller in a photograph. 2. Object Size: The circles are the same size, allowing us to directly compare their apparent size in the image. 3. Comparison: Circle D appears larger than the other circles, indicating that it is closer to the camera. 				
D. Point D is closest Reasoning: 1. Foreground and Background Analysis:				
 Point D is located on the road, which is in the immediate foreground of the image. Points A, B, and C are situated further back in the field, which is in the background. 2. Perspective and Depth: The road in the foreground appears larger and more detailed, indicating it is closer to the camera. The field and the fence posts in the background appear smaller and less detailed, indicating they are further away. 				
 3. Relative Positioning: Point D is positioned at the bottom of the image, which typically represents the closest point to the viewer in a two-dimensional perspective. Points A, B, and C are higher up in the image, indicating they are further away from the camera. Based on these observations, Point D is the closest to the camera. 				
To solve this task, we need to analyze the image and determine which point is closest to the camera based on the perspective and the size of the points relative to each other. 1. Point A is located at the top of the image. 2. Point B is located to the left of the image. 3. Point C is located to the right of the image. 4. Point D is located at the bottom of the image.				
From the perspective of the camera, the points that are closer to the camera will appear larger and more detailed, while the points that are further away will appear smaller and less detailed. In the image, Point D appears to be the largest and most detailed, while Points A, B, and C appear smaller and less detailed. Therefore, Point D is the closest point to the camera.				
The answer is D. Point D is closest to the camera.				

Figure 67: A sample case of physical object relationships-depth. Back to List of Figures.

Relationships: Distance						
Question: Which object appears closest to the camera in the video? <video 1=""> Option: (A) The metal plate (B) The string (C) The yellow ball (D) The person's hand</video>						
 video 1> 						
The answer is C.The yellow ball.						
Here is the reasoning chain:						
 The yellow ball is the only object that is directly attached to the string and swings in the video. The string is attached to a fixed point above the metal plate. Therefore, the yellow ball is closest to the camera at all times in the video because it is swinging in front of the plate and the person's hand. While the person's hand is closer to the camera at the start, the yellow ball moves to the very front in the second half of the video. 						
Therefore, the yellow ball appears closest to the camera in the video.						
S C. The yellow ball						
Step-by-step explanation:						
1. Observation of Images: By examining the series of images, we can see the relative positions of the objec in each frame.	ts					
2. Depth Perception: Depth perception in images can be inferred by noting which objects overlap others an which objects appear larger or smaller due to perspective.	d					
 3. Relative Positioning: The metal plate (A) is a large, flat object that serves as a background for the other objects. The string (B) is thin and appears to be in the middle of the scene, attached to the top and holding the yellow ball. The yellow ball (C) is held by the string and appears to be in front of the metal plate. 						
 The person's hand (D) is interacting with the yellow ball and is positioned behind it in most frames. 4. Overlapping Objects: The yellow ball overlaps the metal plate and the string, indicating it is in front of them. The person's hand is behind the yellow ball in most frames, indicating the ball is closer to the camera. 						
5. Conclusion: Based on the overlapping and relative positioning, the yellow ball (C) appears closest to the camera in the video.						
To determine which object appears closest to the camera in the video, we need to analyze the image and identify the object that is most in focus and has the smallest depth of field. The metal plate (A) is in the foreground and is in sharp focus, indicating it is the closest object to the camera. The string (B) is also in focus but slightly behind the metal plate. The yellow ball (C) is in focus but further away than the metal plate. The preson's hand (D) is in focus but even further away than the yellow ball. Therefore, the metal plate appears closest to the camera.	*					

Figure 68: A sample case of physical object relationships-distance. Back to List of Figures.

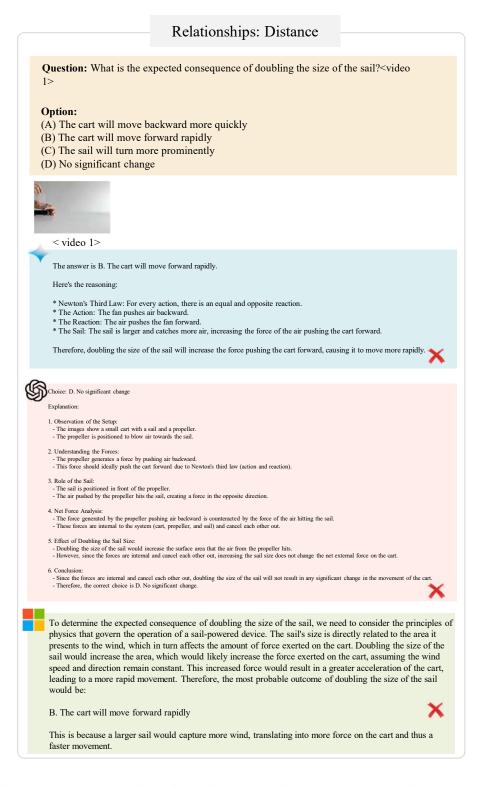


Figure 69: A sample case of physical object relationships-distance. Back to List of Figures.

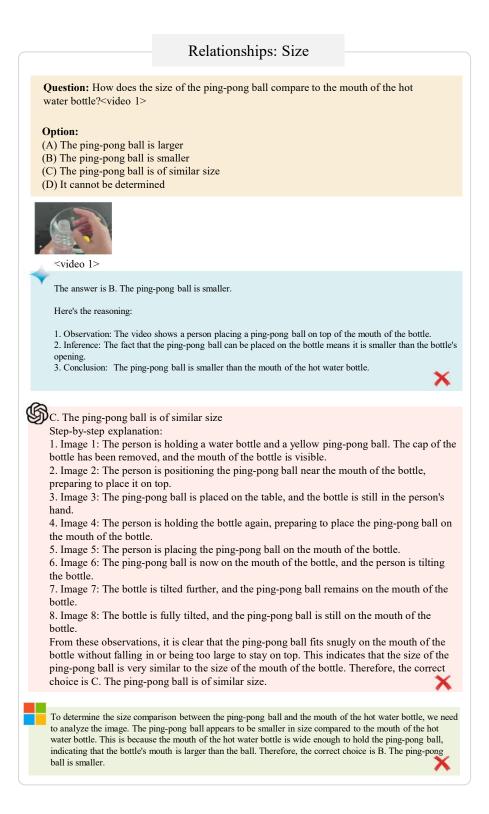


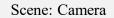
Figure 70: A sample case of physical object relationships-size. Back to List of Figures.

Dynamics: Others						
Question: What type of wave property is predominantly being demonstrated in the video? <video 1=""></video>						
Option: (A) Diffraction (B) Interference (C) Refraction (D) Reflection						
<video 1=""></video>						
The answer is C. Refraction.						
Here's why:						
 What is Refraction? Refraction is the bending of light as it passes from one medium to another (in this case, from the air to the water in the bucket). This bending occurs because the speed of light changes as it moves from one medium to another. 						
2. Observing the Video: The laser beam is clearly changing direction as it enters the water in the bucket. It bends downwards. This is a direct visual indication of refraction.						
3. Eliminating other Options:						
 * Diffraction: Diffraction is the spreading of light waves as they pass through a narrow opening or around an obstacle. There's no clear example of this in the video. * Interference: Interference occurs when two or more waves overlap, resulting in a new wave pattern. The video doesn't show waves interacting in this manner. * Reflection: Reflection is the bouncing of light off a surface. While there is some reflection off the side of the bucket, the primary phenomenon is the bending of the light as it enters the water, which is refraction. 						
C. Refraction						
The series of images predominantly demonstrates the property of refraction. Here is the detailed reasoning:						
 Observation of the Light Path: In the images, a beam of light is seen traveling through a medium (likely water) and bending as it exits the medium. This bending of light is a key indicator of refraction. 						
2. Medium Change: Refraction occurs when light passes from one medium to another and changes speed, causing it to bend. In the images, the light is initially traveling through a transparent medium (possibly water) and then exits into the air, causing the light to bend.						
3. Consistent Bending: The consistent bending of the light path in the images aligns with the behavior of light undergoing refraction. The light beam is not spreading out (diffraction), nor is it showing patterns of constructive or destructive interference (interference). It is also not bouncing back from a surface (reflection).						
4. Contextual Clues: The setup, including the container and the light beam, suggests an experiment designed to show how light behaves when transitioning between different media, which is a classic demonstration of refraction.						
Therefore, the predominant wave property being demonstrated in the video is refraction.						
The video predominantly demonstrates the property of refraction. Refraction is the bending of light as it passes from one medium to another, which is what we see as the red light bending around the edges of the objects in the image. The light is entering the glass at an angle, causing it to change direction, which is a classic example of refraction. This is a common phenomenon that occurs when light passes through transparent materials like glass, where the speed of light changes, causing the light to bend. The other options, such as diffraction, interference, and reflection, do not primarily describe the observed effect in the video. Diffraction involves the spreading of light waves around obstacles or through small openings, interference is the phenomenon where two or more waves superimpose to form a resultant wave of greater, lower, or the same amplitude, and reflection is the bouncing back of light from a surface, which is not the main focus of this video. Therefore, the correct answer is C. Refraction.						

Figure 71: A sample case of physics-based dynamics—others. Back to List of Figures.

Relationships: Size	
Question: Compared to the horse drawing, how is the size of the striped	
paper? <video 1=""></video>	
Option: (A) Smaller than the drawing (B) Exactly the same as the drawing (C) Larger than the drawing (D) Not relevant	
<pre>svideo 1></pre>	
The answer is C. Larger than the drawing.	
Here's why:	
 The striped paper covers the entire horse drawing. This means the striped paper has to be at least as large as the drawing. The striped paper extends beyond the horse drawing. The edges of the striped paper can be seen extend past the boundaries of the drawing. This indicates the striped paper is larger than the drawing. The striped paper is not a perfect fit. The drawing is centered on the striped paper. If it were the same si the striped paper would be exactly the same dimensions as the drawing. 	ing
Therefore, the striped paper is larger than the horse drawing.	
C. Larger than the drawing	
Detailed Explanation: 1. Observation of the Images: - The first two images show a drawing of a horse on a piece of paper The first two images show a drawing of a horse on a piece of paper The first two images show a drawing of a horse on a piece of paper The first two images show a drawing of a horse on a piece of paper The first two images show a drawing of a horse on a piece of paper The first two images show a drawing of a horse on a piece of paper The first two images show a drawing of a horse on a piece of paper The first two images show a drawing of a horse on a piece of paper The first two images show a drawing of a horse on a piece of paper The first two images show a drawing of a horse on a piece of paper The first two images show a drawing of a horse on a piece of paper The first two images show a drawing of a horse on a piece of paper The first two images show a drawing of a horse on a piece of paper The first two images show a drawing of a horse on a piece of paper The first two images show a drawing of a horse on a piece of paper The first two images show a drawing of a horse on a piece of paper The first two images show a drawing of a horse on a piece of paper The first two images show a drawing of a horse on a piece of paper The first two images show a drawing of a horse on a piece of paper The first two images show a drawing of a horse on a piece of paper The first two images show a drawing of a horse on a piece of paper The first two images show a drawing of a horse on a piece of paper The first two images show a drawing of a horse on a piece of paper The first two images show a drawing of a horse on a piece of paper The first two images show a drawing of a horse on a piece of paper The first two images show a drawing of a horse on a piece of paper The first two images show a drawing of a horse on a piece of paper The first two images show a drawing of a horse on a piece of paper The first two images show a dra	
 The subsequent images show a striped paper being placed over the horse drawing. Comparison of Sizes: In the first two images, the horse drawing is clearly visible and occupies a certain area on the paper. In the later images, the striped paper is placed over the horse drawing, and it covers the entire drawing and extends beyond i 	t.
 Edges and Coverage: The striped paper not only covers the horse drawing completely but also extends beyond the edges of the drawing, indicating that it is larger than the drawing itself. 	ş
 Conclusion: Since the striped paper covers the entire horse drawing and extends beyond it, it is evident that the striped paper is larger that the horse drawing. 	n
Therefore, the correct choice is C. Larger than the drawing.	
To determine the size of the striped paper compared to the horse drawing, we need to analyze the image and the text provided. The text "4. motion illusion" is repeated multiple times, which suggests that this is a sequence of images or a video. The striped paper appears to be larger than the horse drawing, as the horse drawing is partially obscured by the striped paper. The striped paper covers the entire drawing, indicating that it is larger in size. Therefore, the correct answer is:	d
C. Larger than the drawing	

Figure 72: A sample case of physical object relationships-size. Back to List of Figures.



Question: Based on the effects in the video, which of these camera changes would result in the observed phenomenon? <video 1>

Option:

- (A) The camera rotates along the vertical axis (upside or downside)
- (B) The camera moves upward or downward
- (C) The camera rotates along the horizontal axis (left or right)
- (D) The camera is farther away from the objects



<video 1>

The answer is C. The camera rotates along the horizontal axis (left or right).

Here's the reasoning:

1. Observe the motion: The objects are moving in a way that suggests a rotation around a horizontal axis. The bagel and cereal bowl move in an arc, indicating a shift in their position relative to the camera's viewpoint. The milk splash appears to be moving in a circular pattern.

2. Eliminate other options:

* A. The camera rotates along the vertical axis (upside or downside): This would cause the objects to appear to move up and down, not in the arcing motion we see.

* B. The camera moves upward or downward: This would make the objects appear closer or farther away, not change their positions relative to each other in the way we see. * D. The camera is farther away from the objects: This would make the objects appear smaller, but not change their relative

positions in the frame.

3. Conclusion: The only camera movement that aligns with the observed motion is a rotation along the horizontal axis (left or right). This would cause the objects to appear to move in arcs as the camera's perspective shifts.

Choice: C. The camera rotates along the horizontal axis (left or right)

Explanation

. Understanding the Phenomenon: The question asks about the observed phenomenon in the video based on a series of images sampled at equal intervals. To etermine the correct camera change, we need to understand how each type of camera movement affects the images.

2. Analyzing Each Option

Option A (Camera rotates along the vertical axis): If the camera rotates upside or downside, the images would show a tilting effect. Objects would appear to tilt either upwards or downwards, which would be noticeable in the sampled images.
 Option B (Camera noves upward) or downward): If the camera moves vertically, the perspective of the objects would change. Objects would appear to move up or down in the frame, but their orientation would remain the same.

- Option C (Camera rotates along the horizontal axis): If the camera rotates left or right, the perspective of the scene would change horizontally. Objects

Option C (cancer to that's along in the total status) in the cancer to the status of th

 Matching the Phenomenon to the Camera Change:
 The key to identifying the correct camera change is to match the observed phenomenon in the images to the expected effect of each camera movement - If the images show a change in the horizontal perspective, where objects appear to shift left or right and the angle of view changes, this indicates a horizontal rotation of the camera.

4. Conclusion

The observed phenomenon in the images is best explained by the camera rotating along the horizontal axis (left or right). This would result in a change in the horizontal perspective of the scene, which matches the description of the observed phenor , the correct choice is C. The camera rotates along the horizontal axis (left or right). The observed phenomenon in the video is the appearance of floating objects, such as the bowl of nuts and the cinnamon rolls, against a plain background. This effect is created by manipulating the camera's position and orientation. To achieve this effect, the camera needs to be positioned at a certain distance from the objects and then rotated along the vertical axis (upside or downside). This rotation creates the illusion that the objects are floating in the air.

Therefore, the correct choice is A. The camera rotates along the vertical axis (upside or downside).

Figure 73: A sample case of physical scene understanding-viewpoint. Back to List of Figures.

		Relationships: Location				
	Question: Where does the projection of the butterfly appear in the video? <video 1=""> Option: (A) On the ceiling</video>					
	(B) On the wall behind t(C) On the floor(D) On the table	he bowl				
	<video 1=""></video>					
The answer is D. On the table.						
	 Perspective: The bo the table. Illusion: The butter created by the pyramid Actual Location: A 	We see the butterfly hovering within the pyramid-shaped owl is placed on a table, and we can see its reflection on t fly appears suspended in mid-air inside the bowl, which i d's geometry and the way light refracts through it. Ithough the butterfly appears to be suspended, it is actual ole surface, which creates the illusion of depth and move	he surface of is an illusion ly a			
	Therefore, the project	ion of the butterfly appears on the table.	×			
	D. On the table					
	Detailed Explanation: 1. Observation of the Setup: The images show a transparent, pyramid-like structure placed on a flat surface, which appears to be a table. This structure is commonly used for creating holographic projections.					
	or a tablet. This is a typical	base of the pyramid is placed on a flat, reflective surface, which is lise setup for a holographic display where the image is projected from the pyramid to create a 3D effect.				
	butterfly is not projected or	: In the series of images, the butterfly appears within the pyramid st to the ceiling, wall, or floor, but rather it is seen floating inside the	pyramid.			
		vramid is placed on the table and the butterfly appears within the py en or tablet) is on the table. Therefore, the projection of the butterfly				
÷	Thus, the correct choice is	D. On the table.	~			
	image and the context	e projection of the dog appears in the video, we need to a provided by the question. The image shows a dark room bject with a projection of a butterfly on it. The projection swer is unknown.	with a stone			

Figure 74: A sample case of physical object relationships-location. Back to List of Figures.

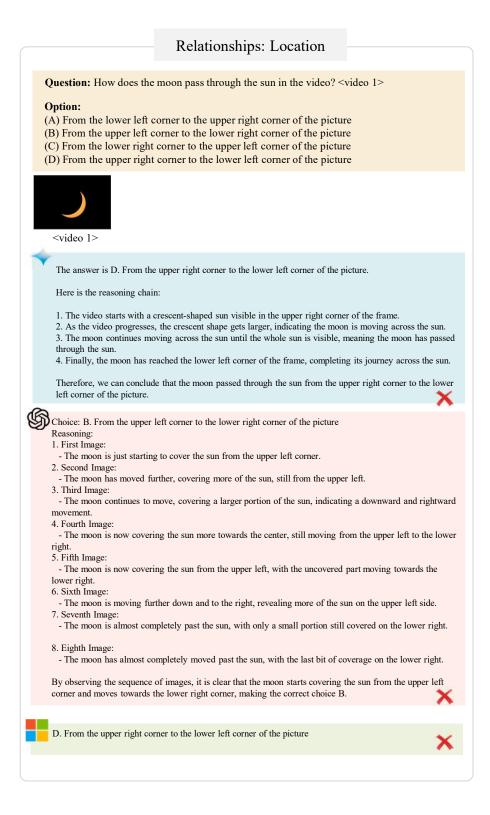


Figure 75: A sample case of physical object relationships-location. Back to List of Figures.

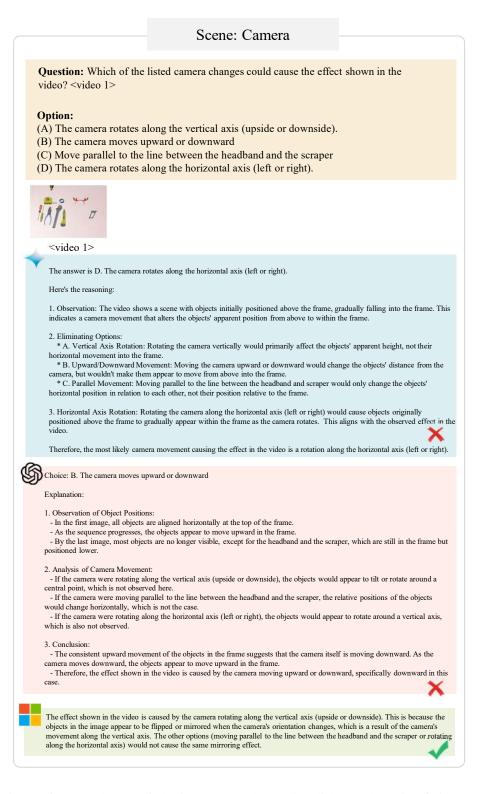


Figure 76: A sample case of physical scene understanding-light. Back to List of Figures.

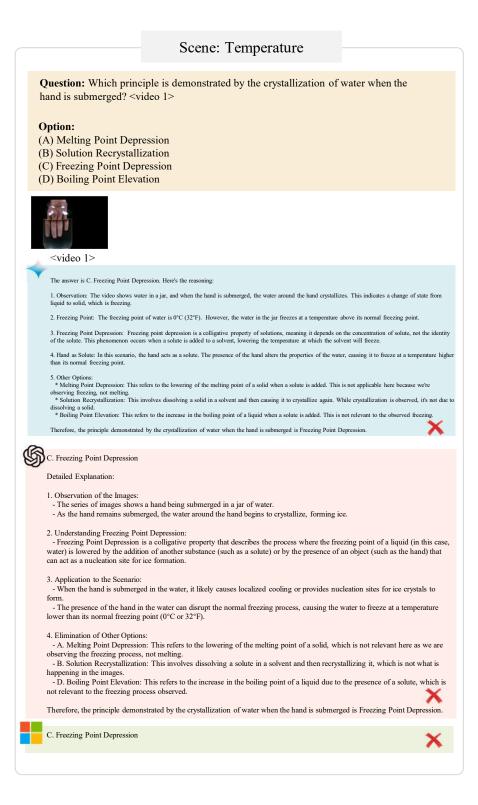


Figure 77: A sample case of physical scene understanding-temperature. Back to List of Figures.

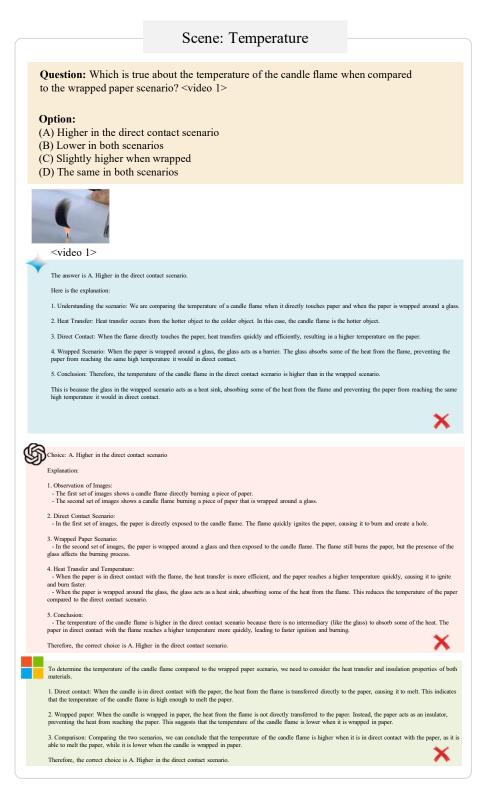


Figure 78: A sample case of physical scene understanding-temperature. Back to List of Figures.

Dynamics: Gas	
Ĵ	
Question: Which option accurately represents the correct sequence of events in gasification from the choices below? <image 1=""/> <image 2=""/> <image 3=""/>	
Option: (A) 3 - 2 - 1 (B) 2 - 1 - 3 (C) 1 - 2 - 3 (D) 2 - 3 - 1	
<pre><image 1=""/></pre> <image 2=""/> <image 3=""/>	
Ý	
The correct answer is C. 1 - 2 - 3	
Here's the reasoning:	
 Image 1: Shows a dry whetstone, indicating the starting point. Image 2: Depicts water being added to the whetstone. This is the first step in the gasification proces where water is introduced. Image 3: Shows the whetstone soaked in water, illustrating the final stage of gasification. 	s, 🗙
Therefore, the sequence 1-2-3 accurately represents the steps involved in the gasification of the whetse	ione.
(S) C. 1 - 2 - 3	
The correct sequence of events in the images is as follows:	
1. Image #1: The block is dry and has no visible liquid on its surface.	
2. Image #2: Some liquid has been applied to the block, but it is not fully covered. There are a few pate	hes
of liquid. 3. Image #3: The block is now more thoroughly covered with liquid, indicating that more liquid has be applied over time.	en
The sequence shows the progression from a dry block to a block with some liquid, and finally to a bloc with more liquid. Therefore, the correct order is 1 (dry block), 2 (some liquid), and 3 (more liquid).	k X
To determine the correct sequence of events in gasification, we need to analyze the images and the changes they show.	
image #1 shows the box before any gasification process has occurred. It is a solid black color with a clear silhouette of a h it.	orse on
image #2 shows the box after the first step of gasification. The silhouette of the horse is now partially obscured by a white substance, which is likely the gas produced during the first step.	
image #3 shows the box after the second step of gasification. The white substance has spread out and is now covering the surface of the box, indicating that the gas has been released and is filling the box.	entire
Based on this analysis, the correct sequence of events is:1. The box is placed in the gasifier (image #1).2. The gasification process begins, and the horse silhouette is partially obscured by the gas (image #2).3. The gas is released and fills the box (image #3).	
Therefore, the correct answer is C. 1 - 2 - 3.	×

Figure 79: A sample case of physics-based dynamics—air. Back to List of Figures.

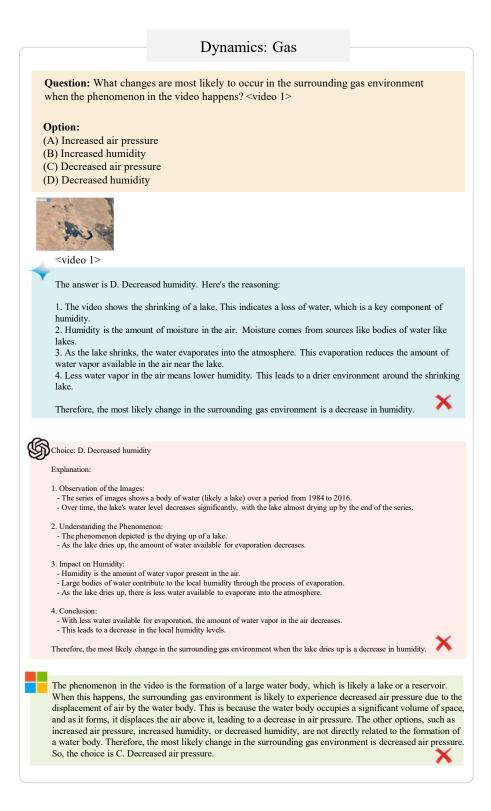


Figure 80: A sample case of physics-based dynamics-air. Back to List of Figures.

Dynamics: Manipulation
Question: To mix the tongs, which point is most suitable? <image 1=""/>
Option: (A) Point A (B) Point B (C) Point C (D) Point D
<image 1=""/>
The answer is D. Point D. Here's why:
 Purpose: The goal is to mix the tongs. This requires a grip that allows for twisting and turning. Point D's Grip: Point D is located at the juncture of the two tongs, where they form a "V" shape. This position provides a strong grip and allows for leverage. Other Points: Point A: Is near the end of the tong, providing less grip and making it difficult to twist. Point B: Is at the base of the tong, where the metal is thinner, making it prone to bending. Point C: Is in the middle of the tong, offering a decent grip but not as much leverage as point D.
In conclusion, Point D offers the best combination of grip and leverage for twisting and mixing the tongs effectively.
Choice: B. Point B
Reasoning:
 Function of Tongs: Tongs are typically used to grip and lift objects. The design of the tongs in the image suggests they are used for handling small items, possibly sugar cubes or similar.
 Structure Analysis: Point A: This is part of the handle, which is not suitable for mixing as it is designed to be held by the user. Point C: This is also part of the handle, closer to the gripping end but still not designed for mixing. Point D: This is the inner part of the gripping end, which is not ideal for mixing as it is designed to grip objects. Point B: This is the outer part of the gripping end, which is rounded and spoon-like, making it suitable for mixing. Design Consideration: The rounded, spoon-like end at Point B is designed to interact with the items being handled. This shape
is ideal for mixing as it can stir and combine ingredients effectively. 4. Practical Use: When mixing, a rounded end like Point B can move through the mixture smoothly, ensuring even distribution of ingredients. The other points (A, C, and D) are either flat or designed for gripping, not for stirring.
Therefore, Point B is the most suitable for mixing.
To mix the tongs, the most suitable point would be Point C.
 Here's the reasoning chain: Point A is the topmost point of the tongs, which is not ideal for mixing as it's the farthest from the handle. Point B is the bottom point of the tongs, which is also not ideal for mixing as it's the farthest from the handle. Point C is the middle point of the tongs, which is the most suitable for mixing as it's the closest to the
handle. 4. Point D is the point where the tongs are bent, which is not ideal for mixing as it's not a straight line.
So, the most suitable point for mixing the tongs is Point C.

Figure 81: A sample case of physics-based dynamics—manipulation. Back to List of Figures.

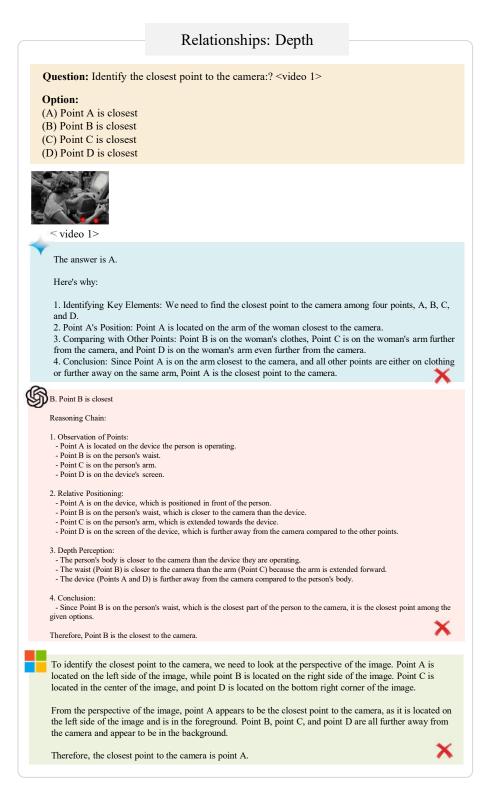


Figure 82: A sample case of physics-based dynamics-fluid. Back to List of Figures.

D	•	T1 · 1
1)vna	mics:	F11110
L y IIa	unico.	I IUIU

Question: Based on the visual phenomena in the video, which alteration to the light source is most likely to be the cause? <video 1>

Option:

(A) It's just that the light source is weaker and the light source position remains the same (B) The color of the light changes from purple to yellow

(C) It's just that the light source is stronger and the light source position remains the same (D) The color of the light changes from green to limeyellow



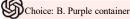
< video 1>

The answer is D. Blue container.

Here's the reasoning:

- 1. The cyan fluid is initially blocked by the purple stick.
- 2. If the purple stick were removed, the cyan fluid would flow downwards freely.
- 3. There's no other obstacle in the path of the cyan fluid, so it would continue downwards until it reaches the blue container. х

4. Therefore, the cyan fluid would flow into the blue container.



Explanation:

1. Initial Setup:

- The images show a setup where colored fluids flow from the top to the bottom through a series of sticks that direct the flow into different containers.

2. Observation of Fluid Paths:

- The cyan fluid starts from the top left and flows downwards.
- The purple stick is positioned such that it directs the cyan fluid towards the green container.
- 3. Effect of Removing the Purple Stick:

the cyan fluid to flow into the purple container.

- If the purple stick is removed, the cyan fluid will no longer be directed towards the green container. - Instead, the cyan fluid will follow the path of least resistance, which is directly downwards.
- 4. New Path of Cyan Fluid:
- Without the purple stick, the cyan fluid will flow straight down.
- The next obstacle in its path is the orange stick, which will direct the cyan fluid towards the right.

5. Final Destination:

- After being directed to the right by the orange stick, the cyan fluid will flow into the purple container.

Therefore, if the purple stick were removed, the cyan fluid would flow into the purple container. If the purple stick were removed, the cyan fluid would flow into the purple container. This is because the purple stick is acting as a barrier between the cyan and purple containers, preventing the cyan fluid from flowing into the purple container. With the purple stick removed, there would be no obstruction, allowing

Figure 83: A sample case of physics-based dynamics—fluid. Back to List of Figures.

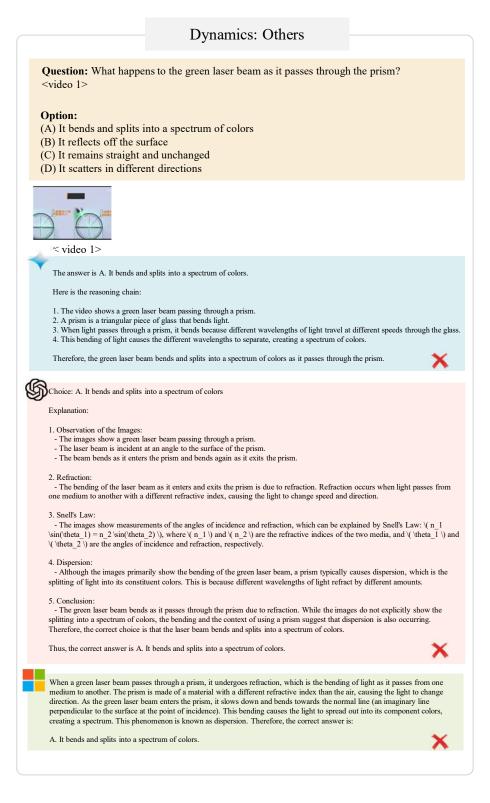


Figure 84: A sample case of physics-based dynamics----others. Back to List of Figures.

	Dynamics: Others
	Question: What is shown happening in the video? <video 1=""></video>
	Option: (A) Can't tell (B) Flowers bloom (C) Flowers grow (D) Flowers wither
	<video 1=""></video>
	The answer is A. Can't tell.
	Here's the reasoning:
	 The video is static: The video only shows a single image of a flower. No movement or change: There is no visual indication of growth, blooming, or withering. Lack of context: The video provides no information about the flower's life cycle or the time period captured.
	Therefore, based on the provided information, we cannot determine what is happening in the video.
5	B. Flowers bloom
	Step-by-step explanation:
	1. Observation of Initial Images: The first few images show a flower that is partially open. The petals are not fully spread out, and the central part of the flower is not fully visible.
	2. Progression Over Time: As we move through the series of images, the petals of the flower gradually spread out more, and the central part of the flower becomes more prominent and visible.
	3. Final Images: In the last few images, the flower appears to be fully open, with the petals spread wide and the central part fully visible.
	4. Conclusion: The sequence of images shows the flower transitioning from a partially open state to a fully open state, indicating that the flower is blooming.
	Therefore, the correct choice is B. Flowers bloom.
	The image shows a single yellow daffodil in focus with a blurred background. The daffodil appears to be in full bloom with a bright yellow center and petals that are slightly curled at the edges. There is no clear indication of movement or change over time, so it is not possible to determine what is happening in the video based on this still image. Therefore, the answer is A. Can't tell.

Figure 85: A sample case of physics-based dynamics—others. Back to List of Figures.

Dynamics: Collision
Question: If the green sphere were much heavier, which direction would the red pulley move? <video 1=""></video>
Option: (A) Stationary (B) Up (C) Down (D) Left
الم ج video 1>
The answer is C. Down.
Here is the reasoning chain:
 If the green sphere is much heavier than the pink sphere, the green sphere will pull down on the yellow rope it's attached to. The yellow rope is also attached to the blue pulley, so the blue pulley will also be pulled down. The blue pulley is connected to the red pulley by a separate yellow rope. When the blue pulley goes down, this rope will also be pulled down. The red rollow is extrached to the integration of the problem of the pulley down.
- The red pulley is attached to this yellow rope, so it will also be pulled down. Therefore, the red pulley will move down.
Choice: C. Down
Explanation:
 Understanding the System: The images show a system of pulleys with weights attached to them. The red pulley is connected to a grey weight. The green sphere is part of a different pulley system but is connected to the same overall structure.
2. Observing the Motion:- In the series of images, the red pulley and its grey weight remain stationary.- The green sphere and the blue weight are moving downwards.
3. Effect of Increasing the Green Sphere's Weight:If the green sphere were much heavier, it would exert a greater downward force on its pulley system.This increased force would cause the green sphere to move downwards more rapidly.
 4. Impact on the Red Pulley: The pulley systems are interconnected. The increased downward force from the heavier green sphere would create a greater tension in the connecting ropes. This increased tension would pull the red pulley downwards as well, as the system seeks to balance the forces.
 Conclusion: Given the interconnected nature of the pulley systems, a much heavier green sphere would result in a downward movement of the red pulley due to the increased tension in the ropes.
Therefore, the red pulley would move down.
C. Down

Figure 86: A sample case of physics-based dynamics-collision. Back to List of Figures.

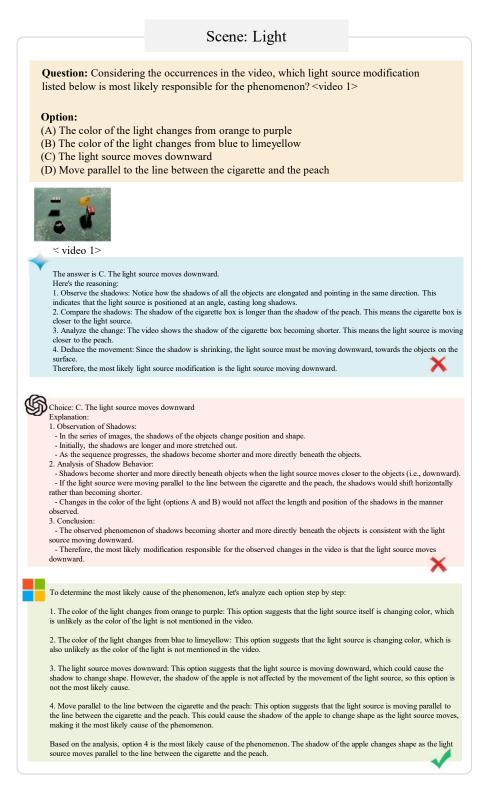


Figure 87: A sample case of physical scene understanding-light. Back to List of Figures.

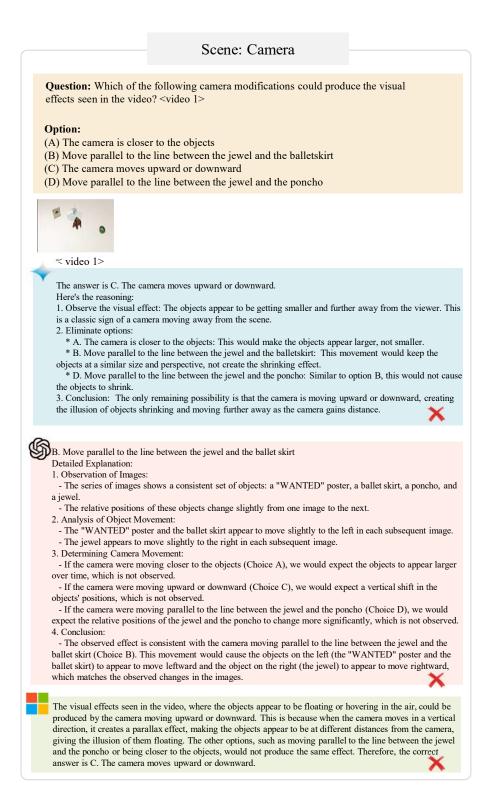


Figure 88: A sample case of physical scene understanding-viewpoint. Back to List of Figures.

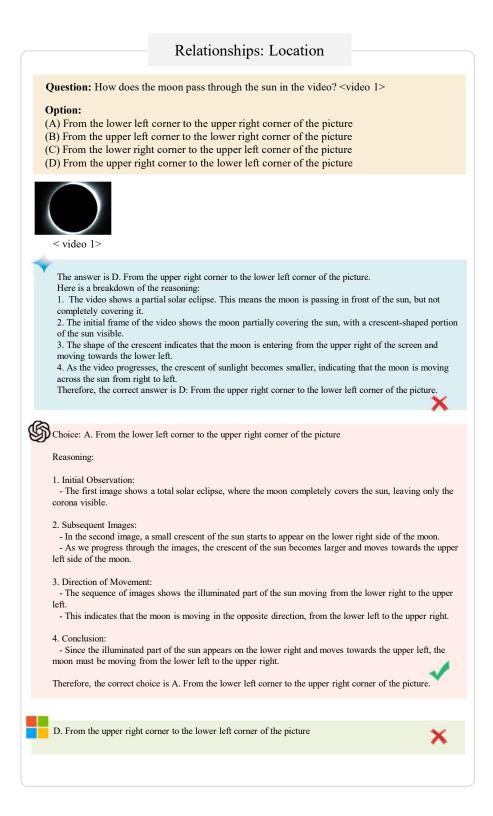


Figure 89: A sample case of physical object relationships-location. Back to List of Figures.

Property: Attribute
Question: Which point with option in the image represents the object that possesses the most brittle? <image 1=""/>
Option: (A) Point A (B) Point B (C) Point C (D) Point D
The answer is A.
 Here's why: 1. Understanding Brittleness: Brittleness refers to a material's tendency to break or fracture under stress, with little to no deformation. 2. Analyzing the Objects: * A (Axe): An axe is made of metal, specifically steel. Steel is known for its strength but can be brittle, especially if the axe is made of a lower quality steel or has been damaged. * B (Bowl): The bowl appears to be ceramic, which is generally brittle. However, it's a relatively simple shape, designed to withstand some pressure. * C (Barrel): The bornel is made of wood, which is known for its flexibility and resistance to bending. It is not inherently brittle. * D (Life Jacket): The bife jacket is likely made of a combination of materials like nylon and foam. These materials are designed to be flexible and resistant to tearing, not brittle. 3. Conclusion: Based on these factors, the axe (Point A) is the most likely object to be brittle. While the bowl could be brittle, the axe's design and potential for lower quality steel make it the most probable choice.
Choice: B. Point B
Reasoning:
 Understanding Brittleness: Brittleness is a material property that describes the tendency of a material to fracture or break without significant deformation when subjected to stress. Brittle materials absorb relatively little energy prior to fracture.
 Analyzing the Objects: Point A (Axe): An axe is typically made of metal, which can be tough and durable. Metals used for tools like axes are usually not brittle; they are designed to withstand impact and stress. Point B (Bowl): The bowl appears to be made of a material that could be ceramic or glass. Both ceramics and glass are known for their brittleness. They can shatter or break easily when dropped or struck. Point C (Barrel): The barrel is likely made of wood or metal. Wood is generally not brittle; it can bend and absorb impact to some extent. Metal barrels are also designed to be durable and not brittle. Point D (Life Jacket): A life jacket is made of soft, flexible materials like foam and fabric. These materials are not brittle; they are designed to be buoyant and flexible.
 Conclusion: Among the objects, the bowl at Point B is the most likely to be brittle. Ceramics and glass are classic examples of brittle materials, as they can break or shatter easily under stress.
Therefore, the object at Point B represents the most brittle material.
 To solve this task, let's examine each object and its corresponding point in the image: Point A: A wooden stick. Point B: A metal bowl. Point C: A wooden barrel. Point D: A leather bag. Now, let's analyze the brittleness of each object: Wooden stick (Point A): Wood is a natural material that can be brittle, especially when it's dy. Metal bowl (Point B): Metal is a strong material that can be brittle. Wooden barrel (Point C): Wood is a natural material that can be brittle, especially when it's old or dy. Leather bag (Point D): Leather is a natural material that can be brittle, especially when it's old or dy.
Based on this analysis, the objects that possess the most brittleness are the wooden stick (Point A) and the wooden barrel (Point C). Therefore, the answer is D. Point D (the leather bag) and A. Point C (the wooden barrel) represent the objects that possess the most brittleness.

Figure 90: A sample case of physical object property-attribute. Back to List of Figures.





Figure 91: A sample case of physics-based dynamics----manipulation. Back to List of Figures.

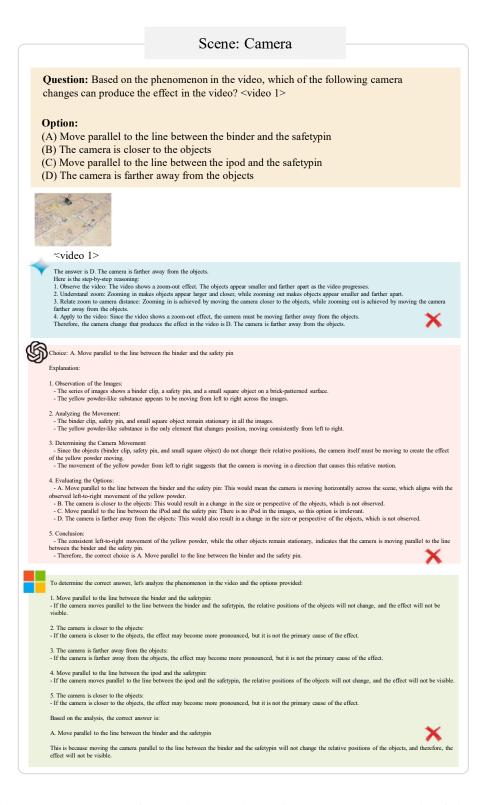


Figure 92: A sample case of physical scene understanding-viewpoint. Back to List of Figures.



Question: Referring to the phenomenon shown in the video, which light source change from the options below would most likely be the cause? <video 1> **Option:** (A) The color of the light changes from limeyellow to pink (B) It's just that the light source is weaker and the light source position remains the same (C) It's just that the light source is stronger and the light source position remains the same (D) Move parallel to the line between the backpack and the cake <video 1> The answer is D. Move parallel to the line between the backpack and the cake. Here's the rea 1. Observe the shadows: The shadows in the video are elongated and clearly defined, indicating a light source that is positioned relatively close to the objects. 2. Analyze the shadow changes: The shadows of the objects are moving over time. This indicates that the light source itself is also moving, not just changing in intensity or color 3. Identify the shadow movement pattern: The shadows appear to be moving in a direction that is parallel to the line connecting the backpack and the cake. 4. Deduce the light source movement: For the shadows to move in this way, the light source must also be moving in a direction parallel to the line connecting the backpack and the cake. 5. Eliminate other options: * A. Color change wouldn't affect shadow movement. * B. A weaker light source would make the shadows less defined, not move them. х * C. A stronger light source wouldn't change the direction of the shadows. Therefore, the most likely cause of the shadow changes in the video is a light source moving parallel to the line between the backpack and the cake Choice: D. Move parallel to the line between the backpack and the cake Reasoning Chain: 1. Observation of Shadows: - The series of images shows a consistent shadow cast on the ground. - The shadow's shape and position change slightly across the images. 2. Analysis of Shadow Movement: - The shadow appears to move horizontally across the images. - The objects (backpack, cake, ham, and barrel) remain stationary, indicating that the change is due to the light source movement. 3. Light Source Position: - The shadow's movement suggests that the light source is moving. - The direction of the shadow's movement indicates the direction of the light source's movement. 4. Direction of Light Source Movement: The shadow moves in a manner that suggests the light source is moving parallel to the line between the backpack and the cake. - This movement would cause the shadow to shift horizontally as observed in the images. х 5. Elimination of Other Options - Option A (Color Change): The images do not show any change in the color of the light. - Option B (Weaker Light Source): A weaker light source would result in a dimmer scene, not a change in shadow position. - Option C (Stronger Light Source): A stronger light source would result in a brighter scene, not a change in shadow position. Therefore, the most likely cause of the phenomenon shown in the video is that the light source is moving parallel to the line between the backpack and the cake. The most likely cause of the change in light source is that the light source is weaker and the light source position remains the same. This is because the shadow of the backpack and the cake appears to be getting larger, indicating that the light source is moving further away from the objects. The other options do not explain the change in shadow size.

Figure 93: A sample case of physics-based dynamics—collision. Back to List of Figures.

Relationships: Location
Question: Relative to the movement of the rope, what is the position of the hand initiating the wave? <video 1=""></video>
Option: (A) At the rope's middle point. (B) At the free end of the rope. (C) Near the rope's starting end. (D) At both ends simultaneously.
 video 1>
The answer is C. Near the rope's starting end.
 Here's the breakdown: Observe the motion: The rope is shown oscillating in a standing wave pattern. Standing waves occur when waves traveling i opposite directions interfere with each other. Identify the fixed point: The rope is fixed at the top, indicating that the end attached to the ceiling is a node (a point of no displacement). Recognize the pattern: The hand holding the rope is moving up and down, generating the wave. The rope oscillates, creating alternating nodes (N) and antinodes (A) along its length. Analyze the hand's position: The hand is always near the rope's starting end, not at the middle or the free end, and it's not at both ends simultaneously. Confirm the choice: The hand's movement is responsible for initiating the wave and creating the standing wave pattern, whic aligns with the choice of being near the rope's starting end.
Therefore, the position of the hand initiating the wave is near the rope's starting end.
 C. Near the rope's starting end Explanation: Observation of the Images: The images show a rope exhibiting different harmonic modes (1st, 2nd, 3rd, and 5th harmonics). The hand initiating the wave is visible in each image, and it is consistently positioned at one end of the rope. Understanding Harmonics: Harmonics are standing wave patterns that occur at specific frequencies. The 1st harmonic fundamental frequency) has one antinode (A) in the middle and nodes (N) at the ends. The 3rd harmonic has three antinodes and three nodes. The 3rd harmonic has three antinodes and four nodes. The 5th harmonic has free antinodes and six nodes. In each image, the hand is seen moving the rope to create these standing wave patterns. The hand is always at the same end of the rope, which is the starting end where the wave is initiated. Conclusion: Since the hand is consistently at the same end of the rope and not in the middle or at both ends, the correct answer is that the hand is near the rope's starting end.
To determine the position of the hand initiating the wave, we need to analyze the image and the movement of the rope. The rope is shown in motion, and we can see the hand at the end of the rope. The hand appears to be at the end of the rope, as it is the only hand visible and the rope is extending from it. The rope is moving from the top left to the bottom right of the image, indicating that the hand is pulling the rope from the top left to the bottom right. Therefore, the hand initiating the wave is at the end of the rope. The correct answer is: C. At both ends simultaneously

Figure 94: A sample case of physics-based dynamics——throwing. Back to List of Figures.

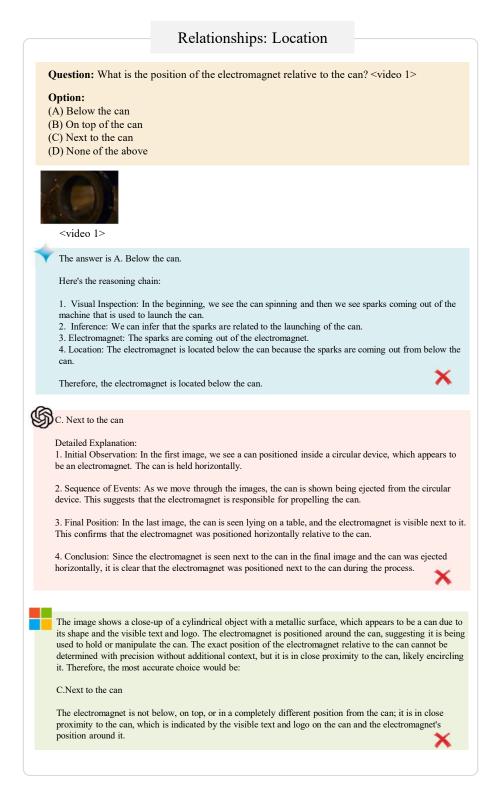


Figure 95: A sample case of physical object relationships-location. Back to List of Figures.

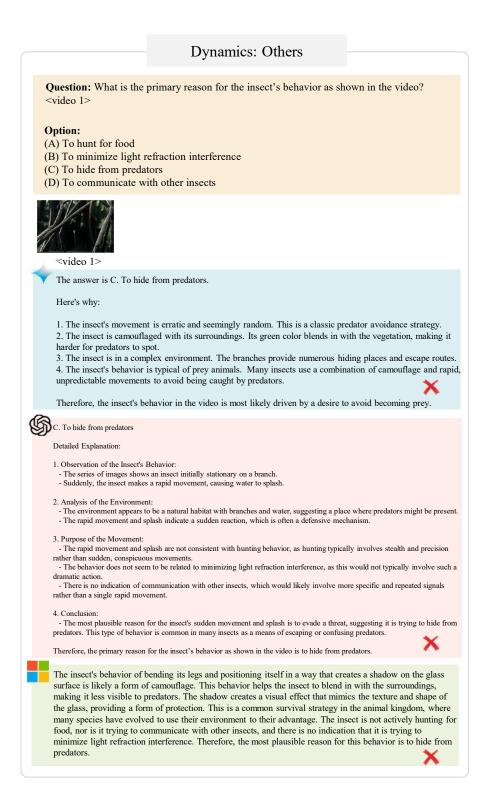


Figure 96: A sample case of physics-based dynamics—fluid. Back to List of Figures.

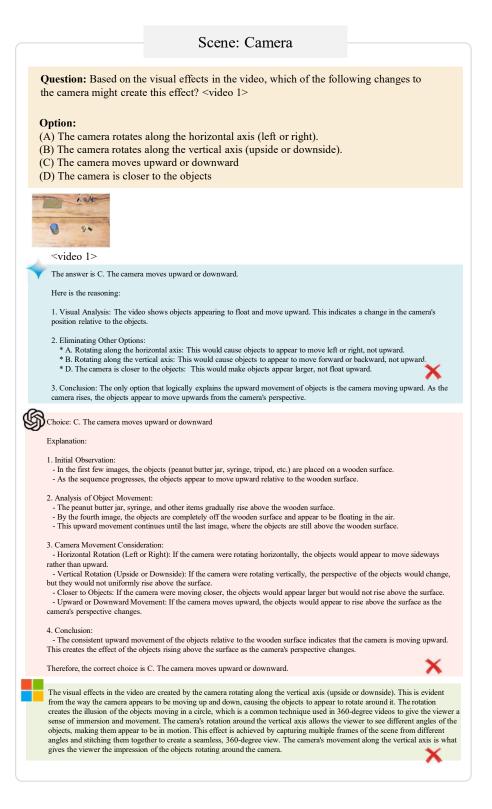


Figure 97: A sample case of physical scene understanding-viewpoint. Back to List of Figures.

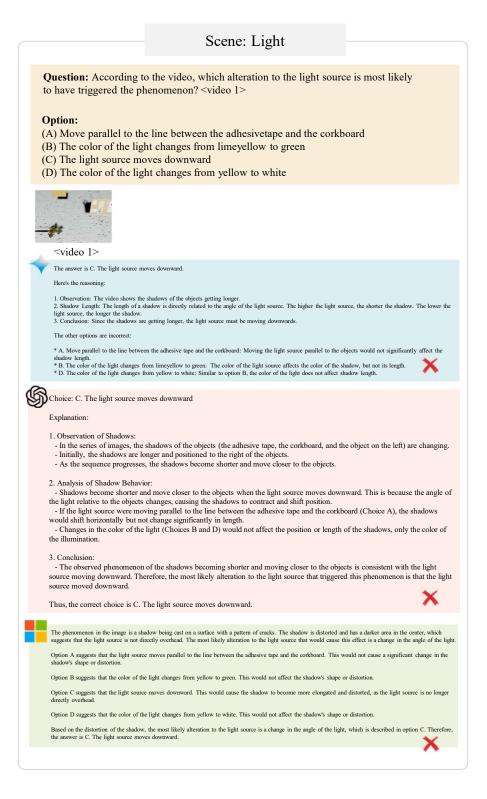


Figure 98: A sample case of physical scene understanding-light. Back to List of Figures.

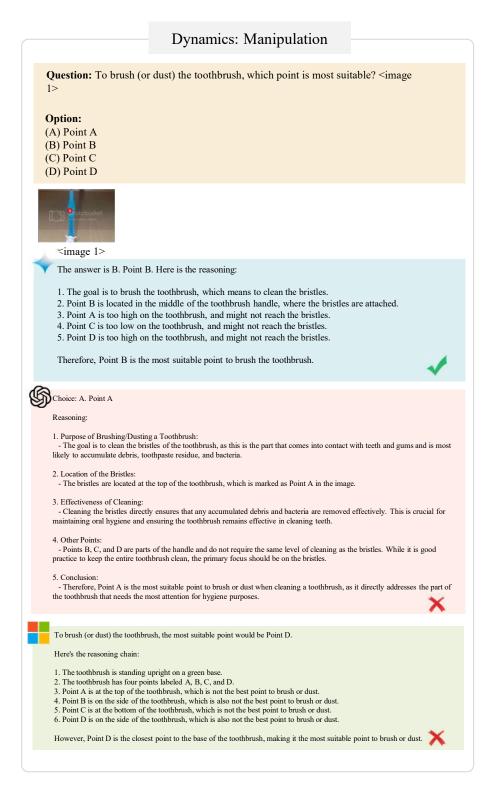


Figure 99: A sample case of physics-based dynamics-manipulation. Back to List of Figures.

	Dynamics: Collision
h C (/	Question: If the red sphere were much heavier, which direction would the purple ollow pulley rotate? <video 1=""> Option: A) Anti-clockwise 3) Clockwise</video>
	C) Stationary D) Uncertain
	video 1>
-	The answer is A. Anti-clockwise.
	Here's the step-by-step explanation:
	 Identify the forces: The system has three main forces: & Gravity: Pulling the red sphere down. * Tension in the purple belt: This tension is created by the weight of the red sphere. * Tension in the green belt: This tension is created by the weight of the red sphere and the weight of the white sphere (though the weight of the white sphere is irrelevant in this case since the green belt is not directly connected to the purple pulley).
	 Analyze the purple pulley: The purple pulley is connected to the red sphere via the purple belt. Since the red sphere is heavier, it exerts a larger downward force. This force will cause the purple belt to move downward on the right side and upward on the left side. Determine the rotation: The upward movement of the purple belt on the left side of the pulley will cause the pulley to rotate anti-clockwise. This is because the belt is fixed to the pulley, and as the belt moves upward, it pulls the top portion of the pulley
~	with it, causing the rotation.
\$	Choice: B. Clockwise Explanation: 1. Understanding the System:
	 The system consists of a series of pulleys and weights connected by ropes. The purple hollow pulley is the one in question, and it is connected to other pulleys and weights.
	 Current Movement: From the series of images, it is observed that the red sphere is moving upwards while the white sphere is moving downwards. This indicates that the current setup has the red sphere being lighter than the white sphere, causing the white sphere to descend and the red sphere to ascend.
	 3. Effect of Heavier Red Sphere: - If the red sphere were much heavier, it would exert a greater downward force compared to the white sphere. - This increased downward force would cause the red sphere to move downwards instead of upwards.
	 4. Pulley Rotation: - As the red sphere moves downwards, it would pull the rope connected to the purple hollow pulley. - The direction of the rope's movement would cause the purple hollow pulley to rotate in the direction that allows the red sphere to descend.
	5. Determining Rotation Direction: Observing the setup, if the red sphere moves downwards, the rope on the right side of the purple hollow pulley would be pulled down. This downward pull on the right side would cause the purple hollow pulley to rotate in a clockwise direction.
	Therefore, if the red sphere were much heavier, the purple hollow pulley would rotate clockwise.
	C. Stationary

Figure 100: A sample case of physics-based dynamics-collision. Back to List of Figures.

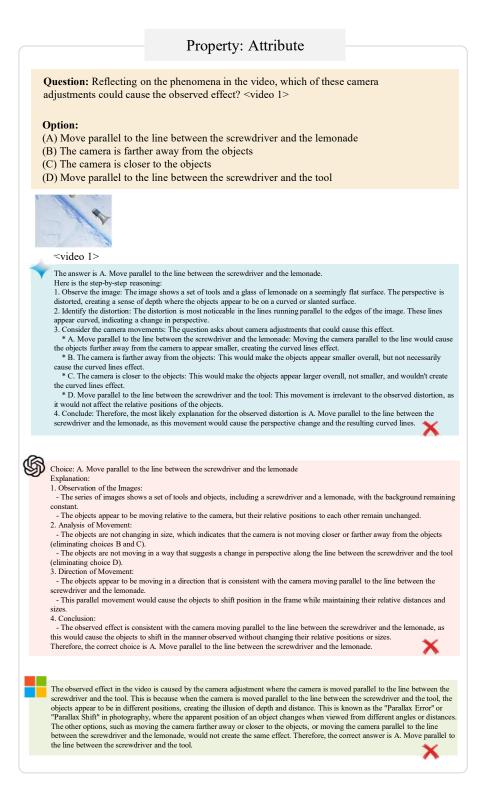


Figure 101: A sample case of physical object property-attribute. Back to List of Figures.

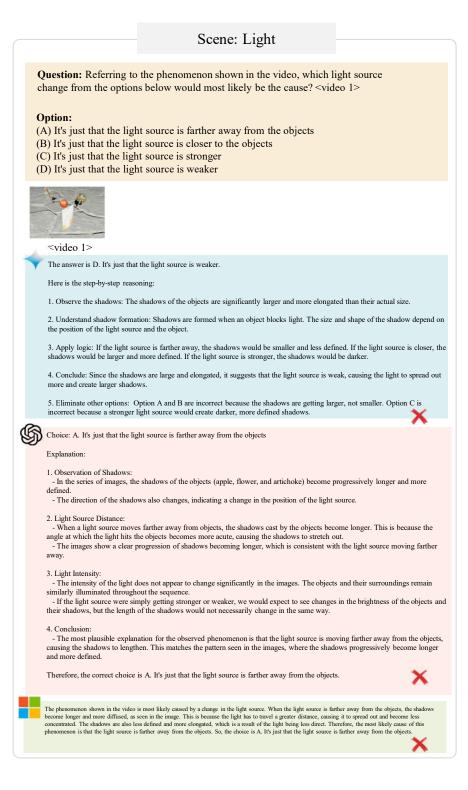


Figure 102: A sample case of physical scene understanding-light. Back to List of Figures.

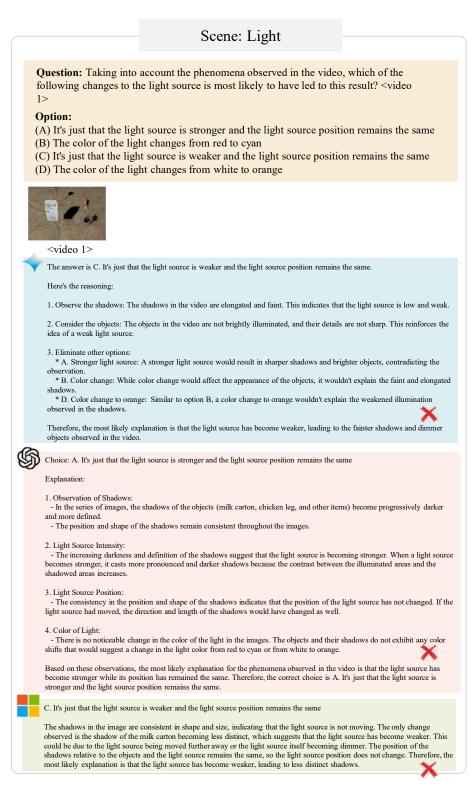


Figure 103: A sample case of physical object property-attribute. Back to List of Figures.

			Dynami	cs: Throwing	
	th < 0 (A (H (0	•	e cabinet's right door.	h one outlines the proper s , then open its left door? <i< th=""><th></th></i<>	
		<pre><image 1=""/></pre>	< image 2>	< image 3>	
1	-	The answer is A. 1 - 2	- 3.		
				6 dh - mar - main - main fan dhia ah	
		Here is the detailed, sto	ep-by-step explanation o	f the reasoning chain for this ch	oice:
		hanging the coat hange 2. Image #2 shows the	er. robot's arm now in the p	wards the right door of the cabi process of hanging the coat hang left door of the cabinet. This is	ger on the right door.
		Therefore, the correct of action, and the opening		2 - 3, which corresponds to the	e initial position, the hanging
					×
¢	Þ	Choice: B. 1 - 3 - 2			×
¢	F	Choice: B. 1 - 3 - 2 Reasoning Chain:			×
¢	F	Reasoning Chain: 1. Image #1: - The robot arm is holding	g the coat hanger and is positi he coat hanger on the cabinet	oned in front of the open cabinet. Thi 's right door.	s indicates the initial step where the
¢	F	Reasoning Chain: 1. Image #1: - The robot arm is holding robot is preparing to hang th 2. Image #3:	he coat hanger on the cabinet hung on the cabinet's right do		
¢	F	Reasoning Chain: 1. Image #1: - The robot arm is holding robot is preparing to hang the 2. Image #3: - The coat hanger is now hanger has been successfull 3. Image #2:	he coat hanger on the cabinet hung on the cabinet's right de ly placed on the door. osed, and the robot arm is po	's right door.	g the hanger, indicating that the
¢	F	Reasoning Chain: 1. Image #1: - The robot arm is holding robot is preparing to hang the 2. Image #3: - The coat hanger is now hanger has been successfull 3. Image #2: - The cabinet doors are of to open the left door of the	he coat hanger on the cabinet hung on the cabinet's right do ly placed on the door. osed, and the robot arm is po cabinet. ence to hang the coat hanger of ang the coat hanger) g on the right door)	's right door. or. The robot arm is no longer holding	g the hanger, indicating that the uggests that the robot is now ready
¢	5	Reasoning Chain: 1. Image #1: - The robot arm is holding robot is preparing to hang the 2. Image #3: - The coat hanger is now hanger has been successfull 3. Image #2: - The cabinet doors are cle to open the left door of the Therefore, the proper seque 1. Image #1 (preparing to h 2. Image #3 (hanger is hung	he coat hanger on the cabinet hung on the cabinet's right de ly placed on the door. osed, and the robot arm is po cabinet. ence to hang the coat hanger of ang the coat hanger) g on the right door) the left door)	's right door. or. The robot arm is no longer holding sitioned in front of the cabinet. This se	g the hanger, indicating that the uggests that the robot is now ready
	5	Reasoning Chain: 1. Image #1: - The robot arm is holding robot is preparing to hang the 2. Image #3: - The coat hanger is now hanger has been successfull 3. Image #2: - The cabinet doors are cle to open the left door of the Therefore, the proper seque 1. Image #1 (preparing to h 2. Image #2 (ready to open Thus, the correct choice is b	he coat hanger on the cabinet hung on the cabinet's right dc ly placed on the door. osed, and the robot arm is po cabinet. ence to hang the coat hanger of ang the coat hanger) g on the right door) the left door) B. 1 - 3 - 2. nger hanging on the right doo	's right door. or. The robot arm is no longer holding sitioned in front of the cabinet. This se	g the hanger, indicating that the uggests that the robot is now ready en its left door is:
	\$	Reasoning Chain: 1. Image #1: - The robot arm is holding robot is preparing to hang the 2. Image #3: - The coat hanger is now hanger has been successfull 3. Image #2: - The cabinet doors are cle to open the left door of the Therefore, the proper seque 1. Image #1 (preparing to h 2. Image #3 (hanger is hung 3. Image #2 (ready to open Thus, the correct choice is la The image shows a coat har left door, the sequence wou 1. Open the left door.	he coat hanger on the cabinet hung on the cabinet's right dc ly placed on the door. osed, and the robot arm is po cabinet. ence to hang the coat hanger of ang the coat hanger) g on the right door) the left door) B. 1 - 3 - 2. nger hanging on the right doo	's right door. or. The robot arm is no longer holding sitioned in front of the cabinet. This su on the cabinet's right door and then op	g the hanger, indicating that the uggests that the robot is now ready en its left door is:
	5	Reasoning Chain: 1. Image #1: - The robot arm is holding robot is preparing to hang the 2. Image #3: - The coat hanger is now hanger has been successfull 3. Image #2: - The cabinet doors are of to open the left door of the 1. Image #1 (preparing to h 2. Image #3 (hanger is hung 3. Image #2 (ready to open Thus, the correct choice is 1 The image shows a coat har left door, the sequence wou 1. Open the left door. 2. Hang the coat hanger on	he coat hanger on the cabinet hung on the cabinet's right do ly placed on the door. osed, and the robot arm is po cabinet. ence to hang the coat hanger of ang the coat hanger) g on the right door) the left door) B. 1 - 3 - 2. nger hanging on the right door ld be: the right side of the left door.	's right door. or. The robot arm is no longer holding sitioned in front of the cabinet. This su on the cabinet's right door and then op	g the hanger, indicating that the uggests that the robot is now ready en its left door is:
		Reasoning Chain: 1. Image #1: - The robot arm is holding robot is preparing to hang the 2. Image #3: - The coat hanger is now hanger has been successfull 3. Image #2: - The cabinet doors are cle to open the left door of the Therefore, the proper seque 1. Image #1 (preparing to h 2. Image #2 (ready to open Thus, the correct choice is la The image shows a coat har left door, the sequence wou 1. Open the left door. 2. Hang the coat hanger on h 3. Close the left door.	he coat hanger on the cabinet hung on the cabinet's right do ly placed on the door. osed, and the robot arm is po cabinet. ence to hang the coat hanger of ang the coat hanger) g on the right door) the left door) B. 1 - 3 - 2. nger hanging on the right door ld be: the right side of the left door.	's right door. or. The robot arm is no longer holding sitioned in front of the cabinet. This su on the cabinet's right door and then op	g the hanger, indicating that the uggests that the robot is now ready en its left door is:

Figure 104: A sample case of physics-based dynamics—throwing. Back to List of Figures.

Relationships: Size
Question: Which object is the biggest in volume? <image 1=""/>
Option: (A) red cube (B) red cube (C) green ball (D) purple cube
<image 1=""/>
 The answer is C. Here's why: Although we don't have exact measurements, we can visually assess the relative sizes. The green ball is significantly larger than the cubes, even considering the blue cube's shadow. This makes the green ball the biggest in volume among the given objects.
Choice: B. purple cube
 Explanation: 1. Visual Inspection: By looking at the image, we can see several objects: a green ball, a red cube, a yellow cube, a green cube, and a purple cube. 2. Relative Size Comparison: The green ball appears to be smaller in volume compared to the cubes. Among the cubes, the purple cube is noticeably larger than the red, yellow, and green cubes. 3. Conclusion: Based on the visual comparison, the purple cube is the largest in volume among the objects listed.
Therefore, the biggest object in volume is the purple cube (Choice B).
To determine which object has the biggest volume, we need to compare the volumes of the different shapes.
A cube has equal sides, so its volume is calculated by multiplying the length of one side by itself twice. The purple cube has sides of length 1, so its volume is $1 * 1 * 1 = 1$ cubic unit. The yellow cube has sides of length 1, so its volume is also $1 * 1 * 1 = 1$ cubic unit. The red cube has sides of length 1, so its volume is $1 * 1 = 1$ cubic unit.
A sphere has a radius, which is the distance from the center to any point on its surface. The green sphere has a radius of 1, so its volume is calculated by multiplying the cube of the radius by $4/3 * \text{pi}$. The volume of the green sphere is $4/3 * \text{pi} * 1^3 = 4/3 * \text{pi}$ cubic units.
Comparing the volumes, we can see that the green sphere has the biggest volume, followed by the purple, yellow, and red cubes, which all have the same volume.
So, the answer is C. green ball.

Figure 105: A sample case of physical object relationships-size. Back to List of Figures.

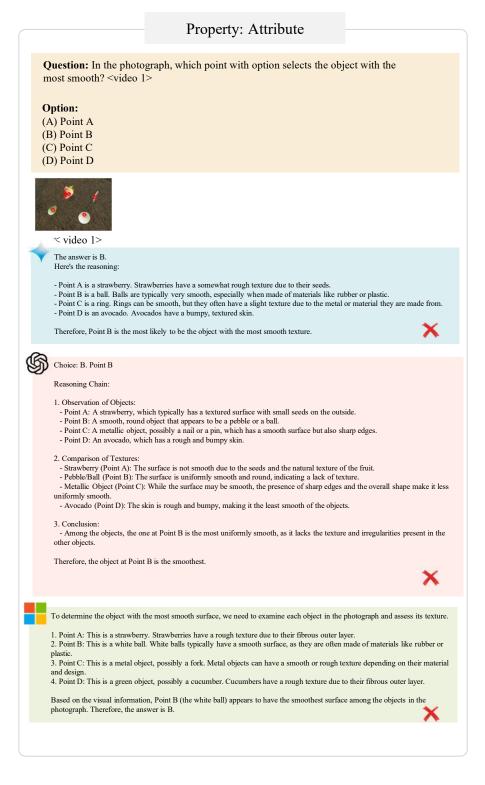


Figure 106: A sample case of physics-based dynamics-fluid. Back to List of Figures.

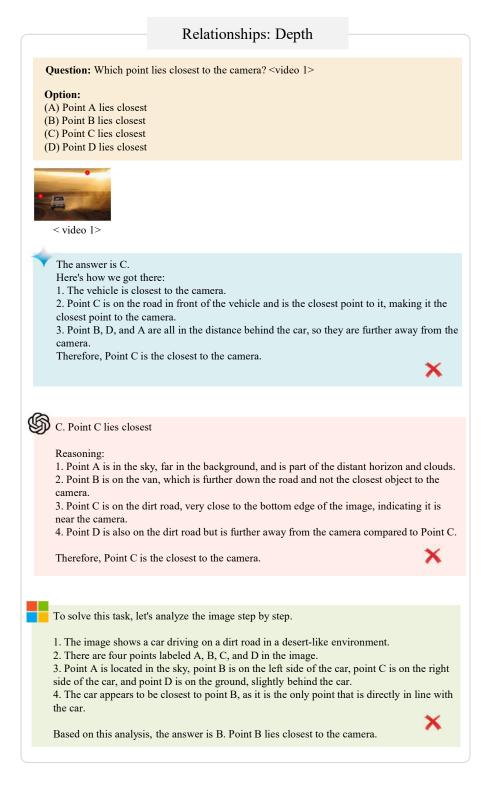


Figure 107: A sample case of physical object relationships-depth. Back to List of Figures.

J DISCUSSION AND STATEMENT

J.1 LIMITATION

Portions of our data are constructed based on pre-existing datasets, as detailed in Table 13. We have made every effort to ensure that the images included in this paper comply with applicable copyright laws and are appropriately credited. Should you be the copyright holder of any image used in our work and believe that its usage conflicts with your licensing agreements, don't hesitate to get in touch with us directly. We are committed to promptly addressing any legitimate concerns.

Although PhysBench is categorized into 4 major categories and 19 subcategories, making it the first benchmark aimed at evaluating a vision-language model's understanding of the physical world, it still does not encompass all aspects of the real physical environment. We invested thousands of hours in data collection, organization, and annotation, following multiple rigorous processes and repeated reviews to ensure data quality. Nevertheless, minor issues may persist in a small portion of the dataset.

In the experiments described in Section 3.4 and 4.1, we utilized GPT-4o-mini to extract answers, which, while currently being one of the most reliable and reproducible methods, may still unavoidably introduce hallucinations. Considering the challenges of using LLMs for evaluation, such as hallucinations and knowledge limitations, assessing open-ended formats is particularly difficult (Yu et al., 2023b; Ge et al., 2024; Li et al., 2023b). Moreover, automatically evaluating the quality of reasoning processes presents additional challenges (Lu et al., 2024b). To address these difficulties and simplify testing, we adopted a multiple-choice format. Nevertheless, PhysBench remains highly challenging, with even the most advanced GPT-40 model achieving less than 50% accuracy. We believe that exploring more complex evaluation formats is a crucial direction for future research.

These challenges are not unique to our dataset but are common across various datasets in VLMs. Nevertheless, we believe that the potential benefits outweigh the associated risks, promoting continued advancement and societal progress. To the best of our knowledge, PhysBench and PhysAgent represent the first effort aimed at benchmarking and enhancing VLMs for physical world understanding, marking a significant step forward in the field. We are committed to the ongoing refinement of our dataset to further improve machine intelligence's comprehension of the physical world, advancing embodied AI toward human-level capabilities.

J.2 BOARDER IMPACT

The broader impact of PhysBench and PhysAgent carries both potential benefits and risks upon deployment and release. While some considerations pertain specifically to the nature of the dataset, others reflect broader challenges inherent to instruction-following vision-language models (VLMs). Below, we outline key risks and corresponding mitigation strategies.

Biases. PhysAgent may inherit biases from its foundational models, both in vision and language foundation models. These biases can manifest in skewed outcomes or unfair representations, necessitating careful evaluation and mitigation efforts.

Anticipated Societal Implications. A major societal concern is the potential misuse of the dataset and system, including the generation of fabricated content, which may contribute to misinformation, privacy infringements, and other detrimental outcomes. To mitigate these risks, strict adherence to ethical guidelines and ongoing oversight are essential.

Environmental Considerations. In alignment with environmental sustainability goals, we commit to publicly releasing the dataset and scripts to reduce unnecessary carbon emissions by regenerating similar datasets. Throughout our experiments, we ensure compliance with model and data licensing requirements.

J.3 ETHICS STATEMENT

This study does not raise any ethical concerns, as it exclusively utilizes publicly available preexisting models, with no involvement of subjective evaluations. All research presented in this paper strictly adheres to the ethical guidelines set forth by the ICLR Code of Ethics.

J.4 REPRODUCIBILITY STATEMENT

We have adhered to the standard baseline settings employed by existing evaluation benchmarks or the original testing benchmarks of specific models. All necessary implementation details of our method are provided in Appendix E and F. Furthermore, we are committed to releasing the data and code under an open-access license, accompanied by comprehensive instructions to ensure the accurate reproduction of the primary experimental results presented in this paper. All research conducted complies fully with the ICLR Reproducibility Requirements.

K LATEST RESULTS

The models listed in Table 3 are current as of August 2024. Given the rapid evolution of VLMs, we evaluated an additional 36 models in December 2024, as shown in Table 28. A description of these newly added models and their hyperparameters, along with those of the original 39 models, can be found in Appendix E.3. Due to space limitations, we have not combined the two tables, but a consolidated version is available on our project page at **Our Project Page**. We will continue to update the results to reflect the latest advancements in VLMs.

In Figure 6(a), the largest model size tested was 13B. In this experiment, we have updated to larger models to evaluate whether increasing the model size significantly impacts performance on Phys-Bench. Based on the new models added in Table 3, we present Figure 108 below.

The results in Figure 108 reveal that models ranging from 1B to larger sizes generally show improvements, while the performance between 3B and 13B does not exhibit significant gains, and in some cases, such as with VILA and PLLaVA, a decrease in performance is observed. This observation constitutes the primary area of interest in Figure 6(a). Notably, at larger scales, particularly at 26B and 40B, we observe substantial improvements compared to previous sizes. However, the scalability patterns in PhysBench differ from traditional VQA benchmarks, which typically demonstrate a strong positive correlation between model size and performance. We selected widely-used benchmarks including TextVQA (Singh et al., 2019), MathVista (Lu et al., 2024b), and MMMU (Yue et al., 2024) for comparison. The relationship between model size and performance on these benchmarks is illustrated in Figures 111, 112, and 113, which demonstrate this consistent scaling pattern.

In contrast, PhysBench exhibits less pronounced scalability compared to these benchmarks, with performance not always correlating positively with model size, as shown in Figures 108, 109, and 110. This phenomenon is particularly evident in the Scene subcategory of PhysBench, where performance remains relatively stagnant in the 5-20B parameter range, only showing notable improvements with models exceeding 25B parameters, as demonstrated in Figure 109.

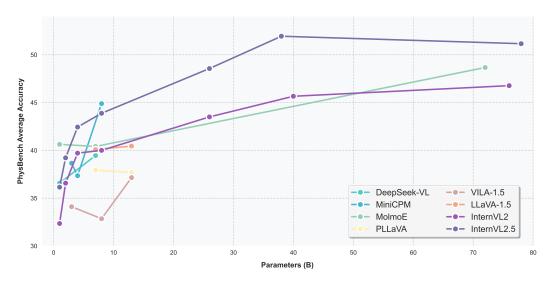


Figure 108: The performance of models of different sizes on PhysBench.

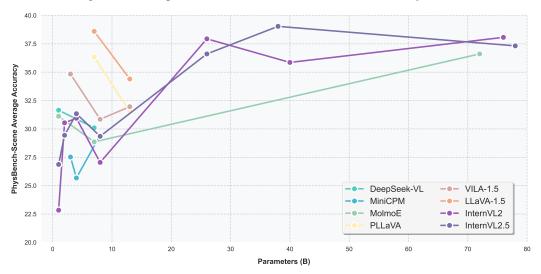


Figure 109: The performance of models of different sizes on PhysBench-Scene.

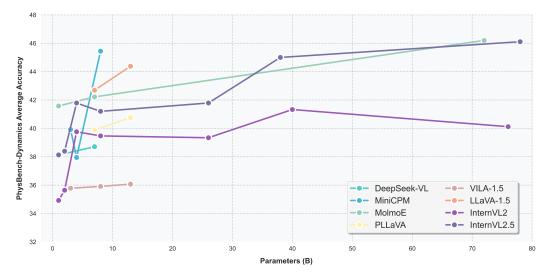


Figure 110: The performance of models of different sizes on PhysBench-Dynamics.

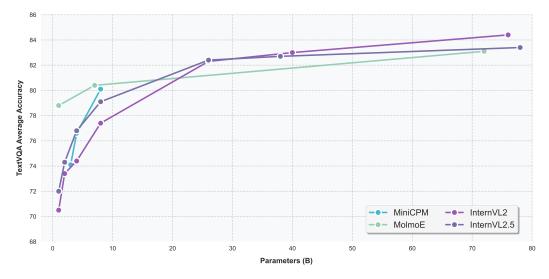


Figure 111: The performance of models of different sizes on TextVQA (Singh et al., 2019).

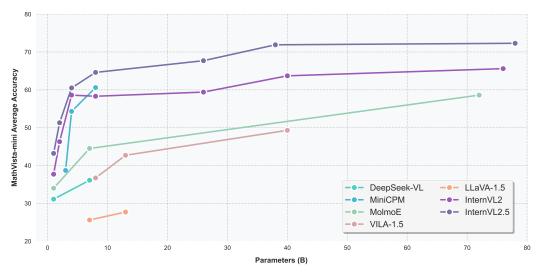


Figure 112: The performance of models of different sizes on MathVista (Lu et al., 2024b).

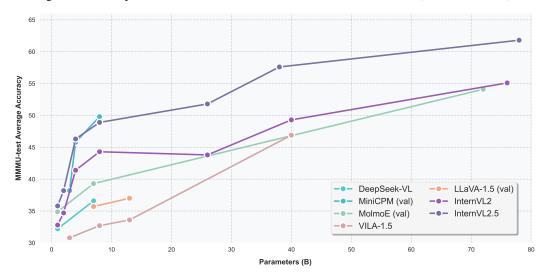


Figure 113: The performance of models of different sizes on MMMU (Yue et al., 2024).

	Size			Relationships	Scene	Dynamics	Avg
		Image					
MolmoE-1B Deitke et al. (2024)	1B	merge	43.17	58.06	31.12	41.58	40.63
MolmoE-7B Deitke et al. (2024)	7B	merge	42.35	63.33	28.86	42.22	40.41
MolmoE-7B-D Deitke et al. (2024)	7B	merge	49.48	67.78	30.81	47.18	45.18
MolmoE-72B Deitke et al. (2024)	72B	merge	55.13	72.08	36.61	46.20	48.67
MiniCPM2 (Yao et al., 2024)	3B	merge	45.62	44.17	27.53	39.92	38.66
MiniCPM2.5 (Yao et al., 2024)	4B	merge	44.26	47.08	25.68	37.95	37.35
MiniCPM2.6 (Yao et al., 2024)	8B	merge	51.43	67.92	29.44	45.44	44.89
Xinyuan-VL (Group, 2024)	2B	merge	47.97	57.50	33.91	42.22	43.09
Aquila-VL (Gu et al., 2024)	2B	merge	47.04	62.50	30.15	45.49	43.22
DeepSeek-VL-1B (Lu et al., 2024a)	1B	merge	38.37	40.28	31.65	38.12	36.58
DeepSeek-VL-7B (Lu et al., 2024a)	7B	merge	43.79	55.97	30.10	38.71	39.46
PaliGemma2-3B (Steiner et al., 2024)	3B	merge	22.03	23.33	24.75	31.73	25.94
PaliGemma2-10B (Steiner et al., 2024)	10B	merge	35.31	41.53	28.73	39.69	35.40
Ge	neral	VLM + 1	Interleaved d	lata			
Phi-3.5V (AzureML, 2024)	4B	seq	45.72	40.15	33.02	39.40	39.75
NVILA-8B (Liu et al., 2024f)	8B	seq	55.79	40.29	33.95	43.43	43.82
NVILA-15B (Liu et al., 2024f)	15B	seq	59.16	42.34	38.78	45.72	46.91
NVILA-Lite-8B (Liu et al., 2024f)	8B	seq	53.81	39.25	34.62	41.17	42.55
NVILA-Lite-15B (Liu et al., 2024f)	15B	seq	55.44	40.15	38.11	44.38	44.93
mPLUG-Owl3-1B (Ye et al., 2024)	1B	seq	38.02	31.54	21.87	33.68	31.68
mPLUG-Owl3-2B (Ye et al., 2024)	2B	seq	40.92	35.11	26.69	35.64	34.87
mPLUG-Owl3-7B (Ye et al., 2024)	7B	seq	49.25	45.62	35.90	40.61	42.83
InternVL2-1B (Wang et al., 2024e)	1B	seq	37.05	33.06	22.84	34.92	32.35
InternVL2-2B (Wang et al., 2024e)	2B	seq	44.17	35.06	30.54	35.64	36.57
InternVL2-4B (Wang et al., 2024e)	4B	seq	47.12	39.96	30.94	39.76	39.71
InternVL2-8B (Wang et al., 2024e)	8B	seq	49.05	43.58	27.05	39.47	40.00
InternVL2-26B (Wang et al., 2024e)	26B	merge	51.92	45.20	37.94	39.34	43.50
InternVL2-40B (Wang et al., 2024e)	40B	merge	55.79	50.05	35.86	41.33	45.66
InternVL2-76B (Wang et al., 2024e)	76B	merge	57.65	52.43	38.07	40.12	46.77
InternVL2.5-1B (Gao et al., 2024b)	1 B	seq	44.25	33.30	26.87	38.13	36.15
InternVL2.5-2B (Gao et al., 2024b)	2B	seq	49.63	38.15	29.44	38.39	39.22
InternVL2.5-4B (Gao et al., 2024b)	4B	seq	51.03	44.77	31.34	41.79	42.44
InternVL2.5-8B (Gao et al., 2024b)	8B	seq	55.87	48.67	29.35	41.20	43.88
InternVL2.5-26B (Gao et al., 2024b)	26B	merge	59.08	58.33	36.61	41.79	48.56
InternVL2.5-38B (Gao et al., 2024b)	38B	merge	58.77	67.51	39.04	45.00	51.94
InternVL2.5-78B (Gao et al., 2024b)	78B	merge	60.32	62.13	37.32	46.11	51.16
ol (Jaech et al., 2024)		merge	59.27	73.79	40.95	49.22	55.11

A C

πъ

Table 28: **Evaluation results for latest 36 VLMs.** The evaluation of General VLMs is based on the data from Video and Image VLM evaluations, with the addition of interleaved data. "Seq" refers to sequential input of frames of videos, while "merge" refers to merging video frames into a single image. Results of original 39 VLMs can be seen in Table 3.

Model	Size	Identify	Comparison			Perception	Prediction	Judgment	Reasoning	Avg
Image VLM										
MolmoE-1B Deitke et al. (2024)	1B	56.76	32.42	64.74	39.07	48.22	37.84	41.88	29.22	40.63
MolmoE-7B Deitke et al. (2024)	7B	54.84	32.49	72.01	37.75	49.85	39.22	45.01	25.20	40.41
MolmoE-7B-D Deitke et al. (2024)	7B	67.04	35.63	74.44	49.67	54.74	43.82	49.00	27.19	45.18
MolmoE-72B Deitke et al. (2024)	72B	68.70	44.51	76.49	58.94	54.33	43.13	50.71	33.00	48.67
MiniCPM2 (Yao et al., 2024)	3B	62.41	32.49	45.71	38.41	47.40	36.33	44.86	24.12	38.66
MiniCPM2.5 (Yao et al., 2024)	4B	49.48	40.07	45.90	51.66	40.88	36.06	41.43	23.62	37.35
MiniCPM2.6 (Yao et al., 2024)	8B	65.82	40.07	72.20	56.95	52.50	42.03	48.57	26.01	44.89
Xinyuan-VL (Group, 2024)	2B	63.12	35.77	63.43	41.06	49.34	39.56	45.30	30.86	43.09
Aquila-VL (Gu et al., 2024)	2B	62.51	35.02	66.04	51.66	50.97	41.00	46.72	28.68	43.22
DeepSeek-VL-1B (Lu et al., 2024a)	1B	48.82	29.90	40.49	43.05	41.59	35.78	40.17	30.47	36.58
DeepSeek-VL-7B (Lu et al., 2024a)	7B	55.36	35.22	59.51	41.72	45.77	35.23	40.74	27.73	39.46
PaliGemma2-3B (Steiner et al., 2024)	3B	18.31	25.19	23.69	21.19	24.57	37.29	20.51	25.20	25.94
PaliGemma2-10B (Steiner et al., 2024)	10B	46.21	27.03	42.35	39.07	44.04	37.57	40.17	26.59	35.40
			General VLM ·							
Phi-3.5-Vision-Instruct (AzureML, 2024)	4B	58.59	35.84	39.09	50.33	48.32	39.55	32.99	30.64	39.75
NVILA-8B (Liu et al., 2024f)	8B	70.71	44.10	38.05	64.71	55.76	44.18	34.02	30.45	43.82
NVILA-15B (Liu et al., 2024f)	15B	75.85	46.28	40.03	64.71	57.70	48.54	33.12	35.42	46.91
NVILA-Lite-8B (Liu et al., 2024f)	8B	69.05	41.77	37.47	59.48	53.82	41.18	33.12	31.16	42.55
NVILA-Lite-15B (Liu et al., 2024f)	15B	68.09	45.60	38.31	58.17	59.53	45.41	31.46	34.71	44.93
mPLUG-Owl3-1B (Ye et al., 2024)	1B	46.56	31.26	30.64	41.83	41.28	36.22	25.83	18.53	31.68
mPLUG-Owl3-2B (Ye et al., 2024)	2B	54.23	30.65	34.24	41.83	40.77	37.58	31.46	23.89	34.87
mPLUG-Owl3-7B (Ye et al., 2024)	7B	65.39	36.59	44.68	56.21	53.62	41.59	30.69	32.50	42.83
InternVL2-1B (Wang et al., 2024e)	1B	48.04	28.67	32.36	39.22	40.06	35.60	30.31	20.68	32.35
InternVL2-2B (Wang et al., 2024e)	2B	60.77	31.19	34.24	43.79	43.12	35.47	33.25	27.62	36.57
InternVL2-4B (Wang et al., 2024e)	4B	61.20	36.18	38.31	56.86	53.62	42.95	27.24	26.28	39.71
InternVL2-8B (Wang et al., 2024e)	8B	64.95	36.79	42.28	56.86	52.19	39.96	32.35	22.40	40.00
InternVL2-26B (Wang et al., 2024e)	26B	66.35	40.55	44.02	58.56	52.31	47.11	38.18	32.18	44.18
InternVL2-40B (Wang et al., 2024e)	40B	69.83	44.91	49.01	60.13	55.66	43.50	28.13	32.17	45.66
InternVL2-76B (Wang et al., 2024e)	76B	71.23	47.37	51.10	64.05	52.91	40.16	33.38	34.47	46.77
InternVL2.5-1B (Gao et al., 2024b)	1B	63.12	29.56	32.41	41.18	47.09	41.39	25.96	24.03	36.15
InternVL2.5-2B (Gao et al., 2024b)	2B	68.35	35.02	37.58	42.48	47.50	39.28	29.92	27.00	39.22
InternVL2.5-4B (Gao et al., 2024b)	4B	66.52	38.84	43.37	60.78	54.43	43.02	30.69	27.91	42.44
InternVL2.5-8B (Gao et al., 2024b)	8B	72.62	43.00	47.39	60.78	51.58	42.82	31.33	26.09	43.88
InternVL2.5-26B (Gao et al., 2024b)	26B	75.94	45.94	58.04	60.78	55.15	40.84	33.89	33.60	48.56
InternVL2.5-38B (Gao et al., 2024b)	38B	74.02	46.89	67.38	69.28	58.92	41.93	38.87	36.57	51.94
InternVL2.5-78B (Gao et al., 2024b)	38B	78.47	46.21	61.17	71.90	60.35	42.61	39.77	34.90	51.16
o1 (Jaech et al., 2024)	-	78.73	44.23	73.38	78.43	55.56	43.29	52.56	40.35	55.11

Table 29: **Evaluation Results for 36 new VLMs Categorized by Ability Dimensions**. PhysBench includes two evaluation dimensions: ability and task. Table 28 presents results categorized by the task-type dimension.

Model			Mass	Color	Attribute		
Image	VLM						
MolmoE-1B Deitke et al. (2024)	1B	56.85	23.89		39.39		
MolmoE-7B Deitke et al. (2024)	7B	48.01	30.03	56.67	39.46		
MolmoE-7B-D Deitke et al. (2024)	7B	65.16	36.52	63.33	42.73		
MolmoE-72B Deitke et al. (2024)	72B	63.95	51.19	64.00	50.25		
MiniCPM2 (Yao et al., 2024)	3B	56.52	42.66	66.56	37.26		
MiniCPM2.5 (Yao et al., 2024)	4B	46.26	50.17	45.82	41.80		
MiniCPM2.6 (Yao et al., 2024)	8B	54.09	58.70	70.23	44.71		
Xinyuan-VL (Group, 2024)	2B	54.25	47.44	71.67	40.38		
Aquila-VL (Gu et al., 2024)	2B	55.63	43.69	64.33	40.38		
DeepSeek-VL-1B (Lu et al., 2024a)	1B	48.18	32.76	49.33	33.29		
DeepSeek-VL-7B (Lu et al., 2024a)	7B	51.99	39.59	52.33	39.46		
PaliGemma2-3B (Steiner et al., 2024)	3B	20.80	17.75	17.67	24.34		
PaliGemma2-10B (Steiner et al., 2024)	10B	40.03	29.01	45.67	32.51		
General VLM + Interleaved data							
Phi-3.5-Vision-Instruct (AzureML, 2024)	4B	49.05	44.37	65.00	40.45		
NVILA-8B (Liu et al., 2024f)	8B	61.35	57.34	75.67	48.90		
NVILA-15B (Liu et al., 2024f)	15B	774.18	55.29	73.67	50.53		
NVILA-Lite-8B (Liu et al., 2024f)	8B	60.14	59.04	75.00	45.42		
NVILA-Lite-15B (Liu et al., 2024f)	15B	61.18	55.97	72.33	49.25		
mPLUG-Owl3-1B (Ye et al., 2024)	1B	37.95	44.37	50.33	34.07		
mPLUG-Owl3-2B (Ye et al., 2024)	2B	44.19	37.54	61.00	35.84		
mPLUG-Owl3-7B (Ye et al., 2024)	7B	57.02	36.52	71.67	43.79		
InternVL2-1B (Wang et al., 2024e)	1B	38.99	34.47	61.67	31.44		
InternVL2-2B (Wang et al., 2024e)	2B	57.89	34.47	69.33	35.13		
InternVL2-4B (Wang et al., 2024e)	4B	49.39	39.93	71.00	42.51		
InternVL2-8B (Wang et al., 2024e)	8B	58.75	36.18	74.67	42.09		
InternVL2-26B (Wang et al., 2024e)	26B	57.19	44.71	68.00	47.69		
InternVL2-40B (Wang et al., 2024e)	40B	64.30	55.29	67.00	49.82		
InternVL2-76B (Wang et al., 2024e)	76B	67.76	60.41	64.67	51.24		
InternVL2.5-1B (Gao et al., 2024b)	1B	58.58	35.49	71.00	34.49		
InternVL2.5-2B (Gao et al., 2024b)	2B	63.95	42.32	72.67	40.38		
InternVL2.5-4B (Gao et al., 2024b)	4B	56.15	52.90	75.00	43.29		
InternVL2.5-8B (Gao et al., 2024b)	8B	67.94	50.85	75.33	47.69		
InternVL2.5-26B (Gao et al., 2024b)	26B	73.31	57.00	72.67	50.67		
InternVL2.5-38B (Gao et al., 2024b)	38B	68.11	51.88	73.00	53.16		
InternVL2.5-78B (Gao et al., 2024b)	38B	5.22	55.63	73.67	52.24		
o1 (Jaech et al., 2024)		75.22	49.83	74.67	51.31		

Table 30: Evaluation Results for 36 new VLMs in PhysBench Physical Object **Property Sub-task** (the fifth last column of Table 28).

Model	Model Size		Location	Depth	Distance	Motion	
	Image VLN						
MolmoE-1B Deitke et al. (2024)	1B	39.29	51.13	72.28	48.33	50.56	
MolmoE-7B Deitke et al. (2024)	7B	42.86	61.65	75.44	53.33	50.56	
MolmoE-7B-D Deitke et al. (2024)	7B	58.93	60.15	79.30	66.67	59.55	
MolmoE-72B Deitke et al. (2024)	72B	76.79	67.29	76.49	68.33	74.16	
MiniCPM2 (Yao et al., 2024)	3B	50.00	45.49	39.65	46.67	59.55	
MiniCPM2.5 (Yao et al., 2024)	4B	66.07	36.84	51.23	43.33	67.42	
MiniCPM2.6 (Yao et al., 2024)	8B	71.43	67.67	68.77	56.67	73.03	
Xinyuan-VL (Group, 2024)	2B	55.36	54.14	62.46	50.00	61.80	
Aquila-VL (Gu et al., 2024)	2B	69.64	60.90	64.56	61.67	59.55	
DeepSeek-VL-1B (Lu et al., 2024a)	1B	41.07	43.23	31.93	50.00	51.69	
DeepSeek-VL-7B (Lu et al., 2024a)	7B	37.50	51.13	61.40	61.67	59.55	
PaliGemma2-3B (Steiner et al., 2024)	3B	23.21	21.05	27.02	26.67	13.48	
PaliGemma2-10B (Steiner et al., 2024)	10B	48.21	45.11	36.14	41.67	50.56	
General VLM + Interleaved data							
Phi-3.5-Vision-Instruct (AzureML, 2024)	4B	57.14	59.45	66.67	55.00	30.36	
NVILA-8B (Liu et al., 2024f)	8B	76.79	67.35	70.88	73.33	26.83	
NVILA-15B (Liu et al., 2024f)	15B	76.79	69.07	80.35	75.00	27.59	
NVILA-Lite-8B (Liu et al., 2024f)	8B	73.21	61.86	71.23	60.00	27.18	
NVILA-Lite-15B (Liu et al., 2024f)	15B	62.50	67.35	73.33	70.00	26.97	
mPLUG-Owl3-1B (Ye et al., 2024)	1B	46.43	39.52	31.93	35.00	29.46	
mPLUG-Owl3-2B (Ye et al., 2024)	2B	60.71	41.58	30.88	43.33	34.09	
mPLUG-Owl3-7B (Ye et al., 2024)	7B	69.64	60.14	69.82	58.33	37.34	
InternVL2-1B (Wang et al., 2024e)	1B	44.64	53.26	35.79	50.00	27.66	
InternVL2-2B (Wang et al., 2024e)	2B	78.57	64.95	73.68	63.33	34.30	
InternVL2-4B (Wang et al., 2024e)	4B	69.64	59.11	75.44	55.00	28.08	
InternVL2-8B (Wang et al., 2024e)	8B	75.00	67.01	77.89	56.67	31.05	
InternVL2-26B (Wang et al., 2024e)	26B	78.57	64.95	73.68	63.33	34.30	
InternVL2-40B (Wang et al., 2024e)	40B	80.36	64.26	77.54	73.33	40.18	
InternVL2-76B (Wang et al., 2024e)	76B	80.36	67.01	82.81	76.67	41.91	
InternVL2.5-1B (Gao et al., 2024b)	1B	48.21	53.26	47.72	50.00	25.73	
InternVL2.5-2B (Gao et al., 2024b)	2B	48.21	57.73	68.07	50.00	28.08	
InternVL2.5-4B (Gao et al., 2024b)	4B	75.00	62.54	72.63	55.00	34.92	
InternVL2.5-8B (Gao et al., 2024b)	8B	67.86	72.16	78.25	75.00	37.00	
InternVL2.5-26B (Gao et al., 2024b)	26B	75.00	65.64	79.65	76.67	51.66	
InternVL2.5-38B (Gao et al., 2024b)	38B	85.71	68.73	75.79	80.00	64.59	
InternVL2.5-78B (Gao et al., 2024b)	38B	80.36	69.42	77.54	86.67	56.43	
o1 (Jaech et al., 2024)		83.93	76.63	78.25	80.00	71.51	

Table 31: Evaluation Results for 36 new VLMs in PhysBench Object **A**Relationships Sub-task (the forth last column of Table 28).

Model		Temperature	Viewpoint	Air	Light			
Ima	Image VLM							
MolmoE-1B Deitke et al. (2024)	1 B	50.00	30.73		30.21			
MolmoE-7B Deitke et al. (2024)	7B	64.71	21.11	36.00	33.76			
MolmoE-7B-D Deitke et al. (2024)	7B	79.41	42.70	86.00				
MolmoE-72B Deitke et al. (2024)	72B	76.79	67.29	76.49	68.33			
MiniCPM2 (Yao et al., 2024)	3B	66.18	20.83	40.00	31.12			
MiniCPM2.5 (Yao et al., 2024)	4B	48.53	13.85	42.00	35.21			
MiniCPM2.6 (Yao et al., 2024)	8B	67.65	19.51	42.00	36.21			
Xinyuan-VL (Group, 2024)	2B	64.71	33.46	48.00	32.21			
Aquila-VL (Gu et al., 2024)	2B	61.76	24.79	28.00	33.48			
DeepSeek-VL-1B (Lu et al., 2024a)	1 B	50.00	32.33	32.00	29.75			
DeepSeek-VL-7B (Lu et al., 2024a)	7B	58.82	25.64	28.00	32.85			
PaliGemma2-3B (Steiner et al., 2024)	3B	17.65	26.20	28.00	23.66			
PaliGemma2-10B (Steiner et al., 2024)	10B	48.53	27.14	40.00	28.57			
General VLM + Interleaved data								
Phi-3.5-Vision-Instruct (AzureML, 2024)		51.47	33.65	50.91	30.85			
NVILA-8B (Liu et al., 2024f)	8B	72.06	31.29	50.91	33.58			
NVILA-15B (Liu et al., 2024f)	15B	83.82	38.36	52.73	35.85			
NVILA-Lite-8B (Liu et al., 2024f)	8B	76.47	31.39		35.30			
NVILA-Lite-15B (Liu et al., 2024f)	15B	82.35	38.55	61.82	34.03			
mPLUG-Owl3-1B (Ye et al., 2024)	1 B	57.35	10.84	50.91	29.48			
mPLUG-Owl3-2B (Ye et al., 2024)	2B	63.24	25.35	29.09	25.75			
mPLUG-Owl3-7B (Ye et al., 2024)	7B	76.47	37.51	78.18	30.66			
InternVL2-1B (Wang et al., 2024e)	1 B	45.59	18.47		25.75			
InternVL2-2B (Wang et al., 2024e)	2B	50.00	28.46	21.82	31.48			
InternVL2-4B (Wang et al., 2024e)	4B	52.94	28.37	54.55	31.39			
InternVL2-8B (Wang et al., 2024e)	8B	73.53	17.91	36.36				
InternVL2-26B (Wang et al., 2024e)	26B	76.47	40.25	29.09	33.30			
InternVL2-40B (Wang et al., 2024e)	40B	94.12	37.89	58.18	29.39			
InternVL2-76B (Wang et al., 2024e)	76B	91.18	39.87	52.73	32.58			
InternVL2.5-1B (Gao et al., 2024b)	1 B	52.94	20.17	14.55	32.03			
InternVL2.5-2B (Gao et al., 2024b)	2B	58.82	21.58	16.36	35.58			
InternVL2.5-4B (Gao et al., 2024b)	4B	67.65	28.09	29.09	32.30			
InternVL2.5-8B (Gao et al., 2024b)	8B	69.12	18.94	47.27	36.49			
InternVL2.5-26B (Gao et al., 2024b)	26B	88.24	34.31	74.55	34.58			
InternVL2.5-38B (Gao et al., 2024b)	38B	88.24	41.47	78.18	32.48			
InternVL2.5-78B (Gao et al., 2024b)	38B	89.71	40.62	90.91	29.30			
o1 (Jaech et al., 2024)		95.59	47.31	81.82	30.30			

Table 32: Evaluation Results for 36 new VLMs in PhysBench Physical **\$**Scene Understanding Subtask (the third last column of Table 28.

Image VL MolmoE-1B Deitke et al. (2024) 1B 32.72 MolmoE-7B Deitke et al. (2024) 7B 28.26 MolmoE-7B-D Deitke et al. (2024) 7B 38.56 MolmoE-72B Deitke et al. (2024) 7B 38.56 MolmoE-72B Deitke et al. (2024) 7B 37.02 MiniCPM2 (Yao et al., 2024) 3B 34.82 MiniCPM2.5 (Yao et al., 2024) 4B 433.44 MiniCPM2.6 (Yao et al., 2024) 8B 35.29 Xinyuan-VL (Group, 2024) 2B 35.94 Aquila-VL (Gu et al., 2024) 1B 32.10 DeepSeek-VL-1B (Lu et al., 2024a) 1B 32.10 DeepSeek-VL-7B (Lu et al., 2024a) 7B 31.64 PaliGemma2-3B (Steiner et al., 2024) 3B 37.63 PaliGemma2-10B (Steiner et al., 2024) 10B 37.17	33.02 28.74 39.43 40.38 34.20 36.82 45.37 39.67 40.14 33.49	43.47 36.68 39.45 30.90 34.92 27.89 38.19 38.44	44.75 53.55 50.15 48.30 34.88 35.03 43.06	71.62 67.57 68.92 63.51 67.57 54.05	57.48 67.01 72.11 80.61 67.69
MolmoE-7B Deitke et al. (2024)7B28.26MolmoE-7B-D Deitke et al. (2024)7B38.56MolmoE-72B Deitke et al. (2024)7B37.02MiniCPM2 (Yao et al., 2024)3B34.82MiniCPM2.5 (Yao et al., 2024)4B433.44MiniCPM2.6 (Yao et al., 2024)8B35.29Xinyuan-VL (Group, 2024)2B35.94Aquila-VL (Gu et al., 2024)2B38.10DeepSeek-VL-1B (Lu et al., 2024a)1B32.10DeepSeek-VL-7B (Lu et al., 2024a)7B31.64PaliGemma2-3B (Steiner et al., 2024)3B37.63	28.74 39.43 40.38 34.20 36.82 45.37 39.67 40.14 33.49	36.68 39.45 30.90 34.92 27.89 38.19 38.44	53.55 50.15 48.30 34.88 35.03 43.06	67.57 68.92 63.51 67.57 54.05	67.01 72.11 80.61 67.69
MolmoE-7B-D Deitke et al. (2024)7B38.56MolmoE-72B Deitke et al. (2024)72B37.02MiniCPM2 (Yao et al., 2024)3B34.82MiniCPM2.5 (Yao et al., 2024)4B433.44MiniCPM2.6 (Yao et al., 2024)8B35.29Xinyuan-VL (Group, 2024)2B35.94Aquila-VL (Gu et al., 2024)2B38.10DeepSeek-VL-1B (Lu et al., 2024a)1B32.10DeepSeek-VL-7B (Lu et al., 2024a)7B31.64PaliGemma2-3B (Steiner et al., 2024)3B37.63	39.43 40.38 34.20 36.82 45.37 39.67 40.14 33.49	39.45 30.90 34.92 27.89 38.19 38.44	50.15 48.30 34.88 35.03 43.06	68.92 63.51 67.57 54.05	72.11 80.61 67.69
MolmoE-72B Deitke et al. (2024)72B37.02MiniCPM2 (Yao et al., 2024)3B34.82MiniCPM2.5 (Yao et al., 2024)4B433.44MiniCPM2.6 (Yao et al., 2024)8B35.29Xinyuan-VL (Group, 2024)2B35.94Aquila-VL (Gu et al., 2024)2B38.10DeepSeek-VL-1B (Lu et al., 2024a)1B32.10DeepSeek-VL-7B (Lu et al., 2024a)7B31.64PaliGemma2-3B (Steiner et al., 2024)3B37.63	40.38 34.20 36.82 45.37 39.67 40.14 33.49	30.90 34.92 27.89 38.19 38.44	48.30 34.88 35.03 43.06	63.51 67.57 54.05	80.61 67.69
MiniCPM2 (Yao et al., 2024)3B34.82MiniCPM2.5 (Yao et al., 2024)4B433.44MiniCPM2.6 (Yao et al., 2024)8B35.29Xinyuan-VL (Group, 2024)2B35.94Aquila-VL (Gu et al., 2024)2B38.10DeepSeek-VL-1B (Lu et al., 2024a)1B32.10DeepSeek-VL-7B (Lu et al., 2024a)7B31.64PaliGemma2-3B (Steiner et al., 2024)3B37.63	34.20 36.82 45.37 39.67 40.14 33.49	34.92 27.89 38.19 38.44	34.88 35.03 43.06	67.57 54.05	67.69
MiniCPM2.5 (Yao et al., 2024)4B433.44MiniCPM2.6 (Yao et al., 2024)8B35.29Xinyuan-VL (Group, 2024)2B35.94Aquila-VL (Gu et al., 2024)2B38.10DeepSeek-VL-1B (Lu et al., 2024a)1B32.10DeepSeek-VL-7B (Lu et al., 2024a)7B31.64PaliGemma2-3B (Steiner et al., 2024)3B37.63	36.82 45.37 39.67 40.14 33.49	27.89 38.19 38.44	35.03 43.06	54.05	
MiniCPM2.6 (Yao et al., 2024)8B35.29Xinyuan-VL (Group, 2024)2B35.94Aquila-VL (Gu et al., 2024)2B38.10DeepSeek-VL-1B (Lu et al., 2024a)1B32.10DeepSeek-VL-7B (Lu et al., 2024a)7B31.64PaliGemma2-3B (Steiner et al., 2024)3B37.63	45.37 39.67 40.14 33.49	38.19 38.44	43.06		(0.00
Xinyuan-VL (Group, 2024)2B35.94Aquila-VL (Gu et al., 2024)2B38.10DeepSeek-VL-1B (Lu et al., 2024a)1B32.10DeepSeek-VL-7B (Lu et al., 2024a)7B31.64PaliGemma2-3B (Steiner et al., 2024)3B37.63	39.67 40.14 33.49	38.44		< 1 a 1	60.88
Aquila-VL (Gu et al., 2024)2B38.10DeepSeek-VL-1B (Lu et al., 2024a)1B32.10DeepSeek-VL-7B (Lu et al., 2024a)7B31.64PaliGemma2-3B (Steiner et al., 2024)3B37.63	40.14 33.49			64.86	76.19
DeepSeek-VL-1B (Lu et al., 2024a) 1B 32.10 DeepSeek-VL-7B (Lu et al., 2024a) 7B 31.64 PaliGemma2-3B (Steiner et al., 2024) 3B 37.63	33.49		39.81	50.00	64.63
DeepSeek-VL-7B (Lu et al., 2024a) 7B 31.64 PaliGemma2-3B (Steiner et al., 2024) 3B 37.63		42.21	42.75	59.46	75.17
PaliGemma2-3B (Steiner et al., 2024) 3B 37.63		38.44	39.35	48.65	52.04
	35.39	35.43	37.04	54.05	61.90
D-1:Commed 10D (Stainer et al. 2024) 10D 27.17	34.68	25.13	34.57	36.49	18.03
PaliGemma2-10B (Steiner et al., 2024) 10B 37.17	40.62	33.92	35.80	56.76	54.08
General VLM + Inte	erleaved d	ata			
Phi-3.5-Vision-Instruct (AzureML, 2024) 4B 33.94	38.72	29.19	43.67	59.46	58.58
NVILA-8B (Liu et al., 2024f) 8B 38.76	45.13	31.24	43.21	70.27	69.75
NVILA-15B (Liu et al., 2024f) 15B 40.42	43.23	29.31	54.17	77.03	71.93
NVILA-Lite-8B (Liu et al., 2024f) 8B 38.31	46.08	28.59	38.43	77.03	65.40
NVILA-Lite-15B (Liu et al., 2024f) 15B 41.48	40.38	31.60	45.83	70.27	72.21
mPLUG-Owl3-1B (Ye et al., 2024) 1B 29.41	32.07	23.16	42.59	51.35	45.78
mPLUG-Owl3-2B (Ye et al., 2024) 2B 34.69	35.63	24.85	38.58	56.76	50.14
mPLUG-Owl3-7B (Ye et al., 2024) 7B 37.10	36.34	28.35	43.06	67.57	64.03
InternVL2-1B (Wang et al., 2024e) 1B 31.83	29.22	30.16	41.82	48.65	43.32
InternVL2-2B (Wang et al., 2024e) 2B 37.10	32.54	29.43	35.65	50.00	47.96
InternVL2-4B (Wang et al., 2024e) 4B 35.29	41.09	27.50	47.53	63.51	52.04
InternVL2-8B (Wang et al., 2024e) 8B 38.46	38.95	29.19	38.43	58.11	61.31
InternVL2-26B (Wang et al., 2024e) 26B 38.91	41.09	26.42	37.96	58.11	64.58
InternVL2-40B (Wang et al., 2024e) 40B 43.14	47.51	20.39	39.20	67.57	74.39
InternVL2-76B (Wang et al., 2024e) 76B 40.27	42.99	22.07	37.04	64.86	74.93
InternVL2.5-1B (Gao et al., 2024b) 1B 40.27	37.05	26.42	43.36	52.70	49.86
InternVL2.5-2B (Gao et al., 2024b) 2B 33.48	40.38	28.11	42.13	62.16	55.86
InternVL2.5-4B (Gao et al., 2024b) 4B 38.76	42.52	28.83	45.37	60.81	63.49
InternVL2.5-8B (Gao et al., 2024b) 8B 39.52	36.82	24.25	46.14	67.57	70.03
InternVL2.5-26B (Gao et al., 2024b) 26B 38.16	43.23	25.69	38.58	67.57	78.75
InternVL2.5-38B (Gao et al., 2024b) 38B 43.89	41.81	31.85	36.88	78.38	83.92
InternVL2.5-78B (Gao et al., 2024b) 38B 42.08	46.32	33.53	37.35	75.68	85.29
o1 (Jaech et al., 2024) - 48.27	41.09		43.52	71.62	89.92

Table 33: Evaluation Results for 36 new VLMs in PhysBench Physics-based Δ Dynamics Sub-task (the second last column of Table 28).